JAVIER CARRETERO GONZÁLEZ

Efecto de la Nanoarcilla en la Estructura y Dinámica del Caucho Natural

MEMORIA PARA OPTAR AL GRADO DE

DOCTOR EN CIENCIAS QUÍMICAS

DIRECTOR:

Miguel Ángel López Manchado

INSTITUTO DE CIENCIA Y TECNOLOGÍA DE POLÍMEROS
(CSIC)
Departamento de Química y Tecnología de Elastómeros

UNIVERSIDAD NACIONAL DE EDUCACIÓN A DISTANCIA
FACULTAD DE CIENCIAS
Departamento de Química Inorgánica y Química Técnica

Madrid, 2009

AGRADECIMIENTOS

El presente trabajo de investigación se ha llevado a cabo en el Departamento de Química y Tecnología de Elastómeros del Instituto de Ciencia y Tecnología de Polímeros perteneciente al Consejo Superior de Investigaciones Científicas (CSIC) durante el periodo de tiempo comprendido entre Septiembre del 2005 y Julio del 2009.

El trabajo de investigación se ha llevado a cabo bajo la dirección del doctor Miguel Ángel López Manchado, a quien quiero agradecer la libertad intelectual que me ha brindado a lo largo de estos años así como el hecho de compartir conmigo sus ilusiones e ideas científicas, hasta el punto de permitir sentirme y hacerme dueño de ellas. Muchas Gracias Miguel Ángel!!.

Así mismo quisiera decir: Muchas Gracias, a Juan López Valentín y a Rebeca Herrero Calderón, por su ayuda en la obtencion de la beca predoctoral que me ha permitido disfrutar de la ciencia y de la vida en la magnitud que lo he hecho y lo sigo haciendo. Gracias chicos!!.

Durante estos últimos años, incluso antes de los años de tesis doctoral, he conocido a mucha gente en este *mundo de ciencia* que me han ayudado no solo a interesarme por seguir en él, sino tambien a ser mejor persona. Quisiera expresar mi agradecimiento a todos ellos. A Nebil Ayape Katcho, por ser mi amigo, mi compañero de carrera, por enseñarme a “parar, mirar y citar”, muchas gracias tío, no cambies, me rio mucho contigo jajajajaja. A Jose Manuel Rivas Mercury, un mulato venezolano-brasileno lleno de bondad, con un corazon tan grande como él, que compartió conmigo cigarillos e ilusión muchos sabados y domingos en Cerámica y Vidrio. A José Manuel Benito por compartir su ciencia conmigo y ayudarme a sacar la mia pa' lante. A Esther ("*Ebony*"), Jesús y Belén, por ser los tres mosqueteros, elegantes compañeros con una *clase* innata, gracias por vuestra exquisita compañía en Catálisis.

Durante los años de Tesis Doctoral, he podido desarrollar mi trabajo de investigación gracias a un numeroso grupo de personas, no solo pertenecientes al Instituto de Ciencia y Tecnología de Polímeros en Madrid, sino también a los centros de investigación de otros países donde llevé a cabo mis estancias predoctorales. Gracias a Juan López Valentín por compartir su ilusión, su inteligencia y su conocimiento y hasta su *gotera*!!! conmigo en la Alemania del Este en tiempos de *guerra espiritual*. I want to thank Prof. Dr. Kay Saalwächter (Martin-Luther Halle-Wittenberg University, Halle, Germany) for accepting me in his laboratory for three months, and teaching me. Thanks especially to Pierre, Volker, Shakeel, Thomas (I'll never forget the bock bier!!), Günter, Walter, Michele and many other so nice mates.

También estuve 7 meses de estancia predoctoral en la prestigiosa Universidad de Cornell, en la ciudad de Ithaca perteneciente al estado de Nueva York. No olvidaré nunca esos 7 meses de duro trabajo en Estados Unidos. La verdad es que agradezco de nuevo a Miguel Ángel el hecho de mandarme allí pues no solo aprendí muchísimo, sino que también fue determinante para el desarrollo posterior del presente trabajo de investigación. I would like to thanks Prof. Emmanuel Paul Giannelis (Cornell University, Ithaca, USA) to permit me living in Ithaca during 7 months and work under his supervision in his laboratory. I especially appreciate the teaching efforts with me of Haris Retsos on the dielectric spectroscopy. I also want to give especially thanks to "Jason" (Chia Che Fang) for being my best friend in Ithaca and to drive me in his amazing *Porsche* during the winery tours….. and Robert Rodriguez, Huiquin Lian, Mamoru Miyata, Luis

Estevez, Michelle, Debra, Jishnu and Loan Vo and for their help and friendship during my stay at Cornell. I'll never forget you guys!!!! and probably you'll never forget me too jajaja!!!!.

I'm very much indebted to Prof. Benjamin S. Hsiao and Shigeyuki Toki for allowing me to visit his lab in the Chemistry Department at the State University of New York (SUNNY) at Stony Brook and permit to me realize the "*key*" X-rays measurements in the National Synchrotron Light Source at Brookhaven National Laboratory in New York.

Muchas gracias a Tiberio Ezquerra por su ayuda, complicidad y enseñanzas vía "e-mail" en el tramo final de mi Tesis Doctoral.

Muchísimas gracias a mis compañeros de departamento y del ICTP en Madrid, Irene Mora Barrantes ("Ayrin") y (and) Justo Brasero Espada ("Yust"), María ("Pintora"), Daniel, Fabi, Raquel, Pedro, Ángel, Alberto, Jose María, Pilar, Celia, Rodrigo Navarro, Leví, Sandra, Zulima, Joanna, Rodrigo París, Mónica, Paula, Cuellas, Jaime, Coro, Miguel, Andrés, Luis Ibarra, Luis González, Juan Pedro, Vanesa, Roberto, Armando (breve pero intenso), Sabino, Carlos ("señor Briones"), Alan, Patricia, (si me olvido de alguien por favor que no me perdone) por ayudarme siempre que he necesitado vuestra ayuda, por estar siempre dispuestos a dar lo mejor que lleváis dentro por los demás, y por aguantarme que también tiene mucho mérito…sois únicos!!! y aunque he pasado poco tiempo a vuestro lado durante los últimos cuatro años, no me he olvidado nunca de vosotros mientras me encontraba lejos y solo.

También me gustaría dar las gracias a los siguientes investigadores que me han ayudado en algún momento de estos últimos años: Ángel Caballero, Miguel Ángel Rodríguez, Inmaculada Rodríguez, Antonio Guerrero, Vicenta Muñoz, Carlos Otero y a Miguel Arroyo (siempre apuntando con una sonrisa, listo para disparar uno de sus chistes!!). Muchas gracias por vuestra confianza!!!

En lo relativo a mis amigos fuera de la ciencia, la verdad no tengo muchos, y me gustaría agradecer especialmente a Juan Bautista Corral Vega, mi amigo desde la juventud, compañero de *juergas y andanzas*, con el que me perdí multitud de noches por las calles de Madrid.

A mi Familia, a mis padres, Tomás y Concha, por lograr que creciera en un ambiente de felicidad plena, idílico, de ensueño, os debo lo que soy. A mi hermana Violeta, a mis sobrinos Aitor y Celia, a Ángel, os quiero mucho.

Y a ti, Elizabeth, *my little turtle*, te debo el hecho de seguir creciendo como un niño cada día, seguir viviendo dentro de un sueño del que no quiero despertar, muchísimas gracias por ser real, por amarnos tanto.

A los artistas

PRÓLOGO

Los nanocompuestos poliméricos son comúnmente definidos como la combinación de una matriz polimérica y aditivos que tienen al menos una dimensión en el rango nanométrico. En los últimos años, han despertado un enorme interés tanto a nivel científico como industrial, debido a las excelentes propiedades que exhiben con solo la incorporación de pequeñas cantidades de nanopartículas. Sin embargo, no han alcanzado las expectativas que se habían marcado hace un par de décadas. Para ello, es necesario profundizar aún más en el conocimiento de estos materiales desde un punto de vista científico. En esta memoria se pretende ahondar en el conocimiento de la microestructura de estos sistemas, las posibles interacciones nanocarga-polímero, el efecto de las nanocargas sobre la dinámica molecular del material o el efecto de las nanocargas sobre la red elastomérica.

El presente trabajo de investigación se ha organizado en cinco grandes capítulos:

Capítulo I. Breve introducción sobre los nanocompuestos poliméricos describiendo la motivación e interés en los mismos por parte de la comunidad científica, así como los objetivos del presente trabajo de investigación.

Capítulo II. Se describen las técnicas y métodos utilizados en la realización de la Tesis Doctoral.

Capítulo III. Se describen los resultados científicos más relevantes alcanzados durante la realización de la Tesis Doctoral. Se presentan en el formato de la revista científica recogida en

Thomson´s Web of Science[1] en lengua inglesa. Para facilitar la lectura y comprensión del presente trabajo de investigación, el orden de los artículos no siempre se corresponde con el orden cronológico en el que éstos fueron publicados.

Capítulo IV. Discusión detallada de los resultados científicos

Capitulo V. Conclusiones científicas más importantes

ÍNDICE

CAPÍTULO I

INTRODUCCIÓN

1. Aspectos Generales

El trabajo de Tesis Doctoral aquí presentado se encuadra en el área de la Nanotecnología, y más en concreto dentro del campo del diseño, preparación y estudio de materiales nanoestructurados. Durante las últimas décadas, la Nanotecnología viene despertando el interés de un mayor número de científicos en todo el mundo y de la sociedad en general.

Como su nombre indica, la *NANOTECNOLOGÍA*, es la tecnología relativa a la escala nano, siendo éste el prefijo de la unidad correspondiente a la milmillonésima (10^{-9}) parte de algo. A escala nanométrica tienen lugar nuevos fenómenos físicos en la materia, así como la observación de propiedades superiores a las ya existentes o incluso nuevas. Y es ahí donde radica el interés del estudio y manipulación de la materia a escala nanométrica, en el descubrimiento y entendimiento de un nuevo *"mundo"* invisible a escalas superiores, que ofrece nuevas oportunidades científico-tecnológicas.

En la imagen (Figura 1) se comparan productos artificiales hechos por el hombre con otros naturales para hacernos una idea de su tamaño, también nos indica hasta que punto se mide en nanómetros o en micrómetros.

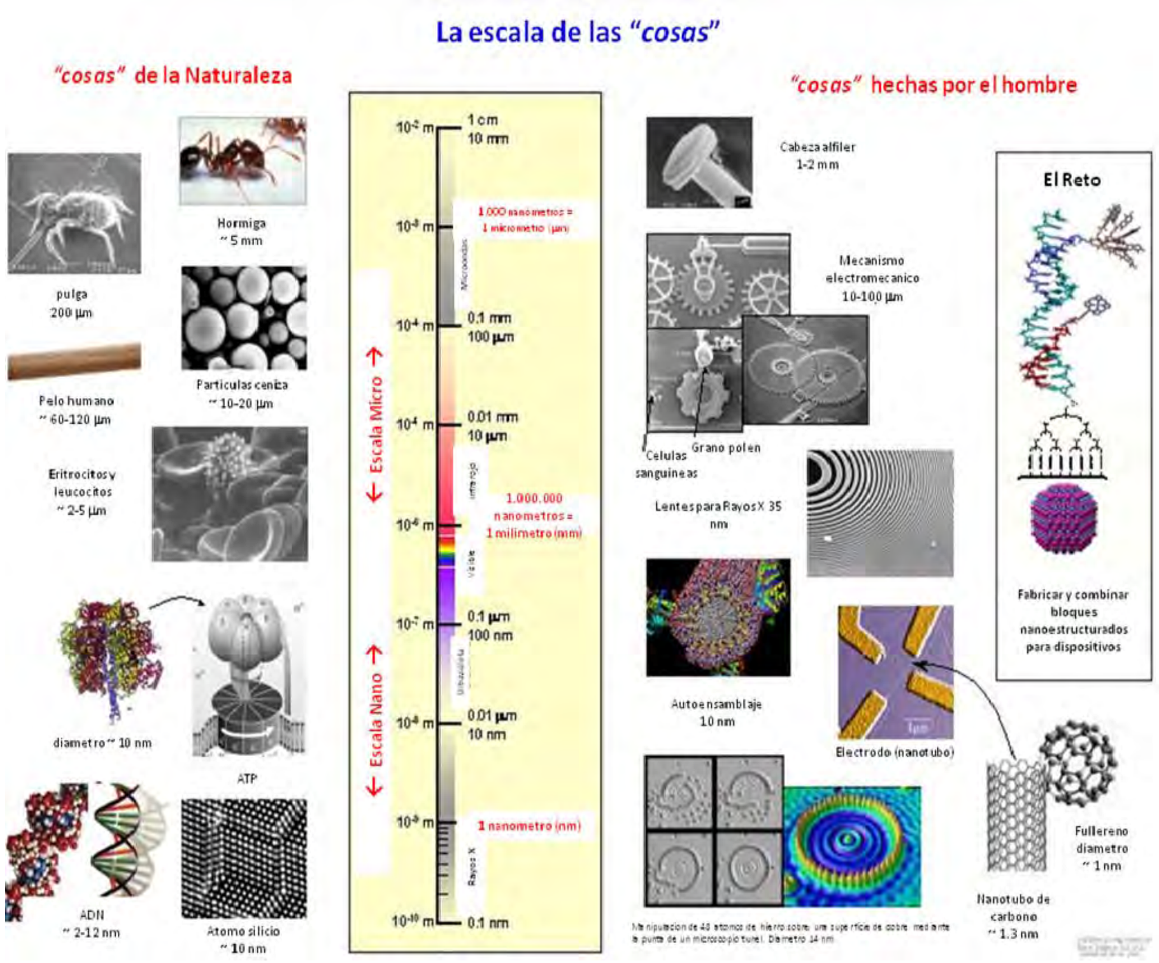

Figura 1. Escala dimensional a modo de comparativa entre las cosas que encontramos en la naturaleza y aquellas fabricadas por el hombre.

2. Nanocompuestos Poliméricos

Un material compuesto se caracteriza por estar constituido principalmente por una fase continua o matriz y una fase dispersa, inmiscibles entre sí y separadas por una interfase.[2] Existe un efecto sinérgico entre los distintos componentes del material compuesto ya que las propiedades del material son superiores a la simple suma de las propiedades de sus componentes.

La gran mayoría de los materiales compuestos se crean artificialmente, pero existen numerosos casos de materiales compuestos en la naturaleza, como por ejemplo, la madera constituida de matriz de lignina y fibras de celulosa o los propios huesos formados de una matriz ósea con fibras de colágeno.

Un nanocompuesto se podría definir a su vez, como un material nanoestructurado ya que está constituido por una fase continua y una dispersión homogénea de elementos que exhiben, en al menos una de sus dimensiones, un tamaño nanométrico, inferior a los 100 nm.[3-7] Aunque el término *nanocompuesto* se acuñó en la década de los 80, la incorporación de partículas finamente divididas o de pequeño tamaño a matrices de distinta naturaleza (metálicas, cerámicas o poliméricas, etc.) ha sido una práctica común en la búsqueda de nuevos materiales reforzados en el área de la ciencia y tecnología de los materiales compuestos.[2]

Más en concreto, en el caso de matrices de naturaleza polimérica, la incorporación de negros de carbono, silicatos y carbonatos de calcio, sílices e incluso zeolitas, etc., han sido empleados como agentes reforzantes desde el siglo pasado,[8-10] estando hoy en día ya reconocidos muchos de ellos como nanopartículas reforzantes o *nanocargas*.

Hay tres características que definen y constituyen la base del comportamiento de los nanocompuestos poliméricos:

i) una matriz polimérica confinada entre las nanopartículas,

ii) un constituyente inorgánico a nanoescala, y

iii) un acoplamiento de estos constituyentes a nanoescala.

La presencia de una gran cantidad de interfases nanopartícula–polímero implica que la mayoría de las cadenas de polímero se encuentren próximas a la superficie inorgánica (Figura 2). Dicha proximidad afectará a la ordenación de las cadenas de polímero y por tanto, a su comportamiento de relajación molecular. En el caso de polímeros que posean una gran capacidad para ordenarse (polímeros semicristalinos), la interfase afectará el grado de ordenamiento y empaquetamiento de las cadenas de polímero, teniendo este hecho a su vez, una indicencia directa sobre la cinética de cristalización, así como en la estructura cristalina del polímero.

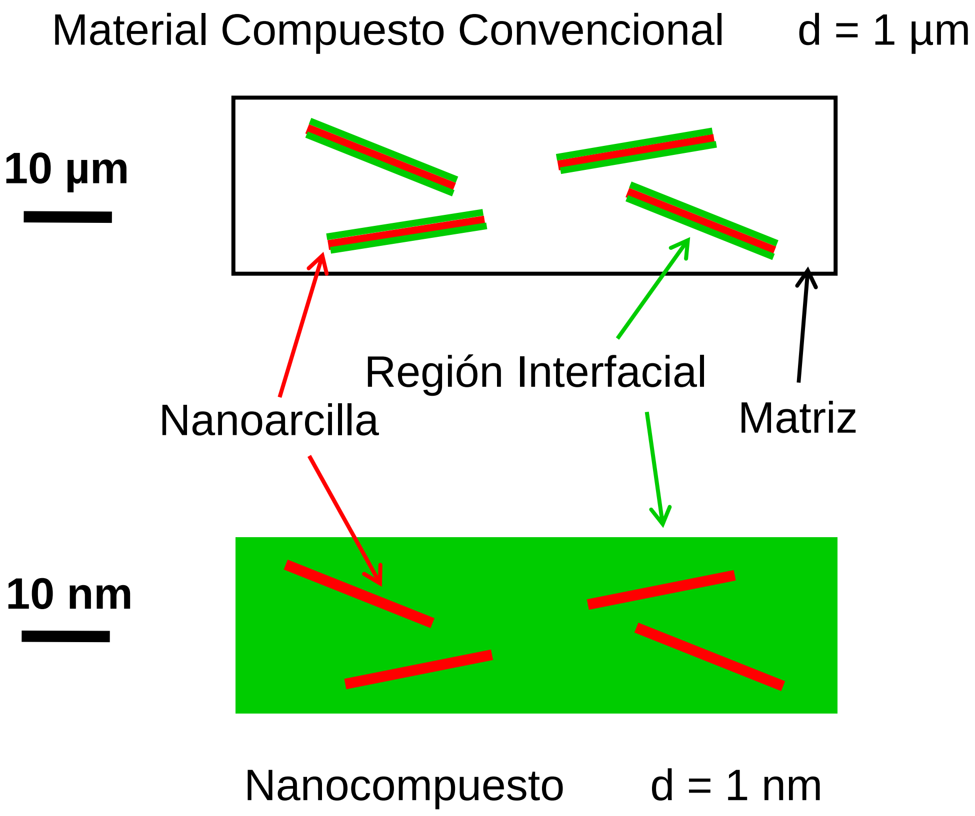

Figura 2. Área interfacial en un material compuesto convencional y en un nanocompuesto.

La segunda característica fundamental de los nanocompuestos viene determinada por las dimensiones de los nanoelementos incorporados. Cuando las dimensiones de los agregados o partículas son del orden o se presentan en la escala de una propiedad física medible (observable), se produce una modificación de la misma o la aparición de nuevos fenómenos que son ausentes a nivel macroscópico sin la presencia de dichos *nanoconstituyentes*.

La principal característica física que tiene que tener una partícula inorgánica para ser considerada como nanocarga, es que tenga al menos una de sus tres dimensiones en el rango nanométrico.[11] Por tanto, dependiendo de que estas nanopartículas dispersas de manera homogénea en la matriz polimérica, tengan una, dos o las tres dimensiones en el rango nanométrico, podemos distinguir entre tres tipos de nanocompuestos poliméricos principalmente:

a) Cuando las tres dimensiones están en la escala nanométrica, estas partículas se llaman isodimensionales y a esta categoría pertenecen partículas esféricas (Figura 3a) principalmente, así como también *clusters*.

b) Si las nanopartículas tienen dos dimensiones de tamaño nanométrico, éstas se presentan en forma de nanofibras o nanotubos, huecos o macizos (Figura 3b) ej. nanotubos de carbono.

c) El tercer tipo pertenece a aquellos nanocompuestos que presentan nanopartículas con una sola dimensión nanométrica. Estas nanopartículas son conocidas como discos o láminas (Figura 3c) ej. silicatos laminares.

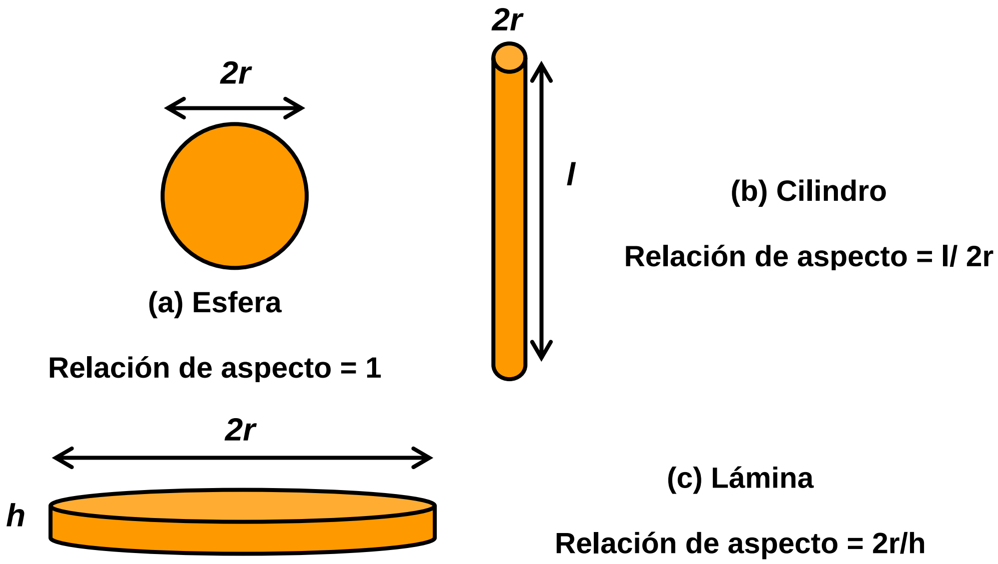

Figura 3. Clasificación de las nanopartículas en función de sus dimensiones en el rango nanométrico.

Finalmente, como en cualquier otro material compuesto, la disposición de los constituyentes determina críticamente el comportamiento del material. Conceptualmente, la ordenación espacial de nanoelementos esféricos, con forma cilíndrica o laminar, originará una gran variedad de sistemas. Estas posibilidades se ven ampliadas por la variación de distintos grados de asociación nanopartícula–nanopartícula, agrupaciones, percolación (formación de una red interconectada de elementos) y distribución heterogénea de partículas. Las propiedades finales de un nanocompuesto dependen de las propiedades individuales de los constituyentes (Tabla 1), de las disposiciones relativas y de las relaciones entre los mismos.

Tabla 1. Características de las cargas tradicionales y nanopartículas.[12]

Características de cargas tradicionales y nanopartículas: Forma, tamaño, propiedades, dimensiones y aplicaciones							
	Forma	Dimensión (nm)	Relación de aspecto	Módulo elástico (GPa)	Conductividad eléctrica (S/cm)	Conductividad térmica (W/mK)	Aplicación comercial
Tradicionales							
Negro de carbono	aglomerados	10-100	1-5	----	10-100	0,1-0,4	neumáticos, zapatos
Fibra de carbono	cilíndrica	5.000-20.000	10-50	300-800	0.1-10	100-1.000	aeroespacial
Grafito	laminar	250-500	15-50	500-600	1-10	100-500	lápices
Fibra de vidrio	cilíndrica	10.000-20.000	20-30	75	----	----	automoción
Sílice	aglomerados	8.000-30.000	5-10	30-200	----	1-10	refuerzo de plásticos
Arcilla	laminar	5.000-20.000	5-10	1-70	----	1-10	industria papelera
Nanopartículas							
Nanofibra	cilíndrica	50-100	50-200	500	700-1.000	10-20	aeroespacial
Nanotubos de carbono	cilíndrica	0.6-1.8	100-10.000	15.000	500-10.000	100-1.000	actuadores
Nanoarcilla	laminar	1-10	50-1.000	200-250	----	1-10	automoción

Esta Tesis Doctoral se centra en el estudio de nanocompuestos poliméricos de matriz elastomérica, concretamente caucho natural reforzado con nanopartículas con una sola dimensión nanométrica, en particular, una montmorillonita, un silicato laminar de la familia de las esmectitas.

A continuación, se describen brevemente las características estructurales de estos materiales y sus atributos para ser usados como nanopartículas.

2.1. Estructura de los silicatos laminares. Reacción de organofilización

Los silicatos intercalados o estratificados, más conocidos como filosilicatos 2:1, están siendo hasta el momento, los nanoelementos inorgánicos más empleados para la preparación de nanocompuestos poliméricos. Estos silicatos poseen las mismas características estructurales que otros conocidos minerales como la mica y el talco y se componen de aluminosilicatos hidratados.

$$Na_x\,(Al_{2-x}Mg_x)\,Si_4O_{10}\,(OH)_2 \cdot nH_2O$$

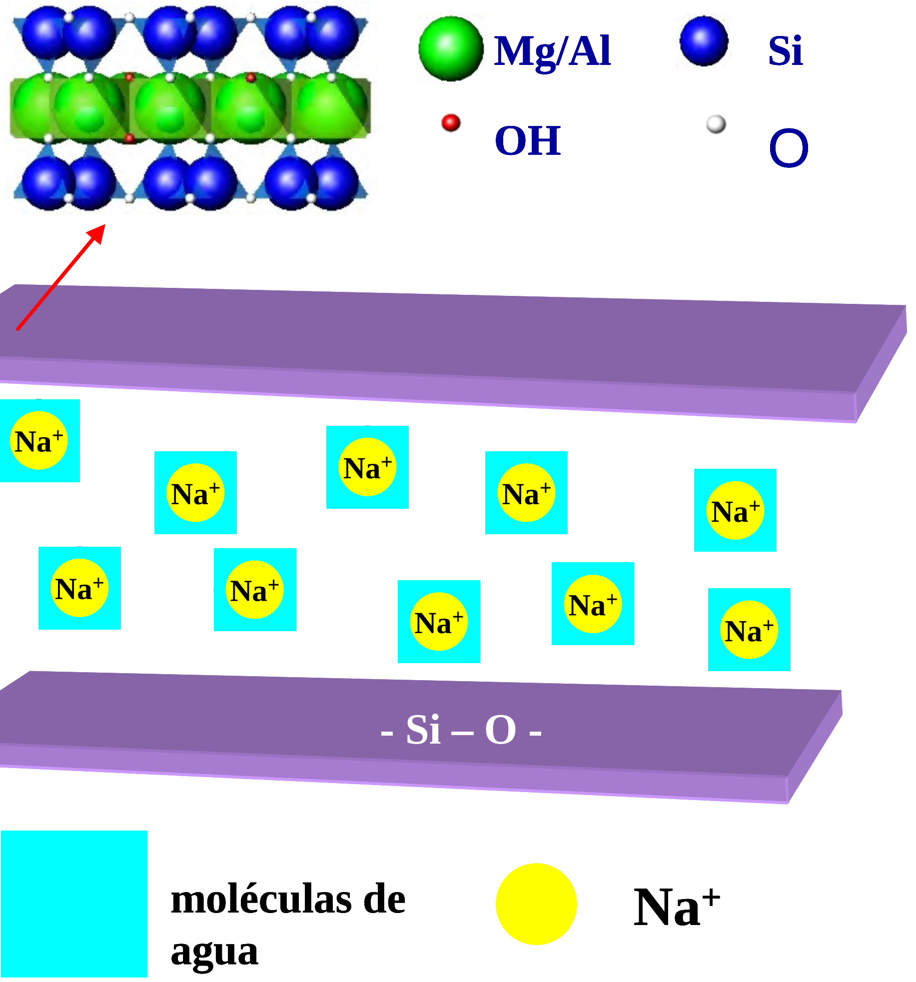

Figura 4. Estructura cristalina de un silicato laminar.

Su estructura cristalina se aprecia en la Figura 4 y consiste en dos capas bidimensionales donde una lámina octaédrica central de alúmina o magnesia se encuentra unida por los extremos a dos tetraedros externos de sílice, de modo que los iones oxígeno de la lámina octaédrica también pertenecen a las láminas del tetraedro. El espesor de la capa es de alrededor de 1 nm y las dimensiones laterales de estas capas varían desde 300 Å a varias micras, en función del tipo de silicato. Estas capas se organizan entre sí, formando agrupaciones o apilamientos con un espaciado regular entre ellas conocido como intercapas o galerías, en el que se encuentran cationes alcalinos, alcalino-térreos y moléculas de agua.

Este carácter laminar le confiere una relación de aspecto muy alta (entre 10 y 5.000) una vez que éstas se encuentran completamente delaminadas en la matriz polimérica, pues el espesor es de 1 nm y las dimensiones laterales varían de 0.5 a 5 micras. La carga neta en el cristal del silicato es negativa siendo contrarrestada por la presencia de cationes generalmente de sodio, calcio o potasio en el interior de la galería.

El desarrollo de estas nanopartículas como refuerzo de matrices poliméricas se debe entre otros factores, a su precio relativamente económico, a la obtención en su forma mineralógica pura y a su rica química de intercalación. Sin embargo, su principal inconveniente es que no se dispersan fácilmente en la mayoría de los polímeros, debido a su tendencia a formar aglomerados.

La nanoarcilla tiene un carácter polar, incluso presenta una esfera de coordinación de agua rodeando a los cationes presentes en el interior de la galería lo que le aporta un carácter hidrofílico que permite el hinchamiento de éstas en medio acuoso.[13] En el caso de matrices poliméricas polares existirá una interacción favorable entre el polímero y la arcilla, pudiéndose originar el proceso de intercalación de forma favorable mediante mezcla directa.

Sin embargo, la mayoría de los polímeros de gran producción[14] (~ 85 %) como son el polietileno, polipropileno, poliestireno, cloruro de polivinilo ó poliisopreno, son apolares y prácticamente incompatibles con la nanoarcilla. Para salvar la barrera energética que nos permita la intercalación del polímero en la galería y una posterior exfoliación (proceso del que hablaremos más adelante) es necesario llevar a cabo una reacción de intercambio catiónico, denominada *reacción de organofilización*.

Los cationes alcalinos y alcalinotérreos presentes en el interior de las galerías proporcionan al silicato una gran versatilidad química, pues éstos se pueden sustituir vía intercambio catiónico por moléculas orgánicas que presentan carga positiva como por ejemplo, sales de alquilamonio o alquilfosfonio, presentando éstas a su vez diferentes grados de sustitución por cadenas alquílicas lineales (Figura 5).

Esta reacción de organofilización no solo aumenta la separación entre las láminas del silicato sino que además, mejora la compatibilidad con la matriz polimérica, facilitando de este modo, la inserción de las cadenas poliméricas en el espaciado interlaminar del silicato.

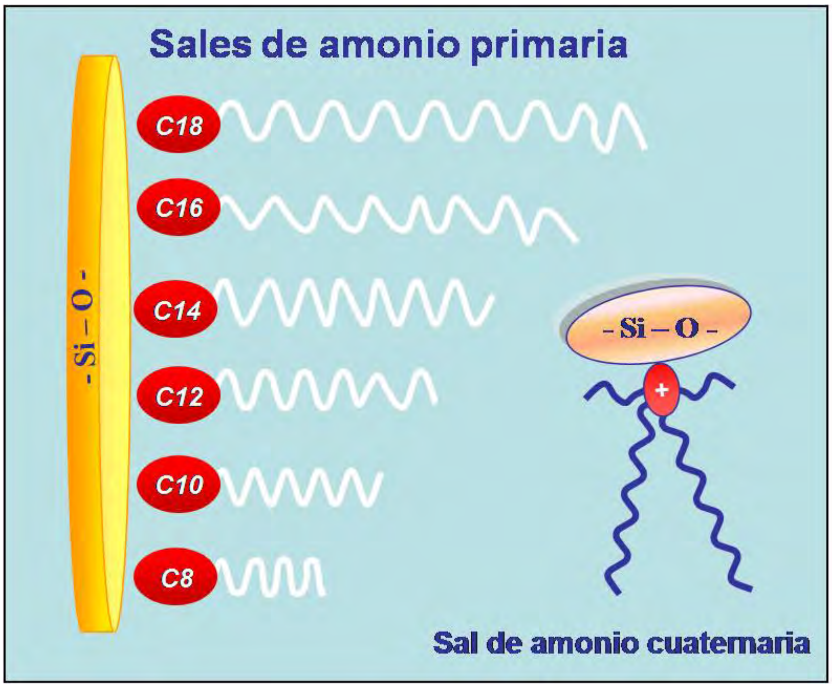

Figura 5. Estructura de las sales de alquilamonio usadas en la reacción de organofilización del silicato laminar. El número indica el número de átomos de carbono en la cadena de surfactante (Ej. C8: 8 átomos de carbono).

Una vez modificada la nanoarcilla con sales de alquilamonio (surfactantes catiónicos) existe una interacción termodinámica favorable con el polímero apolar pudiéndose producir la intercalación. Aunque el proceso de intercalación tenga lugar en parte debido a una ganancia energética en términos entálpicos, éste a su vez tiene un coste entrópico, ya que mientras las cadenas de polímero son nanoconfinadas entre 1.5-2.0 nm en la galería produciéndose un aumento en el orden de las mismas como consecuencia de una disminución del volumen cooperativo entre las cadenas, el balance energético del proceso es favorable gracias a los cambios conformacionales que tienen lugar en las moléculas orgánicas de surfactante empaquetadas en la galería.

Por tanto, una vez optimizada la interacción polímero–nanoarcilla mediante el empleo de moléculas orgánicas, que presentan distinta organización molecular y funcionalidad, o mediante la modificación química del polímero, el proceso de intercalación tiene lugar. La obtención de una estructura en el nanocompuesto presentando una mayor o menor dispersión de las láminas bidimensionales de nanoarcilla vendrá a su vez favorecida por el procesado del nanocompuesto, donde intervienen una serie de parámetros como la temperatura o la fuerza de cizalla ejercida sobre la mezcla polímero y nanoarcilla que tendrá una incidencia directa en la fluidez del polímero y de este modo, en la distribución final de las nanopartículas en la matriz polimérica.

Entre las nanopartículas de silicato laminar tipo 2:1 más empleadas como refuerzo en polímeros se encuentran la montmorillonita, hectorita, fluorhectorita, etc., siendo la principal diferencia entre ellas, la capacidad de intercambio catiónico, es decir el número de equivalentes de un determinado catión presente en la galería del silicato por gramo de nanoarcilla (Tabla 2). La capacidad de intercambio catiónico nos permite no sólo modificar la superficie de la nanopartícula inorgánica sino además, jugar con la concentración de moléculas orgánicas iónicamente unidas a la superficie del silicato para estudiar el efecto de la interacción polímero–nanoarcilla en la estructura y dinámica de los nanocompuestos poliméricos.

Tabla 2. Estructura química de los filosilicatos más comunes

Filosilicato	Fórmula general	Capacidad de Intercambio Catiónico, CEC (eq/g nanoarcilla)
Montmorillonita	$M_x\ (Al_{4-x}\ Mg_x)\ Si_8O_{20}\ (OH)_4$	~ 100
Hectorita	$M_x\ (Mg_{6-x}\ Li_x)\ Si_8O_{20}\ (OH)_4$	~ 25
Fluorohectorita	$M_x\ (Mg_xLi_x)Si_8F_4$	~ 150

M = cation monovalente; x = grado de sustitución isomórfica

3. Nanocompuestos polímero-nanoarcilla

3.1. Propiedades de los nanocompuestos

El primer nanocompuesto de polímero y nanoarcilla conocido fue desarrollado por los investigadores de Toyota en 1985 [15], y consistía en un nylon-6 reforzado con montmorillonita (una arcilla laminar de la familia de las esmectitas tipo 2:1). Los autores observaron una considerable mejora en la resistencia a tracción, en la temperatura de distorsión a calor sin apenas pérdida de la resistencia a impacto del material y todo ello, con la incorporación de tan solo un 2 % en volumen de nanopartículas. Los materiales además, mostraron una menor permeabilidad a gases y agua y un menor coeficiente de expansión térmica. Toda esta mejora de propiedades se producía sin una pérdida en la transparencia del material.

Desde entonces, el número de grupos de investigación interesados en esta área de los nanocompuestos polímero–nanoarcilla así como el número de publicaciones científicas, no ha dejado de crecer como se evidencia en la Figura 6. Se observa un claro crecimiento exponencial del número de publicaciones relacionadas a trabajos sobre nanocompuestos de matriz polimérica conteniendo nanopartículas de arcilla. En el caso de los nanocompuestos constituidos por una matriz elastomérica reforzada por nanoarcillas, se puede observar un claro aumento en el número de publicaciones a partir del año 2004, lo que evidencia el creciente interés en los mismos hasta nuestros días.

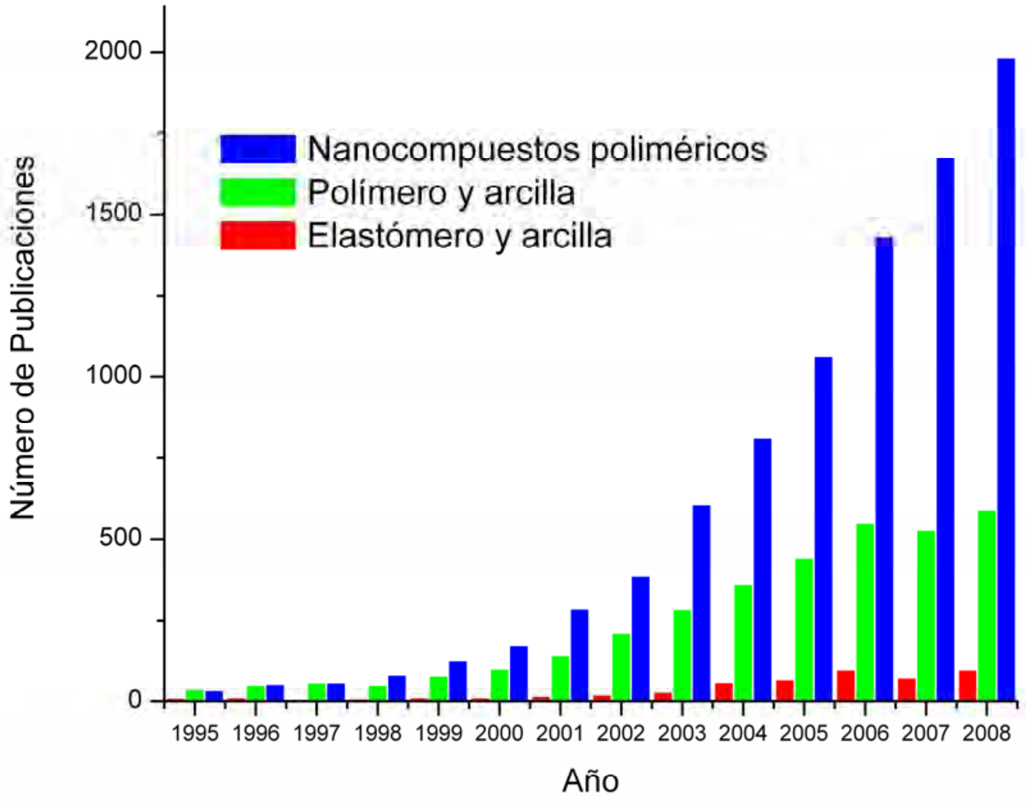

Figura 6. Número de publicaciones por año recogidas en isi web of knowledge

La incorporación de nanopartículas laminares de arcilla (nanoarcilla) con una alta relación de aspecto (entre 10 y 1.000) en matrices poliméricas les proporciona superiores o incluso nuevas propiedades al material, lo que le permite a los nanocompuestos poliméricos competir comercialmente con los materiales tradicionales.

Entre estas mejoras, destacan:

- Eficiente refuerzo con mínima pérdida de ductibilidad y resistencia al impacto
- Mayor estabilidad térmica
- Mayor resistencia a la inflamabilidad
- Mejora de las propiedades barrera a gases y disolventes
- Mayor resistencia a la abrasión
- Menores esfuerzos residuales
- Mejora de las propiedades eléctricas, ópticas y electrónicas
- Una mayor biodegradación de polímeros biodegradables en presencia de las nanopartículas

La incorporación de las nanopartículas también provoca cambios físico–químicos en el material que afectarán a la degradabilidad del polímero tanto térmica (como acabamos de mencionar), mecánica y química (envejecimiento, fotoenvejecimiento, biodegradación), todas ellas, consecuencia directa de la alta dispersión de las nanopartículas laminares de arcilla en la matriz polimérica.[16]

La combinación de esta mejora de propiedades junto con la reducción en peso del material (a diferencia de los materiales compuestos convencionales que requieren altas concentraciones de carga, superiores al 40 % en peso, pequeños porcentajes de arcilla, inferiores al 10 % en peso, son suficientes para alcanzar esta mejora de propiedades) y, el bajo coste de la arcilla (producto natural) ha dado lugar a un aumento en el interés de estos materiales no solo desde un punto de vista académico sino también desde un punto de vista industrial.

La mejora en el refuerzo, estabilidad térmica, conductividad eléctrica y propiedades barrera les convierte en potencial candidatos para aplicaciones en diferentes sectores industriales, como por ejemplo, la automoción o el envase y embalaje. En la Figura 7 se reflejan algunos ejemplos de nanocompuestos poliméricos comercializados a escala industrial. Entre ellos, destacan aquellos relacionados con partes fijas de automóviles, como la cubierta protectora del cinturón de engranaje de distribución en coches (Figura 7a), desarrollada por Toyota y posteriormente, comercializada también por Honywell, donde la nanoarcilla ha sustituido a la fibra de vidrio como partícula reforzante en el Nylon-6 (poliamida),[17] en el escalón de acceso a vehículos monovolumen (Figura 7b) o la carcasa del cuadro eléctrico en vehículos de General Motors donde a un polipropileno y un elastómero termoplástico (TPO) se les incorporó nanoarcillas. Además, General Motors está desarrollando nanocompuestos de polipropileno para aplicaciones en el exterior del automóvil (Figura 7c).

En cuanto al sector del envasado, Kuraray y Nippon Gohsei han comercializado películas basadas en nanocompuestos de poli alcohol vinílico para el envase de alimentos frescos (Figura 7d). Por su parte, Eastman ha desarrollado nanocompuestos de polietilentereftalato, PET para el mercado de botellas para el envase de cerveza, aprovechando la baja difusividad del polímero en presencia de las láminas de nanoarcilla (Figuras 7e y 7f).

Figura 7. Productos que se comercializan hoy en día basados en nanocompuestos poliméricos reforzados con nanoarcillas.

La empresa InMat® desarrolló en el año 2.000 un nanocompuesto basado en caucho butílico y nanoarcilla que dió lugar a la comercialización de pelotas de tenis por parte de la compañía deportiva Wilson® de mayor duración y calidad debido a un novedoso sistema de doble capa ("double core"), que disminuye considerablemente la permeabilidad al oxígeno del interior de la pelota hacia el exterior y aumenta en gran medida la tenacidad de la misma (Figura 7g). Esta misma empresa InMat® ha desarrollado también recubrimientos barrera para guantes de caucho natural (Figura 7h), así como para envases y envoltorios para diferentes productos.

La empresa especializada en biomateriales Foster Corporation, ha desarrollado catéteres quirúrgicos (Figura 7i) basados en Nylon y nanoarcilla que exhiben un aumento considerable en el módulo elástico del nanocompuesto en comparación con aquellos fabricados solo con Nylon.

Finalmente, y sin ser todavía una aplicación real, Michelin® está llevando a cabo un ambicioso programa científico basado en la incorporación de nanoarcillas a las mezclas de caucho comerciales para la fabricación de sus neumáticos.

3.2. Preparación de los nanocompuestos

En la actualidad existen tres principales vías para la obtención de nanocompuestos poliméricos conteniendo nanoarcilla: polimerización in–situ, mezcla en disolución y mezcla directa. Debido a la posibilidad que ofrecen los nanocompuestos basados en una matriz polimérica y nanoarcillas de obtener productos con una aplicación real en el mercado, la polimerización in-situ y la mezcla en disolución pueden ser vistas como alternativas menos atractivas que el proceso de mezcla directa, como consecuencia del coste económico extra que supondría la presencia de disolventes orgánicos así como su posterior eliminación y reutilización.

Sin embargo, en los últimos años, el desarrollo de procesos de polimerización como la intercalación in–situ en ausencia de disolventes, donde uno de los monómeros o reactivos se intercala en el interior de la galería de la nanoarcilla y por consiguiente, la organomodificación de la nanoarcilla in situ tiene lugar sin necesidad de una etapa previa de modificación,[17] e incluso más recientemente el empleo de la nanoarcilla sin modificar como soporte catalítico[18] controlando la selectividad y la conversión del proceso catalítico, hace presagiar un aumento en el empleo e investigación de estas vías de obtención de nanocompuestos. En relación a la intercalación en disolución, cabe destacar los avances que se han producido durante los últimos años en la preparación de nanocompuestos poliméricos con un fuerte carácter hidrofílico en el que se emplea el agua como disolvente.[19]

Vamos a describir brevemente, las características de los tres métodos más utilizados en la síntesis de nanocompuestos poliméricos:

3.2.1. Polimerización in–situ

Fue el primer método empleado para sintetizar nanocompuestos de poliamida 6 con silicatos laminares y en nuestros días, continua siendo el proceso comúnmente usado para la preparación de nanocompuestos de matriz termoestable. En el caso de resinas termoestables, tales como epoxi o poliéster insaturado, se añade un agente de curado o peróxido, respectivamente, para iniciar la polimerización. En el caso de termoplásticos, la polimerización se puede iniciar por la adición de un agente catalítico o bien, por un incremento de la temperatura.

Es necesario controlar el proceso, de manera que el polímero se sitúe entre las láminas intercaladas y así se aumente la separación entre las láminas del silicato. Durante la fase de mezclado, la alta polaridad de la superficie de los silicatos intercalados atrae a las moléculas de monómeros polares, de modo que se difunden entre las láminas del silicato. Cuando se inicia la polimerización, el monómero intercalado comienza a reaccionar con el agente de curado, el cual se difunde entre las galerías del silicato. Esta reacción disminuye la polaridad de las moléculas intercaladas, desplazando el equilibrio temodinámico, de modo que un mayor número de moléculas polares se insertan entre las capas del silicato. A medida que tiene lugar este mecanismo, las moléculas orgánicas van separando las láminas del silicato.

La intercalación del monómero en la galería de la nanoarcilla en polimerizaciones por condensación como es el caso de poliamidas, poliésteres ó poliuretanos, así como algunas siliconas y resinas, no representa en la actualidad un gran handicap como así lo demuestran el gran número de trabajos publicados donde se obtiene con éxito el nanocompuesto.

Caso contrario ocurre cuando la polimerización es de carácter radicálico o están presentes complejos de metales de transición que actúan como catalizadores, en la cual el control de la estereoregularidad (selectividad) y distribución de la masa molecular es crítico, como ocurre con la mayoría de las poliolefinas (polipropileno, polietileno), poliestireno, polimetilmetacrilato, así como algunos elastómeros que presentan una estructura ordenada constituida por bloques. Es en estos polímeros donde reside el verdadero atractivo, pues resulta realmente compleja la incorporación de la nanoarcilla con toda su química superficial en este tipo de polimerizaciones controladas por catalizadores sensibles a cualquier variable físico–química que se introduzca en el medio de reacción.

3.2.2. Mezcla en disolución

En este método, el polímero se disuelve en un disolvente apropiado junto con las partículas de nanoarcilla. Durante el mezclado (agitación vigorosa de la suspensión) tiene lugar la intercalación de las cadenas de polímero en el interior de la galería del silicato. En una última etapa se elimina el disolvente por evaporación bajo vacío, obteniéndose el nanocompuesto. Esta etapa debe realizarse de forma controlada ya que las fuerzas que mantienen unidas las capas de silicatos son muy débiles, por lo que resulta relativamente fácil suspenderlos en un disolvente adecuado. La fuerza motriz que promueve la intercalación del polímero a partir de la disolución, es la entropía ganada por desorción de las moléculas de disolvente, la cual compensa a la disminución de entropía conformacional de las cadenas de polímero intercaladas. De este modo, un gran número de moléculas de disolvente tienen que ser desorbidas del silicato laminar para acomodar las cadenas de polímero incorporadas.

La preparación de nanocompuestos poliméricos mediante mezclado en disolución carece de interés a nivel industrial, como consecuencia de la necesidad de emplear grandes cantidades de disolventes orgánicos. Sin embargo, en los últimos años se ha conseguido una mejora considerable en la obtención de nanocompuestos poliméricos basados en polímeros altamente solubles en agua como se explicó anteriormente, como son el alcohol polivinílico u óxidos de polietileno.[19]

3.2.3. Mezcla Directa

La preparación de nanocompuestos de polímero–nanoarcilla vía mezcla directa se lleva a cabo simplemente mediante el reblandecimiento del polímero (en ausencia de fase líquida), al aplicar una fuerza mecánica durante el procesado y/o por aumento de la temperatura de la mezcla polímero–nanoarcilla. La aplicación de dichos estímulos externos sobre el polímero da lugar a que las cadenas que conforman la estructura macromolecular del mismo comiencen a fluir debido a que se sobrepasa la barrera de transición vítrea y la de fusión en el caso de polímeros semicristalinos. Este aumento en la fluidez del polímero permite la difusión de las cadenas del mismo al interior de las galerías del silicato.

Por supuesto, la intercalación vía mezcla directa de las cadenas de polímero en el interior de la galería de la nanoarcilla no se lleva a cabo sin un balance energético favorable del proceso[20] que influye directamente a su vez en la cinética del mecanismo de intercalación.[21]

3.3 Estructura de los nanocompuestos

Veamos a continuación las distintas estructuras posibles que pueden tener lugar al mezclar un polímero con un silicato laminar, independientemente del método de síntesis empleado. Como hemos comentado, la modificación orgánica vía intercambio iónico de la nanoarcilla facilita la intercalación del polímero en el interior de la galería del silicato. Esta intercalación provoca un aumento en la distancia entre las láminas de silicato, pudiendo permanecer paralelas aún después de la intercalación o una vez superada la barrera energética que las mantiene unidas, produciéndose la delaminación o exfoliación de las mismas.

En la gran mayoría de los casos, los nanocompuestos que presentan las mejores propiedades son aquellos en los que las láminas de nanoarcilla están uniformemente dispersas a lo largo de la matriz polimérica. Dependiendo de la naturaleza de los componentes y del método de preparación utilizado, se obtendrán diferentes estructuras en el nanocompuesto (Figura 8):

a) *Compuestos tradicionales o convencionales* (Figura 8a). El polímero es incapaz de insertarse entre las láminas del silicato dando lugar a un material compuesto de fases separadas con partículas dispersas de tamaño micrométrico como consecuencia de la baja miscibilidad entre el polímero y la arcilla. El silicato laminar se comporta como una carga convencional y las propiedades se asemejan a las de un material compuesto tradicional.

b) *Nanocompuestos Intercalados* (Figura 8b). Consiste en una estructura alterna de polímero y lámina de nanoarcilla, donde el polímero después de incorporarse a la galería del silicato, produce un aumento en la distancia basal del mismo sin llegar a delaminarlo. Este tipo de nanocompuestos presenta mejores propiedades que los tradicionales pues aunque no se alcance la delaminación, la interacción con el polímero es óptima.

En ambos casos, la estructura cristalina del silicato laminar se mantiene, la cual se puede detectar mediante difracción de rayos X (Ver Figura 8 a y b, respectivamente).

c) *Nanocompuestos Exfoliados* (Figura 8c). Se obtienen cuando la nanoarcilla está completamente delaminada y uniformemente dispersa en la matriz polimérica. Como consecuencia de ello, se pierde la estructura multilámina de la nanopartícula de silicato, pues ya sólo existen láminas individuales, así como la continuidad u orden a largo alcance en el apilamiento de las láminas. Este sería la estructura ideal para alcanzar una mejora de propiedades.

En este caso, se pierde la estructura cristalina del silicato que se detecta por la desaparición del pico en el difractograma. (Figura 8c).

En la realidad, la gran mayoría de los nanocompuestos presentan una estructura intermedia entre intercalada y exfoliada. En concreto, las nanopartículas están constituidas por grupos de no más de 10 láminas, aislados unos de otros, sin formar una estructura tipo fractal[22] como las aparecidas en materiales compuestos convencionales con altos contenidos en partículas.

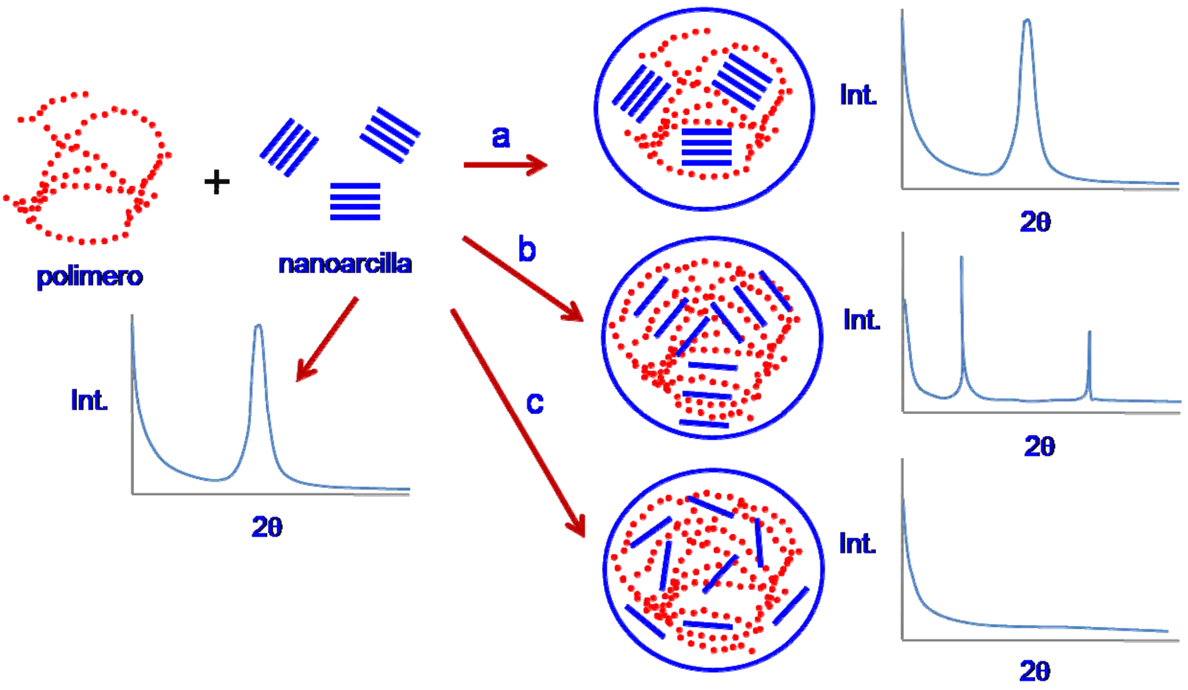

Figura 8. Diferentes estructuras de los nanocompuestos poliméricos.

4. Nanocompuestos de Caucho Natural y nanoarcilla

4.1. Caucho Natural (cis-poliisopreno)

La matriz polimérica empleada en el presente trabajo de investigación ha sido el caucho natural, cuya fase mayoritaria es el cis-poliisopreno (~ 95 %). El aumento en la producción de neumáticos de tipo radial, para los que se requiere una mayor cantidad de caucho natural, ha dado lugar al mayor incremento en el consumo de caucho natural de los últimos veinte años.[23]

El consumo de caucho natural (cis-poliisopreno) supone en la actualidad un 42 % del consumo total de elastómeros en el mundo. Así mismo, el caucho natural es el polímero obtenido de la biomasa de mayor consumo en la actualidad (68 %) con una producción que en el 2007 ascendía a 13 millones de toneladas métricas (Figura 9).

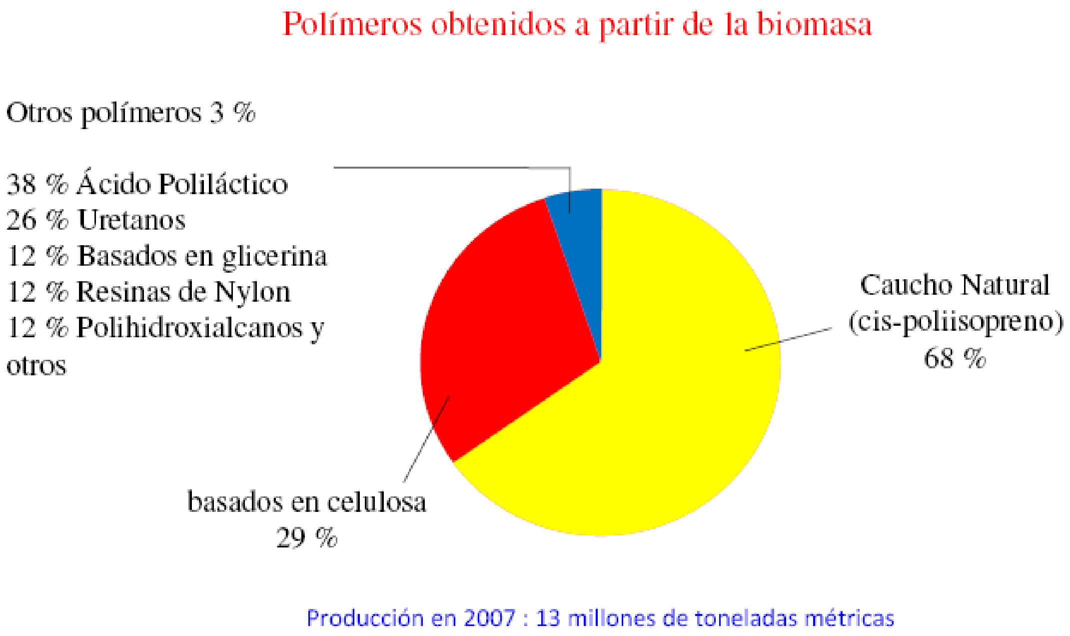

Figura 9. Producción de biopolímeros en 2007.

Además, la existencia en la actualidad de un intenso programa de investigación para el uso potencial de caucho natural epoxidado en neumáticos, prevé un potencial aumento en el consumo del caucho natural en las próximas décadas. Sin embargo, la elección del caucho natural como matriz polimérica objeto de estudio no solo se ha debido a que es uno de los polímeros y elastómeros más importantes desde el punto de vista industrial,[24] sino también y principalmente porque se trata de una matriz ideal desde un punto de vista científico para su estudio, pues presenta una serie de matices[24] que le dotan de una versatilidad no presente en otros polímeros.

Destacan por ejemplo, la posibilidad de preparar los nanocompuestos poliméricos vía mezcla directa en ausencia de disolventes y a temperatura ambiente, debido a la presencia de un valor del modulo elástico alto en fase cruda (solo después de coagularlo desde la emulsión o látex), gracias a la presencia de las impurezas naturales[25] (fosfolípidos y proteínas, principalmente) y al mismo tiempo de una temperatura de transición vítrea por debajo de la temperatura ambiente (~ –60 ºC).

La posibilidad de entrecruzar la matriz químicamente (con azufre o peróxidos) vía vulcanización y obtener un nanocompuesto elástico que permita el estudio de la estructura de la red polimérica. Su capacidad de cristalizar bajo deformación,[26] tanto en fase no entrecruzada químicamente como entrecruzada, debido en última instancia a la presencia de impurezas naturales, así como a la alta estereoregularidad de las moléculas de cis–poliisopreno.[27] La presencia de un momento dieléctrico en la molécula de isopreno[28], con dos componentes uno paralelo a la cadena de polímero y otro perpendicular, que nos permite detectar dos modos de relajación molecular y al mismo tiempo asociarlos con la microestructura del nanocompuesto.

4.2. Estado actual

A pesar de que las matrices elastoméricas no han recibido la misma atención que las matrices termoplásticas o termoestables en la preparación de nanocompuestos poliméricos, si es cierto, que durante los últimos años, se ha producido un importante desarrollo en el campo de los nanocompuestos elastoméricos, siendo el caucho natural una de las matrices más estudiadas. Se han preparado nanocompuestos con estructuras intercaladas o parcialmente exfoliadas mediante la aplicación de diferentes métodos de síntesis, tales como la mezcla directa y posterior proceso de vulcanización, intercalado en disolución o mediante la técnica del látex.

Bala y cols.[29] presentaron el primer estudio en el que se mostraba la intercalación de una montmorillonita orgánicamente modificada con una sal cuaternaria de alquilamonio de 12 átomos de carbono (dodecilamina), en una matriz de caucho natural. Los autores observaron una relativa buena dispersión de las nanopartículas lo que se reflejó en una mejora de las propiedades mecánicas del material. Sin embargo, en este trabajo no se hacía prácticamente hincapié en la microestructura final del nanocompuesto.

En otro estudio coetáneo, Joly y cols.[30] prepararon nanocompuestos de caucho natural con una estructura intercalada, en la que observaron una significativa mejora de las propiedades mecánicas incluso a bajas concentraciones de carga. Los autores demostraron además, que durante la deformación uniaxial de estos nanocompuestos, las cadenas amorfas de poliisopreno exhibían una alta orientación en la dirección de deformación responsable de la mejora de propiedades observadas.

Pero no fue hasta los trabajos realizados por López-Manchado y cols.[31] cuando se obtuvo por primera vez, una estructura exfoliada vía mezcla directa y posterior vulcanización utilizando una montmorillonita químicamente modificada con una sal de amonio de 18 átomos de carbono (octadecilamina).

Se observó que la organoarcilla afectaba las características de vulcanización del caucho natural, disminuyendo considerablemente el tiempo óptimo de vulcanización. Este efecto se atribuyó a la amina primaria empleada como modificador orgánico de la superficie de la nanoarcilla. Además, se observó un incremento del valor del torque, el cual está relacionado con el grado de entrecruzamiento de la red elastomérica, por lo que se podía deducir, que los nanocompuestos con organoarcilla presentaban un mayor número de entrecruzamientos. Este hecho se corroboró mediante medidas de hinchamiento aplicando la teoría de Flory-Rhener[32] y por estudios calorimétricos en condiciones isotérmicas, donde se observó un aumento del calor envuelto durante la reacción de entrecruzamiento en presencia de las nanopartículas.

Además, se demostró que las nanopartículas afectaban a las propiedades térmicas del material, desplazando la temperatura de transición vítrea del caucho natural a temperaturas más elevadas. Este efecto se atribuyó al confinamiento de las cadenas de caucho dentro de las láminas del silicato, que daba lugar a una restricción en la movilidad de las cadenas poliméricas. Por otro lado, se observó una mejora de la estabilidad térmica del material debido a que las nanoláminas de arcilla previenen la difusión de los productos volátiles originados durante el proceso de degradación térmica del material.

En esta misma línea de investigación, el grupo del Instituto de Ciencia y Tecnología de Polímeros del CSIC, demostró que la nanoarcilla podía sustituir al negro de carbono (carga por excelencia en el mundo de los elastómeros) como refuerzo de matrices elastoméricas. La incorporación de tan solo 10 pcc (partes por cien de caucho) de nanoarcilla daba lugar a un material con propiedades mecánicas similares a las de ése con 40 pcc de negro de carbono. Además, el material reforzado con la nanoarcilla mantenía las propiedades elásticas del caucho natural virgen, mientras que éstas se perdían a altos contenidos de negro de carbono.[31]

López-Manchado y cols.[33] sintetizaron nanocompuestos de caucho natural y nanoarcilla mediante intercalación en disolución. En este caso, el caucho natural se disolvió en tolueno y posteriormente, se adicionaba la nanoarcilla. Tras agitación vigorosa durante al menos 24 horas se elimina lentamente el disolvente a temperatura ambiente y a vacío. Este método dio lugar a la obtención de materiales nanocompuestos con una estructura exfoliada en el que las láminas de nanoarcilla se encontraban homogéneamente dispersas en la matriz de caucho natural evidenciando una alta interacción entre las nanopartículas y la matriz polimérica. Esto se reflejó en la obtención de nanocompuestos con excelentes propiedades mecánicas y térmicas incluso superiores a las de los nanocompuestos preparados en estado sólido.

No obstante, este método implica la utilización de disolventes por lo que no es viable a escala industrial.

Otra aproximación para la preparación de nanocompuestos de caucho natural y nanoarcilla es a partir del látex de caucho natural, que consiste en una emulsión de las cadenas de poliisopreno en agua estabilizada con amoniaco.[34] En este proceso, una dispersión acuosa de silicatos de arcilla se mezcla con el látex de caucho natural y se mantiene durante un tiempo determinado bajo agitación hasta alcanzar una mezcla homogénea.

Siguiendo este procedimiento, Karger-Kocsis y cols.[34] prepararon nanocompuestos de caucho natural sin previa modificación química de la arcilla. Aunque se obtienen unas propiedades mecánicas superiores en comparación con la matriz de caucho natural, la dispersión de las nanopartículas en dichos sistemas es menor que la obtenida con nanoarcillas orgánicamente modificadas, por lo que la obtención de propiedades superiores dista todavía de alcanzar. La explicación a este hecho puede deberse a que en los sistemas donde se emplea el látex de caucho natural, las nanopartículas de arcilla se introducen en el látex a partir de una disolución acuosa lo que probablemente limita su dispersión final como consecuencia de la posible floculación (formación de agregados) de la arcilla en el látex debido a la hidrofobicidad de este último.

Es bien conocido, que la organoarcilla se dispera más fácilmente en polímeros polares que en apolares, como el caucho natural. Por ello, otra posible vía de mejorar la dispersión de las nanopartículas en la matriz de caucho natural es mediante la utilización de compatibilizantes. En este sentido, Karger-Kocsis y cols.[35] emplearon caucho natural epoxidado para mejorar la interacción de la nanoarcilla con el caucho natural y de esta manera incrementar su dispersión en este último.

Esta estrategia tuvo su recompensa en la obtención con éxito de una considerable mejora en las propiedades mecánicas finales del nanocompuesto. No obstante, en estos trabajos apenas si se profundizaba en los factores físicos y químicos implicados en esta mejora.

Siguiendo los trabajos iniciados por Karger-Kocsis y cols.[34,35] y con objeto de mejorar la dispersión de las nanopartículas en la matriz polimérica, Arroyo y cols.[36] emplearon un caucho natural epoxidado, ENR como compatibilizante (artículo mostrado en el Anexo de esta memoria). Para ello, se utilizaron dos grados comerciales de ENR (ENR25 y ENR50, con un 25 y un 50 % de unidades epoxídicas, respectivamente). Como nanopartículas, se utilizaron tres montmorillonitas comerciales denominadas Cloisite® (una sódica, C6A y dos orgánicamente modificadas con sales cuaternarias de alquilamonio, C30B y C15A).

Las características estructurales y técnicas de las montmorillonitas empleadas en este trabajo vienen expresadas en el artículo correspondiente (ver Anexo).

Las observaciones llevadas a cabo por difracción de rayos X y microscopia electrónica de transmisión reflejaron la obtención de nanocompuestos con una estructura exfoliada. Debido al carácter polar del caucho natural epoxidado, se observó una mayor interacción con la nanoarcilla mejorando de este modo, su dispersión en la matriz polimérica. Esto se reflejó en una mejora considerable de las propiedades mecánicas, como la resistencia a tracción a distintas deformaciones (50, 100, 300 y 500% de deformación).

No obstante, esta mejora de propiedades no solo se debio al alto grado de dispersión de la nanoarcilla en la matriz, sino también al hecho que las nanopartículas además de actuar como agentes reforzantes se comportaban también como agentes compatibilizantes, disminuyendo la tensión interfacial entre ambas fases poliméricas.

Se observó un sistema con una peculiar morfología, en la que la mayoría de las nanopartículas se encontraban localizadas en la interfase. Las nanopartículas favorecían la dispersión de la fase de ENR, reduciendo sensiblemente el tamaño de las gotitas de ENR dispersas en la matriz de caucho natural.

Comparando las diferentes cargas utilizadas, se observó que este efecto era más marcado en el caso de la C30B, el cual presenta grupos hidroxilo en su estructura, debido a una mayor interacción con el caucho natural epoxidado.

5. Objetivos de la Tesis Doctoral

La mayoría de los estudios llevados a cabo hasta la fecha en el campo de los nanocompuestos poliméricos, se han centrado principalmente en el estudio de la dispersión de la nanoarcilla en la matriz polimérica y su influencia en las propiedades físicas y mecánicas finales del nanocompuesto. Parece evidente, que la obtención de una estructura donde las nanopartículas de arcilla se encuentren homogéneamente dispersas en la matriz polimérica es imprescindible para alcanzar una mejora en las propiedades del material. No obstante, esto no es suficiente para explicar la marcada diferencia de propiedades observadas en estos sistemas en relación a ésos con cargas convencionales, en algunos casos de tamaño nanométrico, como el negro de carbono o la sílice precipitada.

Por ello, el **objetivo** principal del presente trabajo de investigación se centra en el estudio del efecto de la nanoarcilla en la estructura y dinámica molecular de nanocompuestos de caucho natural. Con este estudio, pretendemos entender la relación física y química entre las distintas fases e interfases presentes en el nanocompuesto y su implicación en la mejora de las propiedades finales del mismo.

Además, en el caso particular del caucho natural, sus excelentes propiedades mecánicas incluso sin la presencia de ningún agente reforzante son asociadas a la presencia de proteínas y lípidos que tienen una incidencia directa en su capacidad para cristalizar bajo deformación uniaxial. Es por ese motivo que uno de los objetivos de la presente Tesis Doctoral sea el análisis y estudio del efecto de las nanopartículas de arcilla sobre la cristalización inducida del caucho natural.

Así mismo y como objetivo secundario del presente trabajo de investigación, una vez conseguido un mayor entendimiento de dichas relaciones, se pretende optimizar el proceso de preparación de dichos nanocompuestos, mediante la disminución del número de etapas de procesado. Uno de las grandes inconvenientes que limita el desarrollo de estos nanocompuestos poliméricos a nivel industrial es la necesidad de modificar químicamente los silicatos (reacción de organofilización), lo cual conlleva una etapa previa y el uso de surfactantes.

Por consiguiente, los objetivos científicos marcados en este trabajo de investigación son lo suficientemente atractivos para una amplia comunidad científica y además, sus resultados pueden proporcionar un profundo y valioso conocimiento científico para el desarrollo e integración futura en la sociedad de los nanocompuestos poliméricos, como para justificar la realización de una Tesis Doctoral.

6. Bibliografía

[1] http://www.thomsonreuters.com/products_services/scietific/Web_of_Science

[2] W. D. Callister, *Introducción a la Ciencia e Ingeniería de Materiales*, Reverté, **(2000)**, Vol. 2, Chapter. 17.

[3] R. F. Ziolo, E. P. Giannelis, B. A. Weinstein, M. P. Ohoro, B. N. Ganguly, V. Mehrotra, M. W. Russell, D. R. Huffman, “Matrix-Mediated Synthesis of Nanocrystalline γ-Fe_2O_3: A New Optically Transparent Magnetic Material”, *Science*, **(1992)**, *257*, 219.

[4] H. Gleiter, “Nanostructured Materials”, *Advanced Materials,* **(1992)**, *4*, 474.

[5] B. M. Novak, “Hybrid Nanocomposite Materials-between Inorganic Glasses and Organic Polymers”, *Advanced Materials*, **(1993)**, *5*, 422.

[6] A. Mohammad, G. P. Simon, *Polymer Nanocomposites*, (Eds: Y. W. Mai, Z. Z. Yu), CRC Press, Boca Raton, Cambridge, **(2006)**, Chapter 12, 297.

[7] L. A. Utracki, in *Clay-containing Polymeric Nanocomposites*, (Ed: L. A. Utracki), Rapra Technology Limited, Shawbury, United Kingdom **(2004)**, Vol. 2, 601.

[8] J. B. Donnet, “Nano and microcomposites of polymers elastomers and their reinforcement”, *Composites Science and Technology,* **(2003)**, *63*, 1085.

[9] R. Krishnamoorti, R. A. Vaia, *Polymer Nanocomposites: Synthesis, Characterization, and Modeling*, Oxford University Press, Washington DC (2002)

[10] H. Kunowski, U. Hofmann, “Vergleichende Untersuchung Von Kautschukfullstoffen”, *Angewandte Chemie-International Edition,* **(1955)**, *67*, 289.

[11] R. A. Vaia, J. F. Maguirre, “Polymer-Nanocomposites with Prescribed Morphology: Going Beyond Nanoparticle-Filled Polymers”, *Chemistry of Materials,* **(2007)**, *19,* 2736.

[12] K. I. Winey, R. A. Vaia, “Polymer Nanocomposites”, *MRS Bulletin,* **(2007)**, *32,* 314.

[13] H. van Olphen, *An Introduction to Clay Colloid Chemistry*, 2nd edition, Wiley-Interscience, New York **(1977)**.

[14] L. Leibler, “Nanostructured Plastics: Joys of Self-Assembling”, *Progress in Polymer Science,* **(2005)**, *30,* 898.

[15] U. S. Patent 4739007 (**1988**, priority date: Sep. 30, **1985**), “Composite Material and Process for Manufacturing Same“, Toyota Chuo Kenkyuusho, invs.: A. Okada, A. Fukushima, M. Kawasumi, S. Inagaki, A. Usuki, S. Sugiyama, T. Kurauchi, O. Kamigaito.

[16] J. K. Pandey, K. R. Reddy, A. P. Kumar, R. P. Singh, “An Overview on the Degradability of Polymer Nanocomposites”, *Polymer Degradation and Stability,* **(2005)**, *88*, 234.

[17] A. Okada, A. Usuki, “Twenty Years of Polymer Nanocomposites”, *Macromolecular Materials and Engineering,* **(2006)**, *291*, 1449.

[18] S. Javan Nikkhah, A. Ramazani., H. Baniasadi, F. Tavakolzadeh, “Investigations of Properties of Polyethylene/Clay Nanocomposites Prepared by New in-situ Ziegler Natta Catalyst”, *Materials and Design,* **(2009)**, *30*, 2309.

[19] S. Pavlidoua, C. D. Papaspyrides, “A Review on Polymer-Layered Silicate Nanocomposites”, *Progress in Polymer Science,* **(2008),** *33,* 1119.

[20] R. A. Vaia, E. P. Giannelis, “Lattice Model of Polymer Melt Intercalation in Organically-Modified Layered Silicates”, *Macromolecules,* **(1997)**, *30*, 7990.

R. A. Vaia, E. P. Giannelis, “Polymer Melt Intercalation in Organically-Modified Layered Silicates: Model Predictions and Experiments”, *Macromolecules,* **(1997)**, *30,* 8000.

[21] R. A. Vaia, H. Ishii, E. P. Giannelis, “Synthesis and Properties of Two Dimensional Nanostructures by Direct Intercalation of Polymer Melts in Layered Silicates”, *Chemistry of Materials***, (1993)**, *5,* 1694.

R. A. Vaia, K. D. Jandt, E. J. Kramer, E. P. Giannelis, “Microstructural Evolution of Melt Intercalated Polymer-Organically Modified Layered Silicates Nanocomposites“, *Chemistry of Materials,* **(1996)**, *8,* 2628.

[22] G. Heinrich, M. Klüppel, T. A. Vilgis, “Reinforcement of Elastomers”, *Current Opinion in Solid State & Materials Science,* **(2002)**, *6*, 195;

T. A. Vilgis, “Time Scale in the Reinforcement of Elastomers“, *Polymer***, (2005)**, *46*, 4223.

[23] http://pubs.acs.org/isubscribe/journals/cen/86/i39/html/8639bus1.html

[24] L. Bateman, *The Chemistry and Physics of Rubber like Substances*, MacLaren & Sons, London, **(1963)**.

A. D. Roberts, *Natural Rubber Science and Technology,* Oxford University Press, Oxford, **(1988)**.

J. E. Mark, B. Erman, F. R. Eirich, *Science and Technology of Rubber*; Academic Press, San Diego, **(1994)**.

A. N. Gent, *Engineering with Rubber, How to Design Rubber Components*, Carl Hanser Verlag, Munich, **(2001)**.

J. R. White, S. K. De, *Rubber Technologist´s Handbook,* Rapra Technology, Shawbury, Shrewsbury, Shropshire, **(2001)**.

[25] Y. Tanaka, "Structural Characterization of Natural Polyisoprenes: Solve the Mystery of Natural Rubber Based on Structural Study", *Rubber Chemistry and Technology,* **(2001)**, *74,* 355.

T. Karino, Y. Ikeda, Y. Yasuda, S. Kohjiya, M. Shibayama, "Nonuniformity in Natural Rubber as Revealed by Small-Angle Neutron Scattering, Small-Angle X-Ray Scattering, and Atomic Force Microscopy", *Biomacromolecules"*, **(2007)**, *8,* 693.

[26] P. J. Flory, "Thermodynamics of Crystallization in High Polymers. I Crystallization Induced by Stretching", *Journal of Chemical Physics,* **(1947)**, *15*, 397.

L. Mandelkern, "The Role of Elastomers in the Study of Polymer Crystallization", *Rubber Chemistry and Technology,* **(1993)**, *66*, G61.

J. H. Magill, "Crystallization and Morphology of Rubber", *Rubber Chemistry and Technology***, (1995)**, *68*, 507.

S. Toki, S., T. Fujimaki, M. Okuyama, “Strain-Induced Crystallization of Natural Rubber as Detected Real-Time by Wide-Angle X-Ray Diffraction Technique”, *Polymer*, **(2000)**, *41*, 5423.

[27] Y. Takahashi, T. Kumano, “Crystal Structure of Natural Rubber”, *Macromolecules*, **(2004)**, *37*, 4860.

[28] W. H. Stockmayer, M. E. Baur, “Low-Frequency Electrical Response of Flexible Chain Molecules”, *Journal of the American Chemical Society*, **(1964)**, 86, 3485.

G. Strobl, *The Physics of Polymers*. *Concepts for Understanding their Structures and Behaviour*, Springer-Verlag, Berlin, **(1997)**.

F. Kremer, A. Schönhals, *Broadband Dielectric Spectroscopy*, Springer-Verlag, Berlin, **(2003)**.

[29] P. Bala, B. K. Samantaray, S. K. Srivastava, G. B. Nando, “Effect of Alkylammonium Intercalated Montmorillonite as Filler of Natural Rubber”, *Journal of Materials Science Letters*, **(2001)**, *20*, 563.

[30] S. Joly, G. Garnaud, R. Ollitrault, L. Bokobza, J. E. Mark, “Organically Modified Layered Silicates as Reinforcing Fillers For Natural Rubber”, *Chemistry of Materials*, **(2002),** *14*, 4202.

[31] M. Arroyo, M. A. Lopez-Manchado, B. Herrero, “Organo-Montmorillonite as Substitute of Carbon Black in Natural Rubber Compounds”, *Polymer*, **(2003),** *44*, 2447.

M. A. Lopez-Manchado, M. Arroyo, B. Herrero, J. Biagiotti, "Vulcanization Kinetics of Natural Rubber Organoclay Nanocomposites", *Journal of Applied Polymer Science,* **(2003)**, *89*, 1.

M. A. Lopez-Manchado, B. Herrero, M. Arroyo, "Preparation and Characterization of Organoclay Nanocomposites based on Natural Rubber", *Polymer International,* **(2003)**, *52*, 1070.

[32] P. J. Flory, *Principles of Polymer Chemistry*, Cornell University Press, Ithaca, New York, **(1953)**.

[33] M. A. Lopez-Manchado, B Herrero, M Arroyo, "Organoclay-Natural Rubber Nanocomposites Synthesized by Mechanical and Solutions Mixing Methods", *Polymer International,* **(2004)**, *53*, 1766.

[34] S. Varghese, K. G. Gatos, A. A. Apostolov, J. Karger-Kocsis, "Morphology and Mechanical Properties of Layered Silicate Reinforced Natural and Polyurethane Rubber Blends Produced by Latex Compounding", *Journal of Applied Polymer Science,* **(2004)**, *92*, 543.

S. Varghese, J. Karger-Kocsis, "Natural Rubber-based Nanocomposites by Latex Compounding with Layered Silicates", *Polymer,* **(2003)**, *44*, 4921.

[35] S. Varghese, J. Karger-Kocsis, K. G. Gatos, "Melt Compounded Epoxidized Natural Rubber/Layered Silicate Nanocomposites: Structure-Properties Relationships", *Polymer,* **(2003)**, *44*, 3977.

[36] M. Arroyo, M. A. Lopez-Manchado, J. L. Valentín, J. Carretero, “Morphology/Behaviour Relationship of Nanocomposites based on Natural Rubber/Epoxidized Natural Rubber Blends”, *Composite Science and Technology*, **(2007)**, *67*, 1330

CAPÍTULO II

PARTE EXPERIMENTAL

Con objeto de facilitar el entendimiento y lectura de la presente memoria, a continuación se enumeran y describen las técnicas y métodos empleados durante la Tesis Doctoral, haciendo referencia a cada uno de los artículos científicos que constituyen el capítulo III de resultados.

Artículo titulado: **“Molecular Dynamics of Natural Rubber as Revealed by Dielectric Spectroscopy: The Role of the Natural Cross-linking”**.

En este artículo, la cuidadosa preparación de las muestras fue una etapa esencial para el posterior estudio de la dinámica molecular mediante medidas dieléctricas. Las muestras se prepararon a partir de un látex de caucho natural extraído del árbol *Hevea* en Tailandia. La preparación de las mismas se llevó a cabo en el Departamento de Química de la Universidad de Mahidol (Tailandia) bajo la supervisión del Profesor Jitladda Sakdapipanich. Para la obtención de los distintos compuestos de caucho natural se llevaron a cabo las siguientes etapas:

1.- Primero, se centrifugó el látex durante 30 minutos para separar y eliminar impurezas así como partículas de caucho natural. La fracción sobrenadante se recolectó y secó en una estufa de vacío a 50 ºC. Esta fracción se llamó *CNR*.

2.- Seguidamente, la fracción CNR se disolvió en tolueno en un 1 % en peso. Dicha disolución se almacenó en ausencia de luz durante una semana y sin agitación. A continuación la fracción llamada *GEL* se separó de la fracción SOL mediante centrifugación. La fracción GEL se secó a vacío a 40 ºC. La fracción ligera es la componente SOL que está compuesta de caucho e impurezas naturales solubles en tolueno.

3.- La muestra desproteinizada (*DPNR*) se preparó mediante incubación del látex de caucho natural con una enzima proteolítica (KAO KP–3939) y la presencia de un agente surfactante (Triton® X–100) durante 12 horas a 37 ºC. A continuación se centrifugó durante 30 minutos. La fracción sobrenadante se dispersó empleando un 0.5 % en peso de surfactante por volumen de disolución. Este proceso eliminó el contenido de proteínas en el caucho natural.

4.- Finalmente la muestra sin lípidos y proteínas (*TE–DPNR*) se preparó por reacción del caucho natural con metóxido sódico en tolueno a temperatura ambiente durante 3 horas, seguido de una precipitación de la mezcla de reacción en metanol.

Una vez preparados los materiales se llevó a cabo el análisis de la masa molecular promedio en peso de cada una de las muestras mediante el uso de cromatografía de exclusión por tamaños. Para ello, las muestras se disolvieron en tetrahidrofurano y se filtraron a través de una membrana de teflón con un tamaño de poro de 0.45 micras. El propio tetrahidrofurano se utilizó como eluyente (0.5 ml por minuto a 35 ºC) dentro de las columnas empaquetadas con poliestireno que formaban parte del cromatógrafo de exclusión JASCO–Borwin empleado en la presente Tesis Doctoral.

El análisis de la dinámica molecular de cada uno de los compuestos de caucho natural se llevó a cabo mediante espectroscopia dieléctrica de banda ancha. Los análisis se realizaron en un amplio rango de frecuencia, $10^{-1} < F\ (Hz) < 10^{7}$ Hz, y de temperatura, $-150\ ^{o}C < T < 100\ ^{o}C$, mediante el empleo de un equipo de espectroscopia dieléctrica modelo BDS–40 NOVOCONTROL perteneciente al grupo de Dinámica y Estructura de la Materia

Condensada Blanda *(http://www.iem.cfmac.csic.es/fmacro/softmatpol/)* liderado por el Profesor Tiberio A. Ezquerra del Instituto de Estructura de la Materia (CSIC). Este equipo presenta una interfase dieléctrica tipo ALPHA y un controlador de temperatura tipo QUATRO. La temperatura en los experimentos se controlaba mediante flujo de nitrógeno líquido, posibilitando un error para cada rango de frecuencia de ± 0.1 ºC.

La preparación de las muestras para el análisis por espectroscopia dieléctrica se llevó a cabo mediante la técnica de *"drop casting"* a partir de una didisolución de la muestra de caucho natural en tolueno sobre electrodos cubiertos con oro de 3 centímetros de diámetro. A continuación dichas muestras se secaron a 40 ºC a vacío. Una vez seca la muestra, un electrodo de 2 centímetros de diámetro se situaba sobre la muestra a modo de sándwich para facilitar el contacto con los electrodos.

El análisis matemático de las curvas de relajación de los distintos dipolos dieléctricos se llevó a cabo mediante la aplicación de la ecuación fenomenológica de Havriliak–Negami. A partir de esta ecuación y teniendo en cuenta que el dipolo dieléctrico *(ε')* y la pérdida dieléctrica *(ε")* están relacionadas mediante la relación de Kramer–Kronig, los valores correspondientes con la pérdida dieléctrica se emplearon para describir las distintas relajaciones. Por tanto, la pérdida dieléctrica va a exhibir una dependencia con la frecuencia del siguiente tipo:

$$\varepsilon'' = I_m\left[\varepsilon^*\right] = \left[\varepsilon_\infty + \sum_{x=I,II} \Delta\varepsilon_x \left[1 + \left(i\omega\tau x\right)^{b_x}\right]\right] + \frac{\sigma_{dc}}{\varepsilon_{VAC}\varpi^{s}} \qquad \text{Ecuación 1}$$

donde *I* y *II* corresponden a la relajación segmental y normal, respectivamente, $\omega = 2\pi F$, $\Delta\varepsilon_x$ es la resistencia dieléctrica, τ_x es el tiempo de relajación y *b* y *c* ($0 < b, c < 1$) son los factores de forma que describen la simetría de las curvas de relajación. En esta ecuación, σ_{dc} está relacionado con la conductividad eléctrica, ε_{VAC} es la contante dieléctrica del vacío y *s* es un exponente que depende de la naturaleza del mecanismo de conducción. El tiempo de relajación promedio para la función de distribución de los tiempos de relajación se calculó a partir de la siguiente ecuación (ref. 16 del artículo):

$$\tau = \tau_{HN}\left[\sin\left(\frac{b\pi}{2+2c}\right)\right]^{-\frac{1}{b}}\left[\sin\left(\frac{bc\pi}{2+2c}\right)\right]^{\frac{1}{b}} \qquad \text{Ecuación 2}$$

Artículos titulados: “**Miscibility-Dispersion, Interfacial Strength and Nanoclay Mobility Relationships in Natural Rubber Nanocomposites”**

“Real-Time Crystallization of Organoclay Filled Natural Rubber Under Stretching”

“Effect of Nanoclay on Natural Rubber Microstructure”.

A continuación se detallan las técnicas y métodos que se emplearon en el desarrollo experimental de los tres artículos arriba mencionados.

Primero detallaremos los materiales empleados a lo largo de los tres artículos.

La matriz polimérica que se empleó para la preparación y estudio de los nanocompuestos de nanoarcilla fue un caucho natural (cis–poliisopreno) suministrado por la compañía Malaysian Rubber (Malasia) con una viscosidad Mooney (ML (1+4)) de 60 a 100 ºC. Las arcillas laminares empleadas en el trabajo, las suministró la empresa Southern Clays Products Inc., Gonzales, TX, (EEUU). En concreto, se estudió el efecto tanto de una arcilla laminar tipo montmorillonita conteniendo iones intercambiables de sodio (0.92 mequiv/g) en el interior de la galería, así como sus variantes modificadas con sales cuaternarias de alquilamonio. También, y proveniente de la misma compañía se empleo una arcilla sintética de la familia de las hectoritas, presentando un tamaño de partícula de alrededor de 25 nm y una capacidad de intercambio catiónico de 0.72 mequiv/g.

Así mismo, se emplearon aminas primarias alquílicas de cadena lineal con diferente longitud de cadena provenientes de Sigma Aldrich, para llevar a cabo la modificación mediante intercambio iónico de la montmorillonita sódica.

La reacción de intercambió iónico, se llevó a cabo mediante agitación vigorosa de la arcilla sin modificar (10 % en peso) en agua desionizada durante 12 horas a 70 C. A continuación se adicionó la cantidad estequiométrica deseada de una didisolución correspondiente de amina primaria protonada previo empleo de ácido clorhídrico, también en agua desionizada a 70 ºC. La mezcla de reacción continuó agitándose durante 12 horas a 70 ºC. Una vez transcurrido dicho tiempo, se filtró la suspensión y el sólido obtenido se secó a vacío a 60 ºC. Posteriormente, dicho sólido se tamizó (60 µm), permaneciendo en un desecador hasta su utilización.

La preparación de los nanocompuestos poliméricos se llevó a cabo en el Departamento de Química y Tecnología de Elastómeros del Instituto de Ciencia y Tecnología de Polímeros (CSIC). Los nanocompuestos de caucho natural y nanoarcilla se prepararon mediante mezclado en estado sólido en un mezclador de rodillos de laboratorio, donde de manera secuencial se fueron adicionando cada uno de los componentes que integran el material. De este modo, y tras el *masticado* del caucho se adicionaron los ingredientes de la mezcla, expresada su proporción en partes por cien de caucho (pcc): la nanoarcilla (cantidad variable), el óxido de zinc (5), ácido esteárico (1), un acelerante, el disulfuro de benzotiacilo, MBTS (1), un antioxidante, el fenil-beta-naftilamina, FBN (1) y finalmente el agente de curado, el azufre (2.5). El tiempo utilizado en la preparación de los materiales fue el mismo en todos los casos.

La reacción de vulcanización o curado de los nanocompuestos se llevó a cabo en una prensa hidráulica a 150 ºC tras previa determinación de los tiempos óptimos de vulcanización en un reómetro especial para cauchos (Rubber Process Analyzer, RPA 2000 Alpha Technologies).

Una vez obtenidos los nanocompuestos vulcanizados, éstos se caracterizaron mediante el empleo de diferentes técnicas. Todas las técnicas que se enumeran a continuación forman parte del departamento de Ciencia e Ingeniería de Materiales de la Universidad de Cornell (EEUU), en el cual y bajo la supervisión del Profesor Emmanuel P. Giannelis se llevó a cabo prácticamente toda la caracterización presentada en los tres artículos arriba mencionados.

La dispersión de las nanopartículas de arcilla en la matriz elastomérica se analizó por difracción de rayos X de alto y bajo ángulo, así como por microscopia electrónica de transmisión. Los difractómetros empleados fueron: para los análisis a alto ángulo, se usó un difractómetro tipo Scintag theta–theta con una fuente de cobre de longitud de onda igual a 1.54 Å a una velocidad de barrido de 2 °C/min; por su parte, los análisis a bajo ángulo se llevaron a cabo en modo transmisión en un difractómetro operado a 40 KV y 40 mA de la compañía Bruker (modelo AXS Nanostar) con una longitud de onda de la fuente de cobre igual a 1.54 Å.

Para el análisis de la dispersión y morfología de las nanopartículas por microscopia electrónica de transmisión se prepararon muestras de los nanocompuestos con un espesor de ~ 40 nm con una cuchilla de diamante incorporada a una ultramicrocortadora a la temperatura de -160 °C.

El estudio del grado de curado de los nanocompuestos vulcanizados, se llevó a cabo mediante calorimetría diferencial de barrido en un equipo de la compañía TA Instruments (modelo Q1000). La velocidad de barrido fue de 4 °C/min desde -100 °C hasta 165 °C, siguiendo un ciclo de enfriamiento/calentamiento/enfriamiento en atmósfera de nitrógeno para eliminar la historia térmica del material.

Las propiedades viscoelásticas se examinaron en un analizador mecanodinámico de la compañía TA Instruments (modelo Q800) a una frecuencia de deformación de 1 Hz y una velocidad de calentamiento de 2 °C/min.

El estudio del efecto de la nanoarcilla en la red de caucho natural, se realizó sobre muestras entrecruzadas que fueron hinchadas en tolueno, aplicando la teoría termodinámica de hinchamiento de Flory–Rehner, así como mediante espectroscopia dieléctrica de banda ancha.

En la primera aproximación, el cálculo de los distintos parámetros físicos de la red, se llevó a cabo a través de la ecuación de Flory–Rehner para muestras hinchadas en tolueno durante 48 horas:

$$-\ln(1-\phi_r)-\phi_r-\chi\phi_r^2=\frac{\rho V_0}{M_c}\left[\phi_r^{1/3}-\tfrac{1}{2}\phi_r\right] \qquad \text{Ecuación 3}$$

donde M_c es la masa molecular entre dos entrelazamientos, ϕ_r es la fracción en volumen de polímero en la red hinchada, V_o es el volumen molar del disolvente (106.2 ml/mol para el tolueno), ρ es la densidad del caucho natural (0.92 g/ml), χ es el factor de interacción polímero–disolvente de Flory–Huggins (0.393 para el caucho natural/tolueno).

N_c, el número de monómeros de isopreno entre los entrelazamientos/entrecruzamientos, se calcula a partir de los valores obtenidos por los experimentos de hinchamiento a partir de V_s (mol/ml), donde $N_c = \rho / M_0 V_s$; siendo $M_0 = 68$ g/mol, el peso molecular del monómero de isopreno.

El estudio por espectroscopia dieléctrica se realizó en un equipo idéntico (mismo modelo) al mencionado al principio de este capítulo. Para la realización de los ensayos sobre muestras hinchadas con tolueno, se utilizó una celda especial para líquidos (modelo BDS1308) que evitaba la evaporación del disolvente. Previamente al montaje de la muestra en la celda para líquidos, se llevó a cabo la determinación óptima del espesor inicial de la muestra en seco. El espesor final de la muestra previamente hinchada con tolueno fue de 1 mm. La muestra se mantuvo sellada en la celda para líquidos hasta alcanzar el equilibrio (entre 24 y 48 horas). Las medidas se llevaron a cabo a una frecuencia de 10^3 Hz entre -160 °C y 100 °C.

Los estudios de cristalinidad del caucho natural se llevaron a cabo en el National Synchrotron Light Source (NSLS) perteneciente al Brookhaven National Laboratory (BNL) en EEUU. Dentro del sincrotrón, las medidas se realizaron en la estación experimental X27C bajo la supervisión de los Profesores Sigeyuki Toki y Benjamin S. Hsiao pertenecientes a la Universidad del Estado de Nueva York en Stony Brook (EEUU). Un equipo de tensión–deformación (Instron) acoplado al haz de radiación nos permitió realizar las medidas de difracción de rayos X in-situ durante la deformación del material. La longitud de onda de la radiación de sincrotón fue de 0.1371 nm. El espesor de las muestras fue de 1 mm y la anchura de la zona más estrecha de 0.5 cm. La velocidad de deformación fue de 10 mm/min y el experimento se realizó a temperatura ambiente.

El valor máximo de deformación alcanzado para las muestras fue de un 400 % debido a que mayores deformaciones provocaban el deslizamiento de la muestra de las mordazas.

Las medidas de difracción de rayos X se recogieron como diagramas bidimensionales mediante una cámara CCD MAR. El tiempo de exposición para cada imagen fue de 30 segundos y el intervalo de tiempo entre cada exposición al haz fue de 5 segundos. Para el calibrado del ángulo de difracción se empleó un estándar de Al_2O_3. Cada una de las imágenes se procesó empleando el programa informático “POLAR”, desarrollado en la Universidad del Estado de Nueva York en Stony Brook. Los valores de cristalinidad se calcularon a partir de la integración y posterior corrección de la región de difracción ecuatorial de los diagramas bidimensionales mediante el programa de ajuste “peak fit”. El tamaño lateral del cristal se determinó mediante la ecuación de Scherrer, $L_{hkl} = K\lambda/(\beta \cos \theta)$, donde L_{hkl} es el tamaño de cristal en la dirección perpendicular al plano (*hkl*), λ la longitud de onda y θ el ángulo de Bragg. El valor de la constante K empleado fue de 0.89.

Artículo titulado: **"Natural Rubber/Clay Nanocomposites: Influence of poly(ethylene glycol) on the Silicate Dispersion and Local Chain Order of Rubber Network".**

El caucho natural empleado en el último artículo que conforma la presente Tesis Doctoral es el mismo al de los tres artículos anteriores. En este caso, los nanocompuestos se prepararon empleando la montmorillonita sódica sin modificar (Southern Clay Products Inc., Gonzales, TX) y la adición de polietilenglicol (Flucka) con un peso molecular entre 5.000 y 7.000 g/mol.

En este caso, los nanocompuestos poliméricos se prepararon en un mezclador interno (Haake Rheocord 9000) con un volumen de cámara de 60 cm^3, perteneciente al Instituto de Ciencia y Tecnología de Polímeros de Madrid (CSIC). Los materiales se prepararon a una velocidad de husillos de 100 rpm (revoluciones por minuto), durante 15 minutos y a una temperatura de 80 ºC, permitiéndonos trabajar a temperaturas superiores a la de fusión del polietilenglicol y al mismo tiempo por debajo de la temperatura de degradación del caucho natural.

Se evaluó la aplicación del método de doble cuanto a la determinación cuantitativa de parámetros estructurales y dinámicos de la red elastomérica del nanocompuesto, a partir de medidas de la constante de acoplamiento residual. Para ello, se utilizó un equipo de resonancia magnética nuclear de bajo campo (Bruker minispec mq20) operando a un campo de 0.5 Teslas. Este estudio se realizó en el grupo de resonancia magnética nuclear del estado sólido dirigido por el Profesor Kay Saalwächter en la Universidad de Físicas de Halle (Alemania).

A partir de una secuencia apropiada de pulsos se obtuvo un conjunto de datos formado por una curva creciente que contiene la información relacionada con la estructura de la red (I_{DQ}) y una curva decreciente (I_{ref}) que contiene la información proveniente de la relajación (dinámica) de las cadenas de cis-poliisopreno. Tras un protocolo de normalización obtenemos una curva creciente que viene explicada por la siguiente ecuación:

$$I_{nDQ} = \frac{I_{DQ}}{I_{DQ} + I_{ref} - B \cdot \exp(-2\tau_{DQ} / T_{2B})} \qquad \text{Ecuación 4}$$

donde el denominador contiene la magnetización correspondiente a todos los protones presentes en el nanocompuesto. B es la fracción correspondiente a los componentes de carácter no elástico (defectos) de la red elastomérica y T_{2B} es el tiempo de relajación transversal. Por tanto, la curva normalizada proporciona información de tipo estructural sobre la densidad de entrecruzamiento de la red polimérica, como de la dinámica molecular de las cadenas poliméricas. Esto nos permitió, tras el ajuste de las curvas, calcular los parámetros físicos de la red elastomérica en el nanocompuesto.

Así por ejemplo, considerando que la existencia de un acoplamiento bipolar es causada por el movimiento anisotrópico de las cadenas, debido a la existencia de entrecruzamientos, la relación entre la constante de acoplamiento bipolar y su homóloga en un estado estático se considera el parámetro de orden de la cadena polimérica. A partir de esta relación, y tras la obtención de la constante de acoplamiento residual (D_{res}), obtenida vía RMN de protón mediante la aplicación del método del doble cuanto, era posible determinar la masa molecular (M_c) entre las distintas constricciones topológicas (entrelazamientos físicos y químicos) existentes en las cadenas de cis-poliisopreno. La ecuación que relaciona dicha masa molecular y la constante de acoplamiento es la siguiente:

$$M_C = \frac{3 \times 6300 Hz}{5 D_{res} / 2\pi} \frac{4.7}{4 \times 0.7^2} M_0 = \frac{617 Hz}{D_{res} / 2\pi} kg/mol \qquad \text{Ecuación 5}$$

Una vez obtenida dicha masa molecular, se puede estudiar el efecto de la nanoarcilla en la misma, y por tanto, correlacionar la microestructura del material con sus propiedades macroscópicas.

CAPÍTULO III

RESULTADOS

Molecular Dynamics of Natural Rubber as Revealed by Dielectric Spectroscopy: The Role of Natural Cross–linking

Javier Carretero–González[†,#], Tiberio A. Ezquerra*[,‡], Sureerut Amnuaypornsri[§], Shigeyuki Toki[⊥], Raquel Verdejo[†], A. Sanz[‡], Jitladda Sakdapipanich[§], Benjamin S. Hsiao[⊥], and Miguel A. López–Manchado,[†]

[†]Instituto de Ciencia y Tecnología de Polímeros, CSIC, Madrid 28006, Spain

[‡]Instituto de Estructura de la Materia, CSIC, Madrid 28006, Spain

[§]Department of Chemistry and Center for Excellence for Innovation in Chemistry, Mahidol University, Bangkok 10400, Thailand

[⊥]Department of Chemistry, Stony Brook University, Stony Brook, New York 11794 3400

[#]Present address: The Alan G. MacDiarmid Nanotech Institute, University of Texas at Dallas, Richardson, TX 75083, USA.

[*]Address correspondence to: T. A. Ezquerra (imte155@iem.cfmac.csic.es)

ABSTRACT

In order to understand the molecular dynamics of natural rubber we investigated the dielectric relaxation of its different components. In this work we present the relaxation behavior of: 1) The linear polyisoprene component obtained after deproteinization and transesterification and deproteinization of natural rubber (TE–DPNR). 2) The gel (GEL) fraction, which corresponds to pure natural chain–end cross–linked natural rubber. 3) Deproteinized natural rubber (DPNR) in which the protein cross–links at the ω–end have been removed and 4) Natural rubber (CNR) purified by centrifugation containing the protein, phospholipids and the sol phases. The general relaxation behaviour of the different rubber samples exhibits two processes: the segmental mode (SM), attributed to the segmental motions of the polymer chains and a normal mode (NM) associated to the chain dynamics. While the SM does not depend on the treatment given to samples a significant effect is observed for the NM. The main feature observed in the dynamics of the NM for the different samples is the dependence of the chain mobility with the chain-end cross–linking. TE–DPNR with no chain-end cross–linking exhibits slower chain dynamics than the GEL, with cross–linking in the α– and ω–chain ends. DPNR exhibits the faster dynamics. This effect has been explained considering DPNR as a hybrid star polymer in which the core and the arms have different chemical nature. The faster chain dynamics of DPNR can be understood as caused by a confinement of the phospholipids core. The chain dynamics of natural rubber (CNR) has been explained considering the heterogeneous nature of CNR which consists of a pure network fraction, the gel component, and a linear polyisoprene fraction, the sol. At high temperatures the chain relaxation of CNR is controlled by the dynamics of both cores of the hybrid stars, α–ends and ω–ends, while at lower temperatures the linear polyisoprene sol component tends to slow down the overall CNR chain dynamics.

KEYWORDS: Dielectric Spectroscopy, Natural Rubber, molecular dynamic.

1. Introduction

Natural Rubber (NR) is a complex biomaterial mainly composed of a linear part formed by two trans–1, 4 isoprene units and between 10^3 and $3{\cdot}10^3$ cis–1,4 isoprene units.[1-3] The linear isoprene chain is terminated in one end, the so called α–terminal, by a mono– or di–phosphate group linked with phospholipids.[1-3] The other end, referred to as the α̃–terminal, has been postulated to be a modified dimethylallyl unit linked with a functional group, which can be associated with proteins to form cross–links through intermolecular hydrogen bonding. Additionally, NR contains significant amounts of proteins and lipids as a result of the biosynthesis mechanism of rubber formation.[1] The presence of proteins and phospholipids in NR induces a multi–scaled microstructure characterized by a natural cross–linking among the terminal groups of the linear polyisoprene chains. Proteins are responsible for the cross–linking of the ω–terminal groups by means of hydrogen bonding while interaction among the phospholipids provides cross–linking of the α–terminals. This type of microstructure forms the gel phase of natural rubber, schematized in Fig. 1, which coexists with a sol phase mainly compose by uncross–linked material.[1-3] This unique microstructure endows NR mechanical properties not achieved by its synthetic homologues and makes NR one of the most fascinating and important industrial polymer among engineering plastics. The cross–linking of the ω–terminal groups can be eliminated by deproteinization and that of the α–terminals by transesterification.[1-3] Combining both chemical processes, linear NR can be obtained. The effect of proteins and phospholipids on strain–induced crystallization and their correlation with the tensile strength of NR has been extensively studied by X–ray diffraction and microscopic methods.[3-7] However, to our knowledge there is a lack of systematic work on how the natural impurities, which control the microstructure of NR, affect the molecular dynamics of rubber chains. Most of the studies related the dynamics of polyisoprene (PI) have been accomplished in synthetic samples and only a few in natural ones.[8-11] The dielectric behavior of cis–polyisoprene is characterized by a strong relaxation related to the segmental motions, which appear at temperatures above the glass transition (T_g), and a slower one referred to as the normal mode (NM), which can be related to the end-to–end relaxation of the dipole moment of the cis–PI chain.[12-15]

Consequently the normal mode is related to the chain dynamics and is strongly dependent on the molecular weight. In this work, we use broadband dielectric spectroscopy to study the segmental and chain dynamics of NR with different levels of cross–linking induced by the selective elimination of proteins and phospholipids aiming to characterize dynamically the influence of natural cross–linking natural agents. We have investigated NR with different microstructures including: (a) NR purified by the elimination of non–rubber elements by means of centrifugation (CNR) containing proteins and phospholipids as natural cross–linking agents; (b) the non–soluble gel phase (GEL); (c) deproteinized natural rubber (DPNR) free of proteins and, finally, (d) transesterified and deproteinized and natural rubber (TE–DPNR) consisting essentially of polyisoprene linear chains.

The aim of the present study is to attempt to identify the influence on the relaxation behavior of the different microstructural levels of natural rubber.

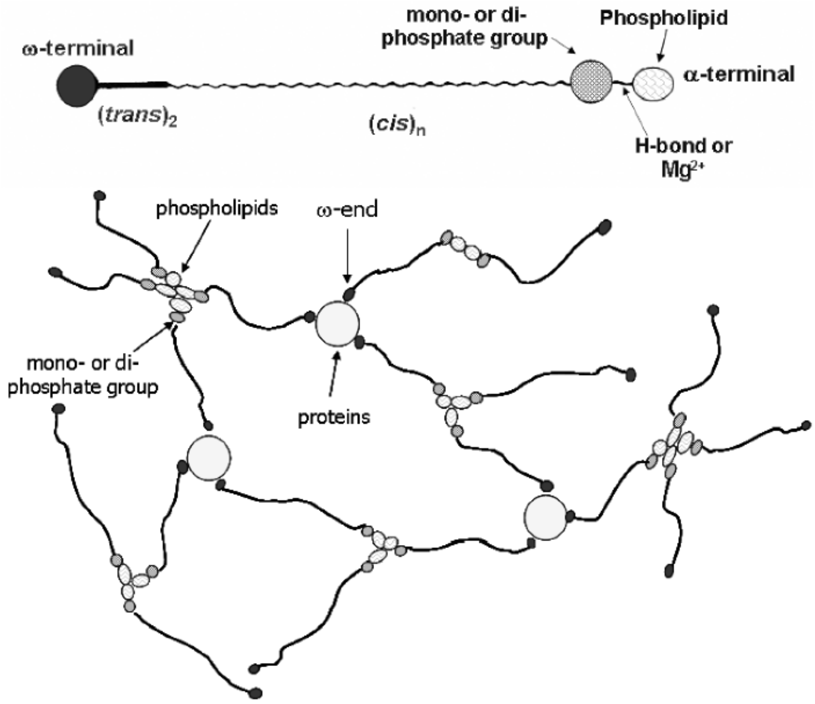

***Figure 1**. Proposed structure of natural rubber (NR) occurring network.[1-3]*

2. Experimental

2.1. Sample Preparation.

Natural rubber (NR) latex used in this study was obtained from regularly tapped *Hevea* tree of RRIM 600 clone, provided by the Thai Rubber Latex Co., Thailand. A systematic procedure to separate the different natural rubber components was accomplished according to the following steps:

1. Firstly, row natural rubber latex was firstly centrifuged at a speed of 13.000 rpm for 30 min in order to remove sludge and water soluble impurities such as amino acids, sugars and metal ions. The cream fraction was collected and dried in an oven at 50 ^oC. This material is referred to as centrifuged natural rubber (CNR).
2. Secondly, CNR was dissolved in toluene solution at a concentration of 1% weight/weight (w/w). This solution was kept in dark without stirring for a week. Then, the gel fraction (GEL) was separated from the sol fraction by centrifugation at the speed of 10.000 rpm for 30 min. The gel fraction was collected and dried in a vacuum oven at 40 ^oC. The lighter part is the sol fraction, about 70 % in weight, which is composed of toluene soluble rubber and soluble natural impurities. The gel fraction contains insoluble rubber and insoluble natural impurities.
3. Thirdly, deproteinized NR (DPNR) was prepared by incubation of NR latex (30% weight/volume (w/v) dry rubber content) with 0.04 % w/v proteolytic enzyme (KAO KP–3939) and 1% w/v Triton® X–100 for 12 h at 37 ^oC followed by centrifugation at 13.000 rpm for 30 min. The cream fraction was re-dispersed with 0.5% w/v Triton® X–100 to make 30% w/v dry rubber content and re–centrifuged at 13.000 rpm for 30 min. This process eliminates the protein content.[1]
4. Fourthly, transesterified and deproteinized NR (TE–DPNR) was prepared by the reaction of DPNR with freshly prepared sodium methoxide in toluene solution at room temperature for 3 h, followed by precipitation using an excess amount of methanol. This process eliminates the phospholipid content.[1]

2.2. Determination of molecular weight and molecular weight distribution

The molecular weight of rubber samples was determined by size exclusion chromatography (JASCO–Borwin) using two columns in series, packed with crosslinked polystyrene gel having the exclusion limits of $2\cdot10^7$ and $4\cdot10^5$. The rubber solution was prepared by dissolving rubber into tetrahydrofurane (THF) (LabScan, HPLC grade) at the concentration of 0.05% (w/v) and filtered through a Millipore prefilter and 0.45 μm membrane filter (Alltech). THF was used as an eluent with a flow rate of 0.5 ml/min at 35 ± 0.01°C, monitoring with refractive index as a detector. Commercially available cis–1,4 polyisoprene (Polymer Standard Service GmbH, Germany) was used as standard sample of the molecular weight. Data of the molecular weight of the different samples are included in Table 1.

Table I. *Insoluble fraction in THF and molecular weight of NR samples.*

Sample	Insoluble fraction in THF (%w/w)	M_w ($\times 10^6$)	M_n ($\times 10^5$)	PDI, M_w/M_n
CNR	30.7	1.87	2.87	6.53
GEL	-	-	-	-
DPNR	4.4	2.16	3.29	6.56
TE–DPNR	~ 0	1.46	2.84	5.13

2.3. Dielectric spectroscopy and data analysis

Dielectric loss measurements, ε” (where ε”=I_m (ε*), being ε* the complex dielectric permittivity) were performed over a broad frequency range ($10^{-1} < F(Hz) < 10^7$ Hz) in a temperature range of -150 $^oC < T < 100$ ^{o}C using a BDS–40 Novocontrol system with an integrated dielectric interface ALPHA and a QUATRO temperature controller. The temperature in these experiments was controlled by a nitrogen jet with a temperature error, during every single sweep in frequency, of ± 0.1 ^{o}C. Samples for dielectric measurements were dissolved in toluene solution at the concentration of 4% w/w. The solution was cast using a dropper on a golden disc of 3 cm in diameter (Novocontrol), which was used as lower electrode. The electrode was rotated and inclined manually in order to cover homogeneously the electrode surface. Subsequently, the samples over the electrode were dried at 40 ^{o}C in a vacuum atmosphere. A smaller golden electrode of 2 cm (Novocontrol) was placed on top of the sample. Both shape and temperature evolution of the observed normal and segmental relaxations were analyzed, as described elsewhere,[14,16] by the phenomenological Havriliak–Negami (HN) description including a conductivity term. Since *ε’ (ω)* and *ε” (ω)* are related to each other via a Kramers–Kronig relation[16], the functional form of the HN description was used to evaluate ε” (ω) values over the entire relaxation range. According to this approach, the dielectric loss, *ε”*, exhibits a frequency dependence of the type:

$$\varepsilon'' = I_m\left[\varepsilon^*\right] = \left[\varepsilon_\infty + \sum_{x=I,II}\Delta\varepsilon_x\left[1+(i\omega\tau x)^{b_x}\right]\right] + \frac{\sigma_{dc}}{\varepsilon_{VAC}\varpi^s} \quad (1)$$

where *I* and *II* indicate the segmental and normal mode relaxations, ω = 2π*F*, $\Delta\varepsilon_X$ is the dielectric strength, τ_x is the central relaxation time of the relaxation time distribution function, and *b* and *c* (0 < b, c < 1) are the shape parameters which describe the symmetric and asymmetric broadening of the relaxation time distribution function, respectively. Here, σ_{dc} is related to the direct current electrical conductivity, ε_{VAC} is the vacuum dielectric constant, and *s* depends on the nature of the conduction mechanism. The average relaxation time of the relaxation time distribution function is calculated through[16]:

$$\tau = \tau_{HN}\left[\sin\left(\frac{b\pi}{2+2c}\right)\right]^{-\frac{1}{b}}\left[\sin\left(\frac{bc\pi}{2-2c}\right)\right]^{\frac{1}{b}} \quad (2)$$

3. Results

3.1. Dielectric Relaxation behaviour.

While CNR can be considered to be a purified natural rubber, cross-linked at the chain ends by natural agents (see Fig. 1), TE–DPNR corresponds to the non cross–linked linear natural polyisoprene. Figure 2 shows the temperature and frequency dependence of the dielectric loss ε” for CNR (Fig. 2a) and for TE–DPNR (Fig. 2b). As expected, the measurements exhibit a low–temperature process just above the glass transition temperature (T_g~ 213 K) which can be assigned to the segmental–mode process (SM). Similarly as for synthetic polyisoprene, it originates from local motions of the perpendicular dipole moment.[14]. A broader relaxation is detectable at higher temperatures in both samples which, again similarly to the polyisoprene case, can be assigned to the normal–mode process (NM).

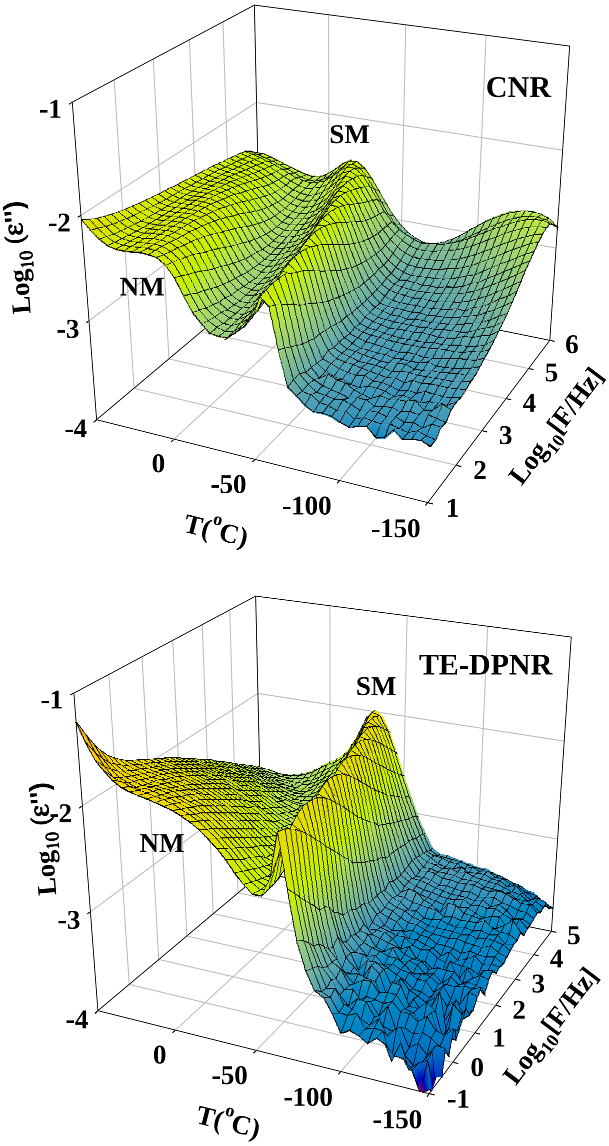

Figure 2. *3D plot of the frequency and temperature dependence of the dielectric loss, ε”, for CNR (top) and TE–DPNR (bottom) samples*

The NM process corresponds to motions of the entire chain caused by dipole components parallel to the backbone.[8,9,14].

This general relaxation behavior is qualitatively similar for all the samples investigated. For the sake of comparison Fig. 3 shows the dependence of *ε”* at 7 Hz as a function of temperature.

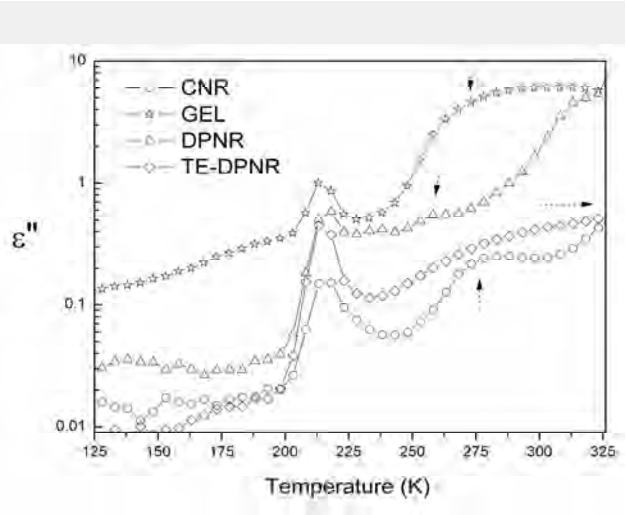

Figure 3*. Temperature dependence of the dielectric loss, ε”, at 7 Hz for: (o) centrifuged natural rubber (CNR), (ψ) Gel fraction of centrifuged natural rubber (GEL), (Δ) Deproteinized natural rubber (DPNR) and (◊) transesterified deproteinized natural rubber (TE–DPNR). The arrows are an indication of the location to the NM process*

In this Figure, the segmental–mode appears as a relatively sharp maximum while the normal–mode appears as a broader one at higher temperatures. It is evident that the SM does not vary from sample to sample. On the contrary, the NM exhibits significant variation with sample treatment. According to these data the NM for TE–DPNR seems to be significantly slower than that of CNR. The NM for the DPNR sample is not well resolved in the isochronal plot shown in Figure 3, therefore isothermal representations are necessary.

Figures 4 and 5 show selected isothermal plots of ε”as a function of frequency corresponding to the SM (Fig.4) and NM (Fig.5) for the different samples. As far as the SM is concerned the data of Fig. 4 clearly show that this process is not significantly affected by the sample treatment.

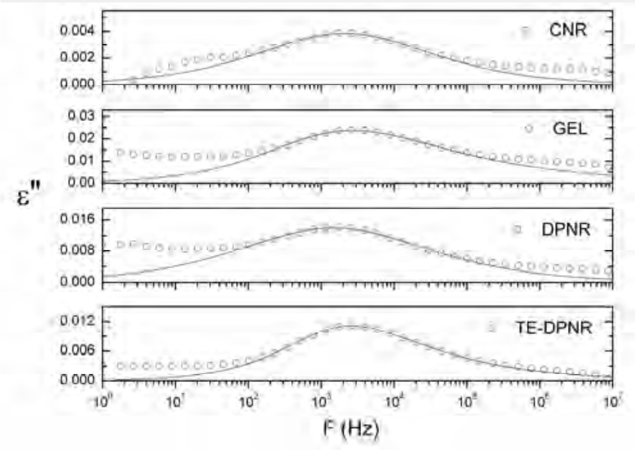

Figure 4. Dielectric loss, ε”, for CNR, GEL, DPNR and TE–DPNR samples as a function of frequency, F (Hz), at 223 K for the segmental mode (SM). The continuous lines represent best fit to the HN relaxation function (eq. 1).

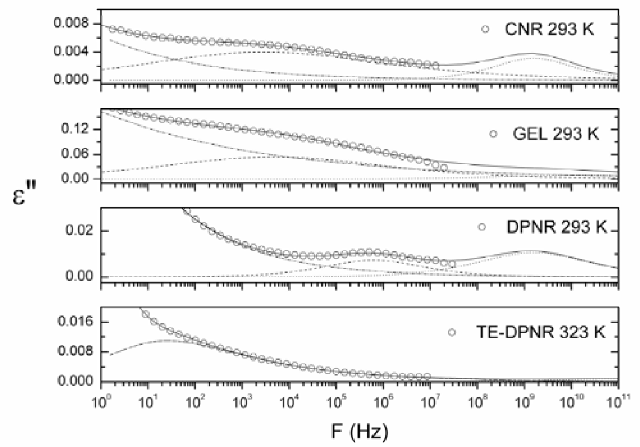

Figure 5. Dielectric loss, ε”, for CNR, GEL, DPNR and TE–DPNR samples as a function of frequency, F (Hz), at selected temperatures where the NM is well resolved. The continuous lines represent best fit to the HN relaxation function (eq. 1).

Fig. 5 shows isothermal plots in the temperature region where the NM appears for the different samples. Contrary to what it was observed for the SM here a significant variation with sample treatment is observed for the NM. NM of the GEL sample becomes faster than that of CNR. Moreover, the NM for the DPNR is even faster than that of the GEL sample. On the contrary the NM of the TE–DPNR sample is the slowest one of all the investigated samples.

3.2 Relaxation times for the segmental and normal modes.

For all the samples, it was possible to analyze the two relaxation processes individually. For this reason the loss curves were resolved into the contributions of the normal and segmental modes. Since the loss curves can be in general broad and asymmetric, the HN function (eq. 1) was used to fit the data.[14,16,17] The continuous lines of Fig. 4 show that the HN function gives a reasonable description of the experimental data for the segmental mode. In these cases only one relaxation term was considered to contribute to eq.1.

The corresponding fitting parameters are collected in Table II.

Table II. Parameters of the HN equation for the segmental mode.

SAMPLE	T(K)	$\Delta\varepsilon_{HN}$	b	c	τ_{HN} (s)
CNR	223	0.019	0.50	1	$7.5\ 10^{-4}$
GEL	223	0.1271	0.58	0.51	0.0017
DPNR	223	0.073	0.46	0.98	0.0011
TE–DPNR	223	0.046	0.55	0.7	0.0013

The analysis of the NM data is more complex because of the segmental mode contribution at high frequencies and of the conductivity term affecting the low frequency tail of the relaxation curves.

For this reason eq. 1 was used with two relaxations, one for SM and other for NM, with an additional conductivity term to fit the data in the temperature range where the NM is analyzed. The SM mode relaxation at high temperatures can be simulated by extrapolation of the HN parameters fitted al lower temperatures.[17,18] . The continuous lines of Figure 5 show the fit of the HN function to the experimental date indicating the contribution of the different terms of eq.1. The corresponding fitting parameters are collected in Table III. The fitting procedure was performed in the whole temperature range for all the samples. By this procedure, the temperature dependence of the average relaxation time can be calculated according to eq. 2. Fig. 6 shows the average relaxation time (eq. 2) as a function of reciprocal temperature for both SM and NM processes and for all the investigated samples. In all cases the temperature dependence of the relaxation time departures from the simple Arrhenius behavior exhibiting a curvature at high temperatures.

Table III. Parameters of the NH eq. for the normal mode

SAMPLE	T(K)	$\Delta\varepsilon_{HN}$	b	c	τ_{HN} (s)
CNR	293	0.04	0.26	0.8	$1.3\text{x}10^{-3}$
GEL	293	0.50	0.26	1	$3.3\text{x}10^{-4}$
DPNR	293	0.03	0.56	1	$2.5\text{x}10^{-6}$
TE–DPNR	323	0.07	0.50	0.46	0.28

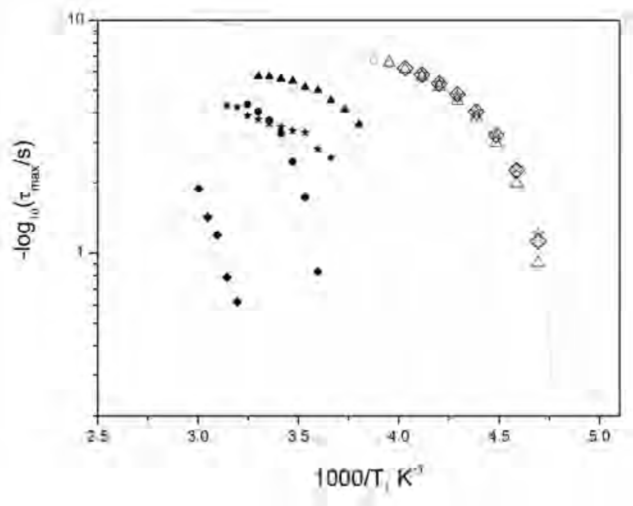

Figure 6. *Activation plot for the segmental (hollow symbols) and the normal (solid symbols) modes for: (○, ●) CNR, (☆,★) GEL, (Δ, ▲) DPNR and (◊, ♦) TE–DPNR samples. The dotted lines represent the fits of the Vogel–Fulcher–Tamann equation to the experimental data.*

This characteristic temperature dependence, which characterizes in general both segmental and normal mode processes,[8,9,14] can be described by means of the Vogel–Fulcher–Tamann (VFT) equation:

$$\tau_{\max} = \tau_0 \exp[A/(T - T_0)] \qquad (3)$$

where τ_0, T_0 and A are constants with $T_0 < T_g$. As far as the segmental mode is concerned, the parameter A can be redefined as $A = D \cdot T_0$ where D is referred to as the fragility strength parameter which can be related with the characteristics of the segmental motions above of glass transition temperature[20]. The dashed lines in Figure 6 indicate the fittings of the VFT equation to the experimental data. The fitting parameters are reported in table IV.

Table IV. VFT parameters for the segmental and normal mode processes

	segmental mode		normal mode	
Sample	D	T_0(K)	A(K)	T_0 (K)
CNR	4.52	157.3	218.4	247.7
GEL	4.17	160.6	191.9	216.5
DPNR	4.22	161.1	161.1	226.3
TE–DPNR	4.27	161.0	2609.3	119.1

5. Discussion

The results presented so far seem to indicate that dielectric spectroscopy is a useful technique to deal with the molecular dynamics of natural rubber specimens with different structural hierarchy. The starting step for the discussion will be to consider that one is dealing with a cross–linked polymer network in which the cross–links affect exclusively the chain ends. While the deproteinization treatment tends to eliminate the cross–linking in the ω–terminal chain ends, the transesterification process tends to eliminate cross–links in the α–terminal ones. Consequently, the combination of deproteinization and transesterification treatments render to natural linear polyisoprene.[1-3] Analogously to synthetic polyisoprene,[8,9,14] the general relaxation behaviour of the different rubber samples exhibit two processes (Fig.2).

5.1. Segmental Mode of Natural Rubber

Starting from lower temperatures, the segmental mode (SM) appears above the glass transition temperature and can be attributed to the segmental motions of the polymer chains[8,9,14]. For synthetic polyisoprene the SM does not depend on the molecular weight[14]. In our case, according to the relaxation time date shown in Figure 6, the SM does not depend on the treatment given to samples. Dielectric experiments performed in polymer networks have shown that the α-relaxation, attributed to the segmental mode, depends on network density and shifts toward higher temperatures as the cross–link density increases[21,22]. However the nature of the cross–linking in natural rubber is very peculiar as it concerns exclusively the chain ends (Fig.1). Therefore, in this case, modification of the cross–linking of natural rubber by the different treatments does not affect significantly the segmental motions since the molecular weight among cross–links is very high, of the order of 10^6 g/mol. The value of the fragility strength parameter, D, does not vary with sample treatment. A D value around 4 indicates that natural rubber is a dynamically fragile system as corresponds in general to polymer materials[23].

5.2. Normal Mode of Natural Rubber

Besides the segmental mode all the investigated samples exhibit at higher temperatures a broad process (Figures 2 and 3) which, in analogy to what it has been reported for synthetic polyisoprene, can be attributed to a normal mode[8,9,14]. The normal mode (NM) appears as a consequence of the chemical structure of the cis–polyisoprene chain which has components of the dipole moment parallel to the chain contour[14]. Therefore, cis–polyisoprene can exhibit a dielectric NM process caused by the parallel dipole moment in addition to the common SM process mainly originated by molecular motions affecting the perpendicular dipole moment. The main effect observed in the dynamics of the NM for the different samples is the dependence of the chain mobility with the chain end cross-linking (Fig. 6). Basically, TE–DPNR with no chain-end cross–linking exhibits slower chain dynamics than the GEL, with cross–linking in the α– and ω–chain ends while DPNR exhibits the faster dynamics. In order to visualize this effect, Figure 7 shows relaxation times extracted from Figure 6 at 321 K as a function of the amount of chain–end cross–linking.

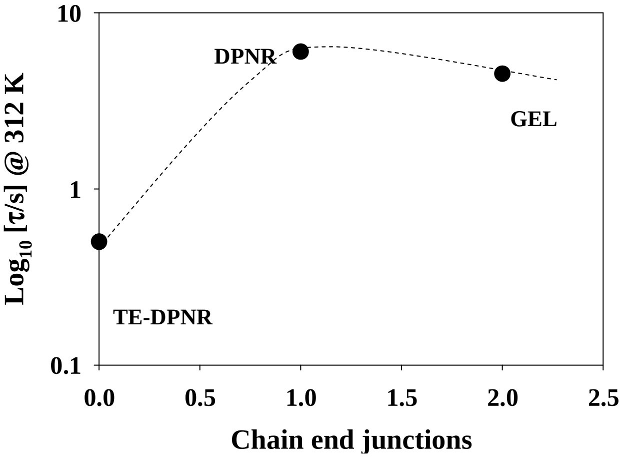

Figure 7. *Relaxation times at 312 K for samples with different treatments: Transesterified and Deproteinized Natural Rubber (TE–DPNR), Deproteinized Natural Rubber (DPNR) and GEL.*

5.2.1. Transesterified and Deproteinized Natural Rubber: Natural cis-polyisoprene

The slower NM is exhibited by the TE–DPNR sample (Figures 6 and 7) which, as mentioned above, can be essentially considered as natural liner polyisoprene[1-3]. The relaxation time of 0.28 s at 323 K for the TE–DPNR sample (Tab. III) is about three orders of magnitude faster than the relaxation time reported for synthetic polyisoprene[14]. Somehow this is expected since the reported results for synthetic polyisoprene refer to samples with very narrow polydispersity[14] ($M_w/M_n \approx 1$). In our case natural rubber samples exhibits much broader polydispersities close to 6 (Tab. I).

5.2.2. Deproteinized Natural Rubber: Natural Hybrid Star Polymer.

The deproteinized natural rubber (DPNR) sample is cross-linked by phospholipids at α–terminal chain ends. In a first approach, we can visualize DPNR as a star polymer[24] in which the centre of the star has a different nature as that of the star arms. Consequently we can consider DPNR as a natural hybrid star polymer as depicted in Figure 8a.

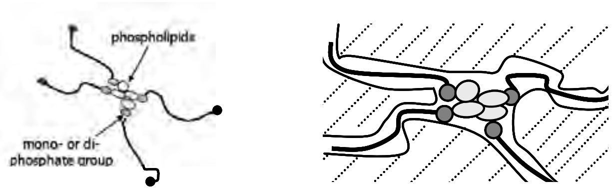

Figure 8. *(a) Proposed structure of DPNR and (b) Idealized picture of the hybrid core topologically confined by the entanglements constrains. Scale is arbitrary.*

The dynamics of star polymers in general and of polyisoprene stars in particular have been investigated by dielectric spectroscopy.[24-26] It has been proposed that star polymers should be around four times slower than the free linear chains of similar length as those forming the star arms.[27] This proposal was corroborated by dielectric relaxation measurements for synthetic cis–polyisoprene stars.[25] In these studies the NM of the polymer stars is shown to be significantly slower than that of the corresponding arms[25]. This effect seems, at first glance, to contradict our own observation since the NM of DPNR is much faster than that of TE–DPNR (Fig. 6). Faster NM processes in cis–polyisoprene stars than those of the linear arms have been observed under confinement[28]. Dielectric spectroscopy was used to study the NM of polyisoprene in microphase separated star diblock copolymers where polyisoprene forms a core and polystyrene forms a corona[28].

According to Floudas et al.[28] the NM process is strongly influenced by the spatial confinement induced by the polystyrene phase. This phase confines the polyisoprene star centre within an effective radius R such that $<(\Delta R)>^{2\ 1/2} \approx b(M_e)^{1/2}$, where b is the statistical segment length (≈ 0.68 nm for PI) and M_e is the molecular weight among entanglements (≈ 5000 for PI). The main effect is an enhancement of the polyisoprene chain mobility which was explained considering that the dielectric NM is mainly determined by the motion of the central star part of size[28]. Calculations based on the Rouse model[28] indicated that the NM process in the star can become faster than that of the arm if $M > 1.5\ M_e$.

Inspired by this ideas we can attempt to explain the enhanced NM dynamics of DPNR as compared with that of TE–DPNR. In our case, DPNR can be considered as a hybrid star polymer because the core of the star is chemically different from the arms.

This chemical heterogeneity is expected to make the molecular mobility of the phospholipid core to be very different from that of the polyisoprene arms.

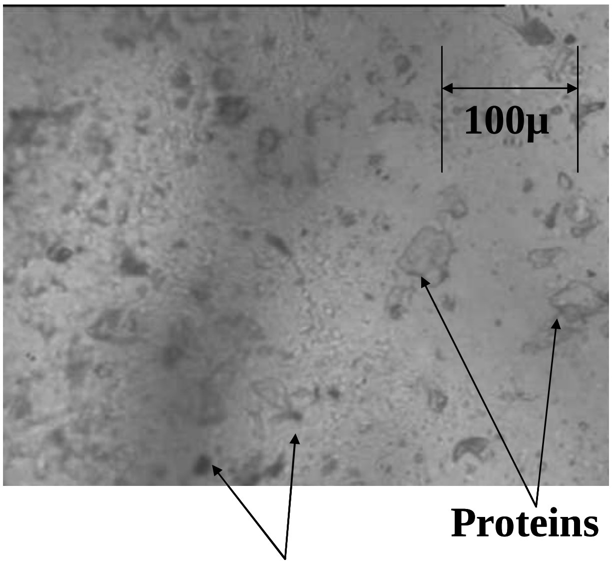

Figure 9. *Optical micrograph of natural rubber indicating the presence of proteins aggregates and phospholipids micelles*

The optical micrography of natural rubber samples shown in Figure 9 indicates the presence of phospholipids micelles with sizes as large as ≈ 10 µm. This suggests that the phospholipids core should be very effective by fixing the α-terminal chain ends

We propose that the phospholipids core has, at least due to its size, a restricted mobility as compared with that of the arms and therefore becomes effectively confined. Additionally, there exists a topological confinement induced by the entanglements[28] which can be idealized by the picture shown in Figure 8b. This effect is expected to be very significant considering that the molecular weight of the polyisoprene arms is about three orders of magnitude higher than M_e.

Due to entanglement constraints the star center is not free to explore the whole space since moving through one tube would provoke modification of the tube diameter to accommodate the hybrid core. To overcome this unfavorable situation the star center tends to be effectively localized. According to Floudas et al.[28] the ratio between the relaxation time of the star polymer, τ_{star}, and that of the arm, τ_{linear}, for an homogeneous, i.e. not hybrid, star should follow that:

$$\frac{\tau_{star}}{\tau_{linear}} \alpha \left(\frac{M_e}{M}\right)^3 \tag{4}$$

where M is the molecular weight of the arm and M_e is the molecular weight among entanglements and the proportionality constant is the number of arms. This relation predicts that the chain mode relaxation will become faster when $M > 1.5M_e$. Considering the molecular weight of the linear polyisoprene (TE–DPNR) of $\approx 10^6$ and that of M_e for polyisoprene of $\approx 5\cdot 10^3$, then it follows that a significantly faster dynamics could be expected for DPNR as compared with that of TE–DPNR as experimentally observed.

5.2.3. Gel component of natural rubber: Natural Chain–end Cross–linked Polymer Network.

The Gel component of natural rubber consists essentially of a natural network with cross–links at the chain–ends (Fig. 1). The chain dynamics of the GEL samples is slightly slower than that of the DPNR one but still significantly faster than that of the TE–DPNR sample.

Considering the arguments provided in the previous sections, this effect can be understood considering that for the GEL the mobility of polyisoprene arms of the DPNR hybrid star become restricted by the fixation of their free ω–ends due to the protein component (Fig.1). The aggregates of proteins can also be of the order of tens of μm and therefore also very effective in fixing the ω–terminals chain–ends. However, in spite of this, the chain dynamics of the Gel sample remains much higher than that of the TE–DPNR linear polyisoprene sample. This indicates that the chain dynamics of the GEL is dictated by the relaxation at the cores of two different hybrid stars associated to the different chain ends of natural polyisoprene.

5.2.4. Chain Dynamics of Natural Rubber

The chain dynamics of natural rubber (CNR) presents a NM which is located close to that of the GEL and in between those of TE–DPNR and DPNR (Fig. 6). This can be understood considering the heterogeneous nature of CNR which consist of a pure network fraction, the GEL component and the Sol (≈ 70 % in weight). Accordingly, it is expected that chain dynamics reflects features of both components. At high temperatures the NM relaxation times practically overlap those of the GEL component indicating that the fast dynamics of both cores of the hybrid stars, α–ends and ω–ends, controls chain relaxation behavior. At lower temperatures the NM of CNR tends to become slower than that of the Gel component probably due to the sol component which contributes to the overall CNR chain dynamics with slower modes.

6. Concluding Remarks

In order to understand the molecular dynamics of natural rubber it is necessary to take into consideration the complexity of this natural product. This can be accomplished by investigating the dielectric relaxation of the different components which form natural rubber. In this work we have investigated by dielectric spectroscopy the relaxation behavior of: 1) The linear polyisoprene component, obtained after deproteinization and transesterification of natural rubber (TE–DPNR). 2) The gel fraction, which correspond to pure natural chain-end cross–linked natural rubber. 3) A deproteinized natural rubber (DPNR) sample in which the protein cross–links at the ω–end have been removed and 4) Natural rubber sample (CNR) purified by centrifugation which contains the protein, phospholipids and the sol phases.

The general relaxation behaviour of the different rubber samples exhibit two processes: the segmental mode (SM), attributed to the segmental motions of the polymer chains and a normal mode (NM) associated to the chain dynamics. While the SM does not depend on the treatment given to samples a significant effect is observed for the NM. The main effect observed in the dynamics of the NM for the different samples is the dependence of the chain mobility with the chain end cross–linking. TE–DPNR with no chain-end cross–linking exhibits slower chain dynamics than the GEL, with cross–linking in the α– and ω–chain-ends. DPNR exhibits the faster dynamics. This effect has been explained considering DPNR as a hybrid star polymer in which the core and the arms have different chemical nature. The faster chain dynamics of DPNR can be understood as caused by a confinement of the phospholipids core. The chain dynamics of the Gel sample slows down as a consequence of the restricted mobility of polyisoprene arms of the DPNR hybrid star induced by the fixation of their free ends due to the protein component. However, the chain dynamics of the GEL remains significantly faster than that of the TE–DPNR linear polyisoprene sample. Finally chain dynamics of natural rubber (CNR) is located close to that of the GEL and in between those of TE–DPNR and DPNR.

This has been explained considering the heterogeneous nature of CNR which consist of a pure network fraction, the GEL component, and the Sol. At high temperatures the chain relaxation of CNR is caused by the dynamics of both cores of the hybrid stars, α–ends and ω–ends, while at lower temperatures the sol component tends to slow down the overall CNR chain dynamics.

ACKNOWLEDGMENT

The authors gratefully acknowledge the financial support of the Spanish Ministry of Science and Innovation (MICINN) through its project MAT 2004-00825. J. Carretero-González thanks the MICINN for the concession of a FPI grant, T. A. E. thanks the financial support from MAT2005-01768 (MICINN) and R. Verdejo also acknowledges a JAE Doc contract from the CSIC.

REFERENCES

1. Tanaka, Y.; Rubber Chem. And Tech. **2001,** 74, 355.
2. Amnuaypornsri, S.; Sakdapipanich, J.; Toki, S.; Hsiao, B.S.; Iichikawa, N.: Tanaka. Y.; Rubber Chem. And Tech. **2009,** 81, 753.
3. Amnuaypornsri, S.; Sakdapipanich, J.; Tanaka. Y.; J. of Appl. Polym. Sci. **2009,** 111, 2127.
4. Toki, S.; Sics, I; Hsiao, B.S.; Murakami, S.; Tosaka, M.; Poompravub, S.; Kohjiya, S.; Ikeda, Y. J. of Polymer Science: Part B: Polym. Phys. **2004**, 42, 956.
5. Rault, J.; Marchal, J.; Judeinstein, P.; Albouy, P. A. Macromolecules **2006,** 39, 8356.
6. Toki, S.; Burger, C.; Hsiao, B.S.; Amnunaypornsri, S.; Saksapipanich, J.; Tanaka, Y. J. of Polym. Sci.: Part B: Polym. Phys. **2008,** 46, 2456.
7. Carretero-Gonzalez, J.; Verdejo, R.; Toki, S.; Hsiao, B.S.; Giannelis, E. P.; López-Manchado, M.A., Macromolecules **2008,** 41, 2295.
8. Adachi, K.; Kotaka, T. Macromolecules **1984,**17, 120.
9. Adachi, K.; Kotaka, T. Macromolecules **1985,**18, 466.
10. Cerveny, S.; Bergman, R.; Schwartz, G.A.; Jacobsson, P. Macromolecules **2002,** 35, 4337.
11. Janik, P.; Paluch, M.; Ziolo, J.; Sulkowski, W.; Nikiel, L. Phys. Rev. E **2001,** 64, 042502.

12. Poh, B. T.; Adachi, K.; Kotaka T.; Adachi, K. Macromolecules **1987**, 20, 2574.

13. Kotaka, T. Prog. Polym. Sci. **1993** 18, 585.

14. Boese, D.; Kremer, F. Macromolecules **1990**, 23, 829,

15. Mijovic, J.; Lee, H.; Kenny, J.; Mays, J. Macromolecules **2006**, 39, 2172.

16. Schönhals, A.; Kremer, F. ‘Broad Band Dielectric Spectroscopy’ (Springer-Verlag: Berlin, **2002**).

17. Havriliak, S.; Negami, S. Polymer **1967**,8, 161.

18. Coburn, J.C.; Boyd, R.H. Macromolecules **1986**,19, 2238.

19. Nogales, A.; Denchev, Z.; Šics, I.; Ezquerra, T. A. Macromolecules **2000**, 33, 9367.

20. Angell, C.A. Polymer **1997,** 38, 6261.

21. Ngai, K. L.; Roland, C. M. Macromolecules **1994,** 27, 2454.

22. Kramarenko, V.Y.; Ezquerra, T. A.; Šics, I.; Baltá-Calleja, F.J.; Privalko, V. P. J. Chem. Phys. **2000**, 113,447,.

23. Böhmer, R.; Ngai, K. L.; Angel, C. A.; Plazek, D. J. J. Chem. Phys. **1993,** 99, 4201.

24. Adachi, K.; Kotaka, T. Macromolecules **1983**, 16, 1936.

25. D. Boese, F. Kremer, L. J. Fetters, Macromolecules 1990, 23, 1826.

26. Roland, C. M.; Bero, C. A.; Macromolecules **1996**, 29, 7521.

27. Graessley, W. W. Adu. Polym. Sci. **1982**, 47, 67.

28. Floudas, G.; Paraskeva, S.; Hadjichristidis, N.; Fytas, G.; Chu, B.; Semenov, A. N. J. Chem. Phys. **1997,** 107, 5502

Miscibility–dispersion, interfacial strength and nanoclay mobility relationships in polymer nanocomposites†

Javier Carretero-González,*[ab] **Haris Retsos,**[b] **Emmanuel P. Giannelis,**[b] **Tiberio A. Ezquerra,**[c] **Marianella Hernández**[a] **and Miguel A. López-Manchado***[a]

Received 7th January 2009, Accepted 5th June 2009
First published as an Advance Article on the web ?????
DOI: 10.1039/b900295b

Fully dispersed layered silicate nanoparticles (nanoclay) in a polymer matrix have provided a new class of multi-functional materials exhibiting several performance improvements over conventional composites. Yet the challenges of miscibility and interfacial strength might prevent nanocomposites from realizing their full potential. In this paper we demonstrate the effect of the chemical characteristics of the nanoclay on the miscibility and dispersion in the polymer matrix as well as on the interfacial strength of the bound polymer and the nanoclay mobility, all of which determine the macroscopic properties of the nanocomposite.

Introduction

The effect of nanoscopic platelets of clay in the morphology of homopolymers,[1] block-copolymers[2] and polymer blends,[3] as well as on their dynamic processes[4–6] have been commonly attributed to the high aspect ratio of the rigid nanoclay layers and to the large interfacial contact area between the clay and the polymer matrix.[7] These effects have a profound impact on the mechanical properties of the nanocomposites due to nanoscale reinforcement. Despite these promising results, and continuous efforts by researchers worldwide to control the dispersion of nanoclay in the polymer, other aspects related to controlling the interfacial strength between the clay and the polymer and, thus, the properties of the nanocomposites remain a challenge.

Theoretical[8] and experimental[9] studies provide evidence that polymer and nanoparticle mobility prevents the failure of polymer nanocomposites during deformation by introducing an additional dissipative energy mechanism through the formation of temporary crosslinks between the polymer chains and the inorganic surface of the nanofiller. Although these studies conclude that the introduction of nanoparticles benefits the toughening and strengthening of polymeric matrices, the bound polymer also seems to play a key role in the material's intrinsic properties. This is likely to be a consequence of the large surface area of nanoclay exposed to the polymer molecules, leading to a huge interfacial volume around the nanofillers. Zhou *et al.*[10] recently concluded that this model of nanoparticle mobility will only result in toughened plastics if both reduced interparticulate interactions and optima nanofiller/matrix interactions are guaranteed and accompanied by sufficient polymer mobility. Effective physical crosslinking thus requires high mobility and strong interaction between the nanoclay particles and the polymer, allowing them to move with the polymer chains during deformation.

In the present work we report the effect of the alkyl chain length, functionality and the grafting density of organic surfactant molecules, covering the surface of the nanoclay, on both the miscibility and the dispersion of nanoclay in natural rubber (NR) nanocomposites by means of X-ray diffraction (XRD) and transmission electron microscopy (TEM). In an effort to understand the role of the interfacial region and the mobility of the nanoclay in determining the properties of polymer nanocomposites, we have studied the polymer dynamics by means of broadband dielectric spectroscopy (BDS) and the microstructure under dynamic deformation by wide angle X-ray diffraction (WAXD). The anisotropic organoclay nanoparticles are aligned within the rubber matrix by stretching. This allows us to monitor microstructural changes, including crystallization, by *in situ* WAXD. Both the alignment capability and the interaction strength with the polymer matrix are ultimately determined by the chemical characteristics of the nanoclay. These two aspects are crucial in designing new types of high-strength polymer nanocomposites.

Most studies on organoclay/polymer nanocomposites focus on the effect that the extent of exfoliation has on the physical and mechanical properties of the material. However the improvement in polymer/NR matrices is dependent not only on the extent of exfoliation but also in other factors as the spatial distribution and orientation of the clay layers. A small degree of agglomeration results in an inevitable decrease in performance. In the first part of this work, we study which chemical features of the nanoclay can improve the miscibility between the polymer and the nanoclay, and so permit nanoparticle dispersions on different length scales. In the second part of the paper the interplay between interfacial strength and nanoparticle mobility in polymer nanocomposites is discussed.

---

[a] *Instituto de Ciencia y Tecnología de Polímeros, CSIC, Madrid 28006, Spain. E-mail: jcarretero@ictp.csic.es; lmanchado@ictp.csic.es*
[b] *Department of Material Science and Engineering, Cornell University, Ithaca, New York 14853, USA*
[c] *Instituto de Estructura de la Materia, CSIC, Madrid 28006, Spain*

† Electronic supplementary information (ESI) available: The dielectric loss values for unfilled and vulcanized NR and the unvulcanized NR containing 10 phr of Q-I nanoclay, and dielectric loss *versus* temperature for the nanocomposite containing 15 phr of Q-I nanoclay in the dry state and in the swollen state. See DOI: 10.1039/b900295b

Results and discussion

Sample processing

A series of montmorillonite clays, organically modified with primary (single tails of varying lengths) and quaternary (stoichiometric and non-stoichiometric dimethyl dehydrogenated tallow) alkyl ammonium salts, were mechanically mixed with NR, $M_w \approx 710$ K, (710×10^3 g mol^{-1}).

Microstructure

Table 1 describes the organoclays used as well as a comparison of the basal spacing, determined by XRD, before and after mixing with the polymer. As expected, a clear correlation between the number of carbon atoms in the primary alkyl chain (with similar surfactant concentration) or the concentration of organic surfactant (for the same type of quaternary ammonium salt) and the initial basal distance for the organoclay is observed. However, after mixing and crosslinking of the rubber matrix the d-spacing is about the same in all the nanocomposites, thus suggesting that the final d-spacing is independent of the initial organoclay spacing but it depends instead on the intercalated polymer.

Nevertheless, as seen in Fig. 1, sharper and better defined X-ray diffraction peaks ((001) reflections) are obtained for the nanocomposites containing the layered silicate nanoparticles modified with quaternary ammonium salt, Q-I and Q-II (Fig. 1, right). This means that more order is retained between the nanoclay layers after polymer mixing in the presence of quaternary ammonium salts. Differences in miscibility as a consequence of the differences in chemical surface modification of the nanoclay are also clearly evident in the TEM analysis shown in Fig. 2 and 3.

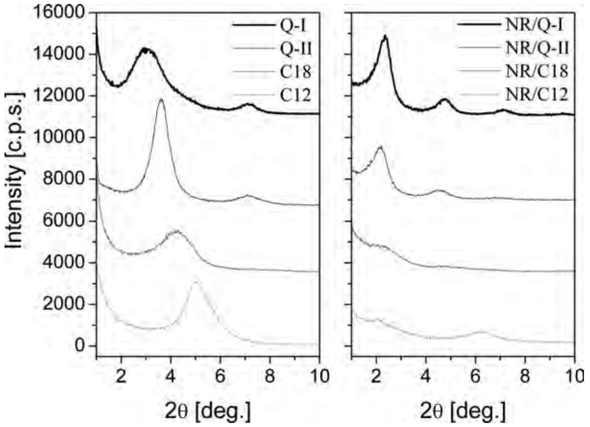

Fig. 1 Left: XRD plots of Q-I (dark line), Q-II (thin line), C18 (medium line) and C12 (light line) nanoclays. Right: XRD plots of NR/Q-I (dark line), NR/Q-II (thin line), NR/C18 (medium line) and NR/C12 (light line) nanocomposites.

TEM images of the nanocomposite system containing the nanoclay organomodified with the linear alkyl ammoniun salt (C18) are shown in Fig. 2. As observed in Fig. 2a, the silicate is present as both individual layers, as well as small multilayer stacks (tactoids). Focusing in more detail (Fig. 2b, 2c and 2d) on the differents areas of the sample, we find that large aggregates co-exist with the individual and smaller tactoids mentioned above. Moreover, besides the breaking apart of big silicate particles into smaller clay particles, a peeling effect from the aggregates forming individual and isolated nanoclay particles, as a consequence of shearing during mechanical mixing, was also observed for the layered silicates organomodified with the linear surfactant (Fig. 2c).

In contrast, the use of organoclays functionalized with a quaternary ammonium salt reduces the micron size agglomerates to smaller tactoids instead of peeling them into individual platelets, as shown in Fig. 3. A highly homogeneous NR nanocomposite system was obtained regardless of a stoichiometric Q-I (Fig. 3Ia and 3IIa) or non-stoichiometric Q-II (Fig. 3Ib and 3IIb) amount of ammonium present. The nanocomposites with Q-type nanoclays exhibit a microstructure characterized by nanoclay particles arranged in small groups of finely dispersed clay tactoids (containing ~10 layers). These tactoids are largely isolated and separated by distances of ~10–50 nm instead of forming a rigid filler network. These observations suggest a different intercalation/exfoliation mechanism for the two types of organic surfactants, each of them exhibiting a different level of miscibility with the polymer matrix.

Due to its homogeneity, the microstructures shown in Fig. 3 may represent an ideal system to study the interplay between the interfacial strength and the mobility of the nanoclay under stretching.

Dielectric relaxation spectroscopy

Fig. 4 shows the dielectric loss, ε'', *versus* temperature for pristine vulcanized NR and for the nanocomposite containing Q-I

Table 1 Selected data for the alkyl ammonium–modified layered silicates and their NR nanocomposites. Note that C*X* (*X* = 12, 14, 16, 18) and Q-*Y* (*Y* = I and II) are the samples based on primary and quaternary (ditallow)[a] ammoniun alkyl chains, respectively

Organoclay	Organic concentration (mmol/g clay)	d-Spacing (nm)		Δd-Spacing (nm)
		Pure organoclay	NR/organoclay	
C12	~1.5	1.7	3.8	2.1
C14	~1.5	1.8	3.8	2.0
C16	~1.5	2.0	3.7	1.7
C18	~1.5	2.1	3.7	1.6
Q–I	1.2	2.9	3.8	0.9
Q–II	0.9	2.4	4.1	1.7

[a] The ditallow was a mixture of dimethylammonium surfactants with various carbon chain lengths of *ca.* 65% of C18, 30% of C16, and 5% of C14. The surfactant concentration (mmol g^{-1} clay) was determined by thermogravimetric analysis after Soxhlet extraction of the organo-modified clay particles.

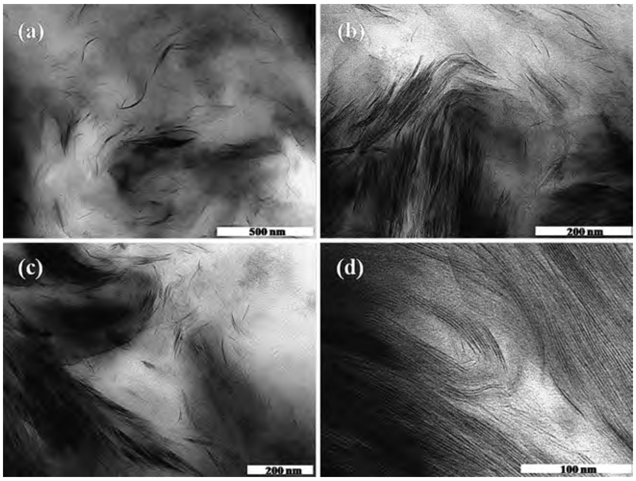

Fig. 2 Different magnification (20 K×–50 K×) TEM images of the NR/C18 nanocomposite.

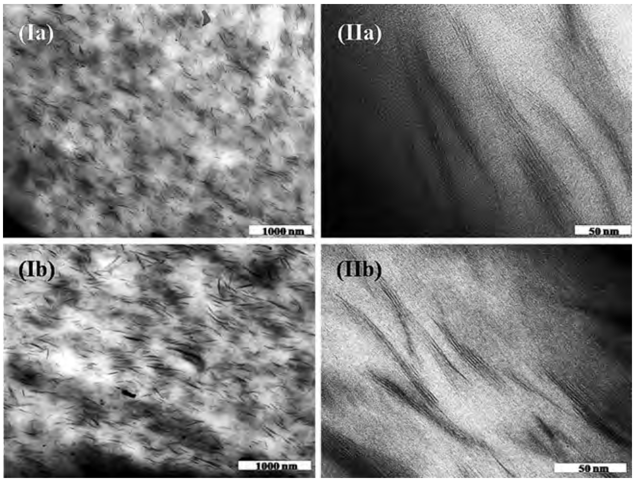

Fig. 3 Low (I) and high (II) magnification TEM images for (a) NR/Q-I and (b) NR/Q-II nanocomposites filled with 15 phr of nanoclay.

nanoclay (15 phr). It is well known that cis-polyisoprene (a major component in NR) exhibits two relaxations.[11] One of them is related to the segmental motion (segmental mode) and a slower one related to the relaxation of whole chains (normal mode).[12] The normal mode disappears after crosslinking due to suppression of large-scale motions of the dipole oriented parallel to the polymer backbone. In our case, vulcanized NR exhibits an intense relaxation around 237.5 K, associated with the segmental mode (SM), accompanied at lower temperatures by another relaxation albeit of lower intensity. No significant changes in the relaxation behavior were observed when the nanoclay was added. This indicates that the segmental motion of cis-polyisoprene is not disturbed by the addition of the nanoparticles. Consequently, both samples must have similar glass transition temperature values. For the NR nanocomposite. a slower relaxation (SR) appears at higher temperatures (T ≈ 325 K). The strong increase of ε'' at even higher temperatures can be associated with a Maxwell–Wagner–Sillars (MWS) process induced by the accumulation of charges at the polymer-nanoclay interfaces.

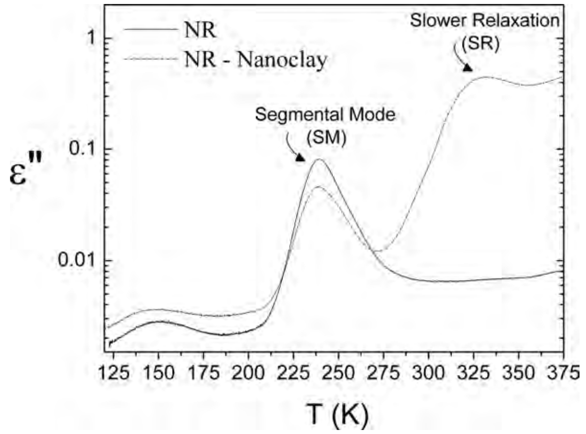

Fig. 4 The temperature dependence of ε'' at 1×10^3 Hz for the unfilled and nanocomposite NR samples after crosslinking. For vulcanized NR the main process is associated with the segmental mode (SM). For the nanocomposite an additional slower relaxation (SR) appears at higher temperatures.

The dielectric relaxations for NR and the nanocomposite as a fucntion of both temperature and frequency are shown in Fig. 5.

The dielectric relaxation spectra were analyzed using the Havriliak–Negami formulation. From this analysis the relaxation time of the different processes were extracted and they are represented in Fig. 6 as a function of the reciprocal temperature. As expected, the relaxation times for the segmental mode of both vulcanized NR and the NR/Q-I nanocomposite follows the characteristic Volgel–Fulcher–Tamann (VFT) dependence

$$F_{max} = F_0\ exp[-DT_0/(T - T_0)]$$

The slower relaxation (SR) of the NR/Q-I nanocomposite also seems to follow a VFT behaviour with the parameters presented in Table 2. We can hypothesise that the SR appears as a consequence of the interaction of the rubber chains with the nanoclay surfaces inducing a slower segmental mode with a new effective T_g of ~90 K higher than in the neat polymer (*i.e.* in the absence of the nanoclay).

Strain induced crystallization

The alignment of the nanoclay in the polymer matrix upon stretching was evaluated by *in situ* monitoring the evolution of the integrated intensity of the I_{200} reflection of the crystalline phase of NR. Fig. 7 (Up) shows the dependence of I_{200} with the deformation ratio α during stretching. The corresponding stress–strain curve for both the unfilled NR and the corresponding nanocomposites are shown in Fig. 7.

Crystallization of neat NR seems to occur in a single step once a critical value of strain $\alpha = 3.4$ is reached. In contrast crystallization in the nanocomposites commences at $\alpha \approx 1.2$ and appears to follow a more complex, two-step pattern.[13] Although the I_{200} intensity values are directly related to the amount of NR crystallites formed during stretching,[14] we must take into account the fact that the motion of the nanoclay particles and the motion of the polymer chains must be coupled. The first step for α-values

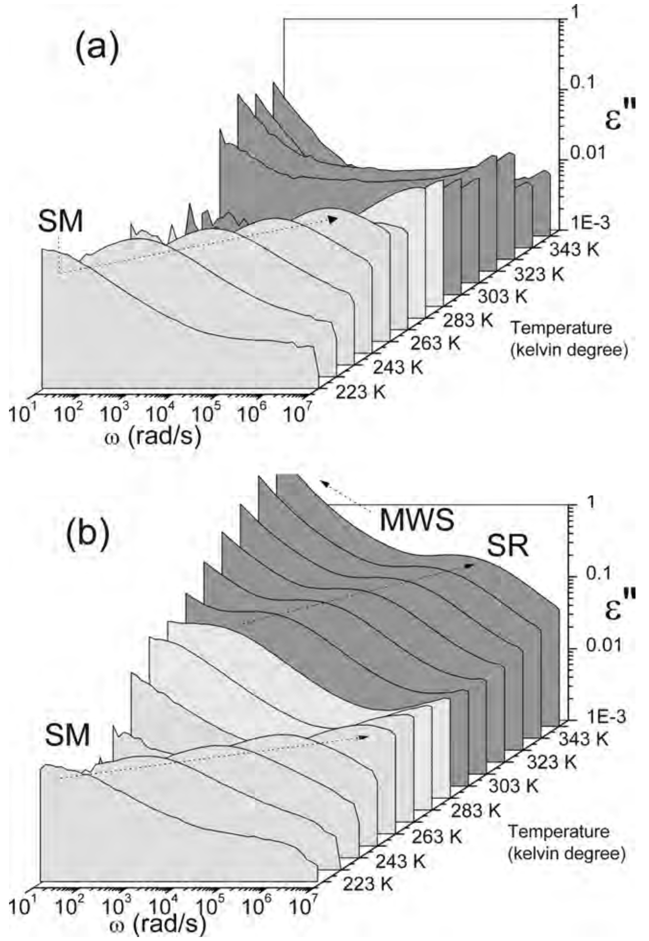

Fig. 5 ε'' values for unfilled NR (a) and the NR nanocomposite containing 15 phr of Q-I nanoclay (b) as a function of frequency and temperature.

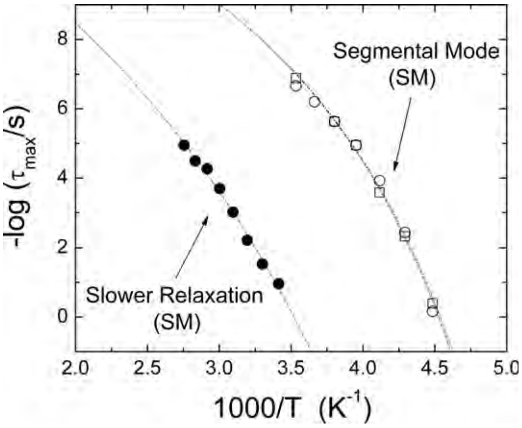

Fig. 6 The dependence of the relaxation time corresponding to the maximum loss (τ_{max}) on the reciprocal temperature for the segmental relaxation (open symbols) for the unfilled polymer matrix (□) and the nanocomposite (○). The slower relaxation mode assigned to the interfacial adsorbed polymer in the nanocomposites is also plotted (●). Dashed lines represent Volger–Fulcher–Tamann fits for each relaxation.

Table 2 T_g and VFT parameters for the unfilled sample and the NR-Q-I nanocomposite

Sample	B	T_0 (K)	T_g (K)
NR(SM)	868	159.0	232
NR15 Q–I (SM)	873	158.6	233
NR 15 Q–I (SR)	1976	142.9	325

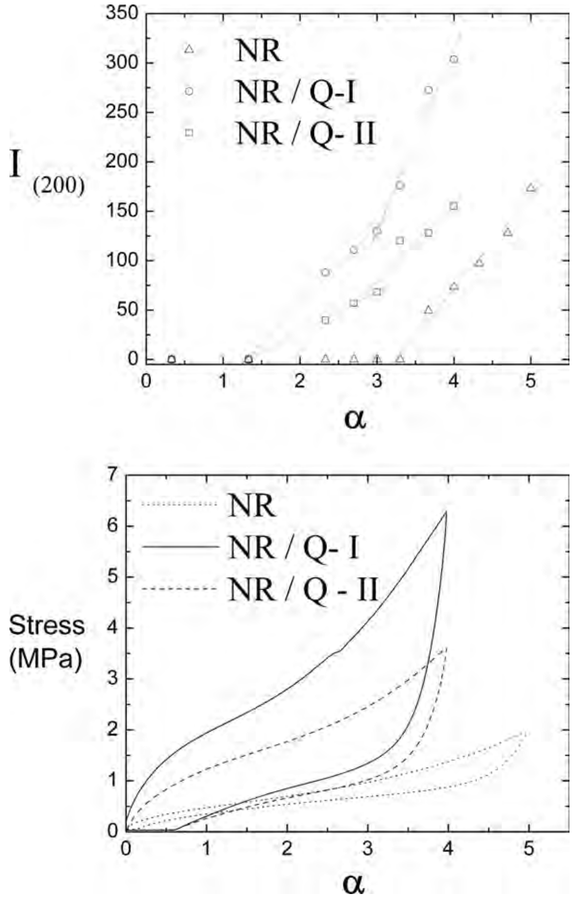

Fig. 7 Upper: Variation of the integrated intensity of the 200 reflection during the stretching process for NR/Q-I (○), NR/Q-II (□) and unfilled NR (Δ). Lower: stress–strain curves for the NR/Q-I (—), NR/Q-II (---) and unfilled NR (···) samples.

<3 is most likely related to the orientation and alignment of the highly anisotropic nanoclay particles. In a second step ($3 \le \alpha \le 4$), these highly anisotropic nanoparticles can be completely aligned along the direction of the deformation and thus a physical network is formed. This physical network may favor the alignment of the rubber chains and the crystallization rate could increase. Moreover, the excess of loosely bound surfactant seems to facilitate the strain-induced crystallization process in NR/Q-I in comparison with NR/Q-II. The change in the crystallizability of the polymer as well as the mobility of the nanoclay can be attributed to the presence of surfactant molecules surrounding the nanoclay fillers. This effect is not expected to be due to the optimum thermodynamic interaction[15] between the organic alkyl chains of surfactant and the polymer at the interface, but rather to the lower friction of polymer chains with the inorganic surface as a consequence of the higher amount of inorganic surface covered by the surfactant alkyl-chains.[16] This is likely also directly related to an increase in dispersion quality as well as a decrease in processing time as a result of employing a quaternary branched alkyl chain instead of a linear ammonium salt as previously demonstrated. Such a change would certainly increase the "*self-lubricating*" effect among the grafted nanoparticles and the polymer. As a result, the final crystalline content of the nanocomposites is higher and there is a more effective toughening as shown in Fig. 7 down.

Conclusions

The influence of the chemical characteristics of the nanoclay on the microstructure and the dynamics of nanoclay–natural rubber nanocomposites has been discussed. We have shown by using broadband dielectric spectroscopy that the nanoclay–polymer interaction induces a new relaxation process which is slower than the segmental relaxation of the rubber matrix. In addition, *in situ* synchrotron X-ray experiments give an indirect measurement of the mobility of the nanoclay during uniaxial elongation. Our results emphasize the importance of the chemical surface modification of nanoclay as being crucial to promote an optimum mechanical reinforcement.

Experimental

Synthesis of the nanocomposites

The natural rubber sample was kindly supplied by Malaysian Rubber (Berhad, Malaysia) under the trade name NR CV60 (mooney viscosity ML (1 + 4) at 100 °C = 60). Nanoclay Q-I (non-stoichiometric dimethyl dehydrogenated tallow ion–exchanged montmorillonite) was supplied by Southern Clay Products (Gonzales, TX, USA) and Q-II was prepared from Q-I after Soxhlet extraction of Q-I. Nanoclays based on linear ammonium alkyl chains surfactants (C12–C18) were prepared by ion exchange with sodium montmorillonite (Southern Clay Products) and the organic surfactants (Aldrich) at 343 K. The formulation of natural rubber compounds expressed in phr (parts per hundred rubber) is as follows: sulfur (2.5), ZnO (5), stearic acid (1), MBTS (1), antioxidant PBN (1) and nanoclays (variable). Nanocomposites were prepared in an open two-roll laboratory mixing mill at room temperature. Vulcanization was carried out in an electrically heated hydraulic press, at 150 °C at the optimum cure time (t_{90}) previously determined with a rubber process analyzer (RPA Alpha Technologies).

X-Ray diffraction

X-Ray diffraction was performed in a θ–θ diffractometer with an integrated germanium detector, using a Cu Kα source with a wavelength of 1.54 Å and a scan rate of 2° min^{-1}.

Microscopy

The dispersion of the nanoparticles in the rubber matrix was determined through transmission electron microscopy (TEM), using a Technai T12 TEM operated at an accelerating voltage of 120 kV. TEM samples (~40 nm) were prepared by sectioning at −160 °C using a Leica Ultracut UCT ultracryomicrotome with a diamond knife.

Broadband dielectric spectroscopy

Dielectric spectroscopy measurements were performed using the Novocontrol Turnkey Concept N40 broadband spectrometer (Hundsangen, Germany). Sample discs were mounted in the dielectric cell (ZGS Alpha Active Sample Cell) between two parallel gold-plated electrodes (BDS 1301 model). The thickness of the gold-plated electrodes was 2 mm and the diameters were 20 mm (upper) and 30 mm (lower), respectively. The sample thickness was 1 mm and the diameter was about 15 mm. The sample/electrode assembly was then mounted in the Novocontrol Quatro Cryosystem.

Synchrotron X-ray measurements

In situ stress–strain experiments coupled with the synchrotron X-ray measurements were carried out at the X27C beamline in the National Synchrotron Light Source, Brookhaven National Laboratory. The wavelength was 0.1366 nm. The deformation rate was 10 mm/min and the experiments were carried out at room temperature. The maximum strain value was 400% due to the slipping of the sample from the clamps. The two dimensional WAXD patterns were recorded using a MAR CCD camera. Exposure time for each image was 30 s and there was an interval of 5 s before the next exposure. The diffraction angle was calibrated by Al_2O_3 standard (provided by the National Institute of Standards and Technology). The images were processed using "POLAR" software (Stony Brook Technology and Applied Research, Inc.). The crystallinity index (C.I.) was calculated from the integration and correction of the equatorial 2D intensity WAXD profiles at the azimuthally range of ±75 using peak fit software.

Acknowledgements

The authors gratefully acknowledge the financial support of the Spanish Ministry of Science and Innovation (MICINN) through projects MAT 2004–00825 and MAT–2005–01768. JCG acknowledges support from MICINN in the form of a FPI grant and EPG acknowledges the support of Award No. KUS–C1–018–02 made by King Abdullah University of Science and Technology (KAUST). Special thanks are due to Shigeyuki Toki and Benjamin S. Hsiao from Stony Brook University and the X27C beamline in the National Synchrotron Light Source at Brookhaven National Laboratory.

References

1 D. M. Lincoln, R. A. Vaia and R. Krishnamoorti, *Macromolecules*, 2004, **37**, 4554.
2 A. S. Silva, C. A. Mitchell, M. F. Tse, H.-C. Wang and R. Krishnamoorti, *J. Chem. Phys.*, 2001, **115**, 7166.
3 M. Arroyo, M. A. Lopez-Manchado, J. L. Valentin and J. Carretero, *Comp. Sci. Tech.*, 2007, **67**, 1330.
4 R. Krishnamoorti and E. P. Giannelis, *Macromolecules*, 1997, **30**, 4097.
5 S. H. Anastasiadis, K. Karatasos, G. Vlachos, E. Manias and E. P. Giannelis, *Phys. Rev. Lett.*, 2000, **84**, 915.

6 S. Salinawal, S. K. Kumar and J. F. Douglas, *Phys. Rev. Lett.*, 2002, **89**, 258301.
7 R. A. Vaia, *Mater. Today*, 2004, **7**, 32.
8 D. Gersappe, *Phys. Rev. Lett.*, 2002, **89**, 058301.
9 D. Shah, P. Maiti, D. D. Jiang, C. A. Batt and E. P. Giannelis, *Adv. Mater.*, 2005, **17**, 525.
10 H. Z. Tong, H. R. Wen, Z. R. Min, Q. Z. Min and L. M. Yu, *Adv. Mater.*, 2007, **19**, 2667.
11 W. H. Stockmayer and M. E. Baur, *J. Am. Chem. Soc.*, 1964, **86**, 3485.
12 K. Adachi and T. Kotaka, *Macromolecules*, 1984, **17**, 120.
13 J. Carretero-González, H. Retsos, R. Verdejo, S. Toki, B. S. Hsiao, E. P. Giannelis and M. A. López-Manchado, *Macromolecules*, 2008, **41**, 6763.
14 S. Toki, I. Sics, S. Ran, L. Liu, B. S. Hsiao, S. Murakami, K. Senoo and S. Kohjiya, *Macromolecules*, 2002, **35**, 6578.
15 R. A. Vaia and E. P. Giannelis, *Macromolecules*, 1997, **30**, 7990.
16 E. Manias, H. Chen, R. Krishnamoorti, J. Genzer, E. J. Kramer and E. P. Giannelis, *Macromolecules*, 2000, **33**, 7955.

Macromolecules

Volume 41, Number 7 April 8, 2008

Communications to the Editor

Real-Time Crystallization of Organoclay Nanoparticle Filled Natural Rubber under Stretching

Javier Carretero-Gonzalez,[†] **Raquel Verdejo,**[†]
Shigeyuki Toki,[‡] **Benjamin S. Hsiao,**[‡]
Emmanuel P. Giannelis,[§] **and**
Miguel A. López-Manchado*[,†]

Institute of Polymer Science and Technology, CSIC, Madrid 28006, Spain; Department of Chemistry, Stony Brook University, Stony Brook, New York 11794-3400; and Department of Material Science and Engineering, Cornell University, Ithaca, New York 14853

Received December 21, 2007
Revised Manuscript Received February 20, 2008

Polymer nanocomposites (PNCs) represent a new class of materials compared to conventional filled polymers or polymer blends, as they can possess enhanced properties through nanoscale reinforcement.[1] Widespread interest in PNCs over the past several years has been fueled by their promise of unprecedented performance, design flexibility, and lower cost. A great deal of effort has been devoted to understanding the reinforcing mechanism of PNCs containing highly anisotropic nanofillers such as nanoclays.[2] In this study, we present experimental evidence of a remarkable enhancement of strain-induced crystallization in natural rubber (NR) nanocomposite under uniaxial stretching due to the presence of nanoclay particles. By using synchrotron wide-angle X-ray diffraction (WAXD), we have monitored the structure changes and crystallinity development during deformation in real time. The behavior of significantly enhanced strain-induced crystallinity in organoclay/NR nanocomposites has not been observed before in systems containing conventional fillers. This effect might be responsible for the observed enhancement in mechanical properties of organoclay/NR nanocomposites.[3] The results suggest a dual crystallization mechanism in nanocomposites, which is absent in the unfilled system. The mechanism consists of spatial reorganization of organoclay at low strains (e.g., less than $\alpha = 3$), followed by rapid strain-induced crystallization of NR. The observed in-situ structure changes in NR nanocomposite enable us to suggest a mechanism that may be universal to crystallizable elastomers containing nanosized fillers.

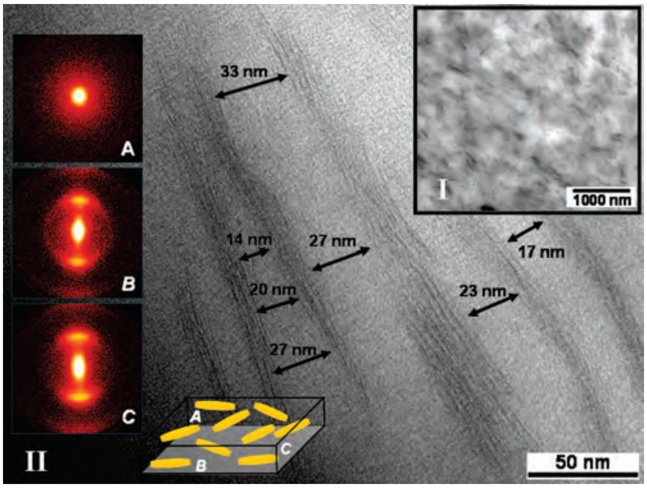

Figure 1. Representative TEM images (I: scale bar 1000 nm; II: scale bar 50 nm) and SAXS patterns (A: face-on view; B and C: edge-on views) of the NR−NC1 nanocomposite.

Layered-silicate nanofillers can improve the physical, mechanical, and thermal properties of polymeric matrices.[4] This behavior has been explained by the formation of a reinforcing nanofiller network (exfoliated or/and intercalated), within which the polymer chains are confined. However, this explanation is not sufficient to paint a complete picture of the reinforcing mechanism taking place in many systems. For example, Giannelis and co-workers[5,6] have reported a unique class of semicrystalline and amorphous nanocomposites having toughness values 1 order of magnitude higher than that of the unfilled polymer matrix. They suggested that the presence of nanoparticles introduces new energy-dissipating mechanisms, and they attributed the mechanical property enhancement to the nanoparticle mobility and orientation during deformation. A study by Joly et al.[7] using birefringence and infrared dichroism on

---

* To whom correspondence should be addressed: Tel +34 912587424, Fax +34 915 644 853, e-mail lmanchado@ictp.csic.es.

[†] CSIC.

[‡] Stony Brook University.

[§] Cornell University.

10.1021/ma7028506 CCC: $40.75

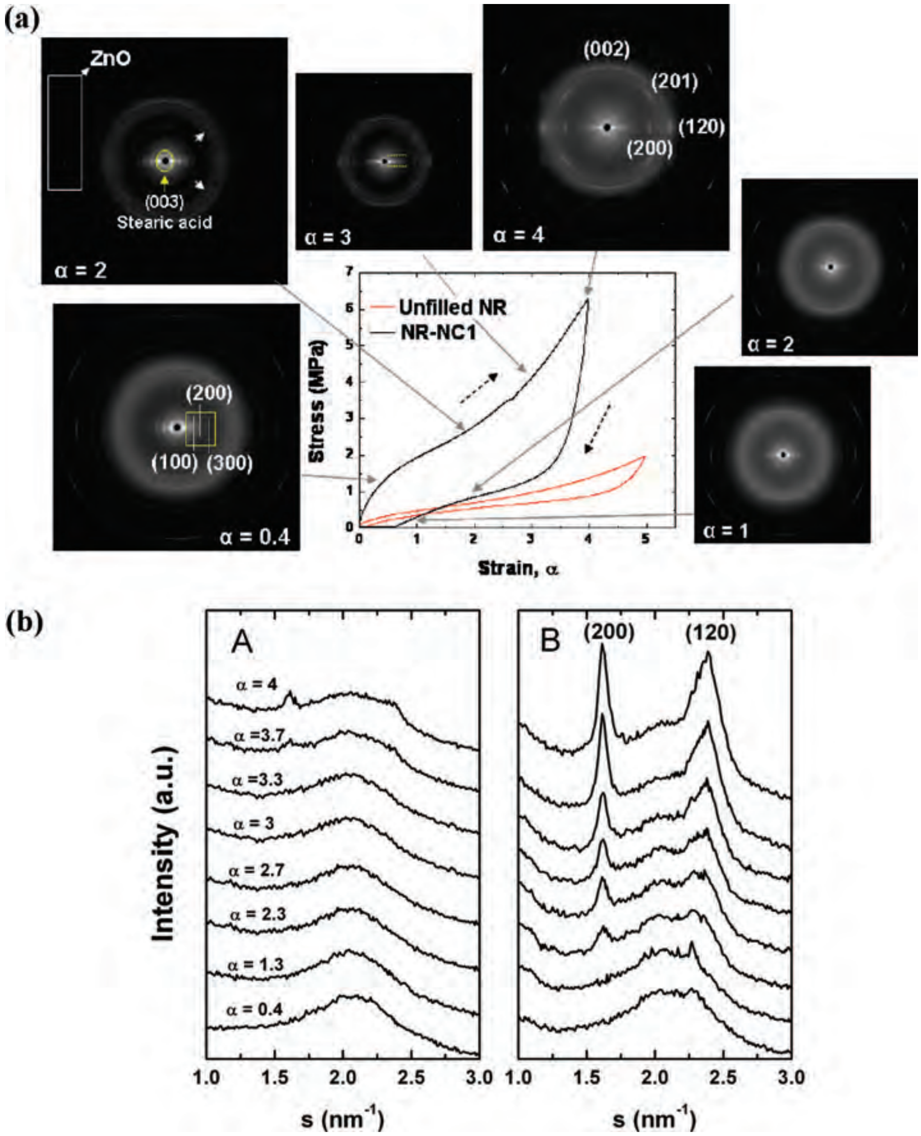

Figure 2. WAXD results for NR−NC1 nanocomposites. (a) Stress–strain curve and selected synchrotron WAXD patterns during extension and retraction cycles. (b) Integrated and corrected intensity profiles from the 2D WAXD patterns at various strains as a function of scattering vector *s* (nm^{-1}).

organoclay/NR nanocomposites also reported a higher orientation of amorphous chains by the addition of nanoclays. However, they did not consider the behavior of strain-induced crystallization in NR, which is the dominant effect in mechanical reinforcement.

The purpose of this study was to investigate the effects of organoclay on strain-induced crystallization under uniaxial stretching in crystallizable natural rubber nanocomposites. In-situ experiments were carried out to couple the stress–strain behavior with structure determination using synchrotron wide-angle X-ray diffraction (WAXD). This method enabled us to monitor the changes at the local molecular structure during deformation in real time.[8]

Two NR/organoclay nanocomposites, NR−NC1 (NC1-filled NR (15 phr)) and NR−NC2 (NC2-filled NR (15 phr)) were prepared by mechanical mixing at room temperature and vulcanized at 150 °C. NC1 is a quaternary ammonium salt modified montmorillonite with a basal distance of 29.4 Å. NC2 was prepared from NC1 after Soxhlet extraction to remove excess surfactant (~6.2 wt %) from the clay. Both nanocomposite samples exhibit an intercalated structure as observed by WAXD (data not shown). Transmission electron microscopy (TEM) (Figure 1) confirmed the presence of finely dispersed tactoids (nanoclay stacks) spaced 10−40 nm apart. In addition, directional small-angle X-ray scattering (SAXS) measurements (A: face-on view; B and C: edge-on views) of the unstretched but pressed specimen showed the preferred orientation of nanoclay stacks aligned parallel to the film plane due to processing. Figure 2a shows the stress–strain curve and corresponding 2D WAXD patterns at selected strains during stretching and retraction for the NR−NC1 nanocomposite. The corresponding stress–strain curve for the unfilled NR is included for comparison. Figure 2b illustrates the normalized and corrected linear diffraction profiles for unfilled NR (A) and the NR−NC1 nanocomposite (B). All images at high strains exhibited preferred orientations of (100), (200), and (300) reflections from layered silicates, indicating that nanoclays became highly orientated along the stretching direction. The orientation began at a relatively low strain ($\alpha = 0.4$) and increased progressively until a maximum alignment was reached (at $\alpha = 4$). In addition to the orientation of nanoclays, WAXD images clearly revealed the strain-induced crystallization of natural rubber chains, which was evidenced by the alignment of (200) and (120) reflections from the rubber matrix. It is

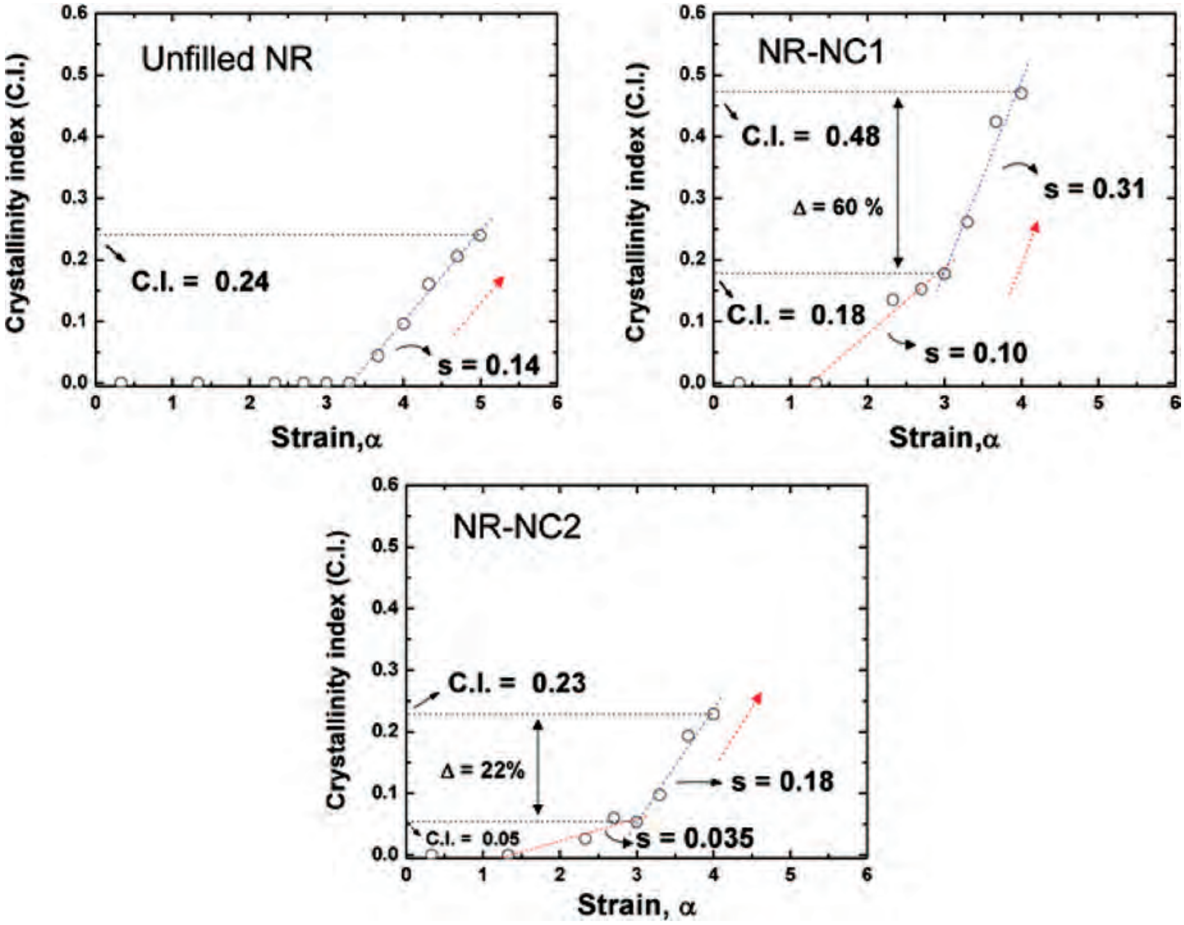

Figure 3. Crystallinity index as a function of strain during the first stretch cycle.

interesting to note that the crystal reflections of NR appeared at a lower strain in the nanocomposite compared to the unfilled NR. In addition, we did not observe strong evidence for orientation of the amorphous phase based on the WAXD analysis. If there was some oriented amorphous phase, the total fraction was small. This is in slight contrast with the study by Rault et al.,[9] who have demonstrated orientation of the amorphous phase using ^{2}H NMR.

Figure 3 shows the evolution of crystallinity index (CI) as a function of strain for the unfilled NR and the nanocomposites. The results indicate that the onset strain (α^0) of deformation-induced crystallization was 3.3 and 1.2 for the unfilled sample and nanocomposites, respectively. The overall crystallinity index was significantly higher in the nanocomposite than in the unfilled sample (e.g., the maximum strain-induced crystallinity in unfilled NR was 25% at a strain $\alpha = 5$[8] while the maximum strain-induced crystallinity in the NR−NC1 nanocomposite was 48% at a strain $\alpha = 4$). In systems containing conventional fillers such as carbon black, silica, or calcium carbonate a lowering of the threshold ($\alpha^0 = 2$) has been reported, but no differences in the overall crystallinity index were observed.[10–12] The difference between these traditional fillers and nanoclays is due to the very high surface-to-volume ratio of 10^3−10^4 m^2/mL for nanoclays compared to 10^{-1}−10^2 m^2/mL for conventional fillers.[2b] Hence, the observed different behavior can be attributed to the high interfacial interactions between the polymer matrix and the nanoclays, resulting in a more efficient transfer of stress across the matrix. The large interfacial region can lead to an early orientation of polymer chains, thus promoting nucleation under stretching.

Our experiment also revealed a different strain-induced crystallization mechanism of NR in the presence of nanoclays. Unfilled NR usually shows a single crystallization step,[8] while the NR nanocomposites exhibit two well-defined crystallization steps: the first one for $\alpha < 3$ is related to the orientation and alignment of nanoclays during elongation forming a physical network while the second ($3 \leq \alpha \leq 4$) corresponds to the conventional crystallization mechanism of unfilled NR,[13] but with a crystallinity index and strain slope approximately twice that of the pristine sample.

Another interesting aspect of our results is the effect of the amount of surfactant on the clay on the behavior of strain-induced crystallization in NR nanocomposites. The quantitative analysis of the WAXD data for NR−NC1 and NR−NC2 samples (Figure 3) revealed that the onset strain ratio did not change in the two nanocomposites. However, the crystallinity index strongly depended on the amount of surfactant. The maximum crystallinity for NR−NC1 and NR−NC2 is 50 and 25%, respectively. This different crystallinity in the nanocomposites can be related to the crystallizability of the NR chains (both nanocomposites showed two crystallization steps, but their slopes were quite different). In the first crystallization step, the NR−NC1 nanocomposite exhibited a slope about 1 order of magnitude higher than the NR−NC2, while the slope of the second step in NR−NC1 was also twice that of NR−NC2. The change in the crystallizability may be attributed to the higher amount of surfactant molecules surrounding the NC1 fillers, resulting in a greater enhancement of chain mobility for crystallization.[14]

In summary, we conclude from this study that the presence of interfacial interactions between nanoparticles (i.e., nanoclays)−polymer matrix and the enhanced mobility of the polymer on the clay surface are crucial in promoting strain-induced crystallization in natural rubber nanocomposites. Addition of nanoclay leads to significantly enhanced crystallinity and lower onset strain for stretch-induced crystallization compared to conventionally filled NR composites.

Acknowledgment. The authors gratefully acknowledge the financial support of the Spanish Ministry of Education (MEC) through its project MAT 2004-00825. J. Carretero-González thanks the Spanish Ministry of Education (MEC) for the concession of a FPI grant, and R. Verdejo also acknowledges a Juan de la Cierva contract from the MEC. B. S. Hsiao also acknowledges the support by the NSF (DMR-0405432).

Supporting Information Available: Nanocomposites preparation and characterization details and synchrotron measurement conditions and analysis. This material is available free of charge via the Internet at http://pubs.acs.org.

References and Notes

(1) Winey, K. I.; Vaia, R. A. *MRS Bull.* **2007**, *32*, 214.
(2) (a) Fornes, T. D.; Paul, D. R. *Polymer* **2003**, *44*, 4993. (b) Vaia, R. A. *Mater. Today* **2004**, *7*, 32. (c) Sheng, N.; Boyce, M. C.; Parks, D. M.; Rutledge, G. C.; Abes, J. I.; Cohen, R. E. *Polymer* **2004**, *45*, 487. (d) Rao, Y. Q.; Pochan, J. M. *Macromolecules* **2007**, *40*, 290.
(3) Arroyo, M.; Lopez-Manchado, M. A.; Herrero, B. *Polymer* **2003**, *44*, 2447.
(4) For comprehensive reviews on polymer−clay nanocomposites the reader is referred to: (a) Giannelis, E. P. *Adv. Mater.* **1996**, *8*, 29. (b) Giannelis, E. P.; Krishnamoorti, R.; Manias, E. *Adv. Polym. Sci.* **1999**, *138*, 107. (c) Pinnavaia, T. J.; Beall, G. W. *Polymer-Clay Nanocomposites*; John Wiley & Sons: New York, 2000. (d) Alexandre, M.; Dubois, P. *Mater. Sci. Eng.* **2000**, *28*, 1. (e) Ray, S. S.; Okamoto, M. *Prog. Polym. Sci.* **2003**, *28*, 1539. (f) Okada, A.; Usuki, A. *Macromol. Mater. Eng.* **2006**, *291*, 1449.
(5) Shah, D.; Maiti, P.; Gunn, E.; Schmidt, D. F.; Jiang, D. D.; Batt, C. A.; Giannelis, E. P. *Adv. Mater.* **2004**, *16*, 1173.
(6) Shah, D.; Maiti, P.; Jiang, D. D.; Batt, C. A.; Giannelis, E. P. *Adv. Mater.* **2005**, *17*, 525.
(7) Joly, S.; Garnaud, G.; Ollitrault, R.; Bokobza, L.; Mark, J. E. *Chem. Mater.* **2002**, *14*, 4202.
(8) Toki, S.; Sics, I.; Ran, S.; Liv, L.; Hsiao, B. S.; Murakami, S.; Senoo, K.; Kohjiya, S. *Macromolecules* **2002**, *35*, 6578.
(9) Rault, J.; Marchal, J.; Judeinstein, P.; Albouy, P. A. *Eur. Phys. J. E* **2006**, *21*, 243.
(10) Poompradub, S.; Tosaka, M.; Kohjiya, S.; Ikeda, Y.; Toki, S.; Sics, I.; Hsiao, B. S. *J. Appl. Phys.* **2005**, *97*, 103529.
(11) Trabelsi, S.; Albouy, P. A.; Rault, J. *Macromolecules* **2003**, *36*, 9093.
(12) Chenal, J. M.; Gauthier, C.; Chazeau, L.; Guy, L.; Bomal, Y. *Polymer* **2007**, *48*, 6893.
(13) Tosaka, M.; Murakami, S.; Poompradub, S.; Kohjiya, S.; Iheda, Y.; Toki, S.; Sics, I.; Hsiao, B. S. *Macromolecules* **2004**, *37*, 3299.
(14) Manias, E.; Chen, H.; Krishnamoorti, R.; Genzer, J.; Kramer, E. J.; Giannelis, E. P. *Macromolecules* **2000**, *33*, 7955.

MA7028506

Macromolecules **2008**, *41*, 6763−6772

Effect of Nanoclay on Natural Rubber Microstructure

Javier Carretero-González,*,[†] Haris Retsos,[‡] Raquel Verdejo,[†] Shigeyuki Toki,[§] Benjamin S. Hsiao,[§] Emmanuel P. Giannelis,[‡] and Miguel A. López-Manchado*,[†]

Institute of Polymer Science and Technology, CSIC, Madrid 28006, Spain; Department of Material Science and Engineering, Cornell University, Ithaca, New York 14853; and Department of Chemistry, Stony Brook University, Stony Brook, New York 11794-3400

Received April 22, 2008; Revised Manuscript Received June 14, 2008

ABSTRACT: The inclusion of highly anisotropic clay nanoparticles (nanoclays) in cross-linked natural rubber (NR) provides a more homogeneous distributed network structure and induces an early onset as well as enhancement of crystallization under uniaxial deformation. The molecular structure of the polymer network and its morphological changes during deformation were characterized by using broadband dielectric spectroscopy and in situ synchrotron wide-angle X-ray diffraction, respectively. It was found that the presence of nanoclay introduces a dual crystallization mechanism due to the alignment of nanoparticles during stretching. The improved properties in NR−nanoclay nanocomposites can be attributed to both microstructural and morphological changes induced by nanoclay as well as to the nanoclay mobility in the NR matrix during crystallization. The interplay of these factors during deformation contributes to the formation of a supernetwork structure containing cross-linked chemical chains, nanofiller, and crystallizable networks with similar length scales.

Introduction

Natural rubber (NR, the major component is *cis*-polyisoprene) is one of the most fascinating and important industrial polymers among many engineering plastics.[1] The principal reasons for the versatility of NR are its high green strength, which is in turn due to the presence of non-rubber components (phospholipids and proteins),[2] and its ability to crystallize upon stretching in unvulcanized[3] and vulcanized state,[4] which is ultimately determined from the non-rubber components and the high stereoregularity[5] of NR.

A common practice to enhance the mechanical properties of NR is the introduction of chemical cross-links as well as the addition of finely divided particulates, typically carbon black or silica.[6] A minimum of 20−30 wt % of conventional filler is required to attain optimal mechanical properties, but this high concentration reduces the processability and increases the weight of the final product. The continuous demand for new, low-cost, low-weight rubber composites with improved properties represents a challenge in the polymer industry.[7] Polymer nanocomposites offer the possibility for new alternatives.[8] The inclusion of nanosized particles, in particular layered silicates (nanoclays),[9] enables the enhancement of properties in polymers with even at small amounts of fillers, a feature not possessed by conventional composites. This was in fact the case for NR−nanoclay nanocomposites. It was found that the inclusion of 10 phr (parts per hundred of rubber) nanoclay greatly improves the mechanical properties of NR compounds over the conventionally filled systems.[10] Nevertheless, the mechanism of the reinforcement is still poorly understood. For example, why does it make NR−nanoclay materials stronger than conventionally filled rubbers without sacrificing properties like elongation at break, resilience, or compression set? According to the molecular models of conventional rubber compounds, for filled and crystallizable vulcanized rubbers, the main reason for the rise in the tensile strength at low deformations (below crystallization) has been considered as the formation of additional cross-links resulting from the filler−elastomer interactions due to the presence of fillers. Regarding the effect of nanoclay, we note that for the same weight/volume fraction of filler the nanosized platelets would lead to 4−6 orders of magnitude more particles per volume than classic mineral fillers.[11] A large amount of surface area will be exposed to the rubber molecules, leading to a huge interfacial volume around the nanofillers.

However, several points must be considered in order to better understand the differences between conventional and nanoclay-filled NR systems. Conventionally filled NR contains rigid aggregates of silica or carbon black particles, which can lead to a filler network with different level of aggregation.[12] Interactions between these micron sized particles forming *clusters* can cause a considerable change in viscoelastic properties.[13] However, this effect is absent in NR−nanoclay systems. The filler network in NR nanocomposites is arranged in small groups of finely dispersed clay tactoids (containing ∼10 layers). These tactoids are largely isolated and separated each other by ∼10−50 nm without forming any rigid filler framework with fractal structure. This is due to the high level of dispersion nanoclay in the nanocomposites. Breakdown or reconstitution of the nanoclay network (Payne effect)[14] by increasing the strain amplitude has not been observed in NR nanocomposites with clay loadings below 30 phr.[15] Therefore, the high elastic modulus and the low hysteresis observed in NR−nanoclay nanocomposites in the low strain regime might be due mainly to the hydrodynamic effect and the interactions between nanoclay and polymer.

Another important issue, mentioned above, is the assumption of the strength increase in NR−nanocomposite has often been attributed to rubber−filler interactions.[16] Such an assumption implies that the ability of the filler to toughen the matrix at any strain is independent of the thermodynamic state of the polymer matrix. Several experimental and theoretical studies have challenged the notion that the polymer−filler interactions are the only factor that is responsible for reinforcing the polymer nanocomposites.[17] It is conceivable that some other energy dissipation mechanism, resulting from the mobility of the nanoparticle that can act as temporary cross-links between polymer chains and nanoparticles, can also hinder the failure during deformation.

---

* To whom correspondence should be addressed. E-mail: jcarretero@ictp.csic.es. or lmanchado@ictp.csic.es.

[†] CSIC.

[‡] Cornell University.

[§] Stony Brook University.

10.1021/ma800893x CCC: $40.75

Table 1. Principal Features of the Layered Silicates Employed in This Work[a]

Clay	platelet size (nm)	CEC[b] (mequiv/g)	*d* spacing (nm)	surfactant (wt %)
Na^+-MMT	∼100−500	0.92	1.1	0
O-MMT	∼100−500	0.97	3.0	40.2
O-LAP	∼25−50	0.74	∼3.0	32.8

[a] The layered silicates were ionically exchanged with dimethyl dehydrogenated tallow quaternary ammonium ion. The ditallow was a mixture of dimethylammonium surfactants with various carbon chain lengths of ca. 65% of C_{18}, 30% of C_{16}, and 5% of C_{14}. [b] Cation exchange capacity (CEC) was determined by thermogravimetric analysis after Soxhlet filtration process of the organo-modified layered silicate particles. CEC for the Na^+-MMT was obtained from Material Safety Data Sheets provided by Southern Clay Products.

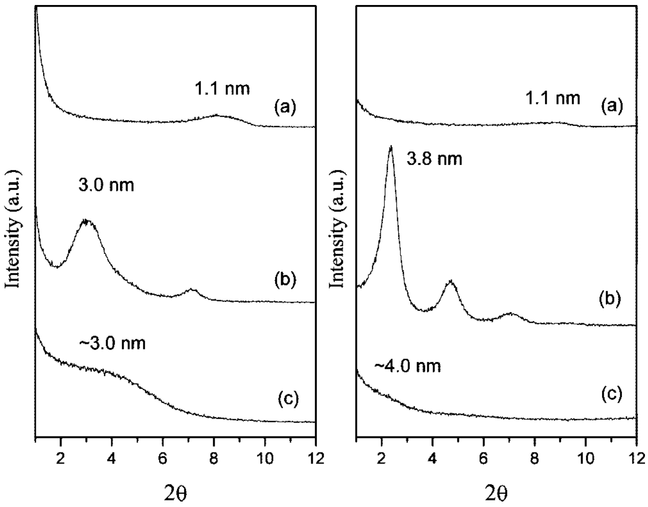

Figure 1. Left: XRD patterns of (a) Na^+-MMT, (b) O-MMT, and (c) O-LAP nanoclays. Right: XRD patterns of (a) NR/Na^+-MMT, (b) NR/O-MMT, and (c) NR/O-LAP compounds.

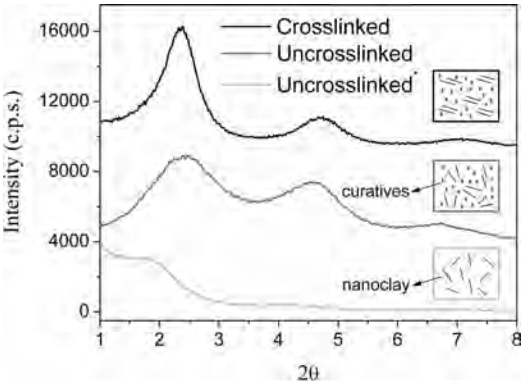

Figure 2. XRD patterns corresponding to the cross-linked NR/O-MMT nanocomposites (dark line), un-cross-linked NR/O-MMT (medium line), and un-cross-linked* NR/O-MMT without curatives (light line).

The above hypothesis is hard to verify because it is difficult to investigate NR−nanoclay nanocomposites under deformation without the induction of crystallization. Generally, strain-induced crystallization (SIC) occurs at strains beyond a critical value. The addition of micron size fillers to NR has been thought of as superimposing another level of filler network at the larger scale in the system.[18] But, this may not be the case for NR nanocomposites, and some interesting questions need to be addressed: (1) Will the dispersed nanoparticles induce a filler network structure with a similar length scale than the chemically cross-linked rubber chains? (2) How would the platelike particles affect the crystallization? To answer these questions, it is necessary to first understand the effect of nanoclay on the final distribution of the network topology (chemical and physical) and the possible network defects. It is well-known that the effective number of network imperfections such as dangling and loops in unfilled NR networks increases by cross-linking as a consequence of heterogeneous distribution of the cross-link junctions[19] and a broad distribution of chain length between the junction points.[20] Both factors will greatly impact the orientation of the polymer chains during deformation and consequently the final crystalline fraction. Thus, network imperfections will not alter the property resulting from the chain orientation due to SIC.[21] In contrast, the dense network region (highly cross-linked) would favor the molecular orientation of the chains at the early stages of deformation.[22] However, the induced crystallization also retards the process of nucleation due to the reduced segment mobility in these regions.[23] For filled NR with conventional fillers, several studies[24] have concluded that although the presence of fillers promotes crystallization, it does not increase the overall crystalline content in comparison with the unfilled systems. This effect could be due to the low volume fraction (0.1) necessary for the aggregation of fillers.[25] In other words, the conventionally filled rubber compounds might possess a nonhomogeneous dispersion of fillers due to the high amount of particles used for reinforcement, approximately 40−60 phr. In addition, the micron size fillers could behave as heterogeneities preventing the rubber chain from aligning and crystallizing, even though the presence of filler could promote strain-induced crystallization. It has been reported that the micron size particles, when they do not interact strongly with the matrix, can effectively decrease the local stress and hinder SIC.[26] Contrary to this observation, a remarkable enhancement of SIC in vulcanized NR nanocomposite under uniaxial stretching due to the presence of nanoclay has recently been reported by Carretero-González et al.[27]

In this work, we present experimental evidence of a more homogeneous NR network microstructure after the addition of nanoclay. The molecular ordering of the polymer network was evaluated by dielectric relaxation spectroscopy. The behavior of SIC was followed in situ by synchrotron radiation. It was found that platelets with a lateral size sufficiently large result in a rapid crystallization rate and different morphology when compared with the system containing small disk size or lower aspect ratio. The results indicate that the addition of nanoclay particles to NR leads to a relatively “homogeneous” distribution of networks containing several different components. In addition, the large interfacial surfaces introduced by nanoclay facilitate the overall chain orientation during deformation, resulting in an increase in final crystallite fraction.

Experimental Section

Materials. NR (CV60) sample with a Mooney viscosity (ML (1+4)) at 100 °C of 60 was supplied by Malaysian Rubber, Berhad, Malaysia. The layered silicates employed in this study were a naturally occurring sodium montmorillonite (Na^+-MMT), an organically modified montmorillonite (O-MMT), and an organically modified synthetic hectorite: laponite clay (O-LAP). All of the clay samples were provided by Southern Clays Products. The main characteristics of the clays are reported in Table 1.

Materials Preparation. The formulation of natural rubber compounds expressed as parts per hundred of rubber (phr) is as follows: sulfur (2.5), ZnO (5), stearic acid (1), MBTS (benzothiazyl disulfide) (1), antioxidant PBN (phenyl β-naphthylamine) (1), and layered silicate (15). The nanocomposite samples were prepared in an open two-roll laboratory mixing mill at room temperature. Vulcanization was carried out in an electrically heated hydraulic press at 150 °C using the optimum cure time (t_{90}) previously determined with a rubber process analyzer (RPA Alpha Technologies). The samples are referred as NR/*y*, where *y* corresponds to the type of clay used.

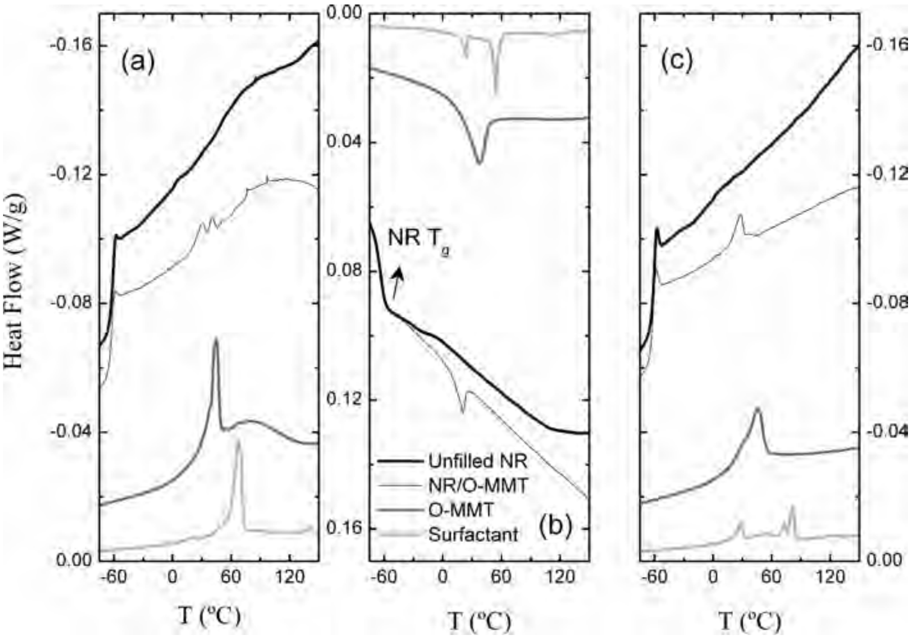

Figure 3. DSC data for (a) heat, (b) cool, (c) second heat cycles corresponding to the surfactant (light line), O-MMT (medium line), NR/O-MMT (thin line), and unfilled NR (dark line) samples.

Characterization. X-ray diffraction was performed in a $\theta-\theta$ diffractometer with an integrated germanium detector, using a Cu Kα source with a wavelength of 1.54 Å and a scan rate of 2° min^{-1}. SAXS experiments were performed on Bruker AXS Nanostar (Cu Kα 1.54 Å) operated at 40 kV and 40 mA in a transmission mode. The dispersion and morphology of the clay nanoparticles in the rubber matrix were determined through transmission electron microscopy (TEM), using a Technai T12 TEM operated at an accelerating voltage of 120 kV. TEM samples with ~40 nm thickness were prepared by sectioning at −160 °C using a Leica Ultracut UCT cryoultramicrotome with a diamond knife. The degree of curing was studied by a TA Instruments Q1000 DSC. A scanning of 4 °C/min from −100 to 165 °C and a heat/cool/heat cycle under a nitrogen atmosphere were employed to eliminate any thermal history in the sample. Dynamic-mechanical properties in the range of −150 to 150 °C were obtained using a TA Instruments Q800 DMA at 1 Hz and 2 °C/min heating rate. The average mass of network chains M_c was determined on the basis of equilibrium swelling experiments (~48 h) using toluene at 30 °C by application of the modified Flory−Rehner equation[28]

$$-\ln(1-\phi_r)-\phi_r-\chi\phi_r^{\,2}=\frac{\rho V_0}{M_c}[\phi_r^{\,1/3}-{}^{1}/_{2}\phi_r] \qquad (1)$$

where ϕ_r is the polymer volume fraction in the swollen network, V_0 is the molar volume of the solvent (106.2 mL/mol for toluene), ρ is the density of the rubber (0.92 g/mL for NR), and χ is the Flory−Huggins polymer−solvent interaction term (0.393 for NR/toluene). The number of monomers between cross-links, N_c, was calculated from V_s (mol/mL) obtained by swelling, where $N_c = \rho/M_0V_s$; $M_0 = 68$ g/mol is the molecular weight of the isoprene monomer.

Dielectric spectroscopy measurements were performed using the Novocontrol Turnkey Concept N40 broadband spectrometer[29] (Hundsangen, Germany). For dry experiments, vulcanized sample discs were mounted in the dielectric cell (ZGS Alpha Active Sample Cell) between two parallel gold-plated electrodes (BDS 1301 model). The thickness of the gold-plated electrodes was 2 mm, and the diameters were 20 mm (upper) and 30 mm (down), respectively. The sample thickness was 1 mm, and the diameter was about 15 mm. The sample/electrode assembly was then mounted in the Novocontrol Quatro Cryosystem. For swollen experiments, vulcanized swelled specimens were fitted into a sealed liquid sample cell (BDS1308 model) to prevent the solvent evaporation. This electrode spacing can be varied to adjust the cell capacity. Preliminary swelling experiments were carried out first, and the results were used to determine the optimum dimensions of the specimen inside the liquid cell. Subsequently, a dry sample with 0.5 mm thickness and ca. 5 mm diameter was used to prepare the swollen sample in the liquid cell. The final sample thickness in the swollen state was around 1 mm. Possible gaps in the liquid cell were eliminated by lowering the electrode, which also avoided the flow of the sample. Two seal rings attached to the Teflon isolation were also employed to prevent the evaporation of solvent. The sample was maintained sealed until equilibrium swelling was reached. The equilibration time for swelling was between 24 and 48 h, enabling the clear detection of different NR dipole movements. The liquid cell (introduced by the Cryosystem) was mounted in the dielectric cell using the similar procedure as in the dry measurements. Both dry and swollen dielectric experiments were carried out at 10^3 Hz from −160 to 100 °C.

In situ stress−strain experiments coupled with synchrotron X-ray diffraction were carried out at the X27C beamline in the National Synchrotron Light Source (NSLS), Brookhaven National Laboratory (BNL). The wavelength was 0.1371 nm. A coupled tensile machine (Instron) permits simultaneous mechanical and X-ray measurements. The dog-bone specimens were molded at 150 °C under 200 bar pressure. The thickness was 1 mm, and the width of the narrower zone was 0.5 cm. The deformation rate was 10 mm/min, and the experiments were carried out at room temperature. The maximum strain value was 400% due to the sample slip from the clamps. Two-dimensional WAXD patterns were recorded using a MAR CCD camera. Exposure time for each image was 30 s, and there was an interval of 5 s before the next exposure. The diffraction angle was calibrated by an Al_2O_3 standard (provided by the National Institute of Standards and Technology). The images were processed using "POLAR" software (Stony Brook Technology and Applied Research, Inc.). The crystallinity index (CI) was calculated from the integration and correction of the equatorial 2D intensity WAXD profiles at the azimuthally range of ±75° using the "peak-fit" routine. All WAXD measurements were corrected for beam fluctuations, sample absorption, and thickness variation during elongation. The calculation of the lateral crystal size was made following the protocol published elsewhere.[30] The crystallite size was estimated by using the Scherrer equation $L_{hkl} = K\lambda/(\beta \cos \theta)$, where L_{hkl} is the crystallite size in the direction perpendicular to

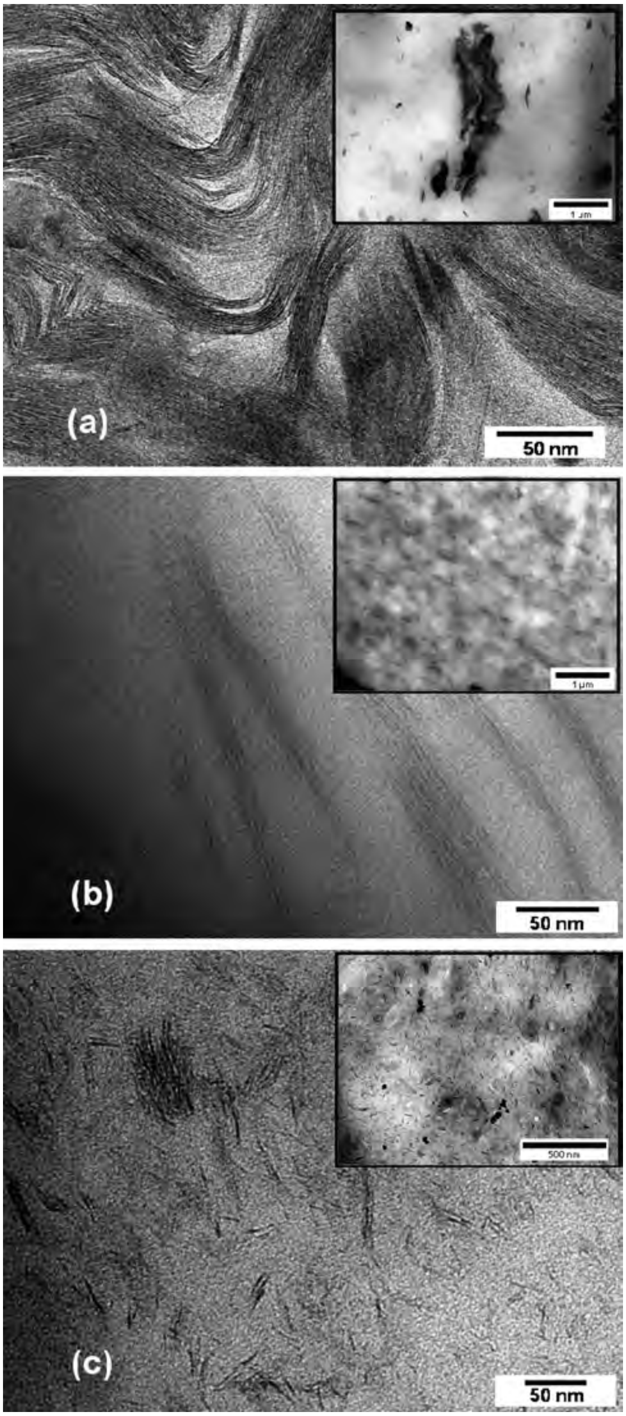

Figure 4. High-magnification TEM images for (a) NR/Na$^+$-MMT, (b) NR/O-MMT, and (c) NR/O-LAP compounds. The inset images represent the dispersion level of nanoclays at low magnification range (20K×−50K×).

the (*hkl*) plane, λ is the wavelength, and θ is the Bragg angle (half of the scattering angle). The value of K used herein was 0.89.

In-situ X-rays and deformation experiment in the simultaneous mode[31] offer the following advantages versus that in the sequential mode: (a) it makes possible to collect WAXD patterns in real time due to the high-intensity synchrotron beam, (b) it permits to follow the exact dynamics of the process, thus avoiding erroneous conclusions regarding the evolution of microscopic mechanism, and (c) it allows to monitor the mechanical response simultaneously with the structural response, enabling the mapping of structural evolution during the stress−strain curve.

Results and Discussion

The X-ray powder diffraction patterns of various NR nanocomposites and corresponding neat clays are shown in Figure 1. As expected, Na$^+$- MMT does not show any changes in the *d*-spacing upon mixing with NR (Figure 1a). This suggests the formation of a conventional composite, where the polymer is not intercalated into the clay galleries. In contrast, both *d*-spacings of O-MMT (Figure 1b, left) and O-LAP (Figure 1c, left) increase after addition of NR. The *d*-spacing value in both O-MMT and O-LAP nanocomposites is about the same, suggesting that a similar amount of polymer chains intercalate into the clay galleries. In the NR/O-LAP nanocomposite, the scattering peak was significantly broadened compared with that of the neat nanoclays, suggesting that the distribution of the particles becomes random. In contrast, sharper peaks are seen in the montmorillonite nanocomposite, suggesting good ordering is retained.

In our opinion the intercalation of the NR chains within clay layers should be related to the curatives like sulfur, accelerators, and activators and also to the cross-linking process. Figure 2 shows the WAXD patterns of cross-linked and un-cross-linked NR/O-MMT nanocomposites with and without curatives. The WAXD pattern of un-cross-linked NR containing only the O-MMT (15 phr) nanoclay particles (light line) showed a broad diffraction shoulder peak, indicating that the silicate layers remained (roughly) parallel, or no longer evenly spaced, or that the distribution of the basal distances are not so regular. On addition of the curatives, some of the clay layers collapsed decreasing the spacing between the groups of nanoclay stacks as evidenced by the appearance of higher order (00*l*) reflections (medium line). A sharper and better defined (001) reflection was evidenced after vulcanization process (shown also above in Figure 1b, right) of the nanocomposite (dark line) in comparison with that of the un-cross-linked nanocomposite (medium line). This peak suggested a larger spatial ordering of the dispersed O-MMT nanoparticles after high-temperature processing, confirming that the cross-linking reaction took place after the intercalation of the NR chains. This suggested that the curatives did not enter in the highly constrained interlayer region. Hence, the portion of the NR chains staying within the interlayer region of the nanoclay would not participate in principle in cross-linking formation. However, this issue requires further consideration.

The behavior of intercalated NR chains can also be supported by the DSC results (Figure 3). The calorimetric data indirectly revealed the effects of thermal history and interlayer organic surfactant on the intercalation processes. The quaternary alkylammonium salt exhibits an endothermic peak, corresponding to the melt transition[32] at 67 °C during the first heating (Figure 3a). The exothermic peaks at 23 and 54 °C observed during cooling (Figure 3b) correspond to the liquid-crystal phase transitions of different surfactant polymorphs. This behavior has been observed in alkyl compounds, such as triglycerides and other lipids with different crystalline forms. These compounds undergo different thermal transitions during crystallization processes.[33] In the second heating step (Figure 3c), multiple endothermic peaks are seen, which confirms the heterogeneity of the ammonium salt having different surfactant crystalline structures during the thermal cycles. Regarding the compound of O-MMT, a well-defined endothermic transitions at 45 °C and an exothermic transition at 37 °C were observed during heating (Figures 3a,c) and cooling (Figure 3b) steps, reflecting the melting and crystallization of local paraffinic packed regions, which is characteristic of 2:1 mica-type phyllosilicates modified with long alkyl chains.[34] The presence of the broad and nonreversible endothermic transition at 100 °C during initial heating (Figure 3a) of O-MMT reflected the release of physically

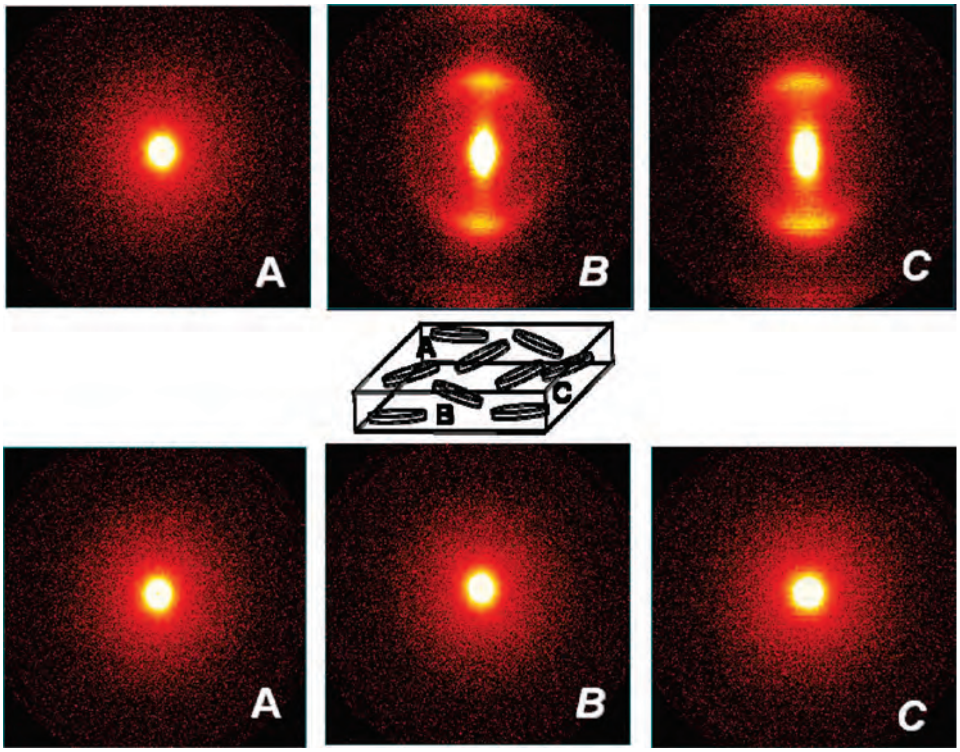

Figure 5. 2D SAXS patterns (A: face-on view; B and C: edge-on views) for the unstretched state of the nanocomposites loaded with 15 phr of nanoclay: (up) NR/O-MMT and (down) NR/O-LAP samples.

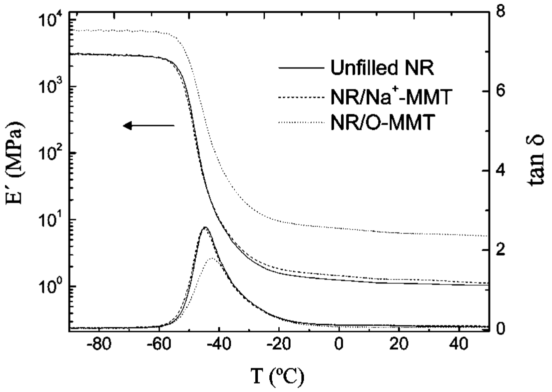

Figure 6. Temperature dependence of elastic modulus E' (left axis) and tan δ (right axis) for vulcanized unfilled NR (solid line), NR/Na$^+$-MMT (dashed line), and NR/O-MMT (dotted line) compounds.

Table 2. Weight-Average Molecular Weight, M_w (g/mol), and Polydispersity Indices, M_w/M_n, for Pristine Unmasticated NR[a] and for NR Extracted from Un-Cross-Linked NR−Nanoclay Materials after Mastication−Mixing Procedure Determined by Gel Permeation Chromatography (GPC) Analysis with THF as Eluant[a]

material	$M_w \times 10^{-4}$ (g/mol)	M_w/M_n	$V_s \times 10^{-4}$ (mol/mL)	$M_c \times 10^{-4}$ (g/mol)	N_c
unmasticated NR	70.8	5.7		2.0[b]	
unfilled NR	24.2	2.5	0.84	1.1	161
NR/Na$^+$-MMT	31.1	2.6	0.68	1.3	197
NR/O-MMT	21.5	2.5	0.96	1.0	140

[a] Cross-linking density, V_s (mol/mL), average mass of network chains, M_c (g/mol), and number of monomers between cross-links, N_c, for the cross-linked materials obtained from swelling experiments (48 h) using toluene at 30 °C are also summarized. [b] According to Elias (Elias, H. G. In *Macromolecules Structure and Properties*; Plenum Press: New York, 1977), the mass of the chains between entanglements for the pristine unmasticated NR is M_e 20 100 g/mol.

absorbed water.[34j] The presence of rubber chains inside the silicate gallery in O-MMT is evidenced via the presence of multiple endothermic peaks in NR/O-MMT nanocomposite during initial heating (Figure 3a). These transitions can be attributed to the conformational changes of surfactant packed in the gallery and to variations of molecular environment due to polymer intercalation. To our knowledge, this is the first report that the use of DSC can trace the polymer intercalation through the thermal transitions of interlayer alkyl surfactant instead of following the intercalated polymer transitions.[35] The pronounced shifts of the exothermic (35 to 21 °C) and endothermic (45 to 27 °C) peaks, corresponding to the crystallization (Figure 3b) and melting (Figure 3c) of organic surfactant in the gallery, respectively, in comparison with the unintercalated state, can be attributed to the disordering of the crystal structure of alkyl chains (e.g., loss of crystal symmetry) and the changes on interlayer packing density created by the penetration of NR chains. Finally, vulcanized NR materials exhibited a near constant secondary transition at −58 °C, which was due to the glass transition temperature of the polymer network.

The TEM images of various nanocomposite systems are shown in Figure 4. A highly inhomogeneous and aggregated microstructure is seen in the system of NR/Na$^+$-MMT (inset, Figure 4a). Both XRD and TEM results suggest that NR/Na$^+$-MMT forms a conventional composite system. In contrast, the presence of finely dispersed and intercalated tactoids (nanoclay stacks) spaced 10−40 nm apart was seen in the systems of O-MMT (Figure 4b) and O-LAP (Figure 4c). However, it is interesting to note that there is some difference in the orientation of the clay particles: a highly oriented distribution of O-MMT nanoparticles is seen (Figure 4b) while a much more isotropic distribution is present for O-LAP (Figure 4c).

Small-angle X-ray scattering (SAXS) provides microstructure information about the distribution of clay particles in the NR matrix. In agreement with the TEM results, the SAXS analysis (A: face-on view; B and C: edge-on views) shows that the O-MMT clay particles are more preferrentially aligned than

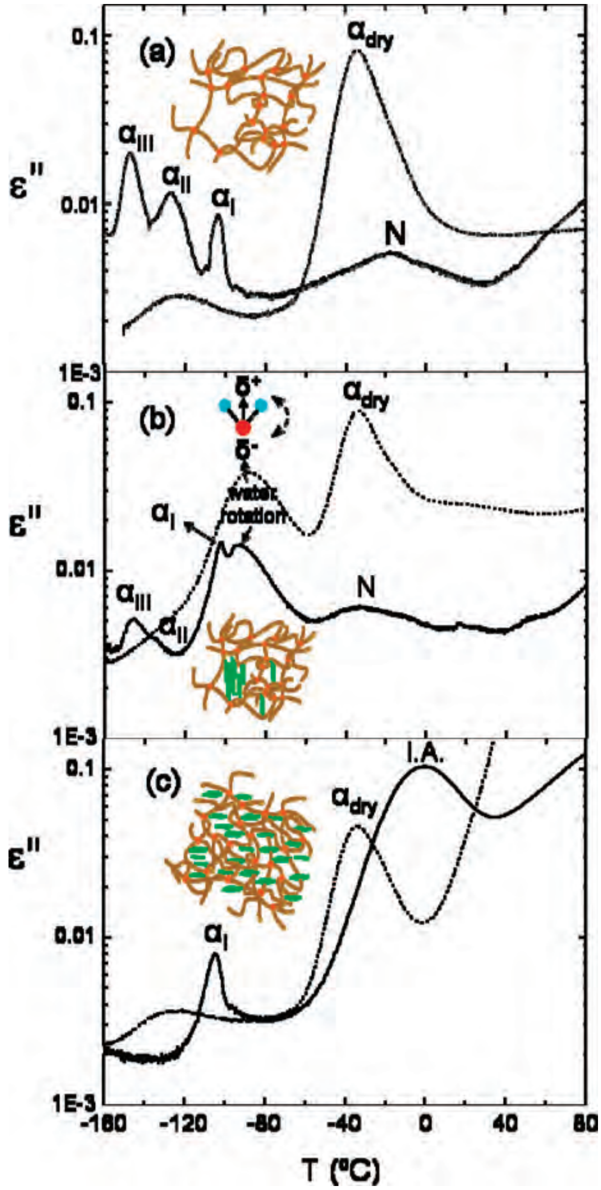

Figure 7. Temperature dependence of ε'' at 10^3 Hz for dry (dashed line) and swollen (solid line) cross-linked NR networks, corresponding to (a) unfilled NR, (b) NR/Na$^+$-MMT, and (c) NR/O-MMT samples. Ideal microstructure including the network points distribution and the layered clay dispersion on the NR matrix are schematically represented in the inset of each graph.

O-LAP. Because of the platy character of the O-MMT clay particles, the edge-on view of the O-MMT-based nanocomposites exhibited a highly anisotropic pattern (top patterns in Figures 5B,C) due to the particle orientation parallel to the plane of the sample. In contrast, the face-on view leads to an isotropic pattern (top Figure 5A) due to the random distribution of the particles with respect to the in-plane direction. In addition, the nanocomposites based on NR with unmodified clay (data not shown) or O-LAP (Figure 5, bottom diagram) also showed an isotropic distribution of the clay particles. The difference between O-MMT and O-LAP can be attributed to the differences in the aspect ratio (the ratio between the lateral dimension and the thickness) of the particle. The larger aspect ratio of MMT particles leads to higher orientation than LAP clays with the smaller aspect ratio.

The effect of dispersion of organically modified layered silicate particles on the viscoelastic properties of the vulcanized NR matrix was studied by DMA, where the dynamic properties of neat NR and NR composites were examined over a wide temperature range (−130 to 50 °C). The storage modulus and tan δ as a function of temperature are shown in Figure 6. It was found that the addition of Na$^+$-MMT did not change the properties of NR. However, an increase in the modulus and a shift in the T_g to higher temperatures compared to pure NR were seen in the O-MMT-based nanocomposite. Since the results from calorimetric analysis (Figure 3) and swelling measurements (Table 2) indicate that the organoclay does not affect the extent of curing, the increase in modulus can be attributed to (a) the hydrodynamic effect of the clay and (b) the formation of physical cross-links due to the presence of clay. On the other hand, the shift in T_g implies a strong interaction between the filler and the matrix, which results in a reduction of the mobility of the polymer chains in the presence of the clay.

Effects of nanoclay on the microstructural network, topological constrain and nonelastically active components of NR have been studied by dielectric spectroscopy. The existence of the dielectric moment on *cis*-poly(isoprene) with two components[36] allows us to monitor two kinds of relaxation modes: one related to the local segmental motion (the segmental mode) and another (slower motion) related to the breathing of the whole chain (the normal mode). Consequently, *cis*-poly(isoprene) can be viewed as a model system to study the dynamics of relaxation modes of entangled[37] or dilute[38] NR and dry cross-linked rubber networks.[39] Figure 7 shows the dielectric loss (ε'') over a wide range of temperatures at the fixed frequency of 10^3 Hz. The dashed and solid lines represent the dry and swollen systems, respectively, for (a) unfilled NR, (b) NR/Na$^+$-MMT, and (c) NR/O-MMT nanocomposites.

Dry vulcanized NR shows a main peak at −34 °C, which can be assigned to the segmental relaxation (α_{dry}), and the secondary relaxations at low temperatures (below T_g) can be assigned to the localized motion in the glassy state. No significant change on the molecular dynamics by the addition of nanoparticles in the bulk state has been observed. The presence of the extra relaxation mode at −80 °C in NR/Na$^+$-MMT nanocomposite (Figure 7b) is most likely due to the electric dipole rotations of the absorbed water in the silicate gallery.[40] However, in the swollen samples, the physical constrains present in the dry samples are no longer effective because of the slippage of the entanglements.[41] Thus, the swelling process induces the occurrence of a low-frequency transition, and a broad normal mode, *N*, due to the much faster chain dynamics. In addition, three narrow distributions of segmental relaxation times, corresponding to the motions of transversal dipoles—α_I (−100 °C), α_{II} (−130 °C), α_{III} (−145 °C)—were also observed in both neat NR (Figure 7a) and NR/Na$^+$-MMT composite (Figure 7b). However, the NR/O-MMT swollen nanocomposite (Figure 7c) shows only one main dipole distribution, which is related to the segmental motion at −100 °C (α_I). It is conceivable that microscale segmental variations due to the distribution of different network components (topological constraints and defects) yield a more homogeneous distribution of transversal dipole domains for the NR/O-MMT nanocomposite. Since all the samples exhibit similar molecular characteristics (i.e., molecular weight (M_w) and polydispersity (M_w/M_n)) before and after processing (see Table 2), the variations on the network microstructure cannot be solely attributed to these molecular variables. Such a difference can best be explained by the presence of a larger amount of dangling end chains, loops, long tail chains, and un-cross-linked chains in neat NR and NR/Na$^+$-MMT samples compared to that in NR/O-MMT. The presence of the long tail components with high mobility has also been observed by NMR studies of swollen cross-linked NR samples.[42] It has been proposed that these components contribute to a larger amount of network defects

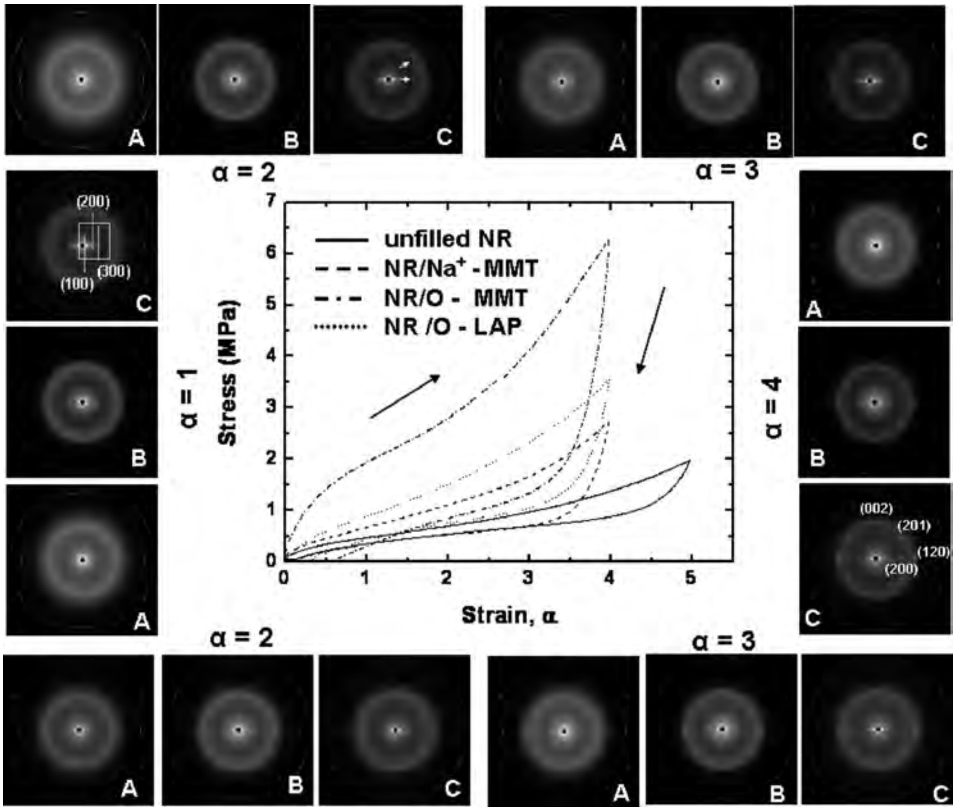

Figure 8. Stress−strain curves and selected synchrotron WAXD patterns during extension and retraction cycles for the chosen samples. The corresponding stress−strain curve for the NR/O-LAP nanocomposites is included for comparison. 2D WAXD patterns for (A) the unfilled NR, (B) NR/Na$^+$-MMT, and (C) NR/O-MMT are illustrated at selected strains.

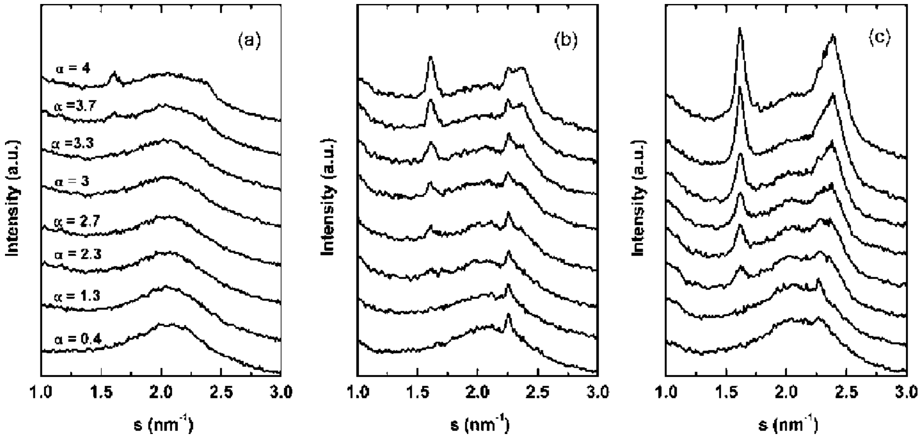

Figure 9. Normalized and corrected linear diffraction profiles for (a) unfilled NR, (b) NR/Na$^+$-MMT, and (c) NR/O-MMT samples. The strain-induced crystallization (SIC) was evidenced by (200) and (120) reflections from the NR. The samples containing the silicate showed an extra diffraction peak at high *s* values corresponding to the layered silicate. This peak did not affect to the crystallinity index calculation.

in the NR matrix and manifest themselves in the presence of an extra and highly mobile region in the loss curve.

The addition of nanoclay in NR appeared to provide a relatively more regular polymer network microstructure, although consisting of several different components. This regular microstructure was attributed both to the presence of a larger amount of shorter network points (physical and chemical) homogeneously distributed and to the high number of interactions between the NR chains and the nanoclay. These interactions would not be present in the unfilled NR matrix or conventional NR composites with poor particle distribution as in those based on unmodified NR/Na$^+$-MMT. The normal mode of the NR/O-MMT nanocomposite overlaps with the dipole distribution due to the NR chains adsorbed on the outer surface of the nanoclay particles (IA: interfacially adsorbed polymer). Further studies of physically adsorbed polymer on the modified nanoclay surface of NR nanocomposites by dielectric spectroscopy are underway and will be published elsewhere.

Figure 8 shows the stress−strain behavior (during stretching and recovery) for unfilled NR (solid line), NR/Na$^+$-MMT (dashed line), NR/O-MMT (dot-dotted line), and NR/O-LAP (dotted line) nanocomposites. WAXD patterns at different strain ratio (α) are also inserted for the unfilled NR (A), NR/Na$^+$-MMT (B), and NR/O-MMT (C) samples as a useful guide to follow the variation of crystallization under stretching. Images corresponding to NR/O-MMT nanocomposites exhibit preferred orientations of (100), (200), and (300) reflections from the nanoclays upon stretching. It is seen that oriented nanoclay reflection peaks (C images) begin to appear at a relatively low strain ($\alpha < 1$). The intensities of these reflections increase with

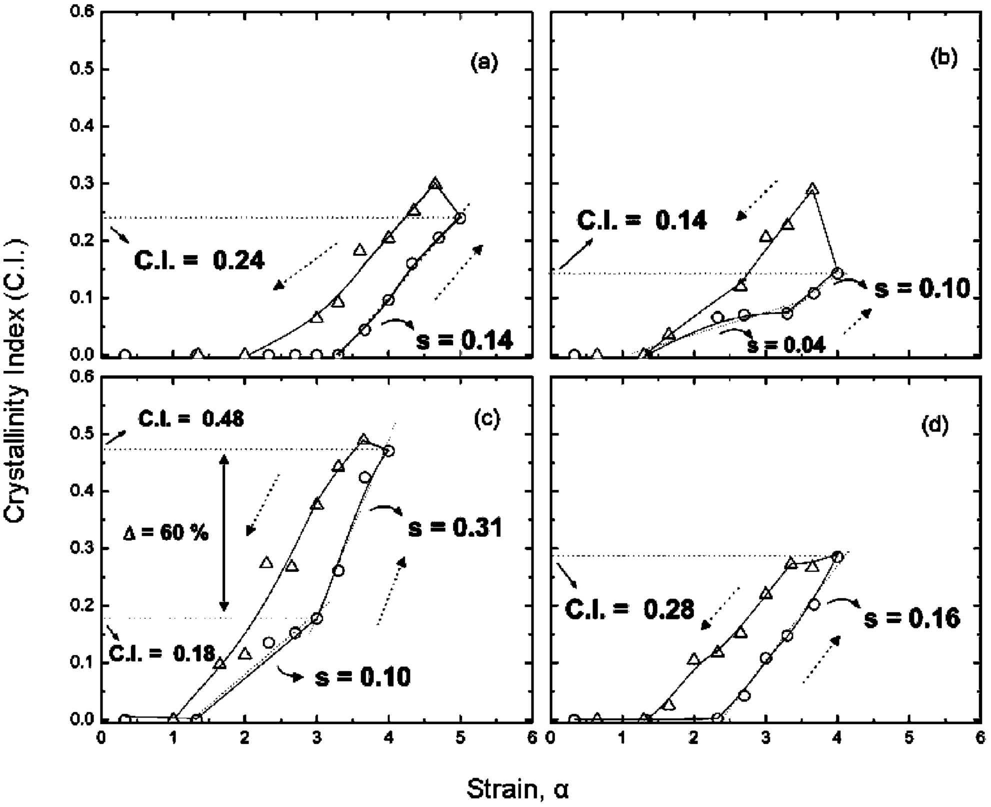

Figure 10. Crystallinity index (CI) as a function of strain during the stretch−recovery cycle for (a) unfilled NR, (b) NR/Na$^+$-MMT, (c) NR/O-MMT, and (d) NR/O-LAP samples. The solid line is only a guide to the eye.

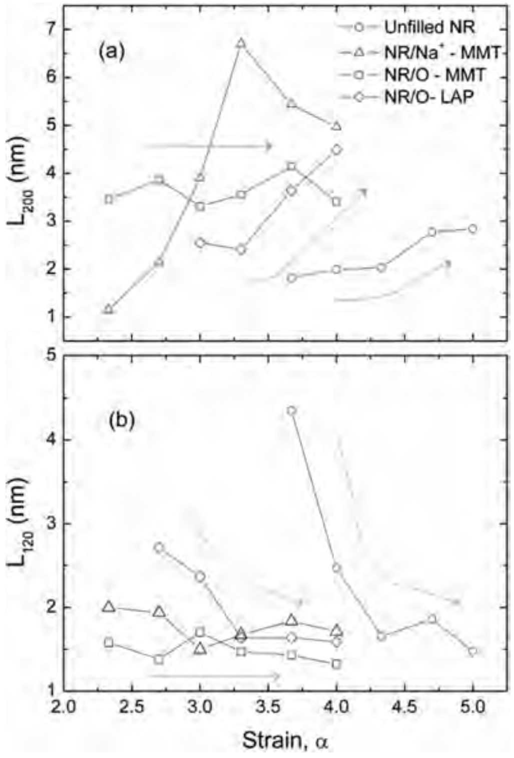

Figure 11. Variations of the lateral crystallite size with strain determined from (a) the 200 (L_{200}) and (b) 120 (L_{120}) reflections during the stretching process (arrows indicate the stretching process).

strain during stretching until a maximum alignment is reached (at $\alpha = 4$). The stress−strain curves show a hysteresis, which was also found in pure vulcanized NR.[30,43] This hysteresis corresponds with the different appearance in the WAXD images collected simultaneously during the tensile test. It has been reported that a dramatic deviation from the behavior of rubber elasticity can take place with the increase of strain,[44] which is seen in the NR/O-MMT nanocomposite. It is interesting to note that the hysteresis cycle is higher for the NR/O-MMT sample than the rest of the samples. In addition, crystal reflections (in WAXD images) of unfilled NR appear at a higher strain than those for the NR/Na$^+$-MMT and NR/O-MMT samples. No evidence of orientation in the amorphous phase has been made based on the WAXD analysis. If there was any oriented amorphous phase, the total fraction must be small. This finding is in contrast with the study by Rault et al.,[24c,d] who have reported orientation of the amorphous phase using H NMR. The degree of crystallization is clearly evidenced from the normalized and corrected linear diffraction profiles as shown in Figure 9.

Figure 10 shows the evolution of crystallinity index (CI) with strain for the chosen samples, which all show a significant hysteresis cycle as in the stress−strain curves in Figure 8. Contrary to the stress values during the stretching−recovery cycle, the CI values are larger during the recovery processes than those during the stretching. This behavior can be explained by the formation of different types of strain-induced crystallites, which has been reported earlier. For example, Andrews et al.[45] suggested a variety of induced-crystallization stages in NR at different strains: spherulitic forms (0−50%), row-nucleated shish-kebabs (100−200%), and extended chain crystals (>400%).

The onset strain for crystallization ($\alpha°$) was determined by the interception of the regression line (dotted line) in the plot of CI against α (Figure 10). In the unfilled NR sample (Figure 10a), the highest $\alpha°$ value observed is in concordance that reported in the previous studies.[31,43] The lowest $\alpha°$ value for NR/Na$^+$-MMT (Figure 10b) and NR/O-MMT (Figure 10c) samples were found to be 1.4 and 1.2, respectively. For NR/O-LAP sample (Figure 10d), the $\alpha°$ value was 2.3, which is also in good agreement with the reported values for NR filled with carbon black,[24a,c,d] calcium carbonate,[24b] and silica.[24e] Regarding the overall CI in NR/O-MMT and NR/O-LAP, the values were significantly higher than those in the rest samples. For unfilled NR (Figure 10a), the maximum CI was 25% at a strain $\alpha = 5$. The highest CI value during the stretching process was found in NR/O-MMT nanocomposite; CI = 48% at a strain $\alpha = 4$ (Figure 9c). For NR/Na^+-MMT and NR/O-LAP samples at $\alpha = 4$, the maximum in CI was 14% and 28%, respectively. It is evidenced that the aspect ratio of the layered silicate particles plays a key role on the apparition of the first crystallites as well as on the final crystalline content during the deformation of the materials.

This effect was also reflected on the strain-induced crystallization mechanism of the chosen nanocomposite samples. While for the unfilled NR (Figure 10a) and the NR/O-LAP (Figure 10d), a single crystallization step during the stretched and recovery stages was detected, a well-defined dual crystallization mechanism was evidenced for the NR/O-MMT (Figure 10c) and NR/Na^+-MMT nanocomposite (Figure 10b) samples. As can be observed in Figure 4a, the NR/Na^+-MMT composite contains single nanoclay platelets (in addition to tactoids) from the delamination process of the micron size silicate particles. This may be the reason for the change in the crystallization rate and the corresponding nearly equal crystallization onset values. Therefore, the first step at $\alpha < 3$ is probably related to the orientation and alignment of highly anisotropic nanoclay particles, while in the second step ($3 \leq \alpha \leq 4$), these highly anisotropic nanoparticles are completely aligned along the direction of the deformation forming a physical network. This physical network would favor the alignment of the NR chain and thus the crystallization rate increase. This behavior was absent in the NR/O-LAP nanocomposite (Figure 10d), where a single crystallization step exhibiting a slope value similar to that of unfilled NR due to lower anisotropy exhibited by the O-LAP nanoparticles in the NR matrix in comparison with that of the O-MMT. Although the crystallization rate in NR/O-MMT is about 2 times more than the rest of the samples, there was no clear relationship between the slope values and the final crystalline content. This implies that some other effects such as crystal morphology may also play a role.

To clarify this hypothesis, the variation of lateral dimension in the crystal during deformation was analyzed. Figure 11 shows the variations of the crystallite size estimated from the 200 and 120 reflections. Interestingly, L_{200} (Figure 11a) and L_{120} (Figure 11b) showed an opposite trend (i.e., the lateral dimension along 200 direction increased while along 120 direction decreased) for all the samples except for NR/O-MMT, where the lateral size dimensions calculated along these two directions were almost unchanged. From these results, we suggest that the morphology of the crystallites formed in the NR/O-MMT nanocomposites under elongation is somewhat different from those formed in the rest of the samples.

Conclusions

The influence of nanoclay on the morphological and microstructural changes of NR network has been analyzed by dielectric spectroscopy and synchrotron wide-angle X-ray diffraction. It is clear that the polymer intercalation can be evidenced through the thermal transitions of the interlayer alkyl surfactant from DSC traces. The inclusion of highly anisotropic nanoparticles leads to microscale segmental variations, in fact, giving rise to the formation of a relatively homogeneous network structures in rubber. The presence of *extra* dipole distribution corresponding to more mobile components which are responsible for the network imperfections can be significantly reduced by addition of the organoclay. Moreover, the presence of strong interfacial adhesions between nanoparticles−rubber matrix can induce an early promotion and enhancement of overall crystallization of NR chains under uniaxial stretching. Furthermore, high anisotropic nanoclay particles induce a crystalline morphology different from those by silicates with lower aspect ratio. The interplay between all of these parameters could explain why the reinforcing effects in NR/clay nanocomposites are manifested at low filler loadings.

Acknowledgment. The authors gratefully acknowledge the financial support of the Spanish Ministry of Science and Innovation (MICINN) through project MAT 2004-00825. This work made use of the Cornell Center for Materials Research Experimental Facilities. Additionally, J. Carretero-González acknowledges support from MICINN in the form of a FPI grant, R. Verdejo a Juan de la Cierva contract from MICINN, and B. S. Hsiao is supported by the National Science Foundation (DMR-0405432).

References and Notes

(1) (a) Bateman, L. *The Chemistry and Physics of Rubber-like Substances*; MacLaren & Sons: London, 1963. (b) Roberts, A. D. *Natural Rubber Science and Technology*; Oxford University Press: Oxford, 1988. (c) Mark, J. E.; Erman, B.; Eirich, F. R. *Science and Technology of Rubber*; Academic Press: San Diego, 1994. (d) Gent, A. N. *Engineering with Rubber, How to Design Rubber Components*; Carl Hanser Verlag: Munich, 2001. (e) White, J. R.; De, S. K. *Rubber Technologist's Handbook*; Rapra Technology: Shawbury, Shrewsbury, Shropshire, 2001.

(2) (a) Tanaka, Y. *Rubber Chem. Technol.* **2001**, *74*, 355. (b) Karino, T.; Ikeda, Y.; Yasuda, Y.; Kohjiya, S.; Shibayama, M. *Biomacromolecules* **2007**, *8*, 693.

(3) (a) Toki, S.; Sics, I.; Hsiao, B. S.; Amnuaypornsri, S.; Kawahara, S. Strain-induced crystallization in un-vulcanized natural rubbers by synchrotron X-ray study. Submitted to Journal. (b) Amnuaypornsri, S.; Toki, S.; Hsiao, B. S.; Sakdapipanich, J.; Tanaka, Y. Strain-induced crystallization of un-vulcanized natural rubber: effect of proteins and phospholipids. Submitted to Journal.

(4) (a) Flory, P. J. *J. Chem. Phys.* **1947**, *15*, 397. (b) Mandelkern, L. *Rubber Chem. Technol.* **1993**, *66*, G61. (c) Magill, J. H. *Rubber Chem. Technol.* **1995**, *68*, 507. (d) Toki, S.; Fujimaki, T.; Okuyama, M. *Polymer* **2000**, *41*, 5423.

(5) Takahashi, Y.; Kumano, T. *Macromolecules* **2004**, *37*, 4860.

(6) Kraus, G. *Reinforcement of Elastomers;* Wiley-Interscience: New York, 1965.

(7) Toki, S.; Minouchi, N.; Sics, I.; Hsiao, B. S.; Kohjiya, S. *Kautschuk Gummi Kunststoffe* **2008**, *61*, 85.

(8) Vaia, R. A.; Maguirre, J. F. *Chem. Mater.* **2007**, *19*, 2736.

(9) For comprehensive reviews on polymer−clay nanocomposites the reader is referred to: (a) Giannelis, E. P. *Adv. Mater.* **1996**, *8*, 29. (b) Giannelis, E. P.; Krishnamoorti, R.; Manias, E. *Adv. Polym. Sci.* **1999**, *138*, 107. (c) Pinnavaia, T. J.; Beall, G. W. *Polymer-Clay Nanocomposites*; John Wiley & Sons: New York, 2000. (d) Alexandre, M.; Dubois, P. *Mater. Sci. Eng.* **2000**, *28*, 1. (e) Ray, S. S.; Okamoto, M. *Prog. Polym. Sci.* **2003**, *28*, 1539. (f) Zhang, Q. H.; Yu, A. B.; Lu (Max) , G. Q.; Paul, D. R. *J. Nanosci. Nanotechnol.* **2005**, *10*, 1574. (g) Okada, A.; Usuki, A. *Macromol. Mater. Eng.* **2006**, *291*, 1449. (h) Winey, K. I.; Vaia, R. A. *MRS Bull.* **2007**, *32*, 314.

(10) (a) Arroyo, M.; López-Manchado, M. A.; Herrero, B. *Polymer* **2003**, *44*, 2447. (b) López-Manchado, M. A.; Herrero, B.; Arroyo, M. *Polym. Int.* **2003**, *52*, 1070. (c) López-Manchado, M. A.; Herrero, B.; Arroyo, M. *Polym. Int.* **2004**, *53*, 1766. (d) López-Manchado, M. A.; Valentín, J. L.; Carretero, J.; Barroso, F.; Arroyo, M. *Eur. Polym. J.* **2007**, *43*, 4143.

(11) Vaia, R. A. *Mater. Today* **2004**, *7*, 32.

(12) (a) Heinrich, G.; Klüppel, M.; Vilgis, T. A. *Curr. Opin. Solid State Mater. Sci.* **2002**, *6*, 195. (b) Vilgis, T. A. *Polymer* **2005**, *46*, 4223.

(13) Wang, M. J. *Rubber Chem. Technol.* **1998**, *71*, 520.

(14) Payne, A. R. *J. Appl. Polym. Sci.* **1962**, *19*, 57.

(15) Vu, Y. T.; Mark, J. E.; Pham, H. L.; Engelhardt, M. *J. Appl. Polym. Sci.* **2001**, *82*, 1391.

(16) (a) Meissner, B. *J. Appl. Polym. Sci.* **1974**, *18*, 2483. (b) Vilgis, T. A.; Heinrich, G. *Macromolecules* **1994**, *27*, 7849. (c) Karásek, L.; Sumita, M. *J. Mater. Sci.* **1996**, *31*, 281. (d) Leblanc, J. L. *J. Appl. Polym. Sci.* **1997**, *66*, 2257. (e) Huber, G.; Vilgis, T. A. *Eur. Phys. J. B* **1998**, *3*, 217. (f) Karásek, L.; Meissner, B. *J. Appl. Polym. Sci.* **1998**, *69*, 95. (g) Klüppel, M. *Adv. Polym. Sci.* **2003**, *164*, 1. (h) Chervanyov, A. I.; Heinrich, G. *J. Chem. Phys.* **2006**, *125*, 084703. (i) Gusev, A. A. *Macromolecules* **2006**, *39*, 5960.

(17) (a) Gersappe, D. *Phys. Rev. Lett.* **2002**, *89*, 058301. (b) Sheng, N.; Boyce, M. C.; Parks, D. M.; Rutledge, G. C.; Abes, J. I.; Cohen, R. E. *Polymer* **2004**, *45*, 487. (c) Shah, D.; Maiti, P.; Jiang, D. D.; Batt, C. A.; Giannelis, E. P. *Adv. Mater.* **2005**, *17*, 525. (d) Tong, H. Z.; Wen, H. R.; Min, Z. R.; Min, Q. Z.; Yu, L. M. *Adv. Mater.* **2007**, *19*, 2667.

(18) Reichert, W. F.; Göritz, D.; Duschl, E. J. *Polymer* **1993**, *34*, 1216.

(19) Flory, P. J. *Chem. Rev.* **1944**, *35*, 51.

(20) Mark, J. E.; Erman, B. *Rubberlike Elasticity A Molecular Primer*; Wiley: New York, 1988.

(21) Flory, P. J. *Principles of Polymer Chemistry*, Cornell University Press: Ithaca, NY, 1953.

(22) (a) Mitchell, J. C.; Meier, D. J. *J. Polym. Sci., Part A* **1968**, *6*, 1689. (b) Tosaka, M.; Senoo, K.; Kohjiya, S.; Ikeda, Y. *J. Appl. Phys.* **2007**, *101*, 084909.

(23) (a) Gent, A. N. *Trans. Faraday Soc.* **1954**, *50*, 521. (b) Gent, A. N. *J. Polym. Sci.* **1955**, *18*, 321.

(24) (a) Trabelsi, S.; Albouy, P. A.; Rault, J. *Macromolecules* **2003**, *36*, 9093. (b) Poompradub, S.; Tosaka, M.; Kohjiya, S.; Ikeda, Y.; Toki, S.; Sics, I.; Hsiao, B. S. *J. Appl. Phys.* **2005**, *97*, 103529. (c) Rault, J.; Marchal, J.; Judeinstein, P.; Albouy, P. A. *Eur. Phys. J. E* **2006**, *21*, 243. (d) Rault, J.; Marchal, J.; Judeinstein, P.; Albouy, P. A. *Macromolecules* **2006**, *39*, 8356. (e) Chenal, J. M.; Gauthier, C.; Chazeau, L.; Guy, L.; Bomal, Y. *Polymer* **2007**, *48*, 6893.

(25) Karásek, L.; Sumita, M. *J. Mater. Sci.* **1996**, *31*, 281.

(26) Reichert, W. F.; Hopfenmüller, M. K.; Göritz, D. *J. Mater. Sci.* **1987**, *22*, 3470.

(27) Carretero-González, J.; Verdejo, R.; Toki, S.; Hsiao, B. S.; Giannelis, E. P.; López-Manchado, M. A. *Macromolecules* **2008**, *41*, 2295.

(28) Flory, P. J. *J. Chem. Phys.* **1950**, *18*, 108.

(29) http://www.novocontrol.de(Novocontrol Technologies GmbH & Co. KG., Germany).

(30) Tosaka, M.; Murakami, S.; Poompradub, S.; Kohjiya, S.; Iheda, Y.; Toki, S.; Sics, I.; Hsiao, B. S. *Macromolecules* **2004**, *37*, 3299.

(31) (a) Murakami, S.; Senoo, K.; Toki, S.; Kohjiya, S. *Polymer* **2002**, *43*, 2117. (b) Trabelsi, S.; Albouy, P. A.; Raoult, J. *Macromolecules* **2003**, *36*, 7624.

(32) Kodama, M.; Kawasaki, Y.; Aoki, H.; Yamamoto, E.; Furukawa, Y. In *Recent Research Developments in Chemistry & Physics of Lipids*, 1st ed.; Pandalai S. G., Ed.; Transworld Research Network: Trivandrum, 2003; Vol. *1*, pp 85−98.

(33) Small, D. M. *The Physical Chemistry of Lipids: From Alkanes to Phospholipids; Handbook for Lipid Research 4*; Plenum Press: New York, 1986; pp 362−369.

(34) (a) Theng, B. K. G. *Formation and Properties of Clay-Polymer Complexes*; Amsterdam: Elsevier, 1979. (b) Lagaly, G. *Solid State Ionics* **1986**, *22*, 43. (c) Vaia, R. A.; Teukolsky, R. K.; Giannelis, E. P. *Chem. Mater.* **1994**, *6*, 1017. (d) Xie, W.; Gao, Z.; Pan, W. P.; Hunter, D.; Singh, A.; Vaia, R. A. *Chem. Mater.* **2001**, *13*, 2979. (e) Osman, M. A.; Ernst, M.; Meier, B. H.; Suter, U. W. *J. Phys. Chem. B* **2002**, *106*, 653. (f) Heinz, H.; Suter, U. W. *Angew. Chem., Int. Ed.* **2004**, *43*, 2239. (g) Zhu, J.; He, H.; Zhu, L.; Wen, X.; Deng, F. *J. Colloid Interface Sci.* **2005**, *286*, 239. (h) Heinz, H.; Koerner, H.; Anderson, K. L.; Vaia, R. A.; Farmer, B. L. *Chem. Mater.* **2005**, *17*, 5658. (i) He, H.; Ding, Z.; Zhu, J.; Yuan, P.; Xi, Y.; Yang, D.; Frost, R. L. *Clays Clay Miner.* **2005**, *53*, 287. (j) Jacobs, J. D.; Koerner, H.; Heinz, H.; Farmer, B. L.; Mirau, P.; Garrett, P. H.; Vaia, R. A. *J. Phys. Chem. B* **2006**, *110*, 20143. (k) Heinz, H.; Vaia, R. A.; Krishnamoorti, R.; Farmer, B. L. *Chem. Mater.* **2007**, *19*, 59.

(35) (a) Vaia, R. A.; Ishii, H.; Giannelis, E. P. *Chem. Mater.* **1993**, *5*, 1694. (b) Vaia, R. A.; Jandt, K. D.; Kramer, E. J.; Giannelis, E. P. *Chem. Mater.* **1996**, *8*, 2628.

(36) (a) Stockmayer, W. H.; Baur, M. E. *J. Am. Chem. Soc.* **1964**, *86*, 3485. (b) Kremer, F.; Schönhals, A. *Broadband Dielectric Spectroscopy*; Spinger-Verlag: Berlin, 2003. (c) Strobl, G. The Physics of Polymers. *Concepts for Understanding their Structures and Behaviour*; Springer-Verlag: Berlin, 1997.

(37) (a) Adachi, K.; Kotaka, T. *Macromolecules* **1984**, *17*, 120. (b) Adachi, K.; Kotaka, T. *Macromolecules* **1985**, *18*, 466. (c) Boese, D.; Kremer, F.; Fetters, L. J. *Polymer* **1990**, *31*, 1831.

(38) Adachi, K.; Kotaka, T. *Macromolecules* **1987**, *20*, 2018.

(39) (a) Poh, B. T.; Adachi, K.; Kotaka, T. *Macromolecules* **1987**, *20*, 2574. (b) Donth, E.; Beiner, M.; Reissig, S.; Korus, J.; Garwe, F.; Vieweg, S.; Kahle, S.; Hempel, E.; Schröter, K. *Macromolecules* **1996**, *29*, 6589.

(40) Calvet, R. *Clays Clay Miner.* **1975**, *23*, 257.

(41) Saalwächter, K.; Herrero, B.; López-Manchado, M. A. *Macromolecules* **2005**, *38*, 9650.

(42) Grinberg, F.; Garbarczyk, M.; Kuhn, W. *J. Chem. Phys.* **1999**, *24*, 11222.

(43) Toki, S.; Sics, I.; Ran, S.; Liu, L.; Hsiao, B. S.; Murakami, S.; Senoo, K.; Kohjiya, S. *Macromolecules* **2002**, *35*, 6578.

(44) Treloar, L. R. G. *The Physics of Rubber Elasticity*, 3rd ed.; Clarendon Press: Oxford, UK, 1975.

(45) Andrews, E. H.; Owen, P. J.; Singh, A. *Rubber Chem. Technol.* **1972**, *45*, 1315.

MA800893X

European Polymer Journal 44 (2008) 3493–3500

Contents lists available at ScienceDirect

European Polymer Journal

journal homepage: www.elsevier.com/locate/europolj

Natural rubber/clay nanocomposites: Influence of poly(ethylene glycol) on the silicate dispersion and local chain order of rubber network

J. Carretero-González [a], J.L. Valentín [a,b], M. Arroyo [a], K. Saalwächter [b], M.A. Lopez-Manchado [a,*]

[a] *Institute of Polymer Science and Technology, CSIC, Madrid 28006, Spain*
[b] *Institut für Physik, Martin-Luther-Universität Halle-Wittenberg, Halle 06108, Germany*

ARTICLE INFO

Article history:
Received 4 March 2008
Received in revised form 30 July 2008
Accepted 22 August 2008
Available online 12 September 2008

Keywords:
Natural rubber
Montmorillonite
Poly(ethylene glycol)
Time-domain NMR
Multiple-quantum NMR

ABSTRACT

A novel preparation of natural rubber (NR)/Na^+–montmorillonite (MMT) nanocomposites in only one step by using poly(ethylene glycol) (PEG) has been investigated. PEG behaves as dispersing agent favouring the intercalation of rubber chains into the silicate galleries and providing substantially improved clay dispersion. Intercalated/exfoliated miscible hybrids were observed by X-ray diffraction (XRD) and transmission electron microscopy (TEM). The influence of PEG on the network structure has also been evaluated by static proton double-quantum nuclear magnetic resonance spectroscopy (^{1}H DQ NMR) at low-field. Silicate nanoparticles with a high aspect ratio (clay tactoids) and a more crosslinked rubber network have been obtained for an optimum PEG/MMT ratio. Both effects were responsible of the enhancement on mechanical properties.

1. Introduction

From the middle of the 90s decade to nowadays, the field of polymer/layered-silicate nanocomposites has experienced an enormous academic development due to their significant enhanced properties in relation to conventional composites [1–7]. However, the acceptance of these promising materials at the industrial level has not yet reached the expectations. A wide-spread use of nanocomposites will be only reached if they are introduced in automotive and packaging applications with commodity polymers such as polyolefins or elastomers [8].

Natural rubber (NR)-organoclay nanocomposites with intercalated, exfoliated or mixed systems have been successfully prepared by several processing techniques, such as vulcanization curing process [9–17], solution blending [18,19] or latex compounding [20–24]. These systems exhibit improved mechanical, thermal and barrier properties. For instance, Arroyo et al. [11] when comparing the organoclay with carbon black as fillers for NR, observed that at similar filler contents the reinforcing effect of the organoclay is more noticeable. Indeed, it was necessary to add four times more of carbon black to obtain similar mechanical properties (modulus at several elongations, maximum strength) as the composite with only 10 phr (parts per hundred of rubber) organoclay. However, high carbon black loadings gave rise to a marked loss in the elastic behaviour of the NR compounds, whilst the organoclay retains the elasticity of the material.

All these studies have been carried out with organoclays, i.e. clays modified chemically by ion exchange reaction with quaternary ammonium salts known as organophilization reaction [25,26]. That is, NR is incompatible with pristine clay, and then, a previous organic treatment of the layered silicate is required to obtain a fine dispersion into the polymer matrix. But, this process dramatically increases the prize of the final material limiting its application at industrial level.

For this reason, great deals of efforts are conducted to find alternative strategies in the manufacturing of polymer nanocomposites removing the organophilization reaction. Moad et al. [27] prepared clay-poly(propylene) (PP) nanocomposites by direct melt mixing from sodium

---

* Corresponding author. Tel.: +34 91 2587424; Fax: +34 91 564 4853.
E-mail address: lmanchado@ictp.csic.es (M.A. Lopez-Manchado).

0014-3057/$ - see front matter © 2008 Elsevier Ltd. All rights reserved.
doi:10.1016/j.eurpolymj.2008.08.046

montmorillonite (MMT) with poly(ethylene oxide)-based non-ionic surfactants as dispersing/intercalating/exfoliating agents. The addition of these surfactants with different molecular "*architecture*", chemical composition and chain length of the PEO-blocks, favoured the breaking down of the clay agglomerates to tactoids providing a partially exfoliated structure. This led to a significant improvement of the mechanical and thermal properties of the nanocomposite. Liao et al. [28] prepared poly(ethylene) nanocomposites by using a polyethylene–poly(ethylene glycol) (PE–PEG) diblock copolymer as compatibilizer. The authors reported a significant improvement of the tensile strength by the addition of small amounts of PE–PEG (1–15 wt%).

In this paper we have prepared natural rubber (NR)/Na^+ montmorillonite (MMT) nanocomposites in only one step by using poly(ethylene glycol) (PEG) as dispersing agent, avoiding the previous organophilization reaction of pristine clay. For this, NR containing 10 phr of as-received clay as filler was processed with different PEG concentrations (1–7.5 phr). Moreover, to study separately the effect of the PEG polymer on the intercalation of NR and on the rubber network microstructure, a series of MMT–PEG (10 and 25 wt% of PEG) hybrid blends were prepared. The nanocomposites were characterized by combination of diverse complementary techniques such as X-ray diffraction, transmission electron microscopy and solid state NMR. In addition, the mechanical properties of the materials are calculated.

2. Experimental

2.1. Materials and preparation of the composites

Natural rubber was kindly supplied by Malaysian Rubber under the trade name CV 60 (Money viscosity, ML (1 + 4) 100 °C 60). Na^+-montmorillonite provided by Southern Clay Products Inc. (Gonzales, TX) was used as filler. Poly(ethylene glycol) with an average molecular weight of $M_n \sim 5000–7000\ \mathrm{g\,mol^{-1}}$ was supplied by Flucka.

Rubber compounds were prepared in a Haake Rheomix internal mixer with a volume of 60 cm^3 and equipped with a pair of high shear roller-type rotors. The temperature of the mixing chamber was set at 80 °C and the blending time was 15 min. The rotors operated at a speed of 100 rpm. The recipe of the compounds is compiled in Table 1. The samples were vulcanized at 150 °C by compression moulding at the optimum cure time (t_{95}) previously obtained from the curing curves measured in a Rubber Process Analyzer (RPA 2000, Alpha Technologies). MMT–PEG hybrids were prepared in the internal mixer during 15 min at 80 °C. Hybrids were called MMT–PEG 10 wt% and MMT–PEG 25 wt%.

2.2. Characterization of the composites

The dispersion at the nanoscale level of the NR/MMT compounds was determined by XRD diffraction and TEM. A Siemens D-5000 X-ray diffractometer with CuKα radiation (λ = 1.54060 Å) operating at 40 kV and 25 mA was used. The scanning rate was $0.02^\circ\ \mathrm{s^{-1}}$ and the data were collected for 2θ from 1° to 60°. A transmission electron microscope (Zeiss CEM 902) with an accelerator voltage of 80 kV was used to examine the dispersed structure and the aspect ratio of the clay particles in the composites. Samples were obtained by means of an ultracryomicrotome equipped with a diamond knife at −160 °C.

Table 1
Recipes of NR compounds

	NR/MMT/PEG	NR/PEG
NR	100	100
ZnO	5	5
Stearic acid	1	1
Na^+ MMT	10	–
PEG	0.5, 1, 2.5, 5, 7.5	0.5, 1, 2.5, 5, 7.5
Sulphur	2.5	2.5
MBTS[a]	1	1
PBN[b]	1	1

Note: The formulation of the compounds is expressed in phr (parts per hundred rubber).

[a] Benzothiazyl disulfide.

[b] Phenyl beta naphthylamine.

^{1}H-multiple quantum (MQ) NMR at low-field experiments were carried out in a Bruker minispec mq20 operating at 0.5 T (90° pulses of 1.7 μs length) according previously published procedures [29,30]. The essential advantage of MQ spectroscopy in polymer network characterization with respect to some other NMR procedures is that it is less susceptible to potential artifacts [31], mainly because in the same experiment, two qualitatively sets of data are obtained: a build-up curve dominated by spin-pair double-quantum (DQ) coherences (I_{DQ}) that reflects the network structure, and a decay (control) curve with signal from other coherences (I_{ref}) that is used to correct for relaxation effects due to chain dynamics. A normalized DQ build-up curved is constructed as

$$I_{nDQ} = \frac{I_{DQ}}{I_{DQ} + I_{ref} - B \cdot \exp(-2\tau_{DQ}/T_{2B})} \tag{1}$$

where the isotropically mobile fraction of rubber is subtracted from the denominator, which represents the full magnetization of the sample subject to relaxation. Therefore, B is the proton integral fraction of the isotropically mobile components, i.e. the fraction of non-elastic network defects (loops and dangling chains) and T_{2B} its apparent transverse relaxation time. The normalized DQ build-up curve contains information on the crosslink density of the rubber matrix without any influence coming from the molecular dynamics. It is encoded in an apparent residual coupling constant (D_{res}) that is proportional to crosslink density. In all the studied samples, as observed previously, distribution (polydispersity) effects of D_{res} do not play a role. This suggests the existence of cooperative dynamics [32] and further indicates that the samples are homogeneous down to the length scale of a few network chain extensions. Therefore, the normalized DQ build-up curves were analyzed in the quasi-static limit in terms of a single D_{res}:

$$I_{nDQ}(D_{res}) = \frac{1}{2}\left(1 - exp\left[-\frac{2}{5}D_{res}^2\tau_{DQ}^2\right]\right) \tag{2}$$

The existence of a residual dipolar coupling is caused by *anisotropic* chain motion due to the existence of crosslinks and other topological restrictions. Therefore, the comparison of D_{res}, with its static counterpart, D_{stat}, gives a dynamic order parameter of the polymer backbone, S_b, which is related to the ratio of the potentially stretched end-to-end vector to its unperturbed melt state (r), and to N, the number of statistical (Kuhn) segments between the constrains,

$$S_{\mathrm{b}} = k\frac{D_{\mathrm{res}}}{D_{\mathrm{stat}}} = \frac{3}{5}\frac{r^2}{N} \tag{3}$$

where k is a constant required by the model in order to rescale D_{stat}. In consequence, Eq. (3) provides the link between the experimental average residual dipolar coupling constant (D_{res}) and the theory of rubber elasticity. According to a model presented in reference [29], the inter-crosslink molecular weight, M_{c}, of natural rubber is given by the following expression,

$$M_{\mathrm{c}} = \frac{3\times 6300\ \mathrm{Hz}}{5D_{\mathrm{res}}/2\pi}\frac{4.7}{4\times 0.7^2} \quad M_0 = \frac{617\ \mathrm{Hz}}{D_{\mathrm{res}}/2\pi}\ \mathrm{kg/mol} \tag{4}$$

To be more rigorous, M_{c} obtained by MQ NMR experiments, represents the molecular weight between constrains, independently of their nature, i.e. crosslinks, entanglements or trapped entanglements.

The residual dipolar coupling results from a time average over the fluctuations of local dipolar tensors that are tied to the network chain segments probing their conformational space. It reaches a plateau region only at sufficiently long times or when the segmental dynamics is sufficiently fast. Therefore, to obtain a proper value of this order parameter, the experimental temperature has to be far above T_{g}. Working at too low temperatures leads to overestimated crosslink densities, in particular for lightly crosslinked rubbers. For this reason, all NMR experiments were performed at 80 °C (far above the glass transition of NR at ca. −65 °C).

The average mass of network chains M_{c}, was also determined on the basis of equilibrium swelling experiments (about 24 h in complete darkness) using toluene at 30 °C by application of Eq. (5), which is derived from the application of a phantom network model to describe the elastic behaviour of the network in swollen state,

$$In(1-\phi_{\mathrm{r}}) - \phi_{\mathrm{r}} - \chi\phi_{\mathrm{r}}^2 = \frac{\rho V_0}{M_{\mathrm{c}}}\left[\phi_{\mathrm{r}}^{1/3} - 1/2\phi_{\mathrm{r}}\right] \tag{5}$$

where ϕ_{r} is the polymer volume fraction in the swollen network, V_0 is the molar volume of the solvent (106.2 mL/mol for toluene), ρ is the density of the rubber, and χ is the Flory–Huggins polymer-solvent interaction term.

The dependence of the Flory–Huggins interaction parameter for swollen NR networks in toluene with respect to the polymer concentration (χ=0.427 + 0.112φ_{r}^2) described in reference [33] was used to calculate M_{c}.

The rubber density was determined via the hydrostatic weighting method. All the measurements were carried out on a Sartorius balance, model Kern 770, with a resolution of ±0.1 mg.

Tensile stress–strain properties were measured according to ISO 37-1977 specifications, on an Instron dynamometer (Model 4301), at 25 °C at crosshead speed of 500 mm min^{-1}.

3. Results and discussion

X-ray powder diffraction patterns of the studied materials are shown in Fig. 1. Sodium MMT shows a diffraction peak at $2\theta = 7°$ that corresponds to an interlayer distance of 12.6 Å (Fig. 1a, right). The existence of water molecules in the interlayer space leads to a swelling of the clay. That is the reason for the deviation from the distance of 9.7 Å measured for dry montmorillonite in [34]. The spacing hardly varies when 10 phr MMT is mixed with NR (Fig. 1a, left). This implies the formation of a conventional composite at a microscopic scale, where the polymer is not intercalated into the silicate galleries. Interestingly, a displacement of the peak towards lower angles $2\theta = 5°$ (∼18 Å) by addition of 1 phr PEG (MMT/NR/1 PEG) is observed (Fig. 1b, left). According to previous reports, this amount of PEG should not be enough in order to fill the basal space with two layers of polymer and therefore, to reach to the maximum interlayer distance (∼18 Å). This indicates that a portion of rubber chains are intercalated into the silicate galleries. Additionally, the appearance of a peak at $2\theta = 44$ Å evidences pronounced intercalation with NR. Similar behaviour was observed for the NR/MMT/2.5 PEG compound in which the diffraction pattern corresponding to 44 Å appears even more defined (Fig. 1c, left).

In order to corroborate this statement, 10 wt% PEG (equivalent amount to that in MMT/NR/1 PEG composite) is added to MMT in absence of rubber. As deduced from XRD, PEG is successfully inserted into the silicate galleries. It increases the distance basal of silicate up to 13.8 Å, i.e. a gallery expansion close to 4 Å, typically attributed to a single layer structure of PEG into the clay [34]. The additional expansion of the interlayer space up to 8 Å observed in NR composites should be attributed to the intercalation of rubber. The *d*-spacing is progressively increased at higher PEG loadings (25 wt%) up to a maximum of 18 Å (Fig. 1c, right). This corresponds to an insertion of two layers of PEG inside the galleries. Further PEG loadings do not increase the interlayer distance of the silicate (data not shown). This statement is in good agreement with the reported results by Chen and Evans [35]. They reported that a maximum of 19 wt% PEG adsorbed on sodium MMT with similar CEC was reached, independently of the polymer molecular weight and processing method. Bujdák et al. [36] attributed this fact to the layer charge density of the silicate rather than to higher attractive electrostatic forces between the layers. That means that the presence of a high CEC in the clay leads to a great surface area covered by the hydrated cations reducing then, the available silicate surface area to the polymer adsorption. However there can be dispersion without intercalation. It is expected that unshared electron pairs of ether oxygen in poly(ethylene glycol) gives tendency for hydrogen bonding with OH groups of clay. Such an interaction can increase the rubber filler interaction leading to enhanced filler dispersion.

These results confirm that the PEG even at small amounts behaves as swelling agent, favouring the diffusion

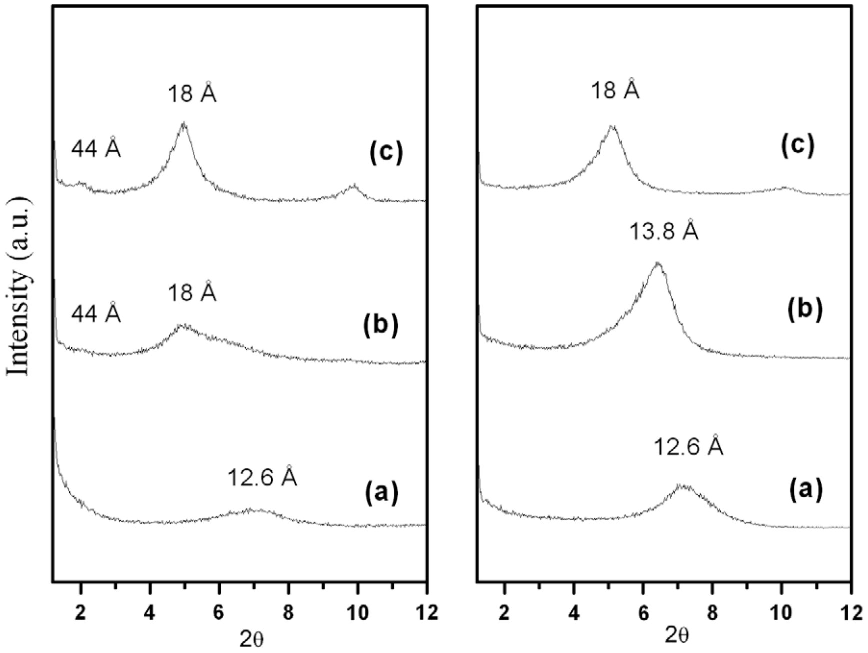

Fig. 1. Left: XRD patterns of NR/MMT (a), NR/MMT/1 PEG (b), and NR/MMT/2.5 PEG (c) composites. Right: XRD patterns of sodic montmorillonite (MMT) (a), MMT–PEG 10 wt% (b), and MMT–PEG 25 wt% (c) hybrids.

of poly(isoprene) chains into the silicate galleries. Therefore, the intercalation of the NR chains in presence of PEG implies that two principal phenomena might take place: first, the overcoming of the higher attractive electrostatic forces between the two silicate layers, which avoid the separation so far than 18 Å for a sodic MMT, and second, the favourable mixing between two thermodynamically immiscible components as the hydrophobic poly(isoprene) chains and the hydrophilic clay.

A likely disposition of the different components of the system into the silicate gallery is schematically represented in Fig. 2. The scheme is based on previous experimental and theorical studies carried out by Giannelis group [36,37]. They evidence that in poly(ethylene

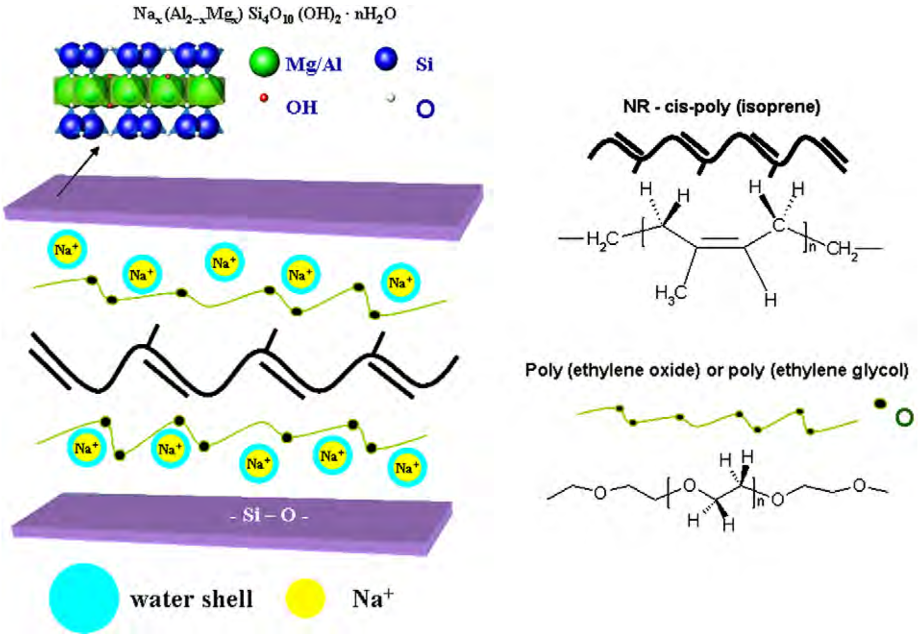

Fig. 2. Schematic showing coordination of Na^+ by water-shell, the PEG chains and the *cis*-poly(isoprene) chains disposition at the inner clay gallery.

oxide)–MMT hybrids a great part of the cations in the galleries exist near to the silicate surface. Moreover, exchangeable cations are in fact the only strongly hydrophilic sites on the silicate surface [38–40] and the water bound to these cations is released only at relatively high temperatures. Thus, PEO does not coordinate directly with the exchangeable cations during the intercalation in the MMT. In the case that we are dealing with herein, poly(isoprene) chains are more hydrophobic than PEG chains. Therefore, it is expected that rubber chains are preferentially located far away from the silicate surface interacting with PEG chains which are acting as interface between the most hydrophobic component in the gallery, poly(isoprene), and the most hydrophilic counterpart, the exchangeable cations with their water coordination shell. This scenario in which exist favourable interactions between the immiscible components of the system is in concordance with the trends found in the literature [41].

TEM images of NR/MMT compounds without and with PEG are shown in Fig. 3. Fig. 3a shows clearly the inhomogeneous dispersion of the original clay into the natural rubber matrix. However, the addition of 2.5 phr PEG favours the dispersion of MMT within the polymer matrix (Fig. 3b). The parallel single-clay layers evidence that some rubber chains indeed diffuse into the silicate galleries leading to an intercalated structure.

To summarize, XRD patterns and TEM images evidence that PEG acts as swelling agent favouring the silicate dispersion into the polymer matrix. We turn to the influence of PEG on the actual rubber network structure by comparing results of swelling experiments and proton multiple-quantum (MQ) NMR spectroscopy [30,42]. Note that this recent and versatile technique can be applied on proton low-field instrumentation [43], it thus provides fully quantitative information on the structure and local chain dynamic of elastomers on a low-cost NMR spectrometer.

Fig. 4 shows representative build-up curves for the control series NR/PEG (Fig. 4a) and the NR/MMT/PEG (Fig. 4b) series at several PEG concentrations. The results obtained by fitting to Eq. (2) are collected in Tables 2 and 3. In agreement with previous experiments on natural rubber [29], the crosslink density distribution determined by numerical inversion of the distribution integral [44] is quite narrow in all samples (see Fig. 5). The relatively small variations in crosslink density, caused by the addition of the clay and PEG, are not linked with any appreciable variation in their distribution. Therefore, we see no evidence for locally heterogeneous structures, e.g., locally higher crosslink density around the clay sheets.

As it is obvious from the data in Table 2 and Fig. 6, the addition of clay has an inhibitory effect on the vulcanization process, depressing the final cure state of the matrix. The filler surface groups react with or absorb the vulcanizing agents, diminishing the vulcanization efficiency, which is reflected in a decrease of D_{res} and $1/M_{\mathrm{c}}$. We observed such behavior on NR samples with different amounts of cure system and filled with different amounts of pristine and organo-modified clay, and details of this study will be published elsewhere. In contrast, the inclusion of PEG in the composite seems to have just the opposite effect, overcoming the undesirable effect of the clay. These tendencies can be best observed in Fig. 6, where the variations of the crosslink density ($\sim 1/M_{\mathrm{c}}$) from NMR and swelling are plotted vs. the PEG content. Note that swelling leads to much lower values apparent for the crosslink density, in agreement with the idea that NMR measures all topological restrictions (crosslinks and entanglements), while upon swelling, entanglement effects are largely relieved (leaving only trapped entanglements).

PEG has rather strong adsorptive interactions that undoubtedly lessen severely or eliminate direct adsorptive interactions of the filler with elastomer. So, it seems unlikely that appreciable filler-polymer interactions occur directly between the clay surface and natural rubber [45]. It is however clear that PEG takes part in the crosslinking process of natural rubber, increasing its efficiency. PEG causes a synergy effect with vulcanizing agents leading to an increase of the crosslinking density. It is of interest to note that this efficiency maximum is reached for an optimal PEG concentration of 1 phr. In contrast, the hybrids containing MMT follow the same trend, but in this case, a higher PEG concentration, 2.5 phr, is required to reach the highest density. This indicates that a fraction of around 1–2 phr PEG is absorbed on the clay and does not

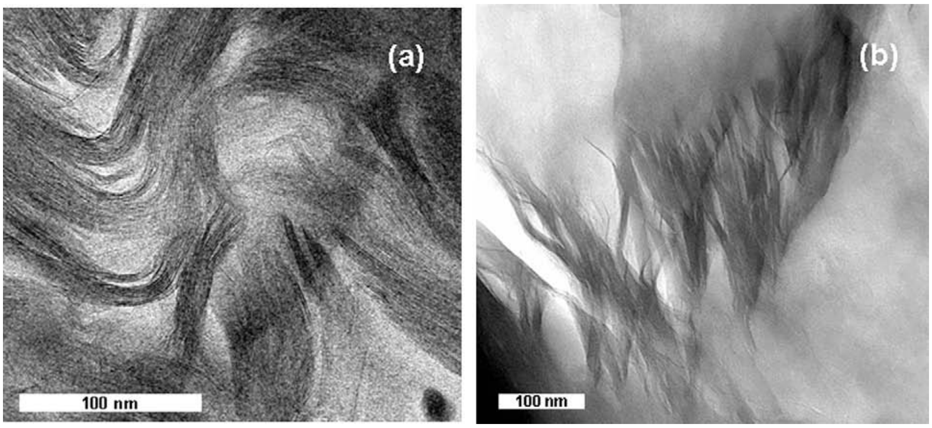

Fig. 3. Representative TEM images of NR/MMT (a), and NR/MMT/2.5 PEG (b) compounds.

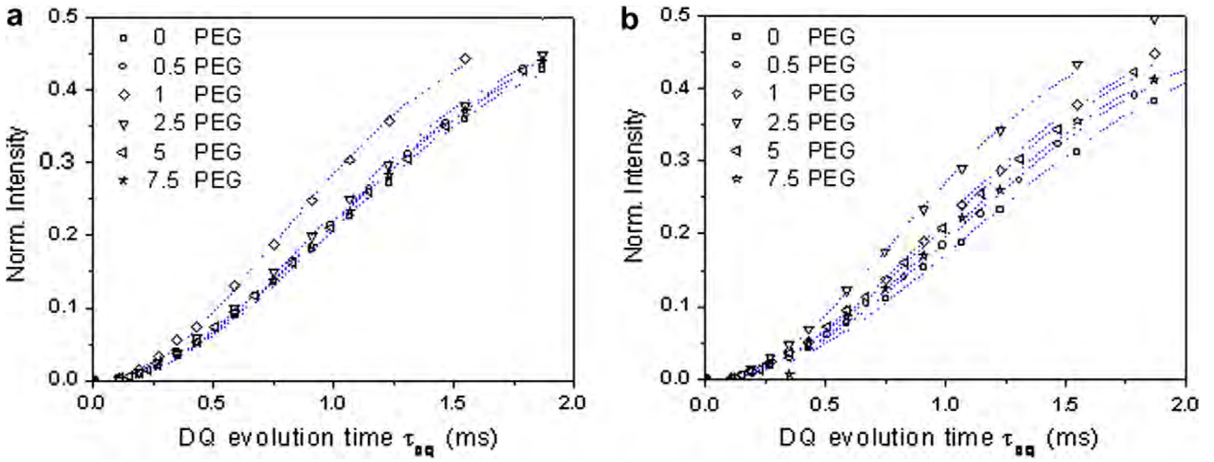

Fig. 4. DQ build-up data for different samples of NR/PEG (a) and NR/MMT/PEG (b) series measured at low-field. The good fitting of the build-up curve in terms of single D_{res}. (Eq. (2)) indicates narrow distributions of residual couplings.

Table 2
Structural parameters of NR networks derived from ^{1}H DQ NMR analysis and solvent swelling measurements for NR/PEG hybrid at several PEG concentrations

Compound	MQ NMR		Swelling		Delta torque
	D_{res}, Hz	M_c, g/mol	Φ_r	M_c, g/mol	ΔS (dN m)
NR	185	3335	0.157	8249	7.43
NR/0.5 PEG	192	3213	0.165	7411	7.72
NR/1 PEG	231	2671	0.169	7037	9.05
NR/2.5 PEG	197	3131	0.164	7510	8.63
NR/5 PEG	190	3247	0.151	8965	8.02
NR/7.5 PEG	189	3264	0.146	9630	6.86

Torque value (ΔS) from RPA are also summarized.

Table 3
Structural parameters of NR networks derived from 1H DQ NMR analysis and solvent swelling measurements for NR/MMT/PEG compound at several PEG concentrations

Compound	MQ NMR		Swelling		Delta torque
	D_{res}, Hz	M_c, g/mol	Φ_r	M_c, g/mol	ΔS (dN m)
NR	185	3335	0.157	8249	7.43
NR/MMT	163	3762	0.151	8965	7.24
NR/MMT/0.5 PEG	174	3545	0.156	8362	7.94
NR/MMT/1 PEG	192	3213	0.167	7221	8.82
NR/MMT/2.5 PEG	222	2779	0.173	6688	9.78
NR/MMT/5 PEG	187	3299	0.148	9356	9.08
NR/MMT/7.5 PEG	178	3466	0.147	9492	7.94

Torque value (ΔS) from RPA are also summarized.

participate in the synergistic enhancement of the vulcanization reaction.

In combination with the XRD and TEM observations that demonstrate that PEG behaves as an effective swelling agent and favours the diffusion of NR chains inside the silicate gallery, we summarize the three effects of PEG:

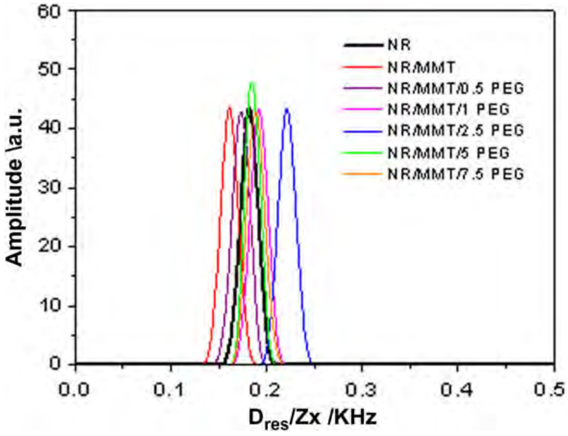

Fig. 5. Distributions of $D_{res}/2\pi$ obtained by Tikhonov regularization of the experimental build-up curves [44].

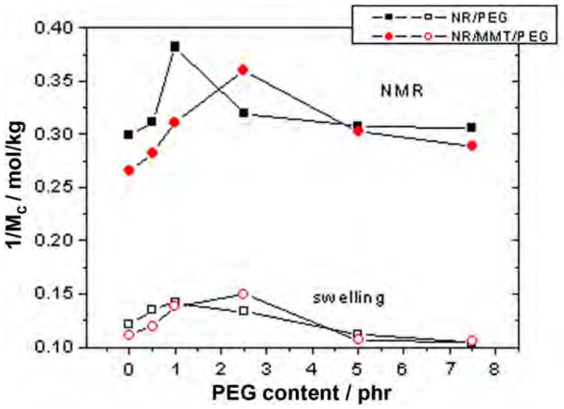

Fig. 6. Variation of the crosslink density obtained from NMR and swelling experiments, plotted vs. the PEG content.

1. PEG takes part in the sulphur vulcanization of NR, increasing its efficiency.
2. PEG behaves as a swelling agent, favouring the dispersion of natural rubber into the silicate galleries.
3. PEG competes with the vulcanization system in its interaction with the clay surface. It thus partially compensates the undesirable effect of the clay and ultimately increases the crosslink density.

The NMR-determined network parameters are now compared with the results from the swelling experiments. The data shown in Fig. 7 nicely prove that the crosslink density calculated from NMR is proportional to that obtained by swelling experiments. The samples in the present study show somewhat larger scatter than data obtained for carefully calibrated NR samples from a model study, which will be published shortly. The latter data evidence the near-perfect linear relationship between NMR and swelling results, as also reported in [23]. The non-zero intercept of the NMR-determined crosslink density is directly related to the entanglement fraction that is revealed in a swelling experiment (without trapped entanglements, the intercept would be $1/M_e$). The delta torque values (Tables 2 and 3) obtained from cure curves actually follow a similar trend when plotted over $1/M_c$ from NMR or swelling, with an expected slight trend of the filled systems toward higher values.

Notably, the data points corresponding to the samples with MMT are systematically shifted to the lower right with respect to the unfilled samples (see arrow). We believe this to be due to the inclusion of some of the NR chains in the MMT, which leads to additional crosslink that are only effective in the swollen sample. In the dry sample, this slight increase is masked by the dominant and much more local entanglement contribution. Note that the size of the MMT tactoids is large, thus restricting such additional effects to a small polymer fraction around the fillers that is hardly observable in a dry sample. On the other hand, the swollen sample is highly heterogeneous, and larger-scale effects become important.

The mechanical properties of the composites are reported in Table 4. The tensile properties are given in terms of the modulus at different strains, maximum strength and elongation at break of the nanocomposites. The low reinforcing effect of original montmorillonite is evident. As previously evidenced by XRD and TEM, a conventional composite at micro scale was obtained due to the poor compatibility filler/polymer. However, a marked increase of the mechanical properties by the addition of small amounts of PEG is observed. Increments of more than 200% in the strength are observed, while the variations in the crosslink density of the matrix as seen by NMR and swelling experiments are only on the 20% range. Obviously, the enhanced swelling and possibly partial exfoliation of the clay sheets lead to a much enhanced mechanically active filler network.

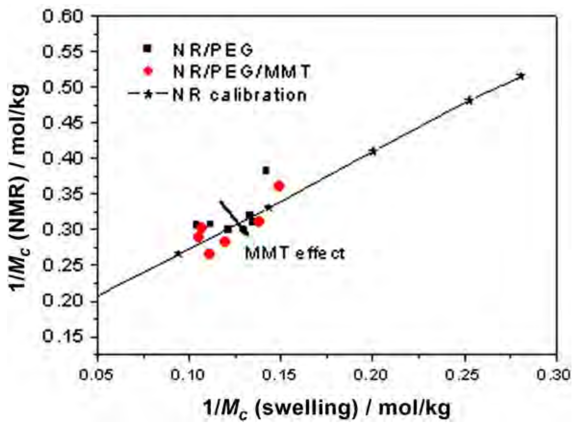

Fig. 7. Correlation the crosslink densities obtained from NMR and swelling experiments.

Table 4
Mechanical properties of the studied NR compounds

Compound	Strength at 100% (MPa)	Strength at 300% (MPa)	Strength at 500% (MPa)	Maximun strength (MPa)	Elongation at break (%)
NR	0.67	1.24	2.08	14.55	1561.19
NR/MMT	0.71	1.44	2.36	9.05	1147.51
NR/1 PEG	0.94	1.88	3.23	14.73	1135.60
NR/MMT/1 PEG	1.05	2.13	3.52	19.92	1419.11
NR/2.5 PEG	0.79	1.55	2.73	14.42	1234.25
NR/MMT/2.5 PEG	1.17	2.63	4.98	18.28	1089.83

4. Conclusions

We have successfully prepared natural rubber/clay nanocomposites in only one step. PEG acts as swelling agent, favouring the dispersion of the silicate into the polymer matrix. The addition of small amounts of PEG sensibly increases the tensile strength without hardly affect the elongation at break in relation with the unmodified MMT filled NR. The promising results reported herein provide new insights into how to tackle the intercalation/exfoliation problem of pristine clays in incompatible polymers without resorting to the organophilization route during the polymer processing. The use of clays with different features and swelling agents with different architectures and chemical composition might permit a wide range of tunable interactions between the components of the system and, in consequence, the preparation of a polymer nanocomposite with similar or enhanced macroscopic properties as compared to those obtained by using conventional organo-modifiers.

Acknowledgements

The authors gratefully acknowledge the financial support of the Spanish Ministry of Science and Innovation (MICINN) through project MAT 2004-00825. We also thank Dr. E. Castillo-Martínez for her invaluable support. J. Carretero-González gratefully acknowledges the FPI fellowship from the MEC. Dr. J.L. Valentin thanks Alexander von Humboldt Foundation for his post-doctoral fellowship.

References

[1] Winey KI, Vaia RA. Polymer nanocomposites. MRS Bull 2007;32:314–22.
[2] Okada A, Usuki A. Twenty years of polymer-clay nanocomposites. Macromol Mater Eng 2006;291:1449–76.

[3] Ray SS, Okamoto M. Polymer/layered silicate nanocomposites: a review from preparation to processing. Prog Polym Sci 2003;28:1539–641.

[4] Pinnavaia TJ, Beall GW. Polymer-clay nanocomposites. In: Pinnavaia TJ, Beall GW, editors. John Wiley & Sons: New York, Inc.; 2000.

[5] Alexandre M, Dubois P. Polymer-layered silicate nanocomposites: preparation, properties and uses of a new class of materials. Mater Sci Eng 2000;28(1–2):1–65.

[6] Giannelis EP, Krishnamoorti R, Manias E. Polymer-silicate nanocomposites: model systems for confined polymers and polymer brushes. Adv Polym Sci 1999;138:107–47.

[7] Giannelis EP. Polymer layered silicate nanocomposites. Adv Mater 1996;8(1):29–35.

[8] Garces JM, Moll DJ, Bicerano J, Fibiger R, Mc Leod DG. Polymeric nanocomposites for automotive applications. Adv Mater 2000;12(23):1835–9.

[9] Bala P, Samantaray BK, Srivastava SK, Nando GB. Effect of alkylammonium intercalated montmorillonite as filler on natural rubber. J Mater Sci Lett 2001;20:563–4.

[10] Joly S, Garnaud G, Ollitrault R, Bokobza L, Mark JE. Organically modified layered silicates as reinforcing fillers for natural rubber. Chem Mater 2002;14:4202–8.

[11] Arroyo M, Lopez-Manchado MA, Herrero B. Organo-montmorillonite as substitute of carbon black in natural rubber compounds. Polymer 2003;44(8):2447–53.

[12] Lopez-Manchado MA, Herrero B, Arroyo M. Preparation and characterization of NR/organoclay nanocomposites. Polym Int 2003;52:1070–7.

[13] Lopez-Manchado MA, Arroyo M, Herrero B, Biagiotti J. Vulcanization kinetics of NR/organoclay. J Appl Polym Sci 2003;89:1–15.

[14] Teh PL, Ishak ZAM, Hashim AS, Karger-Kocsis J, Ishiaku US. Effects of epoxidized natural rubber as a compatibilizer in melt compounded natural rubber-organoclay nanocomposites. Eur Polym J 2004;40:2513–21.

[15] Varghese S, Karger-Kocsis J. Melt-compounded natural rubber nanocomposites with pristine and organophilic layered silicates of natural rubber and shyntetic origin. J Appl Polym Sci 2004;91:813–9.

[16] Teh PL, Ishak ZAM, Hashim AS, Karger-Kocsis J, Ishiaku US. Physical properties of natural rubber-organoclay nanocomposites compatibilized with epoxidized natural rubber. J Appl Polym Sci 2006;100:1083–92.

[17] Arroyo M, Lopez-Manchado MA, Valentín JL, Carretero J. Morphology/behaviour relationship of nanocomposites based on natural rubber/epoxidized natural rubber blends. Comp Sci Tech 2007;67(7–8):1330–9.

[18] Lopez-Manchado MA, Herrero B, Arroyo M. Organoclay-natural rubber nanocomposites synthesized by mechanical and solution mixing methods. Polym Int 2004;53:1762–6.

[19] Magaraphan RW, Thaijaroen W, Lim-Ochakun R. Structure and Properties of natural rubber and modified montmorillonite nanocomposites. Rubber Chem Technol 2003;76:406–18.

[20] Varghese S, Karger-Kocsis J. Natural rubber-based nanocomposites by latex compounding with layered silicates. Polymers 2003;44:4921–7.

[21] Varghese S, Gatos KG, Apostolov AA, Karger-Kocsis J. Morphology and mechanical properties of layered silicate reinforced natural rubber and polyurethane rubber blends produced by latex compounding. J Appl Polym Sci 2004;92:543–51.

[22] Wang YQ, Zhang HF, Wu YP, Yang J, Zhang LQ. Preparation and properties of natural rubber/rectorite nanocomposites. Eur Polym J 2005;41:2776–83.

[23] Stephen R, Ranganathaiah C, Varghese S, Joseph K, Thomas S. Gas transport through nano and micro composites of natural rubber (NR) and their blends with carboxylated styrene butadiene rubber (XSBR) latex membranes. Polymers 2006;47:858–70.

[24] Valadares LF, Leite CAP, Galembeck F. Preparation of natural rubber–montmorillonite nanocomposite in aqueous medium: evidence for polymer–platelet adhesion. Polymers 2006;47:672–8.

[25] Theng BKG. Formation and properties of clay-polymer complexes. In: Theng BKG, editor. Elsevier: Amsterdam Inc.; 1979.

[26] Shmuel Y, Harold C. Organo-clay complexes and interactions. In: Shmuel Y, Harold C, editors. Marcel Dekker: New York Inc.; 2002.

[27] Moad G, Dean K, Edmond L, Kukaleva N, Li G, Mayadunne RTA, et al. Non-ionic, poly(ethylene oxide)-based surfactants as intercalants/dispersants/exfoliants for poly(propylene)-clay nanocomposites. Macromol Mater Eng 2006;291:37–52.

[28] Liao B, Song M, Liang H, Pang Y. Polymer-layered silicate nanocomposites. 1. A study of poly(ethylene oxide)/Na$^+$-montmorillonite nanocomposites as polyelectrolytes and polyethylene-block-poly(ethylene glycol) copolymer/Na$^+$-montmorillonite nanocomposites as fillers for reinforcement of polyethylene. Polymers 2001;42:10007–11.

[29] Saalwächter K, Herrero B, López-Manchado MA. Chain order and cross-link density of elastomers as investigated by proton multiple-quantum NMR. Macromolecules 2005;38:9650–60.

[30] Saalwächter K. Proton multiple-quantum NMR for the study of chain dynamics and structural constraints in polymeric soft materials. Prog NMR Spectrosc 2007;51:1–35.

[31] Saalwächter K, Herrero B, Lopez-Manchado MA. Chemical shift-related artifacts in NMR determinations of proton residual dipolar couplings in Elastomers. Macromolecules 2005;38:4040–2.

[32] Saalwächter K, Sommer JU. NMR reveals non-distributed and uniform character of network chain dynamics. Macromol Rapid Commun 2007;28:1455–65.

[33] Horkay F, McKenna GB, Deschamps P, Geissler E. Neutron scattering properties of randomly cross-linked polyisoprene gels. Macromolecules 2000;33:5215–20.

[34] Harris J, Bonagamba TJ, Schmidt-Rohr K. Conformation of poly(ethylene oxide) intercalated in clay and MoS_2 studied by two-dimensional double-quantum NMR. Macromolecules 1999;32:6718–24.

[35] Chen B, Evans JRG. X-ray diffraction studies and phase volume determinations in poly(ethylene glycol)–montmorillonite nanocomposites. Polym Int 2005;54:807–13.

[36] Bujdák J, Hackett E, Giannelis EP. Effect of layer charge on the intercalation of poly(ethylene oxide) in layered silicates: implications on nanocomposite polymer electrolytes. Chem Mater 2000;12:2168–74.

[37] Hackett E, Manias E, Giannelis EP. Computer simulation studies of PEO/layer silicate nanocomposites. Chem Mater 2000;12:2161–7.

[38] Sposito G, Prost R. Structure of water adsorbed on smectites. Chem Rev 1982;82:553–73.

[39] Chang FC, Skipper NT, Sposito G. Monte carlo and molecular dynamics simulations of interfacial structure in lithium-montmorillonite hydrates. Langmuir 1997;13:2074–82.

[40] Prost R, Koutit T, Benchara A, Huard E. State and location of water adsorbed on clay minerals; consequences of the hydration and swelling-shrinkage phenomena. Clays Clay Miner 1998;46:117–31.

[41] Varghese S, Karger-Kocsis J, Gatos KG. Melt compounded epoxidized natural rubber/layered silicate nanocomposites: structure-properties relationships. Polymers 2003;44:3977–83.

[42] Graf R, Demco DE, Hafner S, Spiess HW. Selective residual dipolar couplings in cross-linked elastomers by ^{1}H double-quantum NMR spectroscopy. Solid State NMR 1998;12:139–52.

[43] Saalwächter K. Detection of heterogeneities in dry and swollen polymer networks by proton low-field NMR spectroscopy. J Am Chem Soc 2003;125:14684–5.

[44] Saalwächter K, Ziegler P, Spyckerelle O, Haidar B, Vidal A, Sommer JU. ^{1}H multiple-quantum nuclear magnetic resonance investigations of molecular order distributions in polydimethylsiloxane networks: evidence for a linear mixing law in bimodal systems. J Chem Phys 2003;119:3468–82.

[45] Wagner MP. Reinforcing Silicas and Silicates. Rubber Chem Tech 1976;49:703–74.

CAPÍTULO IV

DISCUSIÓN INTEGRADORA

El caucho natural, NR es un biomaterial complejo constituido principalmente de una parte lineal formada por unidades cis-poliisopreno (95 %). Estas cadenas de isopreno lineal terminan en uno de los extremos, α-terminal, con grupos mono o difosfatos enlazados a fosfolípidos, mientras que por el otro extremo, ω-terminal, unidades de dimetilalil modificadas se encuentran unidas con grupos funcionales asociados con proteínas para formar entrecruzamientos a través de enlaces de hidrógeno intermoleculares. Además, el NR contiene cantidades suficientes de proteínas y fosfolípidos resultantes del mecanismo de la biosíntesis de formación del caucho, los cuales inducen una microestructura a multiescala caracterizada por un entrecruzamiento natural entre los grupos terminales de las cadenas de poliisopreno lineales. La presencia de estos componentes naturales, lípidos y proteínas, tiene un impacto directo sobre las propiedades mecánicas finales del polímero. De hecho, el NR exhibe propiedades mecánicas no alcanzables por sus homólogos sintéticos, lo que convierte al NR en uno de los polímeros más fascinantes y de mayor interés industrial entre los diferentes plásticos ingenieriles.

Sin embargo, hasta la fecha no se ha estudiado como estas impurezas de origen natural, que controlan la microestructura del caucho natural y por tanto sus propiedades finales, afectan a la dinámica molecular de las cadenas de cis–poliisopreno. La mayoría de los trabajos enfocados a analizar la dinámica molecular del poliisopreno se han centrado en muestras sintéticas y únicamente unos pocos con caucho natural. La técnica empleada en esta Tesis Doctoral para llevar a cabo dicho estudio fue la espectroscopia de relajación dieléctrica de banda ancha.

Se prepararon muestras *“modelo”* a partir de un látex de caucho natural extraído del árbol Hevea en Tailandia. Se realizaron diferentes tratamientos físicos y químicos para obtener muestras que presentasen el mismo peso molecular conteniendo o no las impurezas de origen natural. En concreto, se prepararon y estudiaron cuatro muestras:

(a) un caucho natural purificado tras un proceso de centrifugación del látex y que contiene proteínas y ácidos grasos de cadena larga como agentes de entrecruzamiento y la fase SOL *(CNR)*.

(b) un caucho natural que presenta en su composición solo la fase insoluble conocida como GEL y que contiene las impurezas naturales antes mencionadas, tras eliminación de la fase soluble SOL, compuesta principalmente esta fase SOL por cadenas lineales de cis–poliisopreno.

(c) un caucho desproteinizado, conteniendo solo los componentes lipídicos, en los que se han eliminado los entrecruzamientos proteínicos en el extremo ω de la cadena *(DPNR)*.

(d) un caucho que exhibe únicamente cadenas lineales de cis–poliisopreno por eliminación selectiva de los fosfolípidos y las proteínas, tras procesos de transesterificación y desproteinización, respectivamente, del caucho natural *(TE-DPNR)*.

El comportamiento dieléctrico de la molécula de cis–poliisopreno se caracteriza por presentar un momento dipolar con dos componentes. Uno de ellos, perpendicular a la estructura de la cadena, relacionado con los movimientos de los segmentos de la cadena y cuya relajación se detecta una vez superada la temperatura de transición vítrea del caucho (relajación segmental), y, otro momento dipolar más lento, paralelo al contorno de la cadena polimérica relacionado con el movimiento entre los segmentos contenidos entre los dos finales de una cadena (modo normal).

La relajación segmental del cis–poliisopreno es independiente del peso molecular, pero la relajación asociada con el modo normal está fuertemente influenciada por el peso molecular. De ahí que fuese tan importante lograr sintetizar muestras con diferente microestructura y que presentasen el mismo peso molecular, para poder de esta manera determinar el efecto de la microestructura en la dinámica molecular del caucho natural.

Análogamente al poliisopreno sintético, todas las muestras de caucho natural analizadas exhiben los dos procesos de relajación, segmental y normal. Se consiguió un correcto ajuste de la forma de las curvas de cada relajación con su correspondiente evolución con la temperatura y la frecuencia para todas las muestras analizadas mediante la aplicación de la ecuación fenomenológica de Havriliak–Negami (HN), que es una adaptación a su vez de la ecuación clásica de Debye. Ambos procesos de relajación se pudieron analizar individualmente, lo que permitió una razonable descripción de los datos experimentales. Se pudieron determinar los diferentes parámetros de la ecuación HN para ambos procesos de relajación: resistencia dieléctrica, $\Delta\varepsilon_X$; tiempo de relajación, τ_x; y los parámetros de forma *b* y *c*, que describen el ensanchamiento simétrico y asimétrico, respectivamente, de la función de distribución del tiempo de relajación.

Por su parte, la dependencia del tiempo de relajación con la temperatura para ambos procesos de relajación, se ajustó mediante la ecuación de Vogel-Fulcher-Tamann (VFT).

Los resultados mostraron que la relajación segmental era independiente del tratamiento suministrado a la muestra. En general, se ha demostrado que la relajación α atribuida al modo segmental está íntimamente relacionada con la densidad de entrecruzamiento de la red polimérica, observándose un desplazamiento a mayores temperaturas a medida que aumenta la densidad de entrecruzamiento. Sin embargo, la naturaleza del entrecruzamiento en el caucho natural es muy peculiar, ya que concierne exclusivamente a los extremos de cadena. De este modo, se puede entender que la modificación del entrecruzamiento del caucho natural por los diferentes tratamientos físicos y químicos realizados apenas afecten los movimientos segmentales de la cadena polimérica, ya que el peso molecular entre los entrecruzamientos es muy alto, del orden de 10^6 g/mol. Por su parte, el parámetro de la resistencia de fragilidad, D, relacionado con las características del movimiento segmental por encima de la temperatura de transición vítrea, apenas varía con los tratamientos y muestra un valor alrededor de 4, indicando que el caucho natural es un sistema dinámicamente frágil como se corresponde en general, con materiales poliméricos.

Además del modo segmental, todas las muestras investigadas exhiben otro proceso de relajación a mayores temperaturas asociado al modo normal. El principal efecto observado en la dinámica del modo normal para las diferentes muestras analizadas, es la dependencia de la movilidad de la cadena con el entrecruzamiento en los extremos de la cadena. Así, la muestra con cadenas lineales de poliisopreno sin entrecruzamientos en los finales de cadena (*TE-DPNR*) muestra una dinámica de cadena más lenta que la muestra *GEL* con entrecruzamientos en los extremos de cadena α y ω, mientras la muestra de caucho natural desproteinizada, *DPNR* exhibe la dinámica más rápida.

La muestra de DPNR se encuentra entrecruzada por los fosfolípidos en los extremos de cadena α. En una primera aproximación, se puede considerar al *DPNR* como un *polímero estrella*, en el que la zona central de la estrella tiene una naturaleza diferente a la de los brazos de la estrella. En general, se ha indicado en la literatura, que los polímeros estrella muestran una dinámica de relajación cuatro veces más lenta que las cadenas lineales libres de similar longitud a ésas que forman los brazos de la estrella. Sin duda, estos resultados se contradicen con nuestras observaciones, ya que la muestra desproteinizada, *DPNR* presenta una dinámica mucho más rápida que la muestra de caucho natural lineal, *TE-DPNR*.

Sin embargo, si se ha observado una dinámica de relajación del modo normal más rápida para la estrella del poliisopreno en comparación con los brazos lineales bajo condiciones de confinamiento. Así por ejemplo, Floudas al analizar la dinámica del poliisopreno en copolímeros dibloque donde el poliisopreno forma la zona central y el poliestireno constituye la zona exterior o corona, observó que la relajación del modo normal se encuentra fuertemente influenciada por el confinamiento espacial inducido por la fase de poliestireno. Esta fase confina al centro estrella de poliisopreno dentro de un radio de giro R, tal que $<(\Delta R)>^2 \approx b(M_e)^{1/2}$, donde b indica la longitud del segmento estadístico (~ 0.68 nm para PI) y M_e representa el peso molecular entre entrelazamientos (~ 5.000 para PI). El principal efecto es un incremento de la movilidad de la cadena de poliisopreno, que se puede explicar, considerando que el modo normal dieléctrico viene dado fundamentalmente por el movimiento de la parte estrella central. Según los cálculos realizados aplicando el modelo de Rouse, la relajación del modo normal puede ser mucho más rápida que la de los brazos si se cumple que $M > 1.5\, M_e$.

Según estos estudios, es posible explicar la dinámica de relajación del modo normal más rápida de la muestra de caucho natural desproteinizada, *DPNR* respecto de la muestra constituida por cadenas lineales de poliisopreno, *TE-DPNR*. La muestra de *DPNR* se puede considerar como un polímero estrella híbrido ya que el corazón de la estrella es químicamente diferente a la de los brazos. Es de esperar, que esta heterogeneidad química de lugar a una movilidad molecular muy diferente del núcleo o zona central constituida por los fosfolípidos con respecto a la zona más externa de poliisopreno. La zona central de fosfolípidos, debido a su tamaño, tiene una movilidad restringida respecto a la zona externa, es decir, se encuentra efectivamente confinado. Además, existe un confinamiento topológico inducido por los entrecruzamientos físicos. Es de esperar, que este efecto sea muy significativo, ya que el peso molecular de los brazos de poliisopreno es aproximadamente tres órdenes de magnitud mayor que el M_e.

Debido a los entrecruzamientos físicos, el centro estrella no es libre para explorar el espacio completo ya que su movimiento se encuentra restringido a un espacio delimitado. Para superar esta situación desfavorable, el centro estrella tiende a localizarse. Según los estudios llevados a cabo por Floudas, la relación entre el tiempo de relajación del polímero estrella, τ_{est}, y la del brazo τ_{bra}, para una estrella homogénea viene dada por la relación:

$$\frac{\tau_{star}}{\tau_{linear}} \alpha \left(\frac{M_e}{M} \right)^3$$

Donde M es el peso molecular del brazo y M_e es el peso molecular entre entrecruzamientos y la constante de proporcionalidad es el número de brazos. Esta relación predice que la relajación del modo normal de la cadena se volverá más rápida cuando $M > 1.5 Me$.

Considerando que el peso molecular del poliisopreno lineal (*TE-DPNR*) es de 10^6 g/mol, con un M_e de $5*10^3$, entonces de esperar, que la dinámica molecular del modo normal para la muestra desproteinizada, *DPNR* sea más rápida que la del caucho natural con cadenas de poliisopreno lineales, *TE-DPNR*, como experimentalmente se ha observado.

Finalmente, podemos confirmar, que la espectroscopia de relajación dieléctrica de banda ancha es una técnica idónea para el estudio de la dinámica molecular de compuestos de caucho natural.

Una vez perfectamente analizada la dinámica molecular de nuestro sistema en función de sus componentes biológicos, el objetivo de la Tesis Doctoral se centró en comprender el efecto de las nanopartículas basadas en silicatos laminares sobre la microestructura y dinámica molecular del caucho natural que permitan explicar la considerable mejora de propiedades mecánicas y físicas que exhiben estos sistemas en relación a los sistemas convencionales con cargas micrométricos, como el negro de carbono o la sílice precipitada, con una menor proporción (hasta cuatro veces) de carga en el compuesto.

Es necesario profundizar en el conocimiento de las interacciones nanopartícula-polímero, analizar la dinámica molecular del nanocompuesto y, estudiar, el efecto de las nanopartículas sobre la cristalización inducida del caucho natural bajo deformación uniaxial, así como sobre la red elastomérica.

Antes del mencionado estudio, se optimizaron los parámetros para la obtención de una estructura que exhibiera una delaminación/exfoliación máxima de la nanoarcilla observada mediante difracción de rayos X y microscopia electrónica de transmisión. Para ello se estudió el efecto de la longitud de la cadena de alquilamonio, la estructura y la densidad de injerto de las moléculas orgánicas de surfactante cubriendo la superficie de la nanoarcilla sobre la miscibilidad y dispersión del silicato en el caucho natural.

Las aminas cuaternarias conteniendo en su estructura más de una cadena alquílica de al menos 18 átomos de carbono se mostraron como los candidatos idóneos a la hora de modificar superficialmente la nanoarcilla y obtener una estructura lo más delaminada y dispersa posible. Además, el empleo de sales de amonio cuaternarias como agentes compatibilizantes de la nanoarcilla con el polímero, no afecta al grado de entrecruzamiento de la matriz elastomérica como se comprobó por medidas calorimétricas y de hinchamiento en tolueno. Por tanto, el empleo de sales de amonio cuaternarias no solo nos aporta una microestructura donde la nanoarcilla se encuentra delaminada en su máxima extensión, sino que además, no modifica las características físicas de la red polimérica, pudiendo adscribir el resto de posibles cambios a la presencia de la nanoarcilla.

Esto tiene una enorme importancia en el proceso de cristalización, pues es sabido que regiones con una mayor densidad de entrecruzamiento favorecerán la orientación molecular de las cadenas y por tanto, la cristalización. Sin embargo, al mismo tiempo estas regiones presentarán una mayor dificultad para la nucleación de los cristales debido a su reducida movilidad como consecuencia de la alta densidad de entrecruzamiento. En definitiva, la presencia de una red heterogénea, dificultaría nuestro estudio no pudiendo discernir entre los distintos factores que están afectando a las propiedades observadas.

Las propiedades viscoelásticas de los nanocompuestos también fueron contrastadas con compuestos de caucho natural conteniendo partículas de arcilla sin modificar orgánicamente y por tanto, de tamaño micrométrico, así como con la propia matriz de caucho natural vulcanizada. Solo en presencia de la nanoarcilla, el módulo elástico presenta un aumento considerable en comparación con los otros dos compuestos anteriormente mencionados. Aunque, este aumento en el módulo elástico se debe en gran medida a un efecto hidrodinámico provocado por la alta dispersión de las nanopartículas de arcilla en la matriz, no podemos descartar el efecto también debido a la alta superficie de la nanoarcilla en contacto con las cadenas de polímero. Dicho efecto da lugar a la generación de una gran cantidad de interfase y consecuentemente, a un alto grado de interacción. Esta interacción a su vez, puede estar provocando una disminución en la movilidad de las cadenas de caucho dando lugar a un aumento en la temperatura de transición vítrea observado en el régimen de baja deformación, como es el que se estudió para las propiedades viscoelásticas de los nanocompuestos.

La presencia de una interfase de polímero en la superficie de la nanoarcilla, ha sido también observada mediante el empleo de la espectroscopia dieléctrica de banda ancha. Se ha asignado la presencia de una relajación más lenta que la segmental (“bulk”), proveniente de las cadenas de cis–poliisopreno que se encuentran adsorbidas en la superficie de la nanoarcilla. El estudio y detección de este modo de relajación es muy importante para la comprensión posterior de las propiedades del nanocompuesto, pues la presencia de esta fracción de polímero adsorbida en la superficie de la arcilla es consecuencia directa de la creación de una gran cantidad de área interfacial debido a la alta dispersión de las nanopartículas. Se trata de un parámetro decisivo también en el proceso de cristalización durante deformación del caucho natural como discutiremos a continuación.

Previamente al estudio de cristalización, se evalúo mediante espectroscopia dieléctrica de banda ancha, el efecto de la nanoarcilla en la distribución de los distintos componentes de la red polimérica como son los entrelazamientos (físicos y químicos), así como los defectos (lazos y colgajos). La presencia de la nanoarcilla proporciona una distribución de los componentes de la red polimérica más homogénea así como un decrecimiento de la cantidad de defectos de la red, como se demostró por la presencia de una única distribución en el tiempo de relajación del momento dipolar correspondiente al segmento de la cadena de cis–poliisopreno. Se sugiere que esta homogeneidad en la red polimérica debe tener un efecto directo en el proceso de cristalización de la matriz de caucho natural, pues las imperfecciones de la red (defectos) no intervienen en la orientación de las cadenas poliméricas durante la cristalización inducida por deformación.

Esto se pudo comprobar comparando medidas de muestras en seco e hinchadas en tolueno. Mientras que apenas si hubo diferencias entre las muestras estudiadas en seco en lo que a la posición del modo segmental se refiere, las muestras hinchadas en tolueno presentaban muchas diferencias entre sí. La presencia de un disolvente como el tolueno provocó que los entrelazamientos físicos dejasen de ser efectivos. De manera, que ahora incluso el modo normal se podía incluso observar.

En el caso de las muestras sin partículas reforzantes o aquellas presentando partículas de tamaño micrométrico se detectaron varias distribuciones de tiempos de relajación correspondiente al modo segmental. Sin embargo, para la muestra conteniendo nanoarcilla solo se observó una distribución correspondiente al modo segmental. Por tanto, debido a que las muestras conteniendo o no nanoarcilla presentaban la misma masa molecular y polidispersidad, las variaciones en la red polimérica detectadas mediante la espectroscopia dieléctrica se pueden atribuir principalmente a variaciones en la distribución de los distintos componentes de la red (entrecruzamientos físicos y químicos).

Otra de las características fundamentales, que definen las excelentes propiedades físicas y mecánicas del caucho natural en comparación con sus homólogos cauchos sintéticos, es su capacidad de cristalizar bajo deformación uniaxial. Por lo que se consideró de máximo interés analizar el efecto de la nanoarcilla sobre la cristalización inducida del caucho natural.

Este estudio se llevó a cabo mediante medidas in-situ de difracción de rayos X por radiación sincrotrón durante la deformación uniaxial de las muestras de caucho natural, lo que conlleva las siguientes ventajas:

(a) la obtención de una serie de difractogramas en dos dimensiones y en tiempo real gracias a la alta intensidad de la radiación sincrotrón.

(b) el seguimiento preciso de la dinámica del proceso de deformación así como los cambios microestructurales que están teniendo lugar.

(c) la obtención de la respuesta mecánica del nanocompuesto durante la evolución microestructural del mismo.

Se tomaron difractogramas de las muestras a diferentes deformaciones durante el proceso de estiramiento y de retracción del material. Todas las imágenes mostraban las orientaciones de las reflexiones a 100, 200 y 300 correspondientes a los silicatos laminares, indicando que las nanopartículas de arcilla se orientan en la dirección de la deformación. La orientación comenzaba a bajas deformaciones, $\alpha = 0.4$ (40 % de deformación) e incrementaba progresivamente con la deformación, hasta alcanzar un máximo de alineamiento para un $\alpha = 4$ (400 % de deformación).

Además de la orientación de las nanoarcillas, los difractogramas mostraban la cristalización inducida del caucho natural, la cual se evidenciaba por el alineamiento de las reflexiones a 200 y 120 correspondientes a la matriz de caucho natural. No se detectó la orientación de la fase amorfa, a diferencia de otros autores que la han observado por medidas de resonancia magnética nuclear de protón. Es probable, que si se produjera la orientación de la fase amorfa, ésta fuera muy pequeña para no poderse detectar por difracción de rayos X.

Es interesante destacar, que las nanopartículas provocan la presencia de los primeros núcleos cristalinos a deformaciones inferiores que en ausencia de la nanopartícula o en comparación con partículas de tamaño micrométrico. El valor mínimo de deformación para que se produzca la cristalización inducida del caucho natural sin reforzar es de un 3.3, el cual se reduce notablemente, hasta un 1.2, en presencia de las nanopartículas. Además, la nanoarcilla favorece el proceso de cristalización inducida del caucho natural como consecuencia de la gran cantidad de área interfacial por volumen implicada en el proceso. Esto se refleja en un considerable aumento del índice de cristalinidad total en el nanocompuesto. Así, mientras el caucho natural sin reforzar exhibe una cristalinidad máxima del 25 %, ésta aumenta hasta un 48 % en presencia de las nanopartículas.

Otros estudios de cristalización inducida del caucho natural, han mostrado una disminución en el valor mínimo de deformación, a aproximadamente $\alpha = 2$, en presencia de partículas micrométricas, como el negro de carbono, sílice precipitada o carbonato cálcico, pero no se han apreciado variaciones en la cristalinilidad total del caucho natural.

La principal diferencia entre estas cargas tradicionales y las nanopartículas de arcilla se debe a la alta relación longitud/diámetro de aproximadamente 10^3-10^4 m^2/mL para las nanopartículas en comparación a 10^{-1}-10^2 m^2/mL para las cargas convencionales. Esto puede producir mayores interacciones interfaciales entre la matriz polimérica y las nanopartículas, dando lugar a una más efectiva transferencia de esfuerzos a lo largo de la matriz. Esta mayor región interfacial puede conducir a una prematura orientación de las cadenas poliméricas, y de este modo, promover la nucleación durante la deformación.

Además, se observó un diferente mecanismo de cristalización del caucho natural en presencia de las nanopartículas. El caucho natural sin reforzar mostraba una única etapa de cristalización, mientras que los nanocompuestos de caucho natural exhibían dos etapas de cristalización perfectamente definidas: la primera hasta deformaciones, $\alpha < 3$, relacionada con la orientación y alineamiento de las nanoarcillas durante la deformación formando una red física, mientras la segunda ($3 \leq \alpha \leq 4$), correspondiente al mecanismo típico de cristalización del caucho natural, pero con un índice de cristalinidad y una pendiente aproximadamente el doble que la del caucho natural sin cargar.

También se analizó el efecto de la cantidad de surfactante en la superficie de la arcilla sobre la cristalinidad del caucho natural. Para ello, lo que se hizo fue extraer el exceso de surfactante de la arcilla orgánicamente modificada con una sal cuaternaria de alquilamonio (aproximadamente un 6.2 % en peso).

No se observaron variaciones en el valor mínimo de deformación necesario para inducir la cristalización del caucho natural, pero si se apreció que el índice de cristalinidad depende directamente de la cantidad de surfactante en la superficie de la nanoarcilla. El índice de cristalinidad disminuía de un 50 % a un 25 % al eliminar el exceso de surfactante. Ambas nanoarcillas mostraban dos etapas en el mecanismo de cristalización, si bien sus pendientes eran muy diferentes. La organoarcilla con exceso de surfactante mostraba en la primera etapa de cristalización una pendiente con un orden de magnitud superior, mientras que la pendiente en la segunda etapa era prácticamente el doble que la de la nanoarcilla sin exceso de surfactante.

Es evidente, que la mayor cantidad de moléculas de surfactante en la superficie de las nanopartículas favorece la movilidad de las cadenas de caucho, induciendo su cristalización bajo deformación.

Una vez profundizado en el conocimiento de las interacciones entre la nanocarga y el polímero, otro de los objetivos perseguidos en esta Tesis Doctoral, es preparar nanocompuestos en una sola etapa. Una de las principales limitaciones en el desarrollo masivo de estos materiales a nivel industrial, se debe, como ya se comentó en la introducción, a la necesidad de llevar a cabo una etapa previa de modificación de las nanopartículas, denominada reacción de organofilización, para mejorar la compatibilidad y dispersión de las nanopartículas en la matriz polimérica.

En este estudio, se pretende obtener nanocompuestos de caucho natural y nanoarcilla sin necesidad de llevar a cabo la etapa previa de intercambio catiónico, mediante el empleo de un polímero polar de carácter anfifílico como es el polietilenglicol, PEG. Los materiales se prepararon en estado fundido en un mezclador interno o Haake, en el que se iban incorporando todos los ingredientes del compuesto. Se utilizaron diferentes concentraciones de PEG, y el proceso de intercalación del caucho natural y del polietilenglicol se analizó mediante difracción de rayos X y microscopia electrónica de transmisión.

El PEG es un polímero polar de bajo peso molecular que se intercala fácilmente entre las láminas del silicato, hasta un máximo de un 19 % en peso, correspondiente a una bicapa de PEG insertado en las galerías del silicato. Esta estructura de bicapa impide la inserción de una mayor cantidad de PEG entre las láminas del silicato. Esto proporciona un aumento del espaciado basal de 11.7 Å para la montmorillonita sódica a 18 Å en presencia del PEG.

En presencia del caucho natural, se aprecia un aumento de la distancia interlaminar del silicato, indicando que parte de las cadenas elastoméricas se han insertado en las galerías de la montmorillonita. La inserción de las cadenas de caucho en presencia del PEG implica que dos fenómenos están teniendo lugar:

- superar las altas fuerzas atractivas de carácter electrostático y de Van der Waals entre las dos láminas del silicato, lo cual evita una separación superior a los 18 Å para una montmorillonita sódica.
- el mezclado favorable entre dos componentes termodinámicamente inmiscibles como las cadenas apolares e hidrofóbicas de poliisopreno y la arcilla polar e hidrofílica.

Se sugiere una disposición de las cadenas de caucho natural intercaladas en la zona central de la galería del silicato laminar interaccionando con las cadenas de PEG, las cuales actúan como interfase entre los componentes más hidrofóbicos, poliisopreno, y los más hidrofílicos, las moléculas polares de agua que rodean a los cationes contenidos en el interior de la galería. Se evidenció por tanto, como el polietilenglicol actúa como co–agente de intercalación favoreciendo la intercalación del caucho natural en la galería de la nanoarcilla mejorando de esta manera la dispersión de la misma en comparación con el caso en el que se emplea la nanoarcilla sin modificar.

También, se estudió la influencia del polietilenglicol en la estructura de la red elastomérica mediante resonancia magnética nuclear de protón de campo bajo aplicando el método de doble cuanto. Este es un método novedoso que presenta numerosas ventajas respecto a otros métodos de resonancia magnética nuclear. El empleo del método de doble cuanto nos permite la obtención en un mismo experimento de dos conjuntos de datos: uno de ellos conteniendo información de tipo estructural sobre la red polimérica y el otro aportándonos información sobre la dinámica molecular de las cadenas de polímero que constituyen la red. Otra de las ventajas del empleo de la resonancia magnética nuclear para el estudio de los parámetros físicos de la red polimérica en comparación con los métodos convencionales como el hinchamiento de las muestras en disolvente orgánicos y el cálculo posterior del volumen hinchado, es que los valores de la masa molecular entre entrelazamientos de la red son referidos a nudos físicos y químicos, pues se trata de una medida de carácter no destructiva, donde la muestra está seca, y por tanto, los entrelazamientos físicos siguen formando parte de la red polimérica, a diferencia de otros métodos en húmedo.

Se observó que la arcilla tiene un efecto inhibidor sobre el proceso de vulcanización, disminuyendo el estado final de curado de la matriz. Los grupos superficiales de la carga reaccionan o se absorben con los agentes de vulcanización, disminuyendo la eficiencia de la reacción de vulcanización, lo que se refleja en un descenso de la constante de acoplamiento residual bipolar, D_{res}, y de la densidad de entrecruzamiento, dado por $1/M_c$. Esta tendencia concuerda con los resultados obtenidos mediante medidas de hinchamiento en tolueno, si bien en este caso, los valores absolutos son inferiores, ya que no se tienen en cuenta los entrecruzamientos físicos, mientras que en las medidas realizadas por RMN participan tanto los entrecruzamientos químicos como físicos.

Sin embargo, la adición del PEG producía el efecto contrario, evitando el efecto no deseado de los silicatos laminares. El PEG tiene fuertes interacciones adsortivas que reducen o eliminan las interacciones directas de la arcilla con el caucho. Es evidente, que el PEG forma parte en el proceso de entrecruzamiento del caucho natural, incrementando su eficiencia. El PEG provoca un efecto sinérgico con los agentes de vulcanización, lo que conlleva a un aumento de la densidad de entrecruzamiento. Este efecto es máximo para concentraciones bajas de PEG (1 pcc, partes por cien de caucho), mientras, que en el material compuesto, se requieren concentraciones más altas (2.5 pcc), indicando que una fracción del PEG se encuentra absorbida sobre la superficie de la arcilla y no participa directamente en el proceso de entrecruzamiento.

Mediante estos estudios, se pudo optimizar la relación de polietilenglicol/nanoarcilla a la cual la densidad de entrecruzamiento era máxima, lo que contribuyó también de forma clara a la mejora de las propiedades mecánicas finales del material.

CAPÍTULO V

CONCLUSIONES

En este trabajo de Tesis Doctoral se ha estudiado principalmente la dinámica molecular y la microestructura de nanocompuestos basados en matrices de caucho natural reforzado con nanoarcillas. Los nanocompuestos han sido exhaustivamente estudiados tanto desde el punto de vista estructural por difracción de rayos X y microscopia electrónica de transmisión, así como en términos de dinámica molecular por espectroscopia dieléctrica de banda ancha. La cristalización inducida bajo deformación uniaxial de la matriz de caucho natural en presencia de la nanoarcilla se estudió in–situ por difracción de rayos X mediante el empleo de radiación sincrotrón.

En concreto se llevaron a cabo los siguientes estudios de los que se extrajeron a su vez los siguientes resultados y conclusiones más relevantes:

1. Estudio de la dinámica molecular mediante espectroscopia dieléctrica de diferentes compuestos de caucho natural evidenciando diferente microestructura. Por primera vez, se analizó el efecto de componentes biológicos como proteínas y fosfolípidos en la dinámica molecular del caucho natural. Estos componentes tienen un impacto directo sobre las propiedades mecánicas finales del polímero. La principal evidencia obtenida por espectroscopia dieléctrica fue la presencia de una dinámica molecular dependiente de los entrecruzamientos formados entre los finales de cadena lineal de cis–poliisopreno y los componentes de naturaleza biológica. Se ha propuesto una estructura híbrida tipo *estrella* en la que el núcleo (lípidos y/o proteínas) se haya confinado entre las cadenas unidas a dicho núcleo (cis–poliisopreno), dando lugar a una dinámica más rápida que en el caso de no estar presentes dichos componentes de naturaleza biológica.

2. Se optimizaron los parámetros para la obtención de una estructura que exhibe una delaminación/exfoliación máxima de la nanoarcilla observada mediante difracción de rayos X y microscopia electrónica de transmisión. Para ello se llevaron a cabo tratamientos de modificación superficial de la nanoarcilla con distintas moléculas de surfactante presentando distinta funcionalidad y longitud de cadena. La modificación de la superficie de las nanopartículas de arcilla con sales primarias de alquilamonio presentando una cadena alifática lineal proporcionaba una microestructura donde abundaba la presencia de láminas individuales de nanoarcilla, pero también se observaban agregados de tamaño micrométrico, síntoma de un bajo grado de miscibilidad con el polímero. Sin embargo, el empleo de sales de aminas cuaternarias conteniendo en su estructura más de una cadena alquílica de al menos 18 átomos de carbono, daba lugar a una distribución homogénea de agrupaciones de no más de 10 láminas individuales de nanoarcilla, perfectamente separadas entre sí, como consecuencia del alto grado de miscibilidad de la nanoarcilla con el polímero. A su vez, estos hechos confirmaban la existencia de un mecanismo de exfoliación/delaminación diferente según se emplee una amina primaria lineal o cuaternaria en la modificación superficial de la nanoarcilla.

3. Una vez controlada la dispersión de la nanoarcilla en la matriz de caucho natural, y previo al estudio de cristalización se evalúo mediante espectroscopia dieléctrica de banda ancha el efecto de la nanoarcilla en la distribución de los distintos componentes de la red polimérica como son los entrelazamientos (físicos y químicos) así como los defectos (lazos y colgajos). La presencia de la nanoarcilla proporcionaba una distribución más homogénea de los componentes de la red polimérica y una disminución de la cantidad de defectos de la red,

como se demostró por la presencia de una única distribución de tiempos de relajación del momento dipolar correspondiente al segmento de la cadena de cis–poliisopreno.

Así mismo, se observó una nueva relajación dipolar en los nanocompuestos asignada a la fracción de polímero que se encuentran adsorbido en la superficie de la nanoarcilla, y que no aparecía en el caucho natural en ausencia de nanopartículas. Esta interfase de polímero en la superficie de la arcilla es consecuencia directa de la creación de un enorme área interfacial debida a la alta dispersión de las nanopartículas en la matriz polimérica. Esta relajación exhibe una temperatura de transición vítrea considerablemente mayor que la relajación segmental, por lo que el movimiento de las cadenas de polímero adsorbidas es más lento que el resto de las cadenas que constituyen la matriz polimérica. Es la primera vez que se detecta una nueva relajación en materiales compuestos por espectroscopia dieléctrica, y su detección es de gran importancia para poder explicar la mejora de propiedades físicas y mecánicas de estos nanomateriales en relación a los materiales compuestos convencionales, incluso con la incorporación de una menor cantidad de carga en el material.

4. Se estudió el efecto de las nanopartículas sobre el proceso de cristalización inducida del caucho natural bajo deformación uniaxial mediante medidas de difracción de rayos X in-situ empleando radiación sincrotón. En primer lugar, se observó que las nanopartículas se orientaban a medida que se deformaba el material alcanzando un máximo de alineamiento a altas deformaciones (alrededor de un 400 %). Por otro lado, se evidenció por vez primera, un efecto directo de las nanopartículas en la evolución de los cristales de cis–poliisopreno durante la deformación uniaxial. La nanoarcilla provocaba la presencia de

los primeros núcleos cristalinos a deformaciones menores que en ausencia de la nanopartícula o en comparación con partículas de tamaño micrométrico, como el negro de carbono o la sílice precipitada. También, se observó que las nanopartículas aceleraban el proceso de cristalización como consecuencia de la alta área interfacial por volumen implicada en el proceso. Esto se reflejó en un aumento del índice de cristalinidad total del caucho natural (prácticamente el doble) en presencia de las nanopartículas. Además, las nanopartículas provocaban un diferente mecanismo de cristalización. Mientras el caucho natural sin cargar mostraba una única etapa de cristalización, los nanocompuestos de caucho natural exhibían dos etapas de cristalización perfectamente definidas. Así mismo, también se observó una dependencia directa del índice de cristalinidad total con la cantidad de moléculas de surfactante en la superficie de la nanoarcilla.

Estos resultados son sumamente interesantes ya que las excelentes propiedades del caucho natural en relación con sus homólogos sintéticos, se deben en parte a su capacidad de cristalizar bajo deformación uniaxial. A diferencia de las cargas micrométricas convencionales, las nanopartículas favorecen el proceso de cristalización del caucho natural lo que puede permitir explicar la considerable mejora en las propiedades mecánicas de estos sistemas.

5. Por último, se estudió la producción de nanocompuestos de caucho natural y nanoarcilla sin necesidad de la etapa previa de intercambio catiónico mediante el empleo de un polimérico polar de carácter anfifílico como es el polietilenglicol. Se estudió el proceso de intercalación del caucho natural y del polietilenglicol mediante difracción de rayos X y microscopia electrónica de transmisión.

Se sugiere una disposición de las cadenas de caucho natural intercaladas en la zona central de la galería de la nanoarcilla, mientras que las cadenas de polietilenglicol interaccionan con las moléculas polares de agua que rodean a los cationes presentes en el interior de la galería. Se evidenció por tanto, como el polietilenglicol actúa como co–agente de intercalación favoreciendo la intercalación del caucho natural en la galería de la nanoarcilla y mejorando la dispersión de la misma en comparación con el caso en el que se emplea la nanoarcilla sin modificar.

También, hemos estudiado la influencia del polietilenglicol en la estructura de la red polimérica mediante resonancia magnética nuclear de protón de campo bajo mediante la aplicación del método de doble cuanto. Se encontró una relación óptima de polietilenglicol/nanoarcilla a la cual la densidad de entrecruzamiento era máxima, lo que contribuyó también de forma clara a la mejora de las propiedades mecánicas finales del material.

ANEXO

Available online at www.sciencedirect.com

ScienceDirect

Composites Science and Technology 67 (2007) 1330–1339

COMPOSITES SCIENCE AND TECHNOLOGY

www.elsevier.com/locate/compscitech

Morphology/behaviour relationship of nanocomposites based on natural rubber/epoxidized natural rubber blends

M. Arroyo *, M.A. López-Manchado, J.L. Valentín, J. Carretero

Institute of Polymer Science and Technology, C.S.I.C. C/Juan de la Cierva, 3 28006 Madrid, Spain

Received 11 January 2006; received in revised form 4 August 2006; accepted 28 September 2006
Available online 14 November 2006

Abstract

In order to analyze the effect of an epoxidized natural rubber (ENR) and filler treatment on the morphology and behavior of natural rubber (NR) nanocomposites, blends of these polymers have been prepared. The nature and extent of the clay dispersions in the filled samples were evaluated by X-ray diffraction. In the presence of ENR, an exfoliated structure was obtained which suggests that enough rubbery polymer was incorporated into the interlayer spacing. The effect of clay in rubber compounds was analyzed through rheological, mechanical and swelling characterization. A sensible improvement in the nanocomposite properties was observed by the addition of organoclay. It has been deduced that the properties of the compounds strongly depend on the extent of the silicate nanolayers dispersion into the rubber matrices as well as on the organoclay type and elastomer compatibility.

Keywords: A. Polymer–matrix composites; B. Mechanical properties; A. Nanostructures

1. Introduction

Blending of elastomers have been often used to obtain an optimum number of desirable combinations, physical properties, processability and cost. Natural rubber (NR) shows very interesting physical properties due to its ability to crystallize under stretching. However, NR exhibits a limited ozone resistance and a high dependence of dynamic properties on temperature because of damping derived from high glass transition temperature (T_g). To overcome these limitations, NR is blended with other elastomers such as nitrile rubber (NBR), ethylene–propylene copolymer (EPM), ethylene–propylene–diene terpolymer (EPDM) and epoxidized natural rubber (ENR). ENR obtained by epoxidation of 1,4-polyisoprene shows a higher glass transition temperature than the pristine 1,4-polyisoprene, with an increase in the polarity of the system while retaining the inherent high strength of NR.

In recent years, hybrid organic–inorganic nanocomposites consisting of a polymeric matrix and a layered silicate has inspired scientists to a range of potential applications [1–6]. Due to their nanometer phase dimensions, nanocomposites exhibit significant improvements in physical and mechanical properties in relation to the polymer host [7–12]. The addition of just a low percentage of nanolayered inorganic can increase the stiffness and strength with a minimal loss in ductility and impact resistance, decreases the permeability and swelling in solvents, improves the abrasion, flame resistance and thermal endurance, with an enhancement in electrical conductivity and optical properties [13].

Although clay nanocomposites have been prepared for many thermoplastics and thermosetting polymers, rubber nanocomposites constitute only a minor proportion [11,14–19]. Mohamed and Simon [20] and Utracki [21] recently reported the most significant advances happened in the preparation, characterization and properties of organoclay/rubber nanocomposites based on several rubber matrices, such as natural rubber, synthetic polyisoprene, styrene-butadiene, butyl rubber, polybutadiene,

---

* Corresponding author. Tel.: +34 915622900; fax: +34 915644853.
E-mail address: marroyo@ictp.csic.es (M. Arroyo).

0266-3538/$ - see front matter © 2006 Elsevier Ltd. All rights reserved.
doi:10.1016/j.compscitech.2006.09.019

ethylene–propylene, silicone and nitrile rubbers. Rubber nanocomposites with an exfoliated morphology have been successfully prepared by several methods, in situ polymerization, solution blending, latex compounding and direct melt intercalation. However, scarce information about organoclay/rubber blends ternary nanocomposites can be found [22,23]. The present work focuses on the development of natural rubber/epoxidized natural rubber/organoclay ternary nanocomposites by melt intercalation processing. This processing technique requires information on the rheological behaviour of the system which depend on several factors, such as polymer–polymer or polymer–filler interactions and the morphology of the system. Recent publications on the rheology of rubber–organoclay nanocomposites provide information in this field [24–28]. In addition, since ENR exhibits polar groups, a more fine dispersion of organoclay in these systems can be expected. Varghese et al. [29] and Teh et al. [30] have already demonstrated the efficiency of ENR as compatibilizer for organoclay/NR nanocomposites, which was reflected in an increase of physical and mechanical properties of nanocomposites.

So, in the view of the above exposed, two epoxidized natural rubber (having 25 or 50 mol% epoxidation) and a phyllosilicate with different surface treatments have been used to analyze the effect of matrix polarity and clay treatment on the morphology, rheological behaviour, vulcanization parameters and mechanical properties of NR/ENR/organoclay ternary nanocomposites.

2. Experimental

2.1. Materials

Natural rubber was kindly supplied by Malaysia Rubber (Berhad, Malaysia) under the trade name CV 60 [Mooney viscosity, ML(1+4) 100 °C = 60]. Two commercial grades of epoxidized natural rubber (kindly provided by Kumpulan Guthrie), ENR25 and ENR50, having 25 and 50 mol% epoxidic units, respectively, were used in this study. Three clays supplied by Southern Clay Products (Gonzales, TX) under the trade name of Cloisite® [31], in particular, a natural montmorillonite described as Cloisite-Na$^+$ (C6A) and this montmorillonite modified with quaternary ammonium salts, Cloisite 15A (C15A) and Cloisite 30B (C30B) have also been used. The structural characteristics and X-ray diffraction (XRD) patterns of the clays are reported in Table 1 and Fig. 1, respectively. Prior to be used, the clays were dried under vacuum, at 80 °C, for 12 h.

2.2. Procedures

Rubber compounds were prepared in an open two-roll laboratory mixing mill at room temperature. The rotors operated at a speed ratio of 1:1.4. Firstly, polymer, processing aids and fillers were blended (5 parts of clay per hundred of rubber (phr)). Then, the curatives were added. The formulations of the compounds are compiled in Table 2. Vulcanization was carried out on an electrically heated hydraulic press, at 150 °C, for the optimum cure time (t_{90}), previously determined from an oscillating disk Rheometer. Specimens were mechanically cut out from the vulcanized plaques.

Table 1
Technical characteristics of the fillers used

	Organic modifier	Basal spacing (001), Å	Modifier concentration (meq/100 g clay)
Cloisite-Na$^+$ (C6A)		11.7	
Cloisite 15A (C15A)	2M2HT[a]	31.5	125
Cloisite 30B (C30B)	MT2EtOH[b]	18.5	90

Tallow consists in ∼65% C18, ∼30% C16 and ∼5% C14, and a chloride anion.

Data supplied by Nanocor[19].

[a] 2M2HT: dimethyl,dihydrogenatedtallow, quaternary ammonium.

[b] MT2EtOH: methyl,tallow,bis-2-hydroxyethyl, quaternary ammonium.

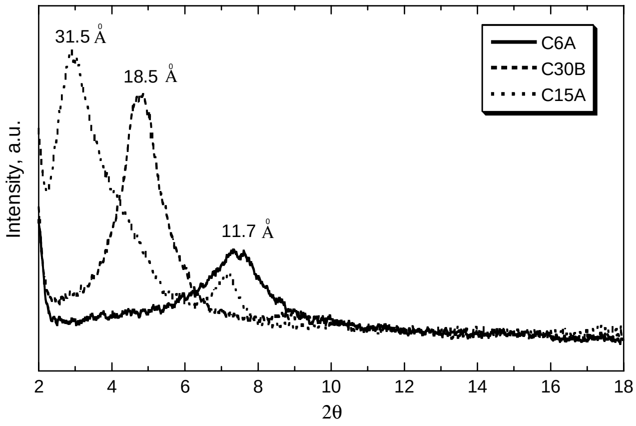

Fig. 1. XRD patterns of clays.

Table 2
Recipe of the rubber compounds

Natural rubber	100	75	50
Epoxidized natural rubber, ENR25/50	–	25	50
Zinc oxide	5	5	5
Stearic acid	1	1	1
Sulfur	1.5	1.5	1.5
MBTS[a]	1.5	1.5	1.5
PBN[b]	1	1	1
Organoclay	5	5	5

[a] Benzothiazyl disulfide.

[b] Phenyl beta naphthyl amine.

2.3. Morphological and mechanical characterization

X-ray diffraction (XRD) was used to characterize the nature and extent of the dispersions of the clays in the filled samples. XRD patterns were collected using a Philips diffractometer at the wage length λ Cu Kα = 1.54 Å, a tube voltage of 40 kV and tube current of 25 mA. Bragg's law was used to compute the crystallographic spacing (d) of the clays.

The dispersion and morphology of the clay particles in the composites were analyzed by transmission electron microscopy (TEM). Samples were prepared by means of a cryo-ultramicrotome and observed on a Jeol JEM 2000 FX microscope with an accelerating voltage of 80 kV.

Morphological changes on NR/ENR by adding of the filler were observed in a Philips XL30 environmental scanning electron microscope (ESEM) at high vacuum mode operated at 30 kV. Samples were coated with Au–Pd in a sputter coated Polaron SC7640 before observation.

Mooney viscosity measurements were performed on a Mooney viscosimeter at 100 °C, with a pre-heating time of one minute and a set time of 4 min.

Cure characteristics of the compounds were determined on a Monsanto MDR 2000E Moving Die Rheometer (Alpha Technologies, Swindon, UK) at 150 °C.

The number of active network chain segments per unit of volume (crosslinking density) was determined on the basis of solvent-swelling measurements (toluene during 72 h, at room temperature) by application of the Flory–Rhener equation.

Stress–strain properties were measured according to ISO 37-1977 specifications on an Instrom dynamometer 4301, at 25 °C, and at a cross-head speed of 500 mm/min. Shore hardness was measured according to ASTM D-2240 by using a Bareiss Rockwell tester Rebound resilience measurements were carried out according to ISO 4662-1978 specifications on a Schob pendulum. In all tests, the results are the average of at least five measurements.

3. Results and discussion

3.1. Structure characterization

The exchange of the interlayer cations of the pristine montmorillonite with alkylammonium ions enlarges the interlayer spacing from 11.7 Å to 31.5 Å and 18.5 Å for C6A, C15A and C30B, respectively, as shown in Fig. 1. In addition, C15A shows a small second peak at higher angles ($2\theta = 7.2°$) which suggests that a portion of the clay layers has not been intercalated after chemical modification. X-ray diffraction spectra of the NR nanocomposites filled with 5 phr of layered silicate are presented in Fig. 2. As can be seen, the composite containing C6A silicate shows a peak about $2\theta = 7{,}5°$ which corresponds to the interlayer platelet spacing of the pristine clay. This suggests that the incorporation of unmodified clay gives rise to a conventional composite at a microscopic scale, where the polymer is not intercalated into the silicate galleries. By adding the C30B clay, XRD diffractogram shows a displacement towards lower angles ($2\theta = 3.6°$), corresponding to an interlayer distance of 24.5 Å, providing thus the existence of layered/polymer intercalates. A further more pronounced intercalation was achieved by the incorporation of the C15A clay. In fact, the peak at $2\theta = 2.9°$ of the C15A disappears, whereas the second peak at $2\theta = 7.2°$ is slightly shifted to lower angles, as shown in Fig. 2. This suggests that enough polymer chains had been introduced into the galleries so that the layered silicates were uniformly dispersed at a nanosize scale in the NR matrix, giving rise to an exfoliated structure.

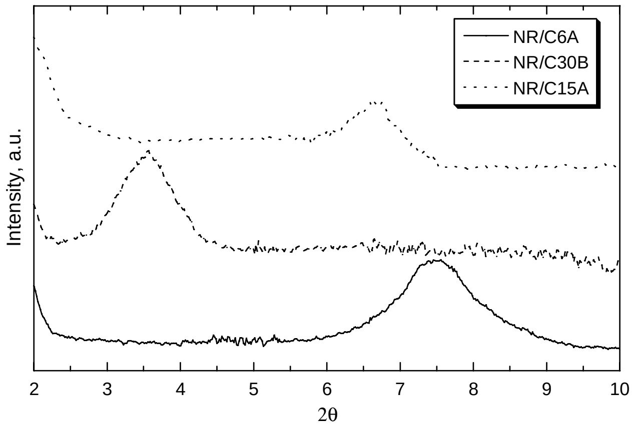

Fig. 2. XRD patterns of clay/NR nanocomposites.

It is important to mention that nanocomposites with an exfoliated structure have been obtained with both C30B and C15A organoclays by addition of 25 phr of epoxidized natural rubber (ENR 25 and ENR 50), as shown in Fig. 3. Both patterns are characterized by the absence of the 001 diffraction peak, providing a strong evidence of the insertion of the elastomer into the silicate galleries, disrupting the regular stacked-layer structure of the organoclays and giving rise to an exfoliated structure. That is, the tactoids of layered silicates tend to disaggregate to individual sheets, which are uniformly dispersed into the elastomer matrix. The polarity of the ENR favours the intercalation of this elastomer into the galleries and the dispersion of the layered silicates in the matrix. Even more, a slight displacement of the C6A diffraction peak to lower angles is observed which

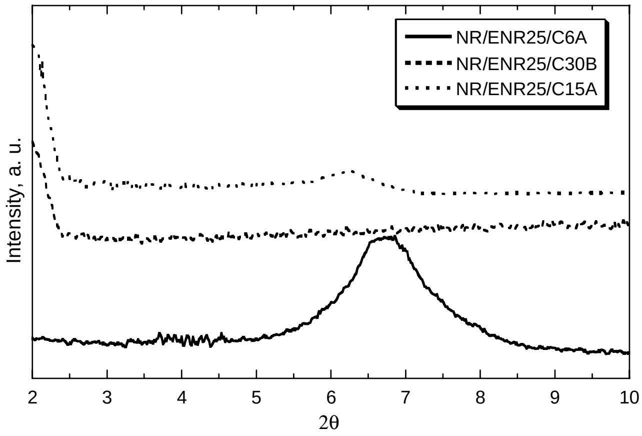

Fig. 3. XRD patterns of clay/rubber nanocomposites based on NR/ENR25 (25 phr) blends.

suggests that a portion of the elastomer chains has been intercalated into the galleries of the pristine clay.

Independently of the type and concentration of ENR employed, similar diffractograms are obtained as shown in Figs. 4–6. An exfoliated morphology is obtained for both organoclays. It is not easy to determine the polymer phase predominantly inserted into the silicate galleries, but, on the basis of these results, it can be suggested that both polymeric phases are capable to be inserted into the interlayer spacing of the organoclay. In the presence of an ENR, it can be thought that its polar character favours their initial insertion into the interlayer spacing of the clay.

Figs. 7(a) and (b) show the TEM micrographs of the NR nanocomposites reinforced with C30B and C15 organo-montmorillonites, respectively. The dark lines represent the cross sections of the clay platelets. Both amine-modified montmorillonites give rise to an intercalated structure. However, in the case of C30B nanofiller agglomerates and nanolayers coexist, whilst a finely intercalated structure is appreciated in the presence of C15A (Fig. 7(a)). In this case, silicate layers of ca. 1 nm and 30–100 nm in length are exfoliated and randomly dispersed throughout the elastomer matrix as monolayers.

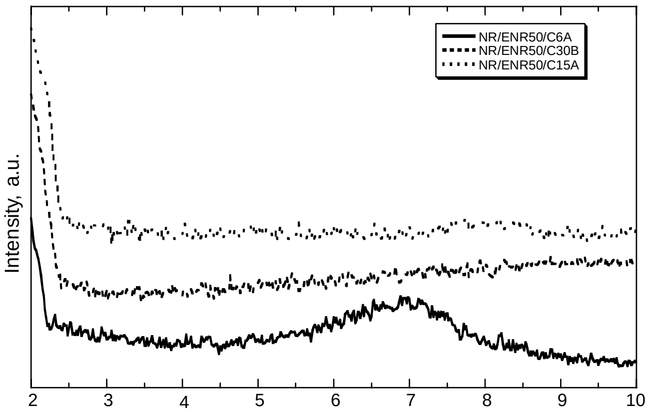

Fig. 4. XRD patterns of clay/rubber nanocomposites based on NR/ENR50 (25 phr) blends.

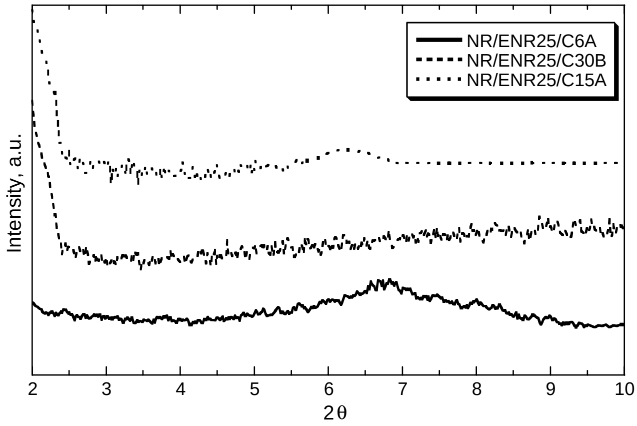

Fig. 5. XRD patterns of clay/rubber nanocomposites based on NR/ENR25 (50 phr) blends.

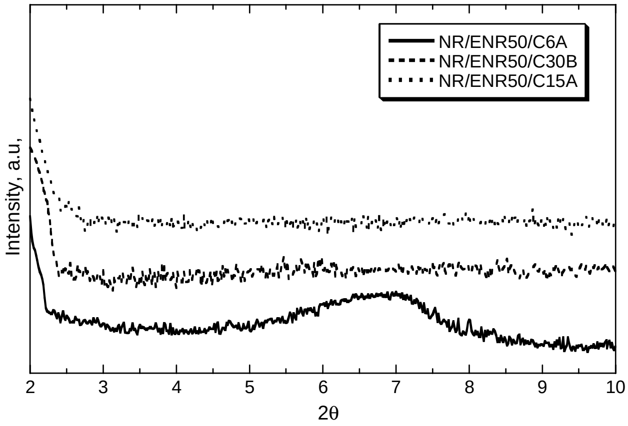

Fig. 6. XRD patterns of clay/rubber nanocomposites based on NR/ENR50 (50 phr) blends.

It is worthy to note that the ENR (Fig. 8) improves the dispersion of the clays in the polymer matrix giving rise in both cases to a predominantly exfoliated structure, particularly in the case of the C30B clay, where nanolayers finely dispersed in the matrix are appreciated (Fig. 8(b)). Due to the polarity of the ENR, a better interaction with the organoclay is expected with an improved dispersion into the polymer matrix.

TEM observations are in concordance with XRD patterns and confirm a better dispersion of the clays in the presence of a polar rubber like ENR. Furthermore, it is important to highlight that the spatial disposition of the nanoparticles varies when the ENR is added. In this case, the dispersed ENR particles are surrounded by the organoclay which probably acts as a compatibilizer between both phases. Similar results were reported by Essawy and El-Nashar [32] when analyzing the use of montmorillonite as a compatibilizing filler for NBR/SBR rubber blends. However, this finding requires a further detailed study.

On the other hand, a more homogeneous morphology with a finer and more uniform dispersion of the ENR phase in the NR matrix is observed from scanning electron microscopy photographs, SEM (Fig. 9). So, a sensible decrease of the dispersed ENR particles size in the presence of the organoclays is observed. This suggests that the organoclay may act as interfacial agents, reducing the interfacial tension with a concomitant breakup of the ENR droplets and, in consequence, a reduction in the particle size [33]. This effect is more significant, when C30B is used as nanofiller. It is expected that the hydroxyl groups present in the structure of the organic modifier are able to react with epoxy groups of ENR, giving rise to a more homogeneous structure.

3.2. Rheological measurements

The rheological behavior of the nanocomposites was investigated through Mooney viscosity measurements. At

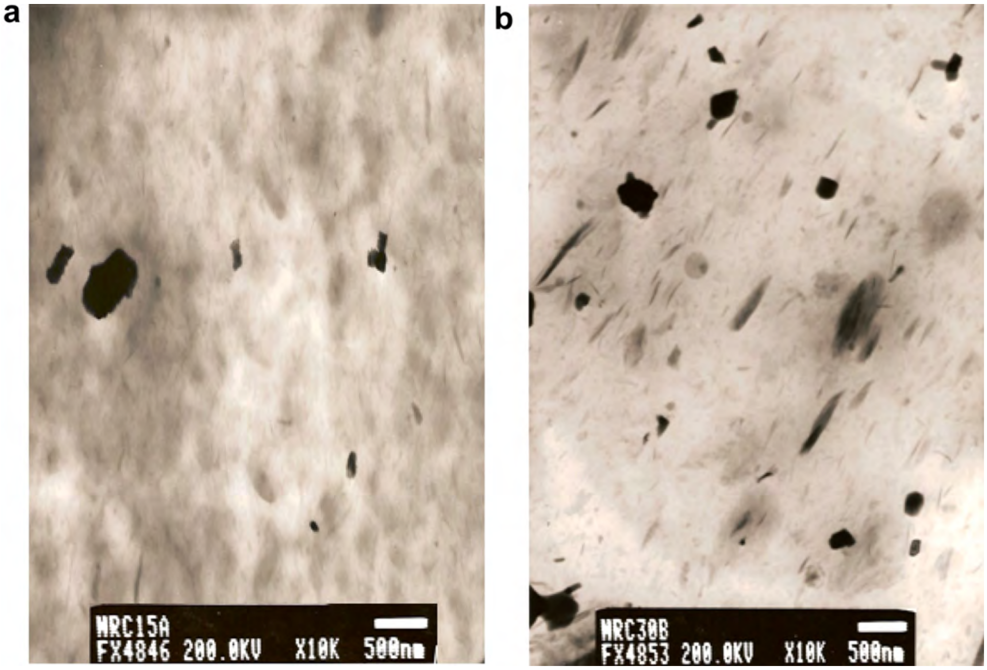

Fig. 7. TEM morphology of NR/organoclay nanocomposite: (a) C15A and (b) C30B.

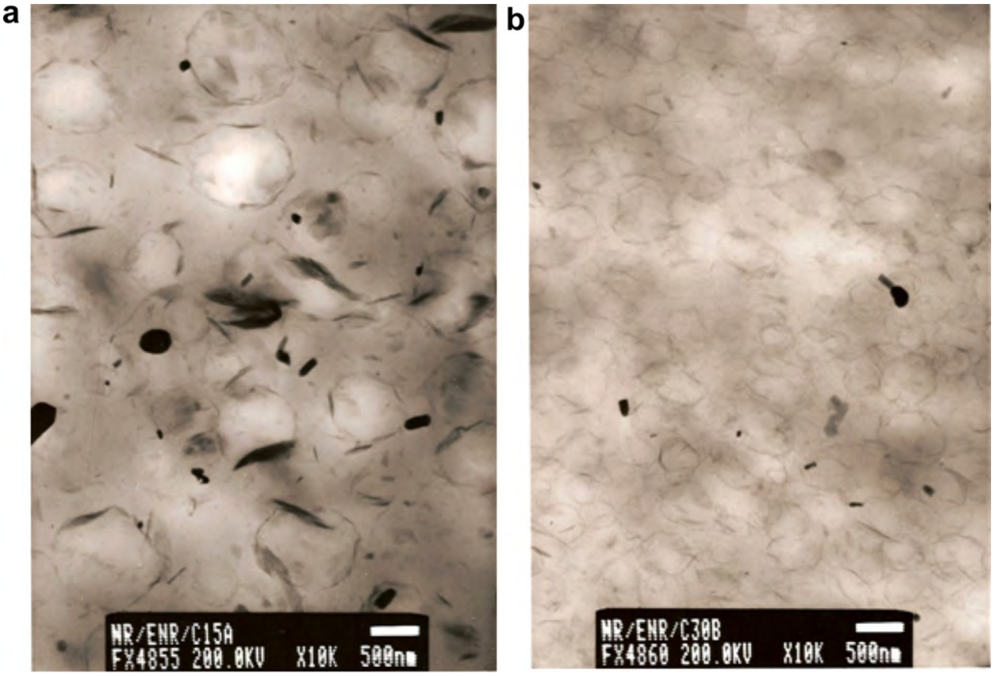

Fig. 8. TEM morphology of NR-ENR50 (25 phr)/organoclay nanocomposite: (a) C15A and (b) C30B.

very low shear rates ($\approx$1–2 s^{-1}), the Mooney viscosity has been shown to be directly proportional to the true shear viscosity. Three parameters can be defined: the peak Mooney viscosity, η_p, the viscosity value after four minutes of shearing, η_4, and a thixotropy parameter $\Delta = \eta_p - \eta_4$, which are given in Table 3.

Prior to shearing the polymer chains have a random Gaussian conformations. During shearing, chains are disentangled and oriented in the direction of shear, facilitating the sliding of chains, and consequently, the viscosity decreases. It has been observed that the Mooney viscosity gradually decreases as ENR content in the blend increases, which is attributed to the relatively low molecular weight of the ENR.

Fig. 10 shows the variation of Mooney viscosity versus time (of shearing) for NR and NR/ENR50 blends and their nanocomposites containing C15A as organoclay. It can be observed that the viscosity of NR compound hardly varies

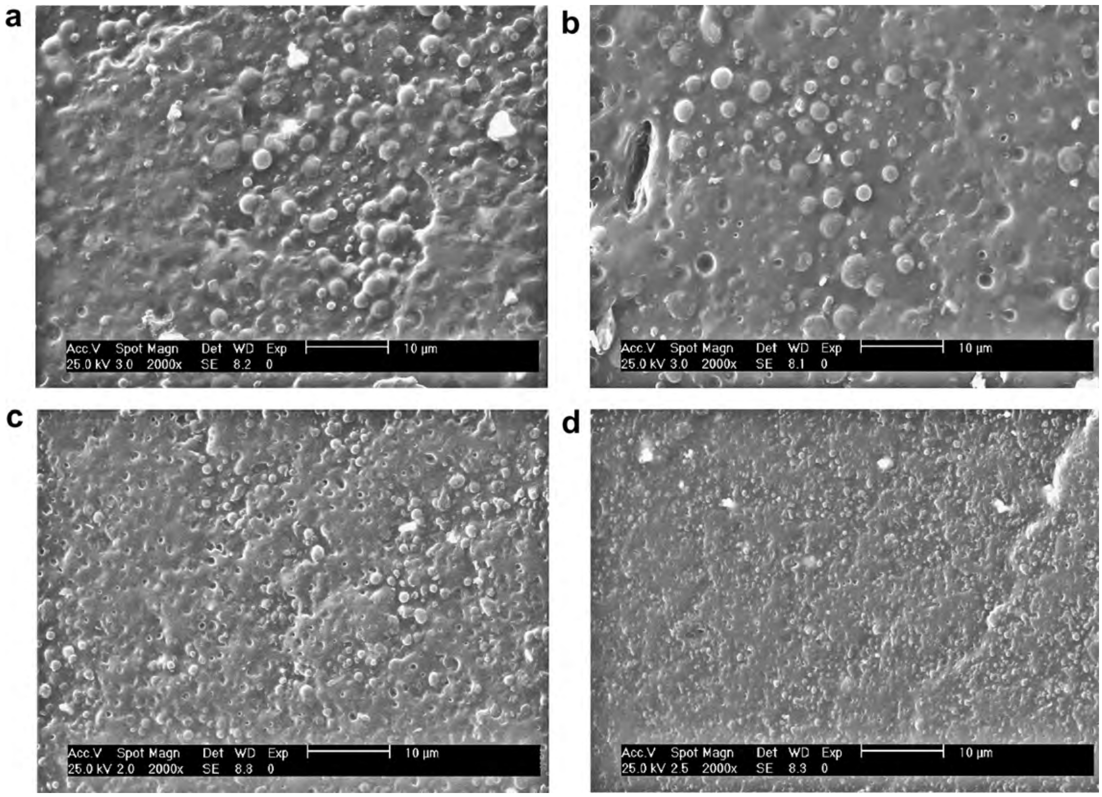

Fig. 9. SEM micrographs of NR/ENR25 (25 phr) blend (a) unfilled and reinforced with clay (b), C15A (c) and C30B (d).

with the incorporation of the organoclay. This behavior does not correspond to that of other conventional fillers, such as carbon black or silica, which normally give rise to an increase in the viscosity and modify the rheological properties of the elastomer [34,35]. In contrast to these traditional fillers, which normally require loadings of 40 phr or more to reinforce elastomers, very low organoclay amounts are needed to achieve strong reinforcing effects (only 5 phr of organoclay are used in the present study). It must be noted that the short organic chains present in the organic modifier can act as plasticizer reducing the viscosity of the compound.

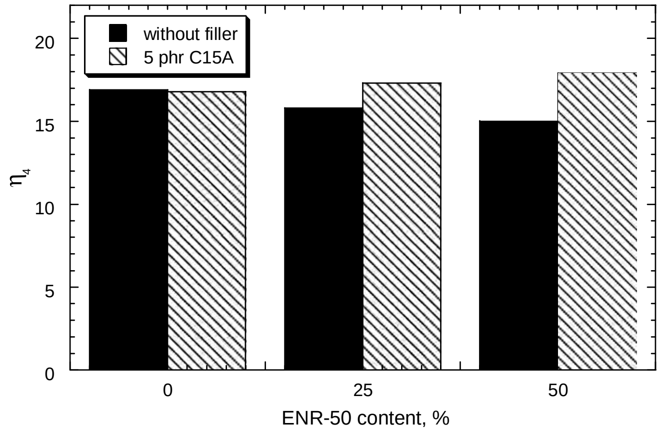

Fig. 10. Variation of Mooney viscosity as a function of ENR50 content in the blend reinforced with C15A (5 phr).

In addition, it is important to note that the incorporation of the fillers hardly affect to the NR/ENR viscosity peak. However, a slight increase in viscosity is detected after shearing, as shown in Table 3 due to both the hydrodynamic effect and the formation of rubber–filler interactions. This effect is more sensible in the presence of the organoclays and as both ENR content and epoxy units in the ENR increase. The improvement in the filler–rubber

Table 3
Rheological properties of the studied compounds

	η_p	η_4	Δ
NR	26.6	16.9	9.7
NR/C6A	26.7	16.8	9.9
NR/C15A	26.4	16.8	9.6
NR/C30B	26.6	16.7	9.9
NR-ENR25 (25 phr)	24.8	15.3	9.5
NR-ENR25 (25 phr)/C6A	24.1	15.5	9.2
NR-ENR25 (25 phr)/C15A	24.7	16.9	8.2
NR-ENR25 (25 phr)/C30B	25.0	16.5	8.5
NR-ENR50 (25 phr)	23.9	15.8	8.1
NR-ENR50 (25 phr)/C6A	23.8	16.0	7.8
NR-ENR50 (25 phr)/C15A	24.0	17.3	6.7
NR-ENR50 (25 phr)/C30B	23.8	16.8	7.0
NR-ENR25 (50 phr)	22.9	14.5	8.4
NR-ENR25 (50 phr)/C6A	22.7	15.1	7.6
NR-ENR25 (50 phr)/C15A	22.8	17.5	5.3
NR-ENR25 (50 phr)/C30B	22.9	17.1	5.8
NR-ENR50 (50 phr)	22.8	15.0	7.8
NR-ENR50 (50 phr)/C6A	22.9	15.8	7.1
NR-ENR50 (50 phr)/C15A	23.1	17.9	5.2
NR-ENR50 (50 phr)/C30B	23.0	17.6	5.4

compatibility by the addition of ENR, not only causes a better dispersion of the clay particles in the rubber matrix with an increase of interphase but also increases the filler–rubber interactions and decreases the agglomeration of filler particles. According to all these factors, an increment in the final viscosity is expected. This confirms that in presence of ENR a stronger polymer–organoclay interaction exists, this effect being more evident with ENR50. It is expected that shearing at 100 °C, is able to cause the cationic opening of the epoxy groups, favoring the interaction between the rubber and the organoclay.

4. Cure characteristics

The curing characteristics of the studied materials, expressed in terms of the scorch time, t_{S2}, optimum cure time, t_{90}, the maximum and minimum values of the torque, $S_{\max}$ and $S_{\min}$, respectively, and delta torque, ΔS, are compiled in Table 4. In the presence of the pristine clay, C6A, the vulcanization reaction of NR and its NR/ENR blends is delayed, as confirmed by an increase in the cure times. This effect is attributed to an interaction between the acid OH groups present on the clay surface and the different components of the cure system. However, when analyzing the optimum cure times it can be deduced that both C15A and C30B organophilic clays accelerate the vulcanization process, acting as effective vulcanizing agents for NR. This effect is essentially attributed to the amine groups present in the nanosilicate structure. It is well assumed that amine groups facilitate the curing reaction of SBR and NR [36], due to the formation of a transition metal complex in which sulfur and amine groups participate. Nevertheless, it is important to note that at high ENR contents (50 phr) in the blend this effect is practically negligible, which could be attributed to an interaction between the amine and epoxy groups.

Delta torque, measured as the difference between the maximum and minimum torque ($\Delta S = S_{\max} - S_{\min}$) was also evaluated, as summarized in Table 4. It is observed that the addition of pristine clay, C6A decreases the torque in relation to unfilled rubber. However, the organoclay nanocomposites show higher torque value, in particular with C15A clay due to a higher interaction between the organoclay and the rubber. It is of interest to emphasize that the delta torque value of the compounds increased with the incorporation of ENR, mainly in the presence of ENR50. In addition, delta torque progressively increased as ENR content in the blend increases. These results suggest that in the presence of ENR, additional crosslinks are formed giving rise to a sensible increase of the torque and the crosslinking density as will be discussed later.

In addition, no changes in the minimum torque values were detected which suggests that the ENR hardly have any effect on the plasticity of the unvulcanized elastomeric compounds.

5. Mechanical properties

The modulus at different elongations (50%, 100%, 300% and 500%), maximum strength and elongation at break of the studied rubber compounds are compiled in Table 5. The incorporation of C6A natural montmorillonite to NR hardly affects to the composite properties which confirms that a composite at microscale has been formed with the filler not showing any reinforcing effect on the elastomer. However, a sensible increase in the mechanical properties is obtained by adding both organoclays, in particular with C15A. These results prove the strong reinforcing effect of these inorganic fillers even at low percentages (5 phr). Moreover, in contrast to other conventional fillers, this increased strength takes place without any loose in the elon-

Table 4
Vulcametric characteristics of the studied compounds

	t_{02} (min)	t_{90} (min)	$S_{\min}$ (dNm)	$S_{\max}$ (dNm)	ΔS (dNm)
NR	6.37	13.02	0.10	7.74	7.64
NR/C6A	8.61	15.26	0.02	4.21	4.19
NR/C15A	1.22	4.88	0.02	11.16	11.14
NR/C30B	2.04	5.93	0.05	7.77	7.72
NR-ENR25 (25 phr)	3.72	8.03	0.26	8.16	7.90
NR-ENR25 (25 phr)/C6A	4.50	9.42	0.03	7.65	7.62
NR-ENR25 (25 phr)/C15A	0.99	5.15	0.07	14.00	13.93
NR-ENR25 (25 phr)/C30B	1.86	6.20	0.00	10.41	10.41
NR-ENR50 (25 phr)	2.98	7.77	0.07	6.44	6.37
NR-ENR50 (25 phr)/C6A	3.93	8.72	0.01	6.62	6.61
NR-ENR50 (25 phr)/C15A	1.20	6.91	0.07	13.66	13.59
NR-ENR50 (25 phr)/C30B	2.04	7.20	0.03	7.83	9.80
NR-ENR25 (50 phr)	1.88	6.08	0.05	8.22	8.17
NR-ENR25 (50 phr)/C6A	2.25	6.98	0.06	9.25	9.19
NR-ENR25 (50 phr)/C15A	0.81	6.32	0.08	16.91	16.83
NR-ENR25 (50 phr)/C30B	0.99	6.15	0.04	13.85	13.81
NR-ENR50 (50 phr)	1.75	6.31	0.00	6.65	6.65
NR-ENR50 (50 phr)/C6A	2.20	7.15	0.03	7.08	7.05
NR-ENR50 (50 phr)/C15A	1.15	6.49	0.13	15.78	15.65
NR-ENR50 (50 phr)/C30B	1.45	6.60	0.04	13.35	13.31

Table 5
Mechanical properties of the studied compounds

	Mod 50% (MPa)	Mod 100% (MPa)	Mod 300% (MPa)	Mod 500% (MPa)	Max. strength (MPa)	Elong. at break (%)	Hardness shore A	Resilience (%)	Cross. degree (%)
NR	0.41	0.63	1.49	2.91	9.45	889	27.5	61.0	8.03×10^{-5}
NR/C6A	0.32	0.46	1.11	2.19	8.10	879	25.1	56.0	6.68×10^{-5}
NR/C15A	0.87	1.35	3.24	6.59	21.00	888	39.7	60.0	1.64×10^{-4}
NR/C30B	0.49	0.78	1.93	3.83	11.81	916	30.5	59.5	8.89×10^{-5}
NR-ENR25 (25 phr)	0.39	0.62	1.58	3.44	11.35	860	30.4	60.5	8.15×10^{-5}
NR-ENR25 (25 phr)/C6A	0.32	0.52	1.43	3.28	10.67	855	28.8	55.0	7.00×10^{-5}
NR-ENR25 (25 phr)/C15A	0.90	1.43	3.52	7.40	24.20	910	45.5	60.0	1.88×10^{-4}
NR-ENR25 (25 phr)/C30B	0.53	0.84	2.19	4.63	16.40	906	35.8	58.5	1.10×10^{-4}
NR-ENR50 (25 phr)	0.36	0.56	1.37	2.95	10.53	893	26.4	60.5	8.10×10^{-5}
NR-ENR50 (25 phr)/C6A	0.35	0.59	1.47	3.19	11.10	830	25.5	55.0	7.38×10^{-5}
NR-ENR50 (25 phr)/C15A	0.92	1.42	3.42	6.80	24.90	907	43.2	60.0	1.99×10^{-4}
NR-ENR50 (25 phr)/C30B	0.61	0.87	2.09	4.32	17.50	890	38.2	58.5	1.35×10^{-4}
NR-ENR25 (50 phr)	0.45	0.81	2.28	4.32	12.15	885	32.5	59.5	8.18×10^{-5}
NR-ENR25 (50 phr)/C6A	0.49	0.88	2.39	4.85	13.25	828	32.3	56.0	7.62×10^{-5}
NR-ENR25 (50 phr)/C15A	1.13	1.92	5.13	9.96	26.60	890	51.4	59.0	2.14×10^{-4}
NR-ENR25 (50 phr)/C30B	0.76	1.23	3.35	6.15	18.25	880	42.4	58.5	1.68×10^{-4}
NR-ENR50 (50 phr)	0.40	0.65	1.71	3.89	11.30	910	24.7	59.0	8.14×10^{-5}
NR-ENR50 (50 phr)/C6A	0.61	0.89	2.29	4.56	14.85	850	25.1	57.5	7.84×10^{-5}
NR-ENR50 (50 phr)/C15A	1.20	1.75	4.45	9.41	27.15	895	50.9	58.5	2.37×10^{-4}
NR-ENR50 (50 phr)/C30B	0.97	1.40	3.75	8.40	23.96	980	44.7	58.5	1.91×10^{-4}

gation at break of the material. The anisotropy and high surface-to-volume ratios of organoclays contribute to the excellent reinforcing capability of these fillers. That is, they act as short reinforcing fibers with a nanoscale architecture, increasing the interphase area between both phases.

The reinforcing effect of the organoclay is more evident for nanocomposites based on NR/ENR blends. However, a different behavior is observed in this case. For NR compounds, at a determined strain, the reinforcing effect of the organoclays is practically constant. Unlike, in the composites based on NR/ENR blends, an abrupt increase of the strength is observed at very low strains (50% elongation). This reinforcing effect tends to decrease as the strain increases and is more evident as ENR level in the blend increases, mainly with ENR50. This behavior can be attributed to the formation of chemical bonding between the ENR functional groups and the organoclay, as was previously suggested from torque measurements. That is, during vulcanization process the epoxy groups interact chemically with the hydroxyl groups of the filler surface and amine groups of the interlayer spacing.

It is also of interest to note, that the reinforcing effect of C30B is gradually more evident as ENR content in the compound increases. Since the alkyl ammonium chains of the C30B organoclay contain polar groups, a better compatibility between this clay and the epoxidized natural rubber should be expected. Thus, it is assumed that C30B is more useful for blends with high ENR contents.

The tensile properties are in agreement with the results obtained from the analysis of the hardness and resilience of these materials. The increase in hardness is related with a higher strength of the composite. On the other hand, as can be suggested from the resilience results, the elastic behavior of the matrix hardly varies with the addition of the organoclay.

5.1. Determination of crosslinking density

Swelling measurements were utilized to determine the crosslinking density of the studied nanocomposites. Since at equilibrium the chemical forces tending to dissolve the rubber in a liquid are balanced by restraining forces exerted by the rubber network, the Flory–Rhener equation can be used to estimate the crosslinking density [37]:

$$-[\ln(1-\phi_r)+\phi_r+\chi\phi_r^2]=V_0n\left[\phi_r^{1/3}-\frac{\phi_r}{2}\right]$$

where Φ_r is the volume fraction of rubber in the swollen mass, V_0 is the molar volume of the solvent (106.2), χ is the Flory–Huggins polymer–solvent interaction term (0.393), and n is the physical degree of crosslinking.

The volume fraction of polymer Φ_r, was calculated by the next expression [38]:

$$\frac{1}{\phi_r}=1+\frac{W_S*\rho_r}{W_i*\rho_S}$$

where W_i and W_s are the weights of the rubber sample in air and in the swollen state, respectively, and ρ_S and ρ_r are the densities of the solvent (0.87 g cm^{-3}) and the rubber (0.92 g cm^{-3}), respectively.

The results are reported in Table 5. The crosslinking density of the pure NR is reduced by the addition of pristine montmorillonite, probably due to the interaction of silanol groups present in the clay surface with the cure system as previously discussed as well as to the incompatibility between both phases, that does not allow the formation of additional interactions. The crosslinking density increases in the presence of the organoclays particularly with C15A. A further increase in the crosslinking density is appreciated when ENR is added to the compound. These results agree with the torque values previously shown, where the formation of additional chemical bonds between the filler and elastomer by ENR was suggested.

6. Conclusions

Exfoliated nanocomposites based on NR/ENR blends and organophilized montmorillonites have been successfully developed. Due to ENR polar character, a higher interaction with organoclay is observed improving the dispersion of the filler in the matrix. In addition, it is of interest to note that a particular morphology for these systems was observed. The most of exfoliated nanoclay layers are selectively located at the NR/ENR interphase, though this finding needs a more detailed investigation. In addition, organoclays give rise to a finer and more homogeneous dispersion of ENR phase. In fact, a clear decrease in the size of the dispersed ENR droplets has been observed which suggests that the organoclays may behave as compatibilizer agents reducing the interfacial tension between both polymer phases. This effect is more evident in the presence of C30B organoclay which is attributed to a higher interaction with ENR. This homogeneous morphology gives rise to a sensible increase in physical and mechanical properties of the nanocomposite.

Acknowledgement

The authors thank the CICyT, MAT 2004-00825, for financial support.

References

[1] Usuki A, Kawasumi M, Kojima Y, Okada S, Kurauchi T, Kamigaito O. A. Swelling behavior of montmorillonite cation exchanged for ω-amino acids by ε-caprolactama. J Mater Res 1993;8(5):1174–8.

[2] Usuki A, Kojima Y, Kawasumi M, Okada A, Fukushima Y, Kurauchi T, et al. Synthesis of nylon 6-clay hybrid. J Mater Res 1993;8(5):1179–84.

[3] Lan T, Pinnavaia TJ. Clay-reinforced epoxy nanocomposites. Chem Mater 1994;6(12):2216–9.

[4] Wang Z, Pinnavaia TJ. Hybrid organic–inorganic nanocomposites: exfoliation of magadiite nanolayers in an elastomeric epoxy polymer. Chem Mater 1998;10(7):1820–6.

[5] Yano K, Usuki A, Okada A, Kurauchi T, Kamigaito O. Synthesis and properties of polyimide clay hybrid. J Polym Sci A: Polym Chem 1993;31(10):2493–8.

[6] Wang Z, Lan T, Pinnavaia TJ. Hybrid organic–inorganic nanocomposites formed from an epoxy polymer and a layered silicic acid (magadiite). Chem Mater 1996;8(9): 220–2208.

[7] Alexandre M, Dubois P. Polymer-layered silicate nanocomposites: preparation, properties and uses of a new class of materials. Mater Sci Eng R-Reports 2000;28(1–2):1–63.

[8] Giannelis EP, Krishnamoorti R, Manias E. Polymer–silicate nanocomposites: model systems for confined polymers and polymer brushes. Adv Polym Sci 1999;138:107–47.

[9] Shi H, Lan T, Pinnavaia TJ. Interfacial effects on the reinforcement properties of polymer–organoclay nanocomposites. Chem Mater 1996;8(8):1584–8.

[10] Ray SS, Okamoto M. Polymer/layered silicate nanocomposites: a review from preparation to processing. Prog Polym Sci 2003;28(11): 1539–641.

[11] Arroyo M, López-Manchado MA, Herrero B. Organo-montmorillonite as substitute of carbon black in natural rubber compounds. Polymer 2003;44(8):2447–53.

[12] Krishnamoorti R, Giannelis EP. Rheology of end-tethered polymer layered silicate nanocomposites. Macromolecules 1997;30(14): 4097–102.

[13] Pinnavaia TJ. Intercalated clay catalysts. Science 1983; 220(4595):365–71.

[14] Zhang L, Wang Y, Wang Y, Dingsheng Y. Morphology and mechanical properties of clay/styrene-butadiene rubber nanocomposites. J Appl Polym Sci 2000;78(11):1873–8.

[15] Wu Y, Zhang L, Wang Y, Liang Y, Yu D. Structure of carboxylated acrylonitrile–butadiene rubber (CNBR)-clay nanocomposites by co-coagulation rubber latex and clay aqueous suspension. J Appl Polym Sci 2001;82(11):2842–8.

[16] Nah C, Ryu H, Han S, Rhee J, Lee M. Fracture behaviour of acrylonitrile–butadiene rubber/clay nanocomposite. Polym Int 2001;50(11):1265–8.

[17] Chang Y, Yang Y, Ryu S, Nah C. Preparation and properties of EPDM/organomontmorillonite hybrid nanocomposites. Polym Int 2002;51(4):319–24.

[18] Usuki A, Tukigase A, Kato M. Preparation and properties of EPDm-clay hybrids. Polymer 2002;43(8):2185–9.

[19] Duquesne S, Jama C, Le Bras M, Delobel R, Recourt P, Gloaguen JM. Elaboration of EVA-nanoclay systems – characterization, thermal behaviour and fire performance. Comp Sci Tech 2003;63(8):1141–8.

[20] Mohammad A, Simon GP. Rubber–clay nanocomposites. In: Mai Y, Yu Z, editors. Polymer nanocomposites. Abington Hall, Abington, Cambridge, England: Woodhead Publishing Limited; 2006 [chapter 12].

[21] Utracki LA. Elastomeric CPNC in clay-containing polymeric nanocomposites. Rapra Technology Limited; 2004.

[22] Stephen R, Alex R, Cherian T, Varghese S, Joseph K, Thomas S. Rheological behaviour of nanocomposites of natural rubber and carboxylated styrene butadiene rubber lattices and their blends. J Appl Polym Sci 2006;101(4):2355–62.

[23] Acharya H, Srivastava SK, Bhowmick A. Ethylene propylene diene terpolymer/ethylene vinyl acetate/layered silicate ternary nanocomposite by solution method. Polym Eng Sci 2006:837–43.

[24] Mousa A, Karger-Kocsis J. Rheological and thermodynamical behaviour of styrene/butadiene rubber–organoclay nanocomposites. Macrom Mater Eng 2001;286(4):260–6.

[25] Kim JT, Oh T, Lee D. Morphology and rheological properties of nanocomposites based on nitrile rubber and organophilic layered silicates. Polym Int 2003;52(7):1203–8.

[26] Oberdisse J, El Harrak A, Carrot G, Jestin J, Boué F. Structure and rheological properties of soft-hard nanocomposites: influence of aggregation and interfacial modification. Polymer 2005;46(17): 6695–705.

[27] Abdul Kader M, Lyu MY, Nah C. A study on melt and thermal properties of fluoroelastomer nanocomposites. Comp Sci Technol 2006;66(10):1431–43.

[28] Zitzumbo R, Alonso S, Avalos F, Ortiz JC, Lopez-Manchado MA, Arroyo M. Structural analysis of nanocomposites based on HDPE/EPDM blends. J Nanosci Nanotech 2006;6(1):1–6.

[29] Varghese S, Karger-Kocsis J, Gatos KG. Melt compounded epoxidized natural rubber/layered silicate nanocomposites: structure–properties relationships. Polymer 2003;44(14):3977–83.

[30] Teh PL, Ishak ZAM, Hashim AS, Karger-Kocsis J, Ishiaku US. Effects of epoxidized natural rubber as a compatibilizer in melt compounded natural rubber–organoclay nanocomposites. Eur Polym J 2004;40(11):2513–21.

[31] Nanocor, Inc, 1500 West Shure Drive, Arlington Heights (IL).

[32] Essawy H, El-Nashar D. The use of montmorillonite as a reinforcing and compatibilizing filler for NBR/SBR rubber blend. Polym Test 2004;23(7):803–7.

[33] Mehta S, Mirabella F, Rufener K, Bafna A. Thermoplastic oelfin/clay nanocomposites. Morphology and mechanical properties. J Appl Polym Sci 2004;94(2):928–36.

[34] Gibala D, Laohapisitpanich K, Thomas D, Hamed GR. Cure and mechanical behaviour of rubber compounds containing ground vulcanizates. 2. Mooney viscosity. Rubber Chem Technol 1996; 69(1):115–9.

[35] Choi SS, Nah C, Lee SG, Joo CW. Effect of filler–filler interaction on rheological behaviour of natural rubber compounds filled with both carbon black and silica. Polym Int 2003;52(1):23–8.

[36] Mousa A, Karger-Kocsis J. Rheological and thermodynamical behaviour of styrene/butadiene rubber–organoclay nanocomposites. J Macrom Mater Eng 2001;286(4):260–6.

[37] Flory PJ, editor. Principles of polymer chemistry. Ithaca (NY): Cornell University; 1953.

[38] Bae YH, Okano T, Kim SW. Temperature-dependence of swelling of cross-linked poly(N,N'-alkyl substituted acrylamides) in water. J Polym Sci Part B: Polym Phys 1990;28(6):932–6.

Available online at www.sciencedirect.com
ScienceDirect
European Polymer Journal 43 (2007) 4143–4150
EUROPEAN POLYMER JOURNAL
www.elsevier.com/locate/europolj

Macromolecular Nanotechnology

Rubber network in elastomer nanocomposites

M.A. López-Manchado *, J.L. Valentín, J. Carretero, F. Barroso, M. Arroyo

Institute of Polymer Science and Technology, CSIC, Juan de la Cierva, 3, 28006 Madrid, Spain

Received 17 April 2007; received in revised form 28 June 2007; accepted 8 July 2007
Available online 24 July 2007

Abstract

The influence of inorganic nanoparticles on crosslinking mechanism of elastomers has been evaluated by applying the tube model on equilibrium statistical mechanics. The results have shown that a highly ordered structure with a huge amount of entanglements, wherein the polymer is nanoscopically confined, is formed by the addition of nanoparticles. These physical links exhibit freedom of movement under stretching, but in a lower volume because of confinement. That is, network molecular parameters such as lateral tube dimensions or average molecular mass of the chains decreased in presence of nanoparticles.

Keywords: Nanocomposites; Rubber networks; Crosslinks; Inorganic nanoparticles; Natural rubber

1. Introduction

In recent years, hybrid organic–inorganic nanocomposites, consisting of a polymeric matrix and a layered silicate has inspired scientists in a range of potential applications. Due to their nanometer phase dimensions, polymer nanocomposites (PNCs) exhibit unique properties even by the addition of just a low weight percentage (<5 wt%), not shared by their microcounterparts or conventional filled polymers [1–4]. Hence, several polymers have been used for preparing nanocomposites. Most of these works are focused on synthesis, characterization and properties of nanocomposites, but, a poor understanding of the nanofiller/polymer interaction mechanism, still exists today. In the particular case of elastomer matrices, a deeper knowledge of the influence of nanoparticles on the rubber network is of crucial importance to explain the improved properties of these nanocomposites.

The statistical mechanics of elastomers, i.e. crosslinked long polymers chains, is one of the most challenging problems in polymer physics [5–8]. Rubber elasticity is a unique phenomenon which has attracted the attention of many researchers. It has been shown that the theory of networks is a typical example of a strong link between modern condensed matter physics and applied materials science [9]. Most of the classic theories on elastomers [10,11] and rubber elasticity have been developed based on the free energy to predict reasonably the stress–strain relation. These theories are based on oversimplified assumptions, i.e., ideal chains where the

---

* Corresponding author. Tel.: +34 91 5622900; fax: +34 91 5644853.
E-mail address: lmanchado@ictp.csic.es (M.A. López-Manchado).

0014-3057/$ - see front matter © 2007 Elsevier Ltd. All rights reserved.
doi:10.1016/j.eurpolymj.2007.07.023

crosslinks did not really move at all, and thus the problem reduces to that of a single chain between two fixed links that deform simultaneously when the solid is deformed. Of course, these classical theories are not realistic due to not only the idealization of real chains to simple random paths where the molecular forces and chain entanglements are neglected, but also are strongly limited by networks interconnectivity. These models rely on strong homogeneous networks, where fluctuations in crosslink densities are not allowed.

Among several versions of the entanglement model on equilibrium statistical mechanics, the most empirically useful and successful seems to be the tube model [12]. This model takes into account the importance of topological constraints or entanglements along the contour of strands. Lateral fluctuations of a polymer strand are limited by the presence of neighbouring chains. Therefore, each individual chain is effectively confined in a determined volume with tube-like geometry. Within this tube, the polymer is free to explore all possible configurations parallel and perpendicular to the axis of the tube. The tube model is particularly successful to explain the uniaxial stress–strain measurements of both unfilled and filled polymer networks. Furthermore, it allows a proper ascription of crosslinks and constraints contribution to the mechanical behaviour and a reliable determination of crosslink densities [13,14].

Therefore, the aim of this work is to analyze the influence of nanoparticles on elastomer crosslinked mechanism by applying the tube model theory in order to explain the improved properties of these elastomer nanocomposites. This will allow to clarify the mechanism of reinforcement by highly anisotropic fillers which at present time is not yet fully understood.

2. Experimental section

Natural rubber was kindly supplied by Malaysian Rubber under the trade name CV 60 (Mooney viscosity, ML $(1+4)$ 100 °C 60). Na^+-activated saponite with cation exchange capacity (CEC) value of 70 meq/100 g was provided by Tolsa (Spain). In order to increase the interlayer spacing, the clay has been organically modified by cation exchange reaction with octadecylammonium salt in our laboratories following a previously described procedure [15]. ISAF carbon black kindly supplied by Cabot, under the trade name N234 with nitrogen adsorption of 120 m^2/g and dibutylphtalate (DBP) adsorption of 125 $cm^3/100$ g, was also used in this work.

Table 1
Recipes of the rubber compounds

	NR	NR/nanoparticle	NR/carbon black
Natural rubber	100	100	100
Zinc oxide	5	5	5
Stearic acid	1	1	1
Sulphur	2.5	2.5	2.5
MBTS[a]	1	1	1
PBN[b]	1	1	1
Nanoparticle	–	5	–
Carbon black, N234	–	–	5

[a] Benzothiazyl disulfide.

[b] Phenyl beta napthyl amine.

Rubber compounds were prepared, at room temperature, in an open two-roll mill. The rotors operated at a speed ratio of 1:1.4. The vulcanization ingredients except sulphur were added to the elastomer previously to the incorporation of the filler and, finally, sulphur was added. The recipes of the compounds are compiled in Table 1. Vulcanizing conditions (temperature and time) were previously determined by means of a Monsanto Moving Die Rheometer MDR 2000E. Rubber compounds were vulcanized at 150 °C in a thermofluid heated press. The vulcanization time of the compounds corresponds to the optimum cure time (t_{95}) derived from the curing curves of the MDR 2000E. Specimens were mechanically cut out from the vulcanized plaques. Details on the characterization of organoclay/elastomer nanocomposites by X-ray diffraction and transmission electron microscopy can be found in previous works [16,17].

Uniaxial stress–strain measurements were performed at 25 ± 1 °C on an Instron dynamometer 4301 model. In order to minimize dynamical contributions, tensile tests were carried out at a cross-head speed of 0.5 mm/min up to break (strain rate $d\varepsilon/dt \approx 2.78 \times 10^{-4}\ s^{-1}$). To obtain a good sensitivity, a load cell of 50 N was used. The results were the average of at least three measurements (standard deviation 0.001–0.03).

3. Results and discussion

The stress–strain curves of the studied materials in uniaxial extension are shown in Fig. 1. As can be observed the organoclay exhibits a stronger reinforcing effect than carbon black on natural rubber compounds as reported in the literature [16]. In

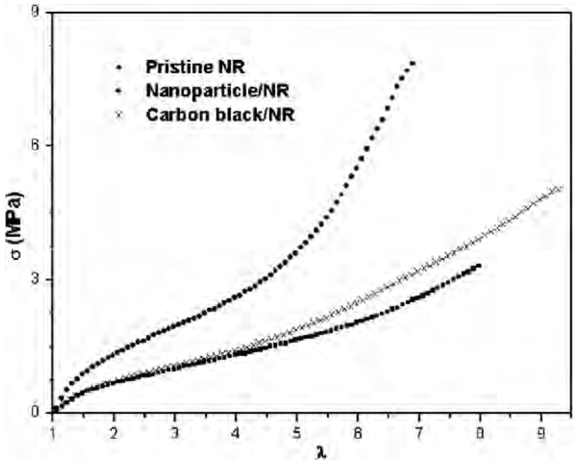

Fig. 1. Stress–strain curves of the studied materials.

order to understand this different behaviour, the filler/polymer interaction mechanism and the influence of these fillers on the crosslinked rubbery network were analyzed by applying the tube model theory. Based on this model, the constitutive equation of a uniaxial deformation of an incompressible sample comes from two contributions:

$$\sigma_M = \frac{\sigma}{(\lambda - \lambda^{-2})} = G_c + G_e f(\lambda) \tag{1}$$

where σ_M is the reduced stress, σ denotes the nominal stress defined as the tensile force required to extend a sample of rubber of a determined undeformed cross-sectional area, λ is the macroscopic extension ratio defined as the ratio of the final length of the sample in the direction of the stretch to the initial length before deformation. G_c is the elastic modulus that corresponds to the contributions of chemical crosslinks, G_e is related to the topological tube-like constraints and $f(\lambda)$ is a deformation function which is given by the following expression:

$$f(\lambda) = \frac{2}{\beta}\frac{\lambda^{\beta/2} - \lambda^{-\beta}}{\lambda^2 - \lambda^{-1}} \quad f(\lambda = 1) = 1 \tag{2}$$

where β can be considered as an empirical parameter which describes the relation between the deformed tube in the stretched state and an undeformed tube corresponding to the equilibrium state. The parameter β was introduced to take into account the strong swelling dependence of constraints. In general, β is taken as 1, i.e., relevant for almost complete converted dry networks made from long primary highly crosslinked chains so that the molecular mass of a strand is much smaller than the molecular mass of the primary chains [13,17]. In addition, this statement has been experimentally corroborated by Marzocca et al. [18] when analyzing NR compounds.

In the case of filled rubbers and in order to consider the likely contributions of matrix overstrain due to the presence of filler particles, the deformation λ, corresponding to the rubber matrix, must be replaced by an intrinsic strain ratio, λ' which is given by the following expression: [19–21]

$$\lambda' = (\lambda - 1)\chi_{\text{eff}} + 1 \tag{3}$$

where the effective amplification factor, χ_{eff}, is expressed as [22,23]

$$\chi_{\text{eff}} = 1 + 2.5f\varphi_{\text{eff}} + 14.1f\varphi_{\text{eff}}^2 = \frac{G}{G_0} \tag{4}$$

where φ_{eff} corresponds to the effective volume fraction of the filler, and G_0 is the modulus of the matrix. This equation is based on the Einstein's equation for the viscosity of a suspension of spherical rigid particles [24]. Guth and Gold generalized the Einstein concept by adding the quadratic term to account for interaction between particles, and then, for non-spherical particles, a shape factor f, defined as the length/width ratio of the particle was introduced. Since in layered silicates the anisotropic character is important, a shape factor has to be taken into account to predict the modulus of a clay reinforced nanocomposite, with an effective volume fraction larger than the theoretical one [25].

Thus, according to Eqs. (1)–(4) when plotting the reduced stress σ_M against deformation function, $f(\lambda')$ (Fig. 2), a curve is obtained, that at the intermediate regions shows a straight line, and G_e and G_c can be calculated from its slope and y-axis intercept at $f(\lambda') = 0$, respectively. For the studied materials these values are reported in Table 2. Obviously, in the case of the unfilled rubber sample $f(\lambda') = f(\lambda)$.

From Fig. 2, it can be seen that at low deformations, the elastic response of the material is given by both contributions (chemical crosslinks and topological constraints or entanglements). As the network chains are stretching, the entanglements slippage takes place, losing effectiveness which leads to a considerable decrease in reduced stress. This effect is more evident in the case of the nanoparticles, which is reflected in a higher slope, as will be discussed later. At higher elongations, a large and rather abrupt upturns in the reduced stress since the entanglements behave as effective crosslinks. This increase in reduced stress is critical to explain

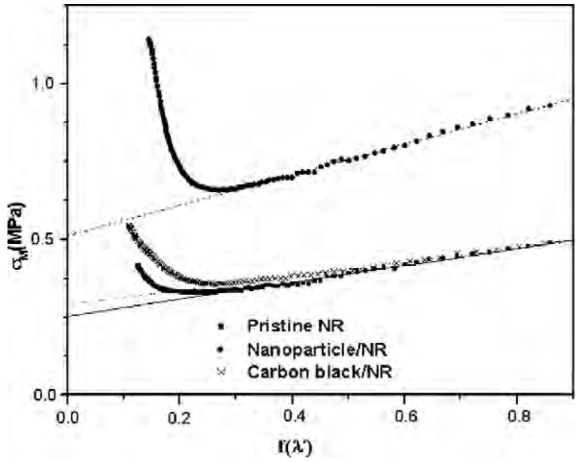

Fig. 2. Reduced stress versus deformation at room temperature.

the ultimate properties of the material. Its molecular origin has been the source of considerable controversy, so, several authors [10,26–29] have attributed it to the finite extensibility of the network chains segments, and others [30,31] have shown that this increase in modulus is associated to the induced crystallization of elastomer under stretching by molecular orientation at high strains. It is worthy to note that this rapid increase in the stress is more noticeable in presence of the organoclay. Similar conclusions have been reported by Joly et al. [25] when analyzing the effect of an organoclay on the orientation level of polymer chains by birefringence and infrared dichroism. The authors verified an increase in the crystallization process of natural rubber under uniaxial extension by the addition of small amounts of organoclay due to strong interactions between the polymer and filler. Further crystallites thus so formed act as additional crosslinks in the network structure, which explains the abrupt increase in the stress at high strains.

Both fillers (carbon black and organoclay nanoparticles) increase the G_c contribution due to the formation of a higher number of interactions, that are not changed under deformation. This means that it is no possible to differentiate between chemical crosslinks and physics entanglements that do not lose their efficiency with the deformation, and therefore act as crosslinks. However, it is noteworthy that in spite of conventional fillers like carbon black, where the contribution corresponding to topological constraints or entanglements is decreased, both contributions are increased in presence of nanoparticles (Table 2).

By applying the tube model theory, both moduli, G_c and G_e are related to the molecular network parameters (Table 2). So, G_c is associated to the effective crosslinks density by the following expression:

$$G_c = A_c \upsilon_c K_B T \tag{5}$$

where υ_c is the network chain density, A_c is a microstructure factor that considers the fluctuation of the crosslinks (a value of 0.5 is assumed since G_c is calculated to infinite deformation where free fluctuation of crosslinks occurs), K_B is the Boltzmann constant and, T is the temperature. It is deduced that the effective network density is increased by the addition of both fillers, this effect being more evident in the presence of organoclay nanoparticles due to a deep interaction filler/matrix at the interface.

In addition, the average molecular mass of the network chains is connected to υ_c according to the relation:

$$M_c = \rho_P N_A / v_c \tag{6}$$

where ρ_P is polymer density (0.92 g/cm^3 for natural rubber) and N_A is the Avogadro number. M_c sensibly decreases by the addition of both fillers, in particular, when the nanoparticles are used as nanoreinforcements. These results are in concordance with the observations carried out by other authors when analyzing the influence of carbon black on the average molecular mass of elastomer network [13]. The authors reported that the decrease in M_c is equivalent to an increase in the formation of polymer-filler couples and short bridging chains between the filler particles which enlarge the extension of the filled network.

The entanglements or physical constraints confine the diffusion of a polymer chain within a tortu-

Table 2
Network molecular parameters

	G_c (MPa)	G_e (MPa)	υ_c (nm^{-3})	M_c (g/mol)	d_0 (nm)	R_c (nm)	n_e
NR	0.259	0.251	0.126	4404	2.23	7.10	6.42
NR/carbon black	0.304	0.196	0.148	3751	2.53	6.55	8.27
NR/nanoparticle	0.521	0.460	0.253	2189	1.65	5.00	3.52

ous path acting as a transient crosslink, restricting the slippage of the chains during deformation under an applied stress [32]. The constraint modulus, G_e is related to the lateral dimensions of the configurational tubes within the bulk rubber by the following expression: [13]

$$G_e = \frac{1}{4(6)^{1/2}} K_B T n_S \left(\frac{l_S}{d_0}\right)^2 \tag{7}$$

where n_S is the polymer segment number density, l_S is the average length of the Kuhn's statistical segment (0.88 nm for natural rubber) and d_0 is the fluctuation range of a chain segment. n_S is a parameter that can be obtained through the next equation:

$$n_S = \left(\frac{9.5}{\beta}\right)\left(\frac{G_N^0}{l_s^3 K_B T}\right)^{1/2} \tag{8}$$

where a value of 3.85 nm^{-3} is obtained for the n_S constant in the system under study. $G_N^0 = 0.46$ MPa was taken from the literature [33,34].

The root-mean-square end-to-end distance of the mobile network chains, R_c, which is related to the average molecular mass of these chains was also calculated by the expression:

$$R_c = l_S \left(\frac{M_c}{M_s}\right)^{1/2} \tag{9}$$

where $M_s = 67.7$ g/mol for the molecular mass of natural rubber calculated through $M_s = \rho N_A / n_s$ is used. It can be observed that for the studied materials $l_s < d_0 < R_c$ which is in concordance with the results reported by other authors on their studies on several elastomers [13,14,35].

The tube radius is also related with the mean number of statistical segments between successive entanglements, n_e, through the expression:

$$d_0 = l_s n_e^{1/2} \tag{10}$$

All network molecular parameters of the studied compounds are summarized in Table 2. According to these results, a different filler/elastomer interaction mechanism for both fillers is evidenced. A likely mechanism of reinforcement is schematically represented in Fig. 3.

The effect of carbon black on filled rubber properties can be successfully described through the entanglement-bound rubber model (EBRM) [36]. On the basis of this model, the carbon black affects the rubber property through its effect on the effective cross-link density υ_c, which is controlled by the entangled bulk rubber with bound rubber in a transition zone between the highly immobilized and localized bound rubber and the mobile bulk rubber phases. Because, a single molecule of bound rubber is likely to adhere on several carbon black surface sites, the bound rubber is essentially immobile in this model. This strong transition layer produces an increase of G_c value, not only because the formation of strong filler–rubber interaction, but also because limits the movement of rubber chains. Thereby, the entanglements slippage in the bound rubber is also reduced, which is reflected in a sensible decrease of G_e value (Fig. 3a). This explains why the rubber samples loaded with high carbon black contents show an increase in strength at different strains but to the detriment of the elastic characteristics of the rubber compound. However, it is important to note that the reinforcement of carbon black is restricted in a zone at the filler/elastomer interface. Therefore, at low filler loads in the compound, carbon black covers only a little rubber percentage, i.e. a huge amount of rubber is still free as reflected in Fig. 3b. So, in relation to the unfilled rubber, the average molecular parameters do not change in a significant way (Table 2).

On the other hand, due to its inorganic nature the nanoparticles mainly exhibit physical absorptions with the elastomer matrix. So, in a particular interphase, the interaction with the rubber is weaker than in carbon black compound, and then, the mobility of the rubber chains is higher (Fig. 3c). Nevertheless, the inorganic nanoparticles are characterized by a high aspect ratio, so the optimum dispersion of even a small quantity of nanoparticles (<5 wt%) is enough to interact with the total rubber mass, i.e., a few rubber chains remain free. So, as corroborated from molecular network parameters, the addition of nanoparticles decreases the tube dimensions, by the presence of neighbouring chains, which restricts the movement of the rubber chains to a lower volume. The rubber is nanoscopically confined forming a highly ordered and entangled structure due to the formation of intense nanoparticle/elastomer interactions. This structure is responsible of the high performance of these materials even at low filler percentages in the compound. However, it is worthy to note that the chains freely move in uniaxial extension since the slippage of the entanglements is not hindered, which explains the good elastic properties of these new materials.

In other words, in an exfoliated nanocomposite, the polymer is nanoscopically confined, with a loss

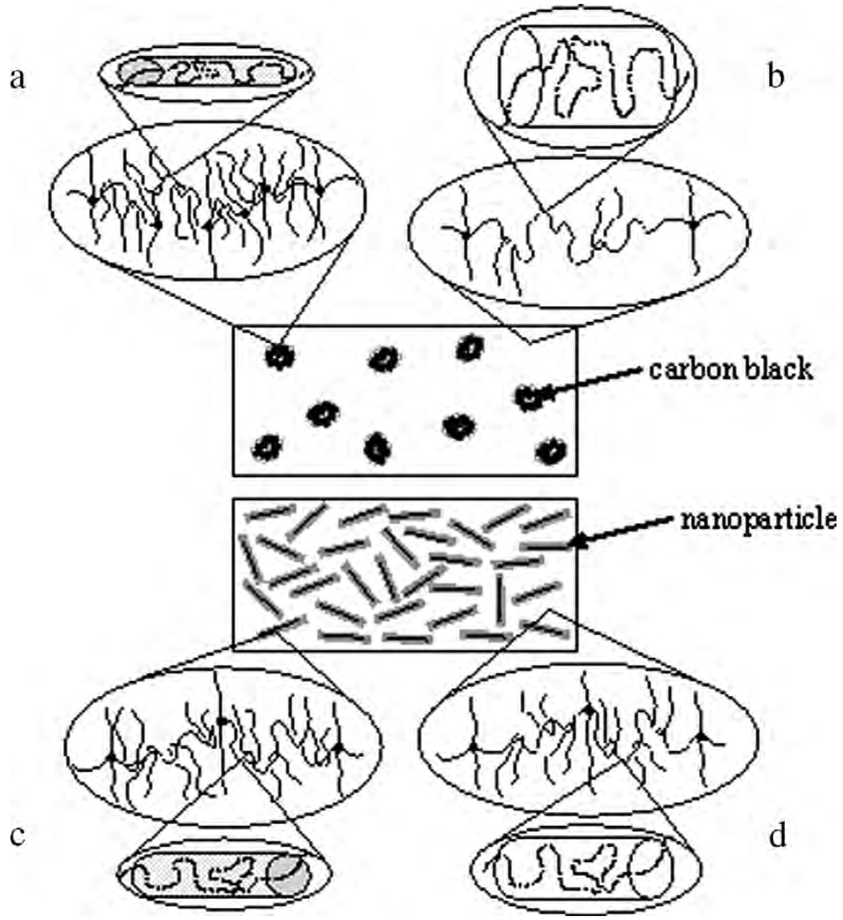

Fig. 3. Schematic representation of filler/polymer interaction.

in chain entropy associated to the reduction in the number of possible chain configurations in comparison with that of bulk rubber (Fig. 3d). This explains the improved properties of these innovative materials [16,17]. These results are supported from a thermodynamic point of view. Since the internal energy term can be considered negligible it is assumed that the elastic retractive force of a rubber-like material depends on the entropy component and then: $f = -T\left(\frac{\partial S}{\partial L}\right)_{\mathrm{T,V}} = \left(\frac{\partial F}{\partial L}\right)_{\mathrm{T,V}}$, where F is Helmholtz free energy, S is the entropy, V the volume of the system, L the length of the sample and T the absolute temperature. Therefore, an increase of f obtained from mechanical measurements is associated with a loss in chain entropy, which reflects a more ordered system due to the confinement, as expected in the presence of nanoparticles.

In addition, in all networks theories based on topological invariants, it has been assumed that the retractive force exhibited by polymeric networks comes not only from the entropic forces generated in deformed elastically active chains, but also from topological interactions among entangled molecules. Due to its inorganic nature, these nanoparticles do not exhibit an optimum compatibility with organic polymers, giving rise, mainly to physical adsorptions. This results in the formation of a highly ordered and entangled structure, wherein the mobility of rubber chains is limited in its lateral fluctuations by the presence of neighbouring chains. Nevertheless, the slippage of the physical joints is hardly hindered decreasing under stretching. This fact is corroborated since the G_e/G_c ratio slightly varies for nanoparticles in relation to pristine natural rubber, whereas a clear decrease in the case of carbon black, is observed. This statement is of crucial importance to understand how the addition of nanoparticles improves the strength and toughness of the material without sacrificing the elastic properties of the rubber compound.

4. Conclusions

Natural rubber network in presence of two fillers, carbon black and inorganic nanoparticles has been evaluated by applying the tube model theory. Molecular network parameters derived from this model point out a different filler/elastomer reinforcement mechanism as a function of filler. In fact, the contribution corresponding to chemical crosslinks is increased by adding both fillers due to the formation of a higher number of interactions. However, in spite of the reduction in the contribution of topological constraints by carbon black, both contributions are increased in presence of nanoparticles. This results in a marked decrease of the tube dimensions due to intense nanoparticle/elastomer interactions, which restricts the movement of the rubber chains to a lower volume.

A likely explanation can be found in terms of the different nature of the fillers. Carbon black forms strong covalent bonds with the elastomer, but restricted in a zone at the filler/elastomer interface which covers only a little rubber percentage. However, the inorganic particles are characterized by a high aspect ratio, so the optimum dispersion of even a small amount of nanoparticles (exfoliated nanocomposites) is enough to interact with the total rubber mass. Furthermore, these nanoparticles mainly exhibit physical adsorptions with the elastomer due to its inorganic nature. This leads to the formation of a highly ordered and entangled structure in which, the mobility of rubber chains is hindered for lateral fluctuations by the presence of neighbouring chains.

Acknowledgement

This work has been supported by CICYT, MAT 2004-00825.

References

[1] Krishnamoorti R, Vaia RA. Polymer nanocomposites: synthesis, characterization and modelling. In: Krishnamoorti R, Vaia RA, editors. American Chemical Society Symposium. Washington, Inc., 2001.

[2] Pinnavaia TJ, Beall GW. In: Pinnavaia TJ, Beall GW, editors. Polymer–clay nanocomposites. New York, Inc.: John Wiley & Sons; 2000.

[3] Giannelis EP, Krishnamoorti R, Manias E. Polymer-silicate nanocomposites: model systems for confined polymers and polymer brushes. Adv Polym Sci 1999;138:107–47.

[4] Suprakas Sinhá R, Okamoto M. Polymer/layered silicate nanocomposites: a review from preparation to processing. Prog Polym Sci 2003;28:1539–641.

[5] Treloar LR. In: Treloar LR, editor. The physics of rubber elasticity. Oxford Inc.: Clarendon Press; 1975.

[6] Flory PJ. In: Flory PJ, editor. Principles of polymer chemistry. New York Inc.: Cornell University; 1953.

[7] Staverman AJ. In: Staverman AJ, editor. Thermodynamic of polymers. Berlin, Inc.: Springer-Verlag; 1962.

[8] Queslel JP, Mark JE. Molecular interpretation of the moduli of elastomeric polymer networks of known structure. Adv Polym Sci 1984;65:135–76.

[9] Vilgis TA. In: Vilgis TA, editor. Comprehensive polymer science. New York Inc.: Pergamon Press; 1989.

[10] Kuhn W, Grün F. Beziehung zwischen elastischen Konstanten und Dehnungsdoppelbrechung hochelastischer Stoffe. Kolloid Z 1942;101:248–62.

[11] James HM, Guth E. Theory of the elastic properties of rubber. J Chem Phys 1943;11:455–81.

[12] Edwards SF. Theory of rubber elasticity. Brit Polym J 1977;9(2):140–3.

[13] Heinrich G, Vilgis TA. Contribution of entanglements to the mechanical properties of carbon black filled polymer networks. Macromolecules 1993;26(5):1109–19.

[14] Heinrich G, Straube E, Helmis G. Rubber elasticity of polymer networks. Theories. Adv Polym Sci 1988;85:33–87.

[15] Lopez-Manchado MA, Herrero B, Arroyo M. Preparation and characterization of organoclay nanocomposites based on natural rubber. Polym Int 2003;52(7):1070–7.

[16] Arroyo M, Lopez-Manchado MA, Herrero B. Organo-montmorillonite as substitute of carbon black in natural rubber compounds. Polymer 2003;44(8):2447–53.

[17] Lopez-Manchado MA, Valentín JL, Herrero B, Arroyo M. Novel approach of evaluating polymer nanocomposite structure by measurements of the freezing-point depression. Macromol Rapid Commun 2004;25(14):1309–13.

[18] Marzocca AJ, Cerveny S, Raimondo RB. Analysis of the variation of molecular parameters of NR during vulcanization the frame of the conformational tube model. J Appl Polym Sci 1997;66(6):1085–92.

[19] Eisele U. In: Eisele U, editor. Introduction to polymer physics. Berlin, Inc.: Springer-Verlag; 1990.

[20] Harwood JAC, Payne AR. Stress softening in natural rubber vulcanizates. 3. Carbon black filled vulcanizates. J Appl Polym Sci 1966;10(2):315–24.

[21] Yuan QW, Mark JE. Reinforcement of poly(dimethylsiloxane) networks by blended and in situ generated silica fillers having various sizes, size distributions, and modified surfaces. Macromol Chem Phys 1999;200(1):206–20.

[22] Guth E, Gold O. On the hydrodynamical theory of the viscosity of suspensions. Phys Rev 1938;53:322.

[23] Guth E. Theory of filler reinforcement. J Appl Phys 1945;16(1):20–5.

[24] Einstein A. Eine neue Bestimmung der Moleküldimensionen. Ann Phys (Leipzig) 1906;19:289–306.

[25] Joly S, Garnaud G, Ollitrault R, Bokobza L, Mark JE. Organically modified layered silicates as reinforcing filler for natural rubber. Chem Mater 2002;14(10):4202–8.

[26] Treloar LRG. The photoelastic properties of short chain molecular networks. Trans Faraday Soc 1954;50(8):881–96.

[27] Isihara A, Hashitsume N, Tatibana M. Statistical theory of rubber like elasticity. 4. (2-Dimensional stretching). J Chem Phys 1951;19(12):1508–12.

[28] Wang MC, Guth E. Statistical theory of networks of non-Gaussian flexible chains. J Chem Phys 1952;20(7):1144–57.

[29] Kuhn W, Kuhn H. Statistiche und energieelastiche rucks-tellkraft bei stark auf dehnung beanspruchten fadenmolekeln. Helvetica Chim Acta 1946;29(5):1095–115.

[30] Flory PJ. Effect of molecular structure of physical properties of butyl rubber. Ind Eng Chem 1946;38(4):417–36.

[31] Mark JE. In: Mark JE, editor. Physical properties of polymers. Cambridge, Inc.: Cambridge University Press; 2003.

[32] Wu S. Chain structure and entanglement. J Polym Sci Part B Polym Phys 1989;27(4):723–41.

[33] Aharoni SM. Correlations between chain parameters and the plateau modulus of polymers. Macromolecules 1986; 19(2):426–34.

[34] Fetters JL, Lohse DJ, Richter D, Witten TA, Zirkel A. Connection between polymer molecular weight, density, chain dimensions, and melt viscoelastic properties. Macromolecules 1994;27(17):4639–47.

[35] Marzocca AJ. Estimation by mechanical analysis of the molecular parameters of SBR vulcanizates at different cure conditions. J Appl Polym Sci 1995;58(10):1839–45.

[36] Funt JM. Dynamic testing and reinforcement of rubber. Rubber Chem Tech 1988;61(5):842–65.

Macromolecules **2008**, *41*, 4717–4729

Uncertainties in the Determination of Cross-Link Density by Equilibrium Swelling Experiments in Natural Rubber

J. L. Valentín,*,[†,‡] J. Carretero-González,[‡] I. Mora-Barrantes,[‡] W. Chassé,[†] and K. Saalwächter*,[†]

Institut für Physik, Martin-Luther-Universität Halle-Wittenberg, Friedemann-Bach-Platz 6, D-06108 Halle, Germany, and Institute of Polymer Science and Technology (CSIC), C/Juan de la Cierva 3, 28006-Madrid, Spain

Received March 6, 2008; Revised Manuscript Received May 15, 2008

ABSTRACT: Equilibrium swelling is a feasible and simple experiment to determine the cross-link density of networks. It is the most popular and useful approach; however, in most of the cases, the given values are highly uncertain if not erroneous. The description of the complex thermodynamics of swollen polymer networks is usually based on the Flory–Rehner model. However, experimental evidence has shown that both the mixing term described by the Flory–Huggins expression and the elastic component derived from the affine model are only approximations that fail in the description and prediction of the rubber network behavior. This means that the Flory–Rehner treatment can only give a qualitative evaluation of cross-link density because of its strong dependence on the thermodynamic model. In this work, the uncertainties in the determination of the cross-link density in rubber materials by swelling experiments based on this model are reviewed. The implications and the validity of some of the used approximations as well as their influence in the relationship of the cross-link densities derived from swelling experiments are discussed. Importantly, swelling results are compared with results of a completely independent determination of the cross-link density by proton multiple-quantum NMR, and the correlation observed between the two methods can help to validate the thermodynamic model.

Introduction

Rubber is an important kind of material with many practical applications and is characterized by a long-range elasticity. This property is obtained after the vulcanization process, where a *plastic* polymer is transformed into an *elastic* material by formation of a three-dimensional network of cross-links that connect the different polymeric chains. For this reason, it is not surprising that the most important properties of rubbers depend on the network structure, and its study allows us to reach a better understanding of the correlation between the microstructure and the macroscopic properties of the rubber.[1–3]

The network structure is defined by several parameters, i.e., the number of cross-links, their functionality and distribution, network defects (dangling chains and loops), and entanglements. However, the difficulty to study the vulcanization reaction in situ, further complicated by the complexity of the polymeric system itself, makes even the number of junctions, which appears to be a rather directly measurable parameter, a hardly accessible quantity.

There are many different experimental approaches to the analysis of cross-linked polymers,[4] such as inverse gas chromatography,[5] osmometry,[6] dynamical mechanical analysis,[7] neutron scattering,[8] or dielectric measurements.[9] However, the most common techniques to determine the cross-link density are mechanical measurements,[10–15] NMR spectroscopy,[16–23] and equilibrium swelling.[24–28]

Although some of the previously mentioned techniques give some extra information about the structure of the network, the equilibrium swelling experiment is nowadays the most widely used approach in rubber science and technology. The technique allows the determination of the average molecular weight between cross-links, M_c, commonly also expressed as cross-link density $\nu = 1/2M_c$ in moles of cross-links per gram of rubber, or $\nu' = \rho_r/2M_c$ when it is defined per volume of rubber using the rubber density, ρ_r.

The thermodynamics of swollen polymer network are usually based on the Flory–Rehner model[24–26] or, more correctly, the Frenkel[29]–Flory–Rehner treatment. They postulate that, in the swollen state, the mixing and elastic components of the free energy are additive and separable, i.e., $\Delta G_{tot} = \Delta G_{mix} + \Delta G_{elas}$. Then, it can be expressed in terms of change in chemical potential of the solvent, $\Delta\mu_s^{total}$, by differentiation with respect to the number of moles of solvent

$$\frac{\Delta\mu_s^{total}}{RT} = \frac{\Delta\mu_s^{mix}}{RT} + \frac{\Delta\mu_s^{elas}}{RT} \quad (1)$$

In equilibrium, the elastic forces compensate the dilation of the network caused by the mixing contribution. Consequently, the total change in the chemical potential vanishes:

$$\frac{\Delta\mu_s^{mix}}{RT} = -\frac{\Delta\mu_s^{elas}}{RT} \quad (2)$$

R and T are the ideal gas constant and temperature, respectively.

It is generally accepted that the Flory–Huggins expression[30,31] is most appropriate to define the mixing term

$$\frac{\Delta\mu_s^{mix}}{RT} = \ln(1-\phi_r) + \left(1 - \frac{V_s}{V_r}\right)\phi_r + \chi\phi_r^{\,2} \quad (3)$$

For a cross-linked polymer, the molar volume of the polymer (V_r) tends to infinity, whereby the expression is simplified to

$$\frac{\Delta\mu_s^{mix}}{RT} = \ln(1-\phi_r) + \phi_r + \chi\phi_r^{\,2} \quad (4)$$

where χ is the Flory–Huggins polymer–solvent interaction parameter and $\phi_r$is the volumetric fraction of rubber (or polymer fraction) at swelling equilibrium.

On the other hand, the elastic contribution to the chemical potential is expressed in terms of a molecular theory.[3,11,12] In

---

* Corresponding authors. E-mail: jlvalentin@ictp.csic.es; kay.saalwaechter@physik.uni-halle.de.

[†] Martin-Luther-Universität Halle-Wittenberg.

[‡] Institute of Polymer Science and Technology (CSIC).

10.1021/ma8005087 CCC: $40.75

the original Flory−Rehner expression, the affine deformation model,[32] which is defined by eq 5 for a swollen network, was assumed

$$\Delta G_{\mathrm{elas}} = \frac{1}{2}\frac{RT}{M_c}(\lambda_x{}^2 + \lambda_y{}^2 + \lambda_z{}^2 - 3) - \frac{2}{f}\frac{RT\ln(V/V_0)}{M_c} \qquad (5)$$

where λ_i represents the elongation in three dimensions, V and V_0 are the total volume of the polymer−solvent system and the pure polymer, respectively, and f is the functionality of the cross-links.

Taking into account the equilibrium requirements (eq 2) and the mixing part defined in eq 4 and deriving eq 5 with respect to the number of moles of solvent, the classical Flory−Rehner equation is obtained

$$\ln(1-\phi_r) + \phi_r + \chi\phi_r{}^2 = -\frac{\rho_r}{M_c}V_s\left(\phi_r{}^{1/3} - \frac{2\phi_r}{f}\right) \qquad (6)$$

However, in the past years some works proposed that the phantom network model[33,34] should be more adequate to represent the behavior of the swollen networks. In that case, the expression is written as

$$\ln(1-\phi_r) + \phi_r + \chi\phi_r{}^2 = -\frac{\rho_r}{M_c}V_s\left(1 - \frac{2}{f}\right)\phi_r{}^{1/3} \qquad (7)$$

Obviously, the real behavior of the swollen network is between the two extremes represented by affine and phantom models. This fact was incorporated in the later Flory−Erman model[35,36] which, by using a variable K parameter, was able to interpolate between the different behaviors of the two models, giving a more realistic picture of the process.

Therefore, and according to the above reasoning, the calculated M_c values from swelling experiments are subject to a large uncertainty, such as the adopted model to define the elastic term. Furthermore, and no less importantly, the parameters that determine the average molecular weight between cross-links, i.e. ϕ_r, χ, or f in eqs 6 and 7, further increase the ambiguity.

Accepting the proposed models, maybe the most important factor which limits the range of confidence is the Flory−Huggins interaction parameter χ. It is usually assumed to be constant for a given polymer−solvent pair. However, this assumption was generally proven incorrect by different experimental and theoretical works[37–45] that showed a dependence of χ on the volumetric fraction of polymer. In addition, the ϕ_r dependence of χ in cross-linked and star polymers is different in comparison with the corresponding linear polymers under the same conditions.[46–61] The quantitative evaluation of M_c from swelling experiments is thus highly uncertain.

Other sources of ambiguity stem from the determination of the volumetric fraction of rubber in the swollen gel at equilibrium. In earlier works, the measurement of the volume of the swollen samples was the most widely used approach,[62] as it represents the most direct and accurate method to determine ϕ_r. However, nowadays the gravimetric method is the most popular, since it is quick and simple.[63–68] As to the gravimetric approaches, the most remarkable point concerns corrections that must be made in order to obtain meaningful results. For instance, it is necessary to take into account the fraction of insoluble ingredients and the “real” rubber density as well as some corrections due to the time dependence of the amount of imbibed solvent observed during the swelling process (as it was pointed out by Ellis and Welding,[63,64] the swelling degree is continually increasing with time of immersion). This again adds another source of considerable uncertainty.

A detailed description of the experimental procedure and the associated accuracy in the determination of the cross-link density is thus not a trivial problem, and revising the scientific literature on the topic, it appeared to us that a unified approach is still missing. On one hand, many of the mentioned ambiguities are not at all addressed in previous work, making it almost impossible to compare data from different sources. On the other hand, and more seriously, it appears that many of the above-mentioned problems have not even come to the attention to a considerable section of the scientific community using equilibrium swelling as a standard tool. This is an important but long neglected problem in rubber science and technology.

This paper reviews the most widely used approaches and approximations to determine the cross-link density via Flory−Rehner swelling experiments and tries to delineate the limitations and errors associated with each one as clearly as possible. We explicitly discuss the range of uncertainty of the obtained M_c values and finally suggest the best approach from our point of view in order to improve the application of this useful methodology.

In order to assess the validity of a method, it is obviously desirable to include results from independent methods. Different combined studies have been published,[69–75] and many of them use NMR. It is in fact well-known that a linear relationship exists between the network parameters determined by equilibrium swelling and by NMR. This suggests that the models used to establish the relationship between the actual NMR observable (an apparent, i.e., averaged residual dipolar coupling, D_{res}) and the cross-link density are at least qualitatively correct. In our previous work,[75] we have identified proton multiple-quantum NMR (rather than the more common measurement of transverse relaxation times) as the most quantitative and reliable method for the measurement of residual dipolar couplings,[76] and we have presented a molecular model that relates D_{res} with M_c. This, as any other model for NMR data interpretation, is also based on a number of assumptions (e.g., the validity of the Kuhn and Grün argument for the calculation of the order parameter S_b of a network chain, the rescaling of the chain based on the known characteristic ratio, etc.). Therefore, the re-evaluation of the validity of our NMR model is another important purpose of this paper. It should be noted that the model uncertainties only pertain to a prefactor, implying that the observation of a linear correlation between swelling and NMR results is an important diagnostic criterion.

Experimental Section

Materials, Preparation of Samples, and Characterization. Then aim of this work is to check the confidence limits of the most popular and useful approach to determine the cross-link density, i.e. swelling experiments, using common rubber samples. The studied compounds, based on standardized natural rubber kindly supplied by Malaysian Rubber (SMR-CV60), were prepared in an open two-roll mill using standard procedures. Sulfur cure systems are nowadays the most useful vulcanization method and therefore the main subject of this work. A conventional cure system was used, increasing the amount of reactive species but maintaining the accelerant/sulfur ratio (0.2) constant. All the details about the composition of the different samples are showed in Table 1.

In some cases, NR samples were also vulcanized with different contents of dicumyl peroxide (DCP) as well as with a different sulfur/accelerant ratio (more information about these samples will be given in following sections). All specimen were cured in a laboratory press at 150 °C at their respective optimum times (t_{97}), deduced from the rheometer curve (Monsanto moving die rheometer, model MDR 2000E).

Determination of the Volumetric Fraction of Rubber, ϕ_r. The volumetric fraction of rubber was determined following different approaches (see the Discussion section), but always on the basis of equilibrium swelling experiments (72 h at 21 °C) using toluene (molar volume V_s = 106.2 mL/mol and density ρ_s = 0.87 g/cm^3) as solvent. In addition, some complementary experiments were

Table 1. Composition and Density of the Studied Compounds

	recipe[a] (phr)		density (g/cm^3)			
sample	sulfur	CBS[b]	compd before swelling ρ_c^b	compd after swelling ρ_c^a	rubber network ρ_r	weight fraction f_{ZnO}
C-1	0.7	0.14	0.949 ± 0.004	0.955 ± 0.005	0.912	0.0464
C-2	1.3	0.26	0.958 ± 0.002	0.959 ± 0.002	0.922	0.0461
C-3	1.9	0.38	0.961 ± 0.004	0.9605 ± 0.0009	0.924	0.0458
C-4	2.5	0.50	0.967 ± 0.007	0.965 ± 0.001	0.929	0.0455
C-5	3.1	0.62	0.965 ± 0.005	0.966 ± 0.001	0.930	0.0452
C-6	3.7	0.74	0.970 ± 0.001	0.970 ± 0.001	0.934	0.0449

[a] Ingredients in parts per hundred of rubber (phr): natural rubber 100; zinc oxide 5; stearic acid 2; CBS; sulfur. [b] *N*-Cyclohexyl-2-benzothiazolesulfenamide.

carried out using methyl ethyl ketone (MEK) as solvent ($V_s = 90.2$ mL/mol and density $\rho_s = 0.805$ g/cm^3).

In all the samples, the procedure to obtain the experimental gravimetric data was the same: Five weighed test pieces of rubber (w_i) were immersed in toluene at 22 °C for a period of 72 h, renewing the solvent every 24 h. Finally, the samples were blotted with tissue paper to remove the excess of the solvent and immediately weighed on an analytical balance with an accuracy of $\sim 10^{-5}$ g (w_s). Finally, the samples were dried in a vacuum oven for ~24 h at 60 °C until constant weight (w_d). It is important to note that in order to obtain a correct ϕ_r the time dependence of this quantity due to gradual network degradation needs to be taken into account. This very important point will be described and discussed in the next section.

To obtain ϕ_r by using gravimetric methods is necessary to know the rubber density in the cross-linked sample. It appears to be common in the literature to approximate this parameter as a constant, $\rho_r^{\text{const}} = 0.92$ g/cm^3. However, it is well-known that this quantity depends on the cross-link density in sulfur-vulcanized samples (in the case of NR vulcanized with DCP, no deviation from 0.92 g/cm^3 is observed). Ellis and Welding[63,64] suggested that an estimated rubber density could be calculated assuming that the volumes of polymer and sulfur are additive, with a fictitious density of 6 g/cm^3 for the combined sulfur

$$\rho_r^{E-W} = \frac{w_{\text{rubber}} + w_{\text{sulfur}}}{\dfrac{w_{\text{rubber}}}{0.92} + \dfrac{w_{\text{sulfur}}}{6}} \tag{8}$$

where w_{rubber} and w_{sulfur} are the nominal weights of rubber and sulfur tabulated in Table 1. The main problem of this approach is the dependence on the density of the pristine rubber. In the literature,[40,41,45] density values for pristine rubber range from 0.906 to 0.9132, with 0.908 g/cm^3 as the most commonly used. The difficulty arrives in the a priori estimation of this value, without any other experimental data. However, it is a good approximation when the real rubber density can not be measured experimentally.

Obviously, the latter approach is the most recommended. In this work, the compound density, ρ_c, was determined via the hydrostatic weighing method, which is one of the best known density measurement techniques.[77] In this method, the apparent weight $\bar{W}$ of a specimen is measured in two different media, e.g. air and water, and the density is obtained from

$$\rho_c = \frac{\overline{W}_{\text{air}}\rho_{\text{water}} - \overline{W}_{\text{water}}\rho_{\text{air}}}{0.99983(\overline{W}_{\text{air}} - \overline{W}_{\text{water}})} \tag{9}$$

where ρ_{water} (0.9977 g/cm^3 at 22 °C) and ρ_{air} (0.0012 g/cm^3) are water and air densities, respectively, and 0.99983 is a geometric balance correction.

All measurements were performed on a Sartorius balance, model Kern 770, with a resolution of ±0.1 mg. It is important to point out that the sensitivity of the weighing balance becomes the limiting factor in precision because the specimens are rather small (around 0.11 g).[78]

The average density of at least three samples per compound (each sample is also measured two times) is summarized in Table 1. The density of the compounds was calculated after (ρ_r^a) and before (ρ_r^b) swelling in toluene in order to established the contribution of all the soluble compounds present in the sample. According to the results in Table 1, the mass loss during the swelling process does not produce any appreciable change in the density value.

With known density of the compounds (values obtained after swelling were used), it is possible to calculate the experimental density of the rubber matrix after the swelling experiments as follows:

$$\rho_r = \frac{w_d - f_{ZnO}w_i}{\dfrac{w_d}{\rho_c^a} - \dfrac{f_{Zno}w_i}{\rho_{ZNo}}} \tag{10}$$

where w_d and w_i are the weight of the dry sample after and before the swelling, respectively, ρ_{ZnO} is the zinc oxide density (5.0 g/cm^3 according to the technical data given by the supplier, Lanxess), and f_{ZnO} is the weight fraction of zinc oxide calculated as $f_{ZnO} =$ (ZnO weight)/(recipe weight).

With eq 10 it is assumed that, after the swelling process, all the remaining ingredients in the sample are part of the rubber network, with the exception of the ZnO. We confirmed that both stearic acid and CBS (*N*-cyclohexyl-2-benzothiazolesulfenamide) are soluble in toluene. Moreover, the weight loss during the swelling process is close to the calculated amount of these ingredients (except for the lowest cross-linked sample C-1). Although sulfur is insoluble in toluene, we assume that it is part of the rubber network and therefore must be included in the calculation of the density.

The influence of the rubber density on the obtained M_c values will be discussed in the Results and Discussion.

Determination of M_c by Equilibrium Swelling. The average mass of network chains between cross-links was determined on the basis of the previously described equilibrium swelling experiments and assuming the formation of 4-functional cross-links during the vulcanization reaction. The given M_c values are the average of five samples per compound, and their associated standard deviation is around 2.5% on average, with a maximum value close to 6.6% and the minimum around 0.7%. These latter values are incorporated in figures of this work as error bars for the *x*-axis. The different approaches used to calculate the M_c value from the swelling experiments, i.e., corrections in the calculation of the volumetric fraction of rubber, different Flory−Huggins interaction parameters, and the use of affine and phantom models, will be further described in the Discussion section.

Determination of M_c by Proton NMR Spectroscopy. Proton NMR spectroscopy is an attractive and powerful tool to study the structure and dynamics of elastomers.[16] The existence of cross-links and other topological constraints in rubber matrices renders the fast segmental fluctuations of the polymeric chains nonisotropic, and as a consequence, residual dipolar couplings (D_{res}) persist.[18,79,80] Many NMR techniques have been used to estimate D_{res}, e.g. Hahn echoes[81] (although the quantitative results obtained from this method have been seriously criticized,[19,82,83] it is still used), combinations of Hahn and solid echoes,[18,84,85] stimulated echoes,[86] and two-dimensional (2D) magnetization exchange spectroscopy.[20] However, the most recent and quantitative approach for the measurement of weak residual dipolar coupling is the double-quantum (DQ) or, more generally, multiple-quantum (MQ) NMR technique.[21–23,87–90]

The essential advantage of MQ spectroscopy is that, in the same experiment, two qualitatively different sets of data, a buildup curve (I_{DQ}) dominated by spin-pair double-quantum (DQ) coherences and a decay curve (I_{ref}), are measured. They can be used to independently analyze residual couplings and the chain dynamics. I_{ref} contains not only the signal from half of the quantum orders of the dipolar-coupled network chains but also the signal from uncoupled components. This uncoupled fraction is characterized by isotropic motion and rather slow relaxation and is formed mainly by network defects, i.e., loops and/or dangling chains. The corresponding long-time tails of I_{ref} can therefore be determined quantitatively and subtracted. In this way, the experimental I_{DQ} can be normalized by point-by-point division by the corrected sum of the two components in order to obtain a buildup function (I_{nDQ}) that is largely independent from the time scale of the segmental motion and is therefore related only to the network structure (i.e., D_{res}).

^{1}H MQ experiments were carried out in a Bruker minispec mq20 operating at 0.5 T (90° pulses of 1.7 μs length). The experiments and the data analysis were performed following the previously published procedures.[22,23,75,76] All samples characterized by NMR were not extracted after the vulcanization, yet we have checked that the extractable content is minor; thus, its removal has virtually no effect on the results (data not shown).

It is important to note that, apart from the fixed segmental time scale, the required time to sweep out the whole conformational space between topological constraints (related to the longest tube-constrained Rouse time), and thus the time required to achieve full averaging, becomes rather long for less cross-linked systems, leading to a residual temperature dependence.[89] Normalized DQ buildup data (I_{nDQ}) of common rubbers can be safely taken to be temperature-independent at 353 K or higher (around 140−145 K above the glass transition, T_g). Only the lowest cross-linked sample of our series (C-1) was evaluated at 373 K (the sample starts to degrade at 393 K). The variations of D_{res} with temperature in the range from 283 to 373 K (i.e., around 75 and 165 K above T_g, respectively) are briefly discussed in the next section.

In all the studied samples, distribution effects of D_{res} (related to different end-to-end separations and polydispersity of network chains) do not play any role. This somewhat surprising finding is explained by cooperativity of the reorientational dynamics on the length scale of a few network chain lengths, which averages the observable.[90] Therefore, the normalized DQ buildup curves were analyzed in the quasi-static limit in terms of a single D_{res}[22,23,75]

$$I_{nDQ}(D_{res}) = \frac{1}{2}\left(1 - \exp\left[-\frac{2}{5}{D_{res}}^2{\tau_{DQ}}^2\right]\right) \tag{11}$$

The obtained *apparent* coupling constant is directly proportional to the cross-link density, $\sim 1/M_c$, and the derivation of the proportionality factor was the subject of a previous paper.[75] In order to clarify that this is in itself a highly model-dependent procedure, we here give some of the details. D_{res}, which represents an average over different internuclear pair couplings, can be divided by its static counterpart, D_{stat}, in order to obtain the dynamic order parameter of the polymer backbone, S_b

$$S_b = k\frac{D_{res}}{D_{stat}} = \frac{3}{5}\frac{r^2}{N} \tag{12}$$

where k is a constant required by the model in order to rescale D_{stat} (determined by fixed proton−proton distances) in order to account for averaging effects that occur on the level below the segmental (Kuhn) length. Therefore, k represents the local coupling topology and intrasegmental motions. From previous spin dynamics simulations, and assuming a reasonable model for the intrasegmental motions, an apparent reference coupling for natural rubber was obtained: $D_{stat}/k = 2\pi \times 6300$ Hz (see ref 75 for a detailed account).

Equation 12 relates the NMR observable with r, i.e., the ratio of the end-to-end vector to its average unperturbed melt state ($r^2 = \mathbf{r}^2/\langle\mathbf{r}^2\rangle_0$), and with N, which represents the number of statistical (Kuhn) segments between constrains. The prefactor only reflects the assumption of Gaussian statistics for **r**. In addition, N provides the link to calculate the molar mass between constrains, M_c.

The latter magnitude is defined as the molar mass of the monomer unit ($M_0 = 68.1$ g/mol for NR) multiplied by the number of monomer units, n, which is in turn related to N via an expression that defines the contour length $L = Nl_K = c4nl$ as a projection length of the fully stretched chain. Therefore

$$M_c = nM_0 = \frac{Nl_K}{c4l}M_0 \tag{13}$$

The ratio between the Kuhn segment length, l_K, and the root-mean-square bond length, l, can be substituted by the known characteristic ratio C_∞ (defined as $C_\infty = N{l_K}^2/4nl^2$ with an average value of 4.7 for NR), leading to the expression

$$M_c = \frac{NC_\infty}{4c^2}M_0 \tag{14}$$

The factor c is the ratio between the projection length l_p of the bond onto the backbone at its maximum extension with respect to l and takes on a value of 0.7 for NR (according to the crystal-structure-based model discussed in ref 75). By the use of eq 12, M_c is finally related with the NMR observable, D_{res}, by the following expression:

$$M_c = \frac{3\times 6300\text{ Hz}}{5D_{res}/2\pi}\,\frac{4.7}{4\times 0.7^2}M_0 = \frac{617\text{ Hz}}{D_{res}/2\pi}\text{ kg/mol} \tag{15}$$

In order to obtain a clear picture on the variation of the results from the different approaches to the swelling experiment, we take these NMR values as an independent reference and always plot their inverse (which reflects cross-link density) vs the *different* values obtained from swelling. Note that very good linear relationships between NMR-based cross-link density determinations, and elastic moduli have been reported for different polymer systems,[91,92] demonstrating the qualitative validity of the models used for the interpretation of NMR results (mainly eq 12) and supporting the use of NMR as a proper reference. Correlating NMR with swelling results, we also found good linear dependencies in most cases. In fact, we hoped to observe more decisive deviations from linearity for certain models (e.g., constant vs ϕ-dependent χ parameter) and thus to be able to even judge the validity of the different thermodynamic models. However, in the investigated M_c range and the limitations set by the (low) experimental error, all models turned out to be linearly related for the common case of the NR−toluene system. However, the possibility of using NMR (that characterizes the bulk unswollen network completely independently from its thermodynamics) to test (and possibly falsify) thermodynamic models is certainly an important strategy for other polymer network−solvent systems. We demonstrate it below for a less common swelling solvent, MEK.

Results and Discussion

The aim of this work is to identify the range of confidence for a given M_c value using the most often used methods in rubber science and technology. For this reason, eq 6 will be used as reference of the Flory−Rehner theory in the following section. In addition, these results will be compared with those obtained by means of NMR, paying particular attention to deviations from this relationship caused by the different thermodynamic models.

We group the problem into three categories, that is, (i) determination of volume fraction of rubber, (ii) the polymer/solvent interaction parameter (χ), and (iii) the applied model of elasticity.

Initially, we will briefly discuss some NMR results that show the D_{res} dependence on the number of cross-links and polymer dynamics. Then, we will present the variations of the average

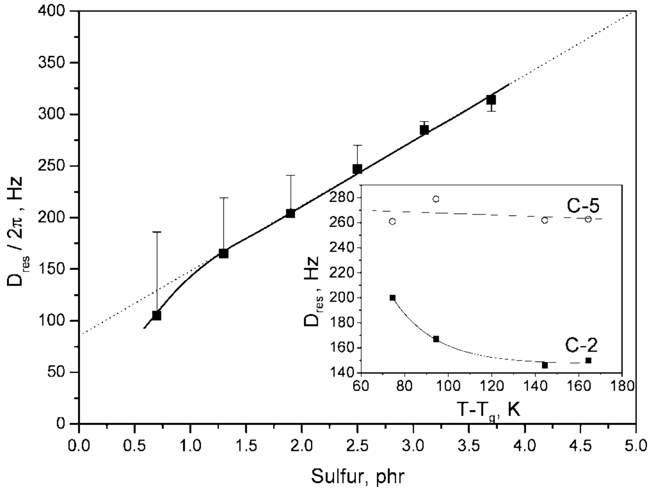

Figure 1. Relationship between the apparent dipolar coupling constant (always measured at the temperature where a constant D_{res} is reached) and the amount of sulfur added to the sample. The dashed line represents a linear fit of the last five points, whereas the solid line is only a guide to the eye. Error bars indicate the temperature dependence of D_{res}, which is also shown in more detail in the inset for the samples C-5 (plateau at $T = T_g + 75$ K) and C-2 (plateau at $T = T_g + 145$ K).

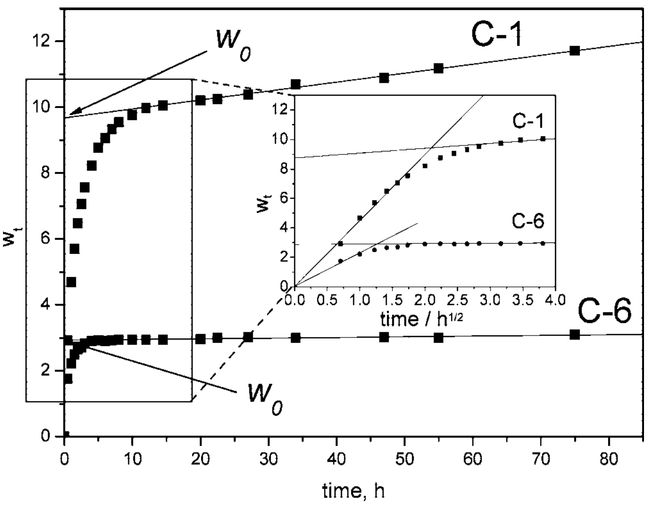

Figure 2. Degree of swelling vs immersion time for the samples C-1 and C-2. Each curve is a representation of the average behavior of three samples. At short times, the process is controlled by diffusion (see inset, where an initial linearity is apparent in a plot vs the square root of time), while at longer times of immersion, a further increase of swelling is caused by network degradation.

molecular weight between cross-links caused by the application of different corrections to evaluate the volumetric fraction of rubber from the gravimetric data. Once the best approach to study our system is identified, the role of the Flory−Huggins polymer−solvent interaction term in the estimation of M_c will be analyzed. Finally, the phantom network approach will be tested in order to delineate the limiting situations established in the Flory−Erman theory, realizing that the true behavior may be somewhere in between. The whole procedure will give us a confidence interval associated with the calculated cross-link density via swelling method. Finally, the significance of the relationship between the results obtained from swelling and NMR techniques will be discussed.

M_c Obtained by NMR. The NMR-determined residual dipolar constant obviously increases with the number of topological restrictions (mainly cross-links), as is shown in Figure 1. We stress the surprisingly good linear relationship between D_{res} and the amount of sulfur, which implies a constant yield in the vulcanization reaction. Only a small deviation is observed in the lowest cross-linked sample C-1, probably because it is a network just above the percolation threshold. Note also the intercept value in the *y*-axis, which is indicative of the fact that NMR is sensitive not only to the cross-links but also to topological constrains, i.e., entanglements, which are equally important restrictions to the segmental motion (and of course contribute to the elasticity). Further explanations on this point will be given in the next sections.

In previous work, we have demonstrated[89] that a residual temperature dependence of normalized DQ data can possibly lead to an overestimated D_{res} and thus cross-link density, in particular for lowly cross-linked systems. The (Rouse) relaxation time of the longest chain between topological restrictions (which roughly corresponds to the entanglement length at low cross-link density) is tied to the segmental relaxation time, which in turn is related to T_g. Therefore, the complete segmental averaging over all possible chain conformations on the time scale of the NMR experiment, and therefore a temperature independence of D_{res}, is only expected far above T_g.

As is obvious from the *y*-axis error bars in Figure 1, the temperature dependence is indeed a very important factor in the less cross-linked samples. This dependence is of course stronger in non-cross-linked samples, where the signal is only due to the entanglement restrictions and further decays due to reptation motion; thus, it never reaches a plateau. For instance, in sample C-1, D_{res} obtained at $T = T_g + 75$ K is 46% higher than the value obtained from the plateau beyond 165 K above T_g. For intermediate samples, D_{res} reaches a plateau at temperatures around $T_g + 95$ K, and $T_g + 75$ K is sufficient for the samples with the highest cross-link density. To take properly the temperature dependence into account and use D_{res} values from the plateau range was particularly important for the present study. Thus, all the measurements were performed at 353 K, which is far above the T_g of all samples (they vary from −65 to −56 °C) and ensures that the segmental dynamics is fast enough in order to average over all the possible conformations (thus reaching the plateau regime). Repeated measurements show that at the measuring temperature of 353 K and the required experimental time around 45 min; therefore, the degradation of the network is not an important factor.

Finally, from the experimental D_{res} and using eq 15, it is possible to obtain the average molecular weight between cross-links. More precisely, the inverse result, reflecting the overall cross-link density, is of course the sum of the density of actual chemical cross-links ($1/M_c$) and entanglements ($1/M_e$), taking into account that the latter also includes trapped entanglements ($1/M_{te}$).

M_c Obtained from Equilibrium Swelling. *1. Swelling Kinetics.* In order to obtain M_c from equilibrium swelling experiments, the first step is to study the swelling kinetics of the networks in order to estimate the most accurate equilibrium weight of solvent, w_0^{sol}. It is common to define the equilibrium weight of liquid as the difference $w_{3d}^{sol} = w_s - w_d$ after 3 days of swelling, which is considered a time long enough to reach the equilibrium. However, according to Figure 2, which shows the degree of swelling (defined as $w_t = (w_s - w_i)/w_i$) as a function of time, an additional slow process appears.

At short times, swelling is dominated by a diffusive process, characterized by a linear behavior when w_t is plotted vs the square root of time (inset in Figure 2). This fast process seems to reach saturation in a rather short time, around 20 h. After that, a continuous but slow increase takes place as a consequence of the degradation of the network, as was stressed by Ellis and Welding.[63,64]

This behavior was also studied by NMR (Figure 3), where a conventionally sulfur-cross-linked sample is compared with a

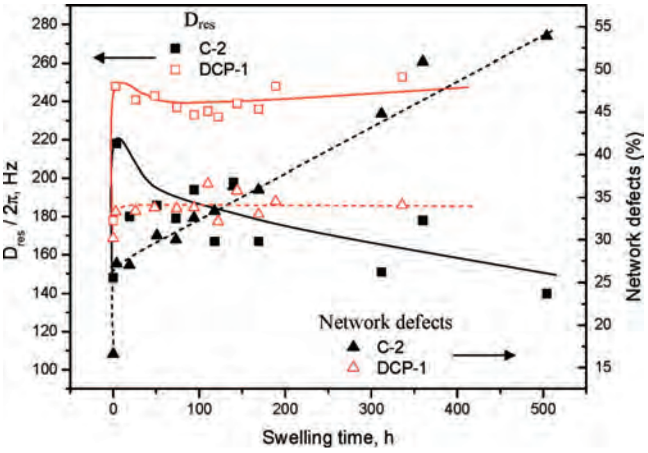

Figure 3. Evolution of D_{res} and the NMR-determined fraction of noncoupled network defects with swelling time for samples vulcanized with a conventional sulfur cure system (C-2) and an organic peroxide (DCP-1). DCP-1 is an NR sample vulcanized with 1 phr of dicumyl peroxide at 150 °C at its optimum cure time (t_{95}). Lines are only guide to the eye.

peroxide-cured sample. In the first stage of swelling, an abrupt increase in both D_{res} and the noncoupled fraction (network defects) as compared to the dry state is observed. This behavior is related to the nonhomogeneous nature of the swelling process in rubber networks.[93,94] More highly swollen areas take on higher chain order parameters, and less swollen can even exhibit reduced order parameters due to relief of entanglements ("des-interspersion"), subaffine local deformation, and genuine excluded-volume effects (on details of which a publication is submitted), whereby the average value of D_{res} increases nonaffinely, while its distribution is strongly broadened (not shown). Moreover, the relief of entanglement constraints by topological reorganization is retarded in time due to its complex nature, which leads to a small local maximum of D_{res} at around 10 h.

After approximately 20−30 h, the system reaches the equilibrium swelling. The uncoupled fraction (defects such as dangling chains and loops) also reaches a plateau, since these structures become increasingly unentangled, with significantly decreased relaxation times (for arm retraction, etc.).

However, while the DCP-cross-linked sample (where the cross-links are carbon−carbon bonds) reaches a plateau for both observables, the sulfur-cured sample shows an increasing amount of defects as well as a decreasing tendency for the residual coupling. This is clearly indicative of a network degradation process. We also note that the large variations in both D_{res} and the uncoupled fractions result from some fitting ambiguities, related to the fact that the system develops a third fraction with higher molecular weight. This fraction does not have a residual coupling (i.e., it is isotropically mobile), but it has a short relaxation time comparable to that of the network fraction.

Obviously, the degradation process is related exclusively with the sulfur bridges. In order to clarify the origin of the degradation, the swelling process in sulfur-cured samples was carried out under different conditions. According to the results shown in Figure 4, the breakdown of the network is caused by a photo-oxidative process, reaching even complete dissolution of the network at longer times (around 1 month at room temperature). The exclusion of light *or* oxygen considerably reduces the destruction of the sulfur bridges, but in both cases a minor increase of the swelling degree with time is still observed (samples under inert atmosphere but exposed to light even showed an exponential increase of the swelling degree at longer times of swelling). Only under a nitrogen atmosphere and complete darkness conditions is it possible to reach the equilibrium swelling in this type of network. The good news is, however, that an extrapolation to zero time gives a swelling degree that is very close to the equilibrium value in all the cases.

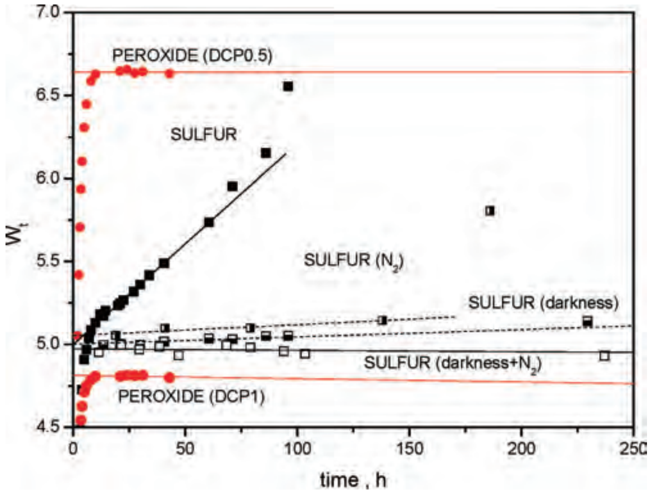

Figure 4. Degree of swelling vs immersion time for the sample C-1 (squares) under different storage conditions: stored in air and exposed to light (solid squares), under inert atmosphere of N_2 but exposed to light (N_2), protecting the sample against light but in air atmosphere (darkness), and stored under nitrogen atmosphere in the darkness (darkness + N_2). The degree of swelling for the samples DCP0.5 and DCP1 (NR vulcanized with 0.5 and 1 phr of DCP, circles) was determined after storage in air and exposed to the light. Lines are linear fits of the experimental data after the step controlled by diffusion.

In conclusion, to obtain a good equilibrium weight of liquid, w_0^{sol}, from which ϕ_r could be calculated, the excess of solvent produced by the network degradation has to be corrected. The best approach is as follows

$$w_0^{sol} = w_{3d}^{sol}(1 - d_{3d}) \qquad (16)$$

where d_{3d} is the increment of swelling degree caused by the degradation processes estimated as $d_{3d} = (w_{3d} - w_0)/w_0$. In this expression, w_0 is the swelling degree at $t = 0$, obtained by extrapolation in Figure 2. It is important to emphasize that, in contrast to the method proposed by Ellis and Welding, w_0 was estimated by using time rather than its square root for the *X*-axis. In this way, the slope more correctly and intuitively reflects the decomposition kinetics (where a linear fit is just an approximation to a first-order growth law), rather than a diffusive process.

2. Determination of the Volumetric Fraction of Rubber, ϕ_r. The definition of volumetric fraction of rubber in swelling experiments is simple and unequivocal, ϕ_r = (rubber volume)/(rubber volume + solvent volume). However, some different approaches have been used in the literature according to the studied system. In rubber compounds that contain insoluble components, it is necessary to properly eliminate this fraction in order to obtain a ϕ_r with a real meaning. The most useful and general method was again described by Ellis and Welding.[63,64]

In a first approximation, the authors suggested to take into account only the polymer in order to calculate ϕ_r. The influence of insoluble components such as sulfur, zinc oxide, or accelerants is corrected according to the following expression

$$\phi_r = \frac{\dfrac{w_d - f_{ins}w_i}{\rho_r}}{\dfrac{w_d - f_{ins}w_i}{\rho_r} + \dfrac{w_0^{sol}}{\rho_s}} \tag{17}$$

where f_{ins} is the weight fraction of insoluble components, defined as f_{ins} = (insoluble components weight)/(recipe weight) (in our case it should be $f_{ins} = f_{ZnO} + f_{sulfur}$). It is the most useful method in rubber science and technology, but in our opinion it could be improved since the substances that are able to create cross-links are not included in the fraction of the actual rubber network.

We favor another approach, also alluded to in the original work[64] of Ellis and Welding, in which ϕ_r is calculated taking into account the rubber network. Consequently, only the zinc oxide is considered insoluble ($f_{ins} = f_{ZnO}$). Conceptually, the latter approach seems to be more correct, and the noninclusion of the sulfur in the network leads to a deviation in the final cross-link densities between 1.5% and 6.3%, depending on the amount of sulfur. In addition, not only the volume of the insoluble particles but also an excess of solvent that arises in the case of noninteracting filler particles (ZnO) should be corrected for. In swollen samples, some amount of solvent is inside a vacuole that is formed at the rubber/ZnO interface and therefore is measured but actually does not take part in the swelling process of the rubber (see inset in Figure 5). This means that the volumetric fraction of rubber measured by eq 17 (here it is defined as ϕ_r* to distinguish it from the *corrected* value ϕ_r which will be defined below) is underestimated because it takes into account the excess of solvent as follows:

$$\phi_r{}^* = \frac{V_r}{V_r + V_s^r + V_s^v} \tag{18}$$

Here, V_r is the volume of rubber, V_s^r is the volume of solvent that swells the rubber network, and V_s^v is the volume of solvent imbibed in the vacuole formed at the ZnO/rubber interface. The volumetric fraction of rubber properly defined should be written as

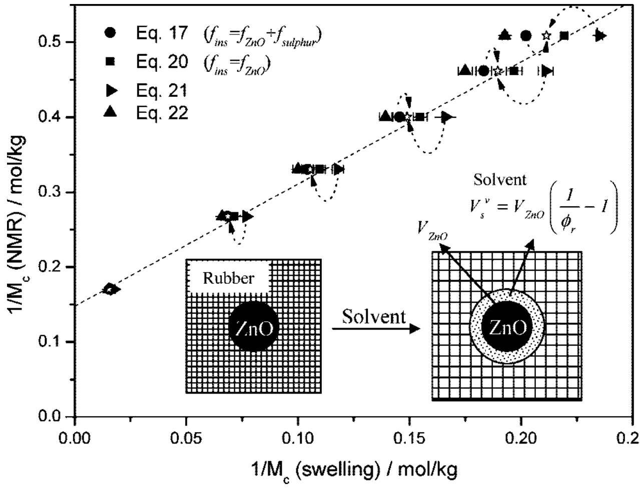

Figure 5. Comparison of swelling-determined reciprocal inter-cross-link molecular weights with corresponding results from NMR experiments. Variations of the estimated cross-link density via equilibrium swelling according to the different approaches used to take account the insoluble substances in the calculation of ϕ_r (see text). In addition, χ = 0.393 and an affine model were assumed. Arrows indicate the variation of the data (from eqs 17 and 21) when the correct density value in relation to the definition of the approach is applied (stars indicate the value). The line connects the corrected values. The inset shows the excess of solvent (assuming an affine deformation) imbibed in the ZnO/rubber interface caused by the noninteraction between the solid particles and rubber.

$$\phi_r = \frac{V_r}{V_r + V_s^r} \tag{19}$$

Assuming an affine deformation, the excess volume should be a function of the volume of ZnO (V_{ZnO}) as well as the volumetric fraction of rubber ϕ_r via $V_s^v = V_{ZnO}(1/\phi_r - 1)$. Therefore, it is possible to define the corrected volumetric fraction of rubber as a function of experimentally accessible parameters:

$$\phi_r = \frac{1 + \dfrac{V_{ZnO}}{V_r}}{\dfrac{1}{\phi_r^*} + \dfrac{V_{ZnO}}{V_r}} = \frac{1 + \dfrac{(f_{ZnO}w_i)/\rho_{ZnO}}{(w_d - (f_{ZnO}w_i))/\rho_r}}{\dfrac{\dfrac{w_d - f_{ZnO}w_i}{\rho_r} + \dfrac{w_0^{sol}}{\rho_s}}{\dfrac{w_d - f_{ZnO}w_i}{\rho_r}} + \dfrac{(f_{ZnO}w_i)/\rho_{ZnO}}{(w_d - (f_{ZnO}w_i))/\rho_r}} \tag{20}$$

The last correction (only valid for particles that do not interact with the rubber) only leads to differences around 2% in these samples with 5 phr of ZnO. However, at higher content of an insoluble fraction, such as actual fillers, it will play a major role in the determination of cross-link density by swelling measurements. This will be reported in future work. The results are shown in Figure 5, where for the first time now the different swelling approaches are represented in relation to the NMR results (in order to avoid interferences with the discussion in the following section, M_c values presented here were calculated using a standard value of χ = 0.393 for the NR/toluene pair[39,95]).

However, if we are consistent with the main idea of the more common approach, i.e., sulfur is not included in the network, ρ_r should be taken as 0.92 g/cm^3. In this case, the error is reduced (around 2.4% in average), as it is indicated in Figure 5 by the arrows. In order to delineate the importance of the insoluble component correction, two other approaches are represented in Figure 5. In the first one, all the sample volume is consider as rubber volume

$$\phi_r = \frac{\dfrac{w_d}{\rho_r}}{\dfrac{w_d}{\rho_r} + \dfrac{w_0^{sol}}{\rho_s}} \tag{21}$$

In the other extreme, all the ingredients, with exception of rubber, can be considered insoluble

$$\phi_r = \frac{\dfrac{w_i f_r(1-\alpha)}{\rho_r}}{\dfrac{w_i f_r(1-\alpha)}{\rho_r} + \dfrac{w_0^{sol}}{\rho_s}} \tag{22}$$

where f_r is the weight fraction of rubber, expressed as f_r = (rubber weight)/(recipe weight) and α is the mass fraction lost during the swelling ($\alpha = (w_i - w_d)/w_i$).

Obviously, the application of both methods to our system is a complete mistake. The M_c values not only are conceptually false but also show deviations up to 10%. In the first case, the overestimation of the cross-link density is lessened by the use of the compound density, which is more appropriate according to the definition of this method, obtaining similar values with respect to the approach of Ellis and Welding. This fact is easily explained since, as is shown in Figure 6, the deviation produced

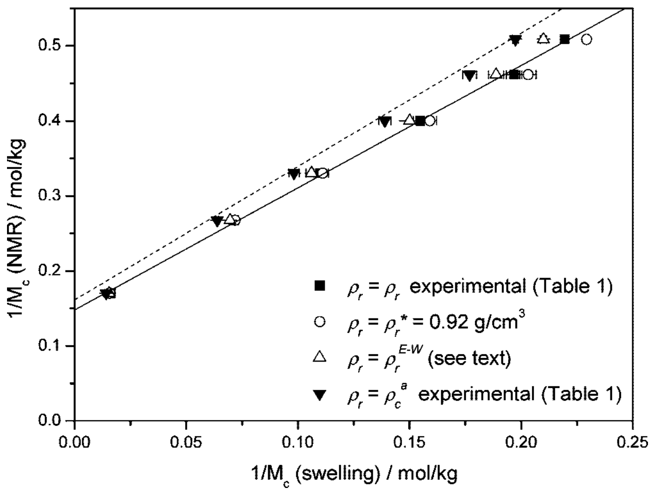

Figure 6. Variation of the reciprocal inter-cross-link molecular weights from equilibrium swelling data with the value of rubber density. The dashed line connects the results if the excess of imbibed solvent during 3 days of immersion time is not suppressed to calculate ϕ_r. The solid line is a linear fit of the values obtained by use of the most correct approach to calculate ϕ_r. In all the cases, eq 20 was used to calculate ϕ_r, and the affine model and $\chi = 0.393$ were assumed.

by using the compound density is partially canceled by the conceptual error of the method. Nevertheless, it is important to remember that even when the values are close to those obtained by the better approach, these values arise from a cancelation of errors in a conceptually false definition (at least within our interpretation). In addition, this "trick" is not recommendable since, for higher insoluble fractions, the deviation respect to the correct approach always increases.

In conclusion, it could be shown that the method described by eq 20 is the most general and correct approach in the estimation of ϕ_r when there are insoluble particles that do not interact with the rubber molecules. The use of any other approach inevitably leads to inconsistencies.

In order to close the discussion about the measurement of the volumetric fraction of rubber, it is important to stress the importance of using the corrected equilibrium weight of liquid in order to eliminate the excess of imbibed solvent caused by the photo-oxidative degradation of the network. As is also shown in Figure 6, the neglect of this correction leads to an underestimation of the cross-link density of about 15% on average. Here, we would like to point out that the use of the solvent weighted after 20 h, or 3 days of immersion gives the same results (discrepancies are inside the experimental error, around 1%) when the above-mentioned correction is taken into account (obviously, the factor of correction is different and it is necessary to calculate it).

3. Influence of the χ Parameter. The Flory−Huggins polymer−solvent interaction parameter χ introduced in eq 3 describes the change in the chemical potential of the solvent accompanying the formation of a real solution, minus the corresponding quantity of solvent in the formation of the reference solution.[43] The parameter χ is a complex parameter influenced by both entropic and heat of mixing terms.[24] It has been used as a measure of the "goodness" of a solvent in a given polymer−solvent pair. Therefore, it is the key parameter to describe solution properties of linear polymer molecules (non-cross-linked polymers) and swelling behavior of networks.

The parameter χ was originally introduced by Flory and Huggins as a measure of the intermolecular potential energy in polymer solutions. Initially, it was defined as being inversely proportional to temperature, $\chi = f(1/T)$, but independent of the polymer concentration.[24,96] However, subsequent experimental and theoretical results demonstrated the necessity of treating χ as a function of ϕ_r.[37–45]

Later on, Flory et al.[36,37] suggested that the χ parameter, originally expressed as a constant, should be replaced by power series:

$$\chi = \chi_0 + \chi_1\phi_r + \chi_2\phi_r^2 + ... \qquad (23)$$

The concentration dependence of χ was included in other thermodynamics of polymer solutions theories, as it was reviewed by Orwoll.[43] However, the most important of them was the equation of state theory described by Flory.[40,97–99] In this theory, the thermodynamics of polymer solutions are deduced from the equation of state of the pure components of the system. Nevertheless, the most significant conclusion concerning our discussion is that the dependence of χ with the temperature and polymer concentration in solution is justified. This new statistical theory of Flory represents a significant improvement over the early approach, which has been a comprehensive model to obtain qualitative information about the properties of polymer solutions.

Gee et al.[46] showed that, for cross-linked natural rubber in benzene, the swelling activity parameter, *S*, went through a maximum near to the maximum swelling and did not go toward zero in the unswollen state. These findings were later related by McKenna and co-workers with the possibility that the Flory−Huggins χ parameter for the cross-linked and un-cross-linked rubbers could be different. This possibility was intensely studied,[46,58–60] in particular by McKenna[47–51] and Horkay[52–57] in diverse polymer systems. These authors showed that, in all studied systems, χ_c of the cross-linked polymer is always higher than the parameter for the un-cross-linked system in solution, χ_u, at identical polymer concentration (i.e., identical volumetric fraction of polymer).

McKenna et al.[47–49] (and some other groups[58,59]), being based upon the works of Freed et al.,[100,101] suggested a linear dependence of the effective value of χ_c with the cross-link density, ν

$$(\chi_c - \chi_u)/\chi_u = \alpha\nu \qquad (24)$$

Along these lines, Tan et al.[58] even claims a dependence of this parameter on the structure of the formed network.

However, some years later, McKenna and Horkay[51] demonstrated that the Flory−Huggins χ_c parameter for cross-linked polymers is dependent on the volumetric fraction of polymer ϕ_r but totally independent of the detailed network structure, i.e., mainly the actual cross-link density. In all cases, the expression $\chi_c > \chi_u$ was demonstrated to be correct. This suggests that the total loss in the degree of translational freedom, caused by the introduction of cross-links, could be the reason for the conceptually different concentration dependence exhibited by χ in polymer gels and solutions. It simply points to an entropic origin of the large value of χ for both cross-linked and star polymers[102] as compared to the linear systems. For more details on this topic, we recommend the original articles of McKenna and Horkay and the recent review of Horta and Pastoriza.[61]

Figure 7 shows the variation of χ with polymer concentration for both un-cross-linked and cross-linked natural rubber, using toluene and methyl ethyl ketone (MEK) as solvents. Note that, in the case of the NR−toluene pair, the original data for the cross-linked system were obtained from poly(*cis*-isoprene) and deuterated toluene.[55] In addition, these values represent a system at 25 °C, therefore, and according to the temperature dependence of natural rubber−toluene system,[103] a deviation of about 3% is expected since we use these values for experiments at 22 °C. It should be emphasized that there is an obvious disproportion between the importance of the χ parameter to describe the

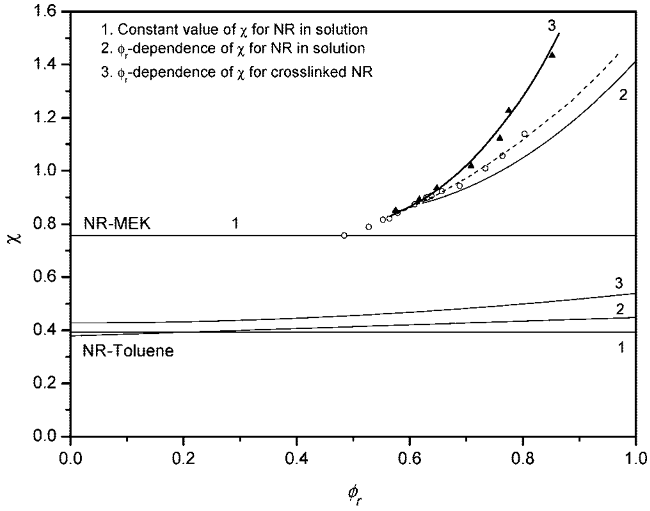

Figure 7. Dependence of the Flory−Huggins parameter on the polymer concentration. For the natural rubber−toluene pair (at 25 °C), χ was taken as 0.393 when it is considered constant,[39,95] $0.378 + 0.07\phi_r$ for in NR solution,[39] and $0.427 + 0.112\phi_r^2$ for cross-linked poly(*cis*-isoprene) swollen with deuterated toluene at 25 °C.[55] In the case of natural rubber swollen with methyl ethyl ketone (MEK), triangles show the dependence of χ on polymer concentration in natural rubber networks according to ref 49 (line is only a guide to the eye). The concentration dependence of χ in solutions of NR in MEK was obtained from ref 96. Circles represent the "experimental" values of χ for the NR samples swollen with MEK that are needed to obtain the same cross-link density as obtained from swelling experiments with toluene. The lowest value ($\chi = 0.757$) was used as a constant χ. Finally, the dashed line represents the χ behavior described in ref 41 for NR dissolved in MEK.

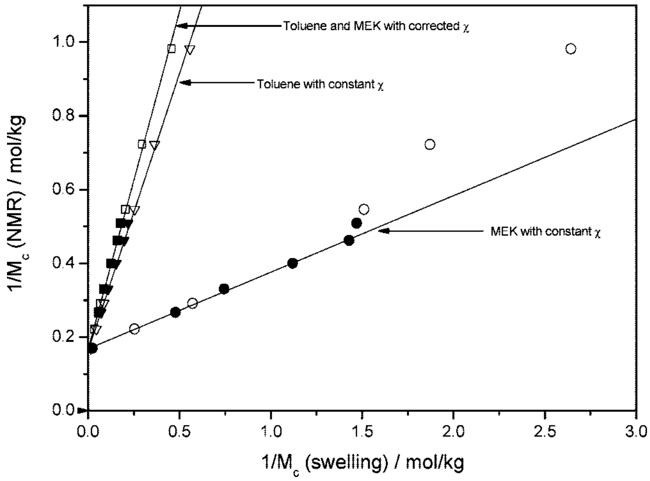

Figure 8. Variation of the reciprocal inter-cross-link molecular weights measured by swelling experiments (affine model) with respect to the value of the Flory−Huggins parameter for natural rubber swollen by toluene and MEK. Filled symbols correspond to sulfur-cured samples, whereas empty ones are for NR vulcanized with different contents of DCP.

swelling properties of cross-linked polymers and the scarce experimental results on its temperature and polymer concentration dependence for many important polymer−solvent pairs. It is even possible to find exactly opposing behaviors for the same polymer−solvent system.[39,104]

From the prior arguments, it is obvious that the use of the Flory−Huggins parameter obtained for polymer solutions (even when the dependence with the polymer concentration is assumed) will lead to overestimated cross-link densities (around 25−30%), as is shown in Figure 8. The central conclusion is that, taking into account the widespread use of the solution-based χ parameter to characterize natural rubber networks, most of the previously reported data for its cross-link density are overestimated.

On the other hand, the deviations between the cross-link densities from constant and concentration-dependent solution values of χ are relatively minor (not shown). Unfortunately, for toluene as solvent, no deviation from linearity is observed in our NMR-correlation plots for any of the adopted Flory−Huggins polymer−solvent interaction parameter models (Figure 8). This is mainly due to the fact that the volumetric fraction of rubber at swelling equilibrium over the typical cross-link density range used for practical purposes coincides with the range of ϕ_r where the crossover between both behaviours occurs (roughly from 0.1 to 0.3; see Figure 7). In addition, the values for the cross-linked systems have a tendency almost parallel to the linear-polymer values in the typical polymer concentration range. Obviously, more significant differences and possible deviations from linearity should be expected for very highly cross-linked NR samples which correspond with higher polymer fractions at swelling equilibrium.

In order to check the feasibility of the NMR correlation approach, another alternative is the use of a poorer solvent, in this case MEK. Significant differences in χ concentration dependence between un-cross-linked NR in solution or swollen NR networks in MEK are reported in the literature.[49,96] However, $1/M_c$ is very sensitive to small variations in the value of χ in this system. It causes large deviations as compared to the results obtained with toluene as swelling agent. In addition, we have not found any value of χ in the literature that covers the lower polymer concentration range of our samples. Therefore, a workaround the problem is to use the cross-link density obtained from the swelling experiments in toluene (assuming those results as being correct) and calculate the corresponding Flory−Huggins parameter for the NR−MEK pair. Of course, in order to obtain the experimental values of ϕ_r in MEK, all the previously mentioned considerations and corrections were taken into account.

For this reason, we used the lower value of χ obtained in this way as constant value for this system instead of the traditional value of 0.835 given by Bristow and Watson[39] (this value was obtained from a system with $\phi_r = 0.5794$, and as a consequence, all our samples, having lower values of ϕ_r at equilibrium, would show a negative and thus meaningless $1/M_c$).

Figure 7 shows that, at lower polymer concentration, our experimental points are superimposed with the χ values obtained for NR networks (ref 49). However, at higher polymer concentration, an inflection point becomes apparent where both tendencies start to differ. In any case, the so-obtained χ values are notably higher than those described in ref 96 for NR solutions in MEK. This again confirms the different concentration dependence of the Flory−Huggins polymer−solvent interaction parameter for linear and cross-linked polymers.

This conclusion is in contradiction to the behavior of χ for this system obtained by Brostow.[41] He corrected the data of Gee et al.[96] in order to obtain χ as a function of segment fractions instead of volume fractions (according to the equation of state of the pure components of the systems proposed by Flory). As is illustrated in Figure 7, the dependence for NR in solution (un-cross-linked NR) perfectly fits our data for swollen NR networks, in clear disagreement with the main idea. However, when Brostow's data are examined in detail, it appears that he calculated the values of χ mixing experimental data obtained from un-cross-linked NR in MEK and cross-linked samples, as Gee et al.[96] explained in their original work. Consequently, he obtained some parameters without physical meaning. The cancelation of errors seems to be the reason for the unexpected coincidence of both results.

Coming back to the main goal at this point, the χ behavior for a NR network swollen in MEK is far away from constant (as traditionally assumed in rubber science). Therefore, it is a perfect system to check the importance of the Flory−Huggins polymer−solvent interaction parameter on the average molecular weight between cross-links calculated by swelling experiments. According to the comparison between the average molecular weight between cross-links calculated by swelling experiments or by NMR (Figure 8), the use of an underestimated and polymer concentration-independent χ parameter (an unrealistic value for the NR−MEK pair) does not only lead to a gross overestimation of $1/M_c$, like in the case of toluene, but now also to very significant deviations from the linearity predicted by a concentration-dependent χ. It is thus demonstrated that, indeed, the comparison of independent experimental methods, in this case NMR, with swelling results is a viable strategy to evaluate models that describe the thermodynamics of swollen rubbers.

Summarizing all results, it can be concluded that the Flory−Huggins polymer−solvent interaction parameter is the key to a better understanding of the thermodynamics of swelling in rubber networks. However, the literature on this topic is not sufficient to completely clarify the meaning of this parameter. In some cases, results are contradictory, and of course only a few polymer−solvent systems have been studied. For this reason, uncertainties in χ are among the most important contribution to the uncertainty in the determination of cross-link density by equilibrium swelling experiments.

4. Dependence on the Theory of Rubber Elasticity. The elastic behavior of a rubber network is usually assumed to be in between the two extreme suppositions of the affine theory[32] and the phantom network model.[33,34] In the first case, the macroscopic deformation is assumed to be essentially the same as the microscopic deformation, and consequently, the cross-links are supposed to be fixed in space. Contrarily, the phantom model implies the free movement of the cross-links around a mean position. The later theory of Flory and Erman[35,36] to explain the thermodynamics of swollen networks assumes that, in the real behavior of rubber networks, the fluctuations of the cross-links are reduced by topological restrictions, i.e., entanglements. These restrictions are considered in the theory by the definition of a K parameter, which varies from 0 (implying an affine network) to ∞ (for phantom behavior).

Traditionally, the most widely used equation to determine the cross-link density in swollen rubbers has been eq 5, which is based on the affine model.[24–26] Nevertheless, several works suggest that the phantom network behavior provides a better approximation to the elastic behavior of swollen networks[55,58,105] (based on the supposition that the topological restrictions are relaxed because of the swelling process). If the latter hypothesis is accepted, a considerable increase of $1/M_c$ is observed (Figure 9).

Obviously, as a consequence of the impossibility to quantify the real behavior of the network, the *true* cross-link density of the system should be in the range delimited by both extremes (accepting of course the validity of such chain-based theories in general). This results in an overall uncertainty of around 40% (taking the phantom model as reference) and is probably the most important problem to be resolved.

Relationship between NMR and Swelling Results. Probably, the most important observation is, again, the linear relationship between $1/M_c$ obtained from equilibrium swelling and NMR, as seen, for instance, in Figure 9 (the obtained R value, using the phantom model, is 0.9999). This means that the relationship $S_b \sim 1/N$ assumed for the NMR analysis is qualitatively correct. If both swelling and NMR gave correct results, the slope in our correlation plots would be the unity.

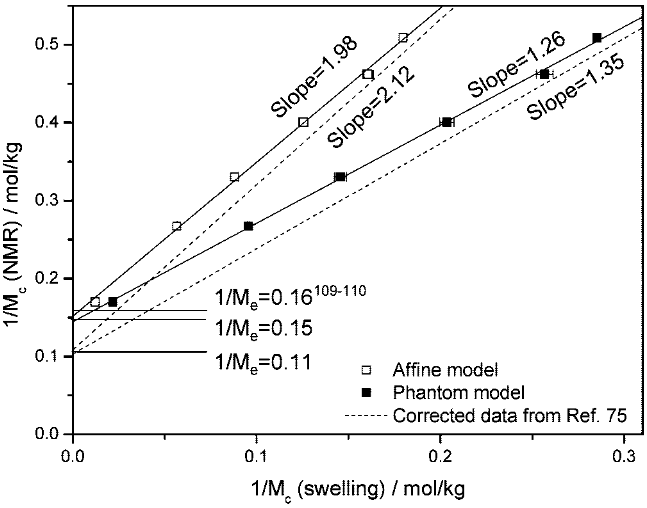

Figure 9. Comparison of swelling-determined reciprocal inter-cross-link molecular weights (using toluene as solvent) with corresponding results from NMR experiments. Variation of the estimated cross-link density via equilibrium swelling assuming the affine model (empty squares) or the phantom network (full squares) to define the elasticity of the swollen network. All other corrections were taken account to calculate the most accurate $1/M_c$ values. Dashed lines represent regressions of the data published in ref 75 (which are from different samples), but taking account all the corrections and the affine or phantom model.

As we have seen, swelling results based on the phantom model are most probably upper limits, with an uncertainty of about 40%. On the other hand, the many assumptions employed to relate the apparent D_{res} with M_c clearly indicate that the NMR value is also subject to an uncertainty, which we estimate to be in the 50% range (see Experimental Section and refs 75 and 94 for an in-depth discussion). An important factor that deserves more discussion is the influence of polydispersity and the type of average obtained by the method. The network chain length distribution is exponential in randomly cross-linked systems; thus $M_{w,c} \approx 2M_{n,c}$. To a first approximation, the swelling experiments "counts" the number of network chains; thus, the cross-link density $\sim 1/M_c$ should be a number-average. NMR measures every monomer unit; thus $D_{res} \sim 1/M_c$ should be a weight-average. NMR should thus be biased toward lower cross-link densities (higher M_c). Yet again, it should be stressed that NMR, even though measured at every monomer unit, gives only a single D_{res} rather than the expected wide distribution.[90] The cooperative reorientation dynamics that extends over a length scale of a few network chains somehow masks the chain-length polydispersity (and also the fact that different end-to-end separations should correspond to different order paramters), and the implications of this phenomenon with respect to the proportionality factor in $S_b \sim 1/N$ are as yet not fully understood.[90,94]

Thus, for truly quantitative results, a proper calibration is desirable, but would only be possible if M_c were directly accessible. This is, for instance, possible for networks based on vinyl-functionalized poly(dimethylsiloxane), cross-linked by a silane and a Pt catalyst, where the cross-link points are chemically distinct and can be "counted" by high-resolution NMR methods. These results will be reported in a future publication.

Apart from these uncertainties, the combination of NMR and swelling measurements carries further complementary information on the network structure[69,71,75] and allows us to draw some further conclusions on the range of uncertainty for both methods. In some previous works[20,75,86,106–108] as well as in this article, a linear relationship between the network parameters determined by both methods was found. The existence of a finite *y*-intercept (see Figure 9) is usually explained by the following relation:

$$\frac{1}{M_c(\mathrm{NMR})} + \frac{1}{M_e} \approx \frac{1}{M_c(\mathrm{swelling})} + \frac{1}{M_{te}} \qquad (25)$$

It is attributed to the fact that additional restrictions caused by lateral chain packing or entanglements (tube constraint) sensed by NMR in bulk samples are at least partially relaxed at swelling equilibrium, i.e., $M_{te} \leq M_e$.[75,109,110] As stated by Flory,[12] the total suppression of entanglement restrictions could only be obtained by preparation under high-dilution conditions. As this is not the case here, the retention of some topological restrictions, i.e. trapped entanglements, is realistic. Consequently, as implied by eq 25, the *y*-intercept cannot simply be equated with the inverse entanglement length. If this is however done, the obtained value for M_e should certainly be *over*estimated (as the experimental intercept is always lowered due to a noninfinite value of M_{te}). In conclusion, the NMR results are sensitive to all types of restrictions (cross-links, entanglements, and trapped entanglements), whereas the elastic response in swelling experiments is determined only by cross-links, and those entanglements that could not be relaxed under the swollen conditions (= trapped entanglements). Therefore, the *y*-intercept could be related to the number of entanglements which effectively *disappear* in swollen state.

In Figure 9, the intercept expected for the literature value of the entanglement length (6.2 kg/mol) is indicated. It is seen to be somewhat higher than the experimental intercepts. We therefore conclude that the NMR result (in terms of M_c) is not too far from the “true” value (with respect to the rheological determination of M_e), and is, if at all, underestimated (cross-link density is somewhat overestimated). This yet again suggests that the phantom model with variable χ gives values that are close to the true ones, as the slope of 1.26 also suggests that the NMR values is overestimated, but not too much (the higher slope from the affine model would imply an even larger overestimation by NMR). However, this fact may only be accidental, and we do not want to imply that swollen rubber chains actually behave phantom-like.

This discussion is also in accord with our previously published data for the NR−toluene pair[75] (the samples are different in both works), which have here been revised with regards to the multiple corrections for the swelling data mentioned in the first part of this article (which in most of the cases were not taken into account in the original work). The corrected results, shown as a regression line in Figure 9, compare well with the new results as far as the slope is concerned. A small but significant difference is exhibited by the *y*-intercept, which could be associated with a different amount of trapped entanglements present in the different natural rubber raw materials. Differences in the chain characteristics (molecular weight, polydispersity, etc.) or in their processing could be the responsible. The control of the entanglements in the formed network thus appears to be the key to improve our understanding of rubber elasticity. In this sense, polymer melts that are free of entanglements, recently published by Lippits et al.,[111] may provide a very worthwhile starting point for future work.

Finally, we stress that all the natural rubber networks (independently of the cure system) swollen with toluene show the same linear relationship (Figure 10), at least over the typical cross-link density range used for practical proposes. This result further supports the correctness of the presented, improved approach to the analysis of swelling experiments, as well as it proves the independence of both methods from differences in the very local structure of these networks. Note that peroxide-cured systems can be assumed to have a certain fraction of highly functional cross-links or clusters due to radical chain reactions.[112]

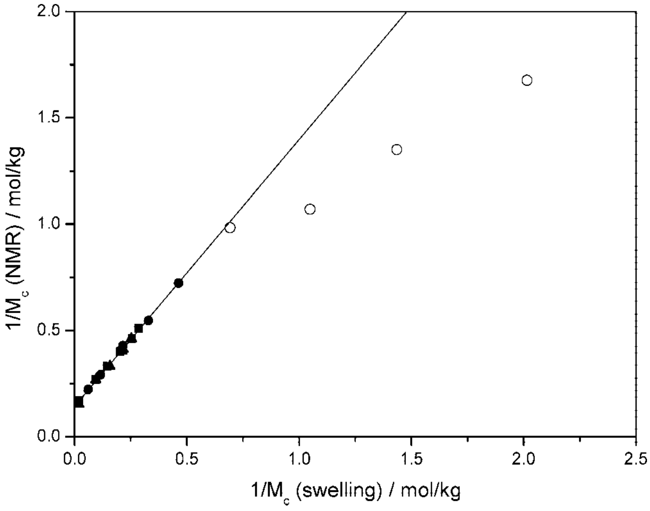

Figure 10. Comparison of swelling-determined reciprocal inter-cross-link molecular weights (using toluene as solvent, all discussed corrections, and the phantom model) with corresponding results from NMR experiments. Natural rubber networks vulcanized with different cure systems are compared: squares correspond to the conventional cure system defined in Table 1, triangles to samples vulcanized with an efficient system based on the same recipe as the conventional one but with different accelerant/sulfur ratio (12 instead of 0.2), and circles are from samples vulcanized with different contents of DCP. Full and empty symbols represent points that were taken into account for the linear fitting and those that do not follow the initial linear relationship, respectively.

Nevertheless, we also observe some deviation from linearity at very high cross-link density. One reason could of course be that very short network may show deviations from the assumed Gaussian deformation behavior (note that such rubbers are in fact technologically unimportant). Another obvious reason is certainly the increasing importance of higher-order corrections for the concentration dependence of χ, which is apparent from Figure 7. Also, the microstructure of very highly cross-linked elastomers might be different; e.g., higher network chain polydispersity or more pronounced spatial heterogeneities may arise, maybe as a consequence of the mentioned peculiarities of radical cross-linking.[112] The chain order distribution in these systems is in fact not as narrow as in sulfur-cured samples, sometimes with a clear bimodality, i.e., a small fraction with higher local cross-link density. Details on this topic will be the subject of a separate publication. Here, we can just conclude that a small number of such heterogeneities may well affect the swelling behavior much more than the bulk NMR response, in which they may lead to a more inhomogeneous local stress distribution in the swollen system. The fact that such effects may play a role also leads us to conclude that networks used to study the concentration dependence of χ should be carefully selected. For instance, McKenna et al.[49] used highly cross-linked samples, also vulcanized with DCP, to determine the behavior of χ in a large range of polymer concentrations. Their samples contained even more DCP than ours (up to 15 phr); therefore, their results could also be affected by the possible change in the swelling behavior.

Conclusions

In this work we have demonstrated the strong dependence of the cross-link density obtained from equilibrium swelling experiments on the model used to describe the thermodynamics of the swollen networks. This makes an accurate determination of this important parameter difficult if not impossible. On the basis of the Flory−Rehner theory, three possible sources of error/uncertainty have been identified and quantified: determination of the volumetric fraction of rubber, the Flory−Huggins polymer−solvent interaction parameter, and the applied model of rubber elasticity.

In the first part, the most important sources of error in the calculation of the volumetric fraction of rubber found in the literature were reviewed. The most general and correct method to calculate the concentration of polymer via gravimetric measurements was described by eq 20, where corrections in the solvent weight and rubber density must be made in order to obtain meaningful results. It was found to be particularly important to consider the kinetics of the swelling process and the degradation of the polymer. In addition, the inclusion of noninteracting solid particles leads to an excess of solvent that is imbibed in vacuoles formed at the particle/rubber interface, which should be corrected for. These problems are easily solved by proper experimental care and accuracy.

Although deviations caused by the calculation of ϕ_r are important, the largest dependences are due to the parameters that describe the thermodynamics of the swollen systems. A large uncertainty (around 50−60%) is associated with the interaction parameter χ. The correct value and concentration dependence of this parameter in cross-linked polymers is still an open challenge, mainly due to the small number of references on the topic. However, one can always define empirical procedures to determine this parameter experimentally; therefore, this issue should be not the main problem for accurate determination and comparison of cross-link densities via swelling experiments.

Finally, it is by far not clear which model should be used to describe the elastic behavior of swollen networks. Although most of our results indicate that the phantom model is the most appropriate, we believe that the better agreement is fortuitous. The elastic answer of swollen samples should be between the two extremes marked by the affine and phantom models, and the correct choice of the model is in fact one of the central problems. Currently, the dependence of the transformation of chain dimensions during swelling is not completely understood.

At this point, we would like to take up a very insightful comment of one of the reviewers, concerning the heuristic value of the Flory−Rehner approach and its relation to physically intuitive (but certainly not fully quantitative and thus here not considered) scaling approaches.[3] Using the series ansatz (eq 23) for χ in combination with the Flory−Rehner or phantom model equations, for lower volume fractions ϕ_r it is in fact possible to reproduce *any* realistic power law $1/M_c \sim \phi_r{}^a$ (e.g., $a = 5/3$ for the Flory−Rehner model in good solvent[25]) predicted by different scaling theories. Therefore, clearly, there are no a priori reasons to favor either scaling theories or empirical determinations/modifications of $\chi = f(\phi_r)$. The way in which the different model assumptions made in scaling approaches are related to an empirically nonconstant and network-specific χ parameter (which may be of thermodynamic origin, but also be due to nonaffine chain deformation, etc.) must be subject of independent interrogations of the swollen system (e.g., by light scattering, NMR).

In conclusion, the cross-link density of a network, which is one of the most important parameters defining the network structure and therefore the macroscopic properties, is a rather ill-defined parameter. Swelling experiments only yield a qualitative approximation to the real cross-link density of the sample, in particular when highly cross-linked samples are considered. The most important conclusion of this paper is therefore as follows: if swelling experiments should be used, as they are a rather simple and easy method, the only way to obtain a posteriori comparable data is to give a detailed description of the experimental procedure.

In contrast, MQ NMR experiments, possibly performed on a low-field instrument, have been proven to be an easy and direct alternative method to measure the total amount of cross-links and topological constraints in the system, and it has two important advantages; i.e., it does not depend of any thermodynamic arguments (although it is also model-dependent), and the NMR signal is more sensitive to the entanglement contributions that ultimately have an impact on the mechanical properties. On the basis of the in-depth comparison with swelling data presented herein, our calibration for the conversion of the measured residual coupling to cross-link density seems to give results that are close to the true value. Further work on independent calibrations is certainly necessary and will shortly be reported for the case of poly(dimethylsiloxane) networks.

Finally, we again stress that the linear dependence of the NMR observable on $1/M_c$ can be used to check the validity of thermodynamic models used to evaluate swelling experiments, which we have here demonstrated for the case of swelling experiments of natural rubber in MEK.

Acknowledgment. We thank the Alexander von Humboldt Foundation for the fellowship of J.L.V. and the Deutsche Forschungemeinschaft (DFG, SFB 418) as well as the Fonds der Chemischen Industrie for financial support. Our acknowledgments also go to R. Herrero for her invaluable assistance in the preparation of swelling samples under inert atmosphere.

References and Notes

(1) Mark, J. E.; Erman, B.; Eirich, F. R. *Science and Technology of Rubber*, 2nd ed.; Academic Press: San Diego, CA, 1994.
(2) Strobl, G. *The Physics of Polymers. Concepts for Understanding their Structures and Behaviour*, 2nd ed.; Springer-Verlag: Berlin, 1997.
(3) Rubinstein, M.; Colby, R. H. *Polymer Physics*; Oxford University Press: New York, 2003.
(4) Harrison, D. J. P.; Yates, W. R.; Johnosn, J. F. *Rev. Macromol. Chem. Phys* **1985**, *C25*, 481–549.
(5) Tan, Z.; Jaeger, R.; Vancso, G. J. *Polymer* **1994**, *35*, 3230–3236.
(6) Arndt, K. F.; Schreck, J. *Acta Polym.* **1985**, *36*, 56–57.
(7) Gillmor, J. R.; Colby, R. H.; Patel, S. K.; Malone, S.; Cohen, C. *Macromolecules* **1992**, *25*, 5241–5251.
(8) Pyckout-Hintzen, W.; Springer, T.; Forster, F.; Gronski, W. *Macromolecules.* **1991**, *24*, 1269–1274.
(9) Imanishi, Y.; Adachi, K.; Kotaka, T. *J. Chem. Phys.* **1988**, *89*, 7585–7592.
(10) Ferry, J. D. *Viscoelastic Properties of Polymers*, 3rd ed.; John Wiley & Sons: New York, 1980.
(11) Treolar, L. R. G. *The Physics of Rubber Elasticity*, 3rd ed.; Clarendon Press: Oxford, UK, 1975.
(12) Mark, J. E.; Erman, B. *Elastomeric Polymer Networks*; Prentice-Hall: Englewood Cliffs, NJ, 1992.
(13) Melley, R. E.; Stuckey, J. E. *J. Appl. Polym. Sci.* **1970**, *14*, 2327–2331.
(14) Matzen, D.; Straube, E. *Colloid Polym. Sci.* **1992**, *270*, 1–8.
(15) Hergenrother, W. L. *J. Appl. Polym. Sci.* **1986**, *32*, 3039–3050.
(16) Litvinov, V. M.; De, P. P. *Spectroscopy of Rubbers and Rubbery Materials*; Rapra Technology Ltd.: Shawbury, UK, 2002.
(17) Simon, G.; Schneider, H. *Makromol. Chem., Macromol. Symp.* **1991**, *52*, 233–246.
(18) Cohen-Addad, J. P.; Vogin, R. *Phys. Rev. Lett.* **1974**, *33*, 940–943.
(19) Brereton, M. G. *Macromolecules.* **1990**, *23*, 1119–1131.
(20) Demco, D. E.; Hafner, S.; Fülber, C.; Graf, R.; Spiess, H. W. *J. Chem. Phys.* **1996**, *105*, 11285–11296.
(21) Graf, R.; Heuer, A.; Spiess, H. W. *Phys. Rev. Lett.* **1998**, *80*, 5738–5741.
(22) Saalwächter, K.; Ziegler, P.; Spyckerelle, O.; Haidar, B.; Vidal, A.; Sommer, J.-U. *J. Chem. Phys.* **2003**, *119*, 3468–3482.
(23) Saalwächter, K.; Klüppel, M.; Luo, H.; Schneider, H. *Appl. Magn. Reson.* **2004**, *27*, 401–417.
(24) Flory, P. J. *Principles of Polymer Chemistry*; Cornell University Press: Ithaca, NY, 1953.
(25) Flory, P. J.; Rehner, J. *J. Chem. Phys.* **1943**, *11*, 521–526.
(26) Fory, P. J. *J. Chem. Phys.* **1950**, *18*, 108–111.
(27) Gee, G. *Trans. Faraday Soc.* **1942**, *38*, 276–282.
(28) Gee, G. *Trans. Faraday Soc.* **1942**, *38*, 418–422.
(29) Frenkel, J. *Rubber Chem. Technol.* **1940**, *13*, 264–274.
(30) Flory, P. J. *J. Chem. Phys.* **1941**, *9*, 660–661.

(31) Huggins, M. L. *J. Chem. Phys.* **1941**, *9*, 440–440.
(32) Kuhn, W.; Grün, F. *Kolloid Z. Z. Polym.* **1943**, *101*, 248–262.
(33) James, H. M.; Guth, E. *J. Chem. Phys.* **1943**, *11*, 455–481.
(34) James, H. M.; Guth, E. *J. Chem. Phys.* **1947**, *15*, 669–683.
(35) Flory, P. J.; Erman, B. *Macromolecules* **1984**, *15*, 800–806.
(36) Erman, B.; Flory, P. J. *Macromolecules* **1984**, *15*, 806–811.
(37) Orofino, T. A.; Flory, P. J. *J. Chem. Phys.* **1957**, *26*, 1067–1076.
(38) Flory, P. J.; Daoust, H. *J. Polym. Sci.* **1957**, *25*, 429–440.
(39) Bristow, G. M.; Watson, W. F. *Trans. Faraday Soc.* **1958**, *54*, 1567–1573.
(40) Eichinger, B. E.; Flory, P. J. *Trans. Faraday Soc.* **1968**, *64*, 2035–2051.
(41) Brostow, W. *Macromolecules.* **1971**, *4*, 742–747.
(42) Flory, P. J.; Tatara, Y.-I. *J. Polym. Sci., Polym. Phys. Ed.* **1975**, *13*, 683–702.
(43) Orwoll, R. A. *Rubber Chem. Technol.* **1977**, *50*, 451–479.
(44) Gottlieb, M.; Herskowitz, M. *Macromolecules* **1981**, *14*, 1468–1471.
(45) Kok, C. M.; Rudin, A. *J. Appl. Polym. Sci.* **1982**, *27*, 353–362.
(46) Gee, G.; Herbert, J. B. M.; Roberts, R. C. *Polymer* **1965**, *6*, 541–548.
(47) McKenna, G. B.; Flynn, K. M.; Chen, Y. H. *Polym. Commun.* **1988**, *29*, 272–275.
(48) McKenna, G. B.; Flynn, K. M.; Chen, Y. H. *Macromolecules* **1989**, *22*, 4507–4512.
(49) McKenna, G. B.; Flynn, K. M.Y. H. *Chen. Polym.* **1990**, *31*, 1937–1945.
(50) McKenna, G. B.; Crissman, J. M. *J. Polym. Sci., Part B: Polym. Phys.* **1997**, *35*, 817–826.
(51) McKenna, G. B.; Horkay, F. *Polymer* **1994**, *35*, 5737–5742.
(52) Horkay, F.; Zrinyi, M.; Geissler, E.; Hecht, A. M.; Pruvost, P. *Polymer* **1991**, *32*, 835–839.
(53) Horkay, F.; Hecht, A. M.; Geissler, E. *J. Polym. Sci., Part B: Polym. Phys.* **1995**, *33*, 1641–1646.
(54) Horkay, F.; Waldron, W. K.; McKenna, G. B. *Polymer* **1995**, *36*, 4525–4527.
(55) Horkay, F.; McKenna, G. B.; Deschamps, P.; Geissler, E. *Macromolecules* **2000**, *33*, 5215–5220.
(56) Mallam, S.; Horkay, F.; Hecht, A. M.; Rennie, A. R.; Geissler, E. *Macromolecules* **1991**, *23*, 543–548.
(57) Horkay, F.; Hecht, A. M.; Mallam, S.; Geissler, E.; Rennie, A. R. *Macromolecules* **1991**, *24*, 2896–2902.
(58) Tan, Z.; Jaeger, R.; Vancso, G. J. *Polymer* **1994**, *35*, 3230–3236.
(59) Hrnjak-Murgić, Z.; Jelenčić, J.; Bravar, M.; Marović, M. *J. Appl. Polym. Sci.* **1997**, *65*, 991–999.
(60) Hedden, R. C.; Saxena, H.; Cohen, C. *Macromolecules* **2000**, *33*, 8676–8684.
(61) Horta, A.; Pastoriza, M. A. *Eur. Polym. J.* **2005**, *41*, 2793–2802.
(62) Scott, J. R. *Trans. Inst. Rubber Ind.* **1929**, *5*, 95–102.
(63) Ellis, B.; Welding, G. N. *Rubber Chem. Technol.* **1964**, *37*, 563–570.
(64) Ellis, B.; Welding, G. N. *Rubber Chem. Technol.* **1964**, *37*, 571–575.
(65) Proske, G. *Rubber Chem. Technol.* **1941**, *14*, 489–500.
(66) Whitby, G. S.; Evans, A. B. A.; Pasternack, D. S. *Trans. Faraday Soc.* **1942**, *38*, 269–275.
(67) Williams, I. *Ind. Eng. Chem.* **1937**, *29*, 172–174.
(68) Scott, R. L.; Magat, M. *J. Polym. Sci.* **1949**, *4*, 555–571.
(69) Klüppel, M.; Menge, H.; Schmidt, H.; Schneider, H.; Schuster, R. H. *Macromolecules* **2001**, *34*, 8107–8116.
(70) Oikawa, H.; Murakami, K. *Macromolecules* **1991**, *24*, 1117–1122.
(71) Menge, H.; Hotopf, S.; Pönitzsch, S.; Richter, S.; Arndt, K.-F.; Schneider, H.; Heuert, U. *Polymer* **1999**, *40*, 5303–5313.
(72) Burel, F.; Feldman, A.; Bunel, C. *Polymer* **2005**, *46*, 483–489.
(73) Villar, M. A.; Vallés, E. M. *Macromolecules* **1996**, *29*, 4081–4089.
(74) Patel, S. K.; Malone, S.; Cohen, C.; Gillmor, J. R.; Colby, R. H. *Macromolecules* **1992**, *28*, 5241–5251.
(75) Saalwächter, K.; Herrero, B.; López-Manchado, M. A. *Macromolecules* **2005**, *38*, 9650–9660.
(76) Saalwächter, K. *Prog. Nucl. Magn. Reson. Spectrosc.* **2007**, *51*, 1–35.
(77) Pratten, N. A. *J. Mater. Sci.* **1981**, *16*, 1737–1747.
(78) Bowman, H. A.; Schoonover, R. M. *J. Res. Natl. Bur. Stand.* **1967**, *71C*, 179.
(79) Cohen-Addad, J. P. *Macromolecules* **1989**, *22*, 147–151.
(80) Cohen-Addad, J. P. *Prog. NMR Spectrosc.* **1993**, *25*, 1–316.
(81) Litvinov, V. M. *Macromolecules* **2006**, *39*, 8727–8741.
(82) Saalwächter, K. *Macromolecules* **2005**, *38*, 1508–1512.
(83) Saalwächter, K.; Herrero, B.; López-Manchado, M. A. *Macromolecules* **2005**, *38*, 4040–4042.
(84) Collignon, J.; Sillescu, H.; Spiess, H. W. *Colloid Polym. Sci.* **1981**, *259*, 220–226.
(85) Callaghan, P. T.; Samulski, E. T. *Macromolecules* **1997**, *30*, 113–122.
(86) Fischer, E.; Grinberg, F.; Kimmich, R.; Hafner, S. *J. Chem. Phys.* **1998**, *109*, 846–854.
(87) Graf, R.; Demco, D. E.; Hafner, S.; Spiess, H. W. *Solid State Nucl. Magn. Reson.* **1998**, *12*, 139–152.
(88) Schneider, M.; Gasper, L.; Demco, D. E.; Blümich, B. *J. Chem. Phys.* **1999**, *111*, 402–415.
(89) Saalwächter, K.; Heuer, A. *Macromolecules* **2006**, *39*, 3291–3303.
(90) Saalwächter, K.; Sommer, J.-U. *Macromol. Rapid Commun.* **2007**, *28*, 1455–1465.
(91) Cohen-Addad, J. P.; Phan Thanh, B.; Montes, H. *Macromolecules* **1997**, *30*, 4374–4380.
(92) Litvinov, V. M.; Dias, A. A. *Macromolecules* **2001**, *34*, 4051–4060.
(93) Saalwachter, K.; Kleinschmidt, F.; Sommer, J. U. *Macromolecules* **2004**, *37*, 8556–8568.
(94) Sommer, J. U.; Saalwachter, K. *Eur. Phys. J. E* **2005**, *18*, 167–182.
(95) Wagner, H. L.; Flory, P. J. *J. Am. Chem. Soc.* **1952**, *74*, 195–200.
(96) Booth, C.; Gee, G.; Holden, G.; Williamson, G. R. *Polymer* **1964**, *5*, 343–353.
(97) Eichinger, B. E.; Flory, P. J. *Discuss. Faraday Soc.* **1968**, *64*, 2035–2052.
(98) Flory, P. J.; Orwoll, R. A.; Vrij, A. *J. Am. Chem. Soc.* **1964**, *86*, 3507–3514.
(99) Flory, P. J.; Orwoll, R. A.; Vrij, A. *J. Am. Chem. Soc.* **1964**, *86*, 3515–3520.
(100) Freed, K. F.; Pesci, A. I. *J. Chem. Phys.* **1987**, *87*, 7342–7344.
(101) Freed, K. F.; Pesci, A. I. *Macromolecules* **1989**, *22*, 4048–4050.
(102) Moerkerke, R.; Koningsveld, R.; Berghmans, H.; Dušek, K.; Šolc., K. *Macromolecules* **1995**, *28*, 1103.
(103) Tewari, Y. B.; Schreiber, P. *Macromolecules* **1972**, *5*, 329–331.
(104) Brandrup, J.; Immergut, E. H.; Grulke, E. A. *Polymer Handbook*, 40th ed.; John Wiley & Sons: New York, 1999.
(105) Braun, J. L.; Mark, J. E.; Eichinger, B. E. *Macromolecules* **2002**, *35*, 5273–5282.
(106) Fry, C. H. G.; Lind, A. C. *Macromolecules* **1988**, *21*, 1292–1297.
(107) Sotta, P.; Fülber, C.; Demco, D. E.; Blümich, B.; Spiess, H. W. *Macromolecules* **1996**, *29*, 6222–6230.
(108) Cohen-Addad, J. P.; Thanh, B. P.; Montes, H. *Macromolecules* **1997**, *30*, 4374–4380.
(109) Abdel-Goad, M.; Pyckhout-Hintzen, W.; Kahle, S.; Allgaier, J.; Richter, D.; Fetters, J. L. *Macromolecules* **2004**, *37*, 8135–8144.
(110) Krushev, S.; Paul, W.; Smith, G. D. *Macromolecules* **2002**, *35*, 4198–4203.
(111) Lippits, D. R.; Rastogi, S.; Talebi, S.; Bailly, C. *Macromolecules* **2006**, *39*, 8882–8885.
(112) Valentin, J. L.; Fernandez-Torres, A.; Posadas, P.; Marcos-Fernandez, A.; Rodriguez, A.; Gonzalez, L. *J. Polym Sci., Part B: Polym. Phys.* **2007**, *45*, 544–556.

MA8005087